NSF/NOAA ATM 8418204
ATM 8720488

DOD-NAVY-ONR N00014-87-K-0203

THE STRUCTURAL EVOLUTION OF TYPHOONS

by Candis L. Weatherford

P.I.-William M. Gray

Colorado State University

DEPARTMENT OF ATMOSPHERIC SCIENCE

PAPER NO.
446

THE STRUCTURAL EVOLUTION OF TYPHOONS

By
Candis L. Weatherford

Department of Atmospheric Science
Colorado State University
Fort Collins, CO 80523

September, 1989

Atmospheric Science Paper No. 446

ABSTRACT

A three phase life cycle characterizing the structural evolution of typhoons has been derived from aircraft reconnaissance data for tropical cyclones in the western North Pacific. More than 750 aircraft reconnaissance missions at 700 mb into 101 northwest Pacific typhoons are examined. The typical life cycle consists of the following: phase 1) the entire vortex wind field builds as the cyclone attains maximum intensity; phase 2) central pressure fills and maximum winds decrease in association with expanding cyclone size and strengthening of outer core winds; and phase 3) the wind field of the entire vortex decays.

Nearly 700 aircraft radar reports of eyewall diameter are used to augment analyses of the typhoon's life cycle. Eye characteristics and diameter appear to reflect the ease with which the maximum wind field intensifies. On average, an eye first appears with intensifying cyclones at 980 mb central pressure. Cyclones obtaining an eye at pressures higher than 980 mb are observed to intensify more rapidly while those whose eye initially appears at lower pressures deepen at slower rates and typically do not achieve as deep a central pressure. The eye generally contracts with intensification and expands as the cyclone fills, although there are frequent exceptions to this rule due to the variable nature of the eyewall size. Disappearance of the eye coincides, on average, with the filling of central pressure to 955 mb. Concentric eyes are observed nearly as often in the deepening as in the filling stage for central pressures below 945 mb.

By extracting the symmetric portion of the tangential wind field of the cyclone vortex and the cyclone motion vector, the residual wind in the cyclone's interior region can be studied for various cyclone stratifications. These analyses show that tropical cyclones move faster than and to the left of the ambient 700 mb wind field. The residual wind field data also show systematic differences for cyclones with differing latitude, direction of motion, and core intensity.

TABLE OF CONTENTS

LIST OF SYMBOLS AND ACRONYMS

CYCLONE : Tropical cyclone of intensities ranging from tropical depression to super-typhoon.

INNER CORE : The region of the tropical cyclone from the center to 1° radius.

INTERIOR REGION : The region of the tropical cyclone extending from the center to 2.5° latitude radius.

JTWC : Joint Typhoon Warning Center (US Air Force and Navy) based on Guam.

MOT : Motion or storm-relative cylindrical coordinate system where the current, speed and direction of each storm is removed from all wind observations prior to compositing.

MOTROT : A combination of the MOT and ROT systems, hence a cyclone-relative cylindrical coordinate system in which the cyclone's motion vector is subtracted from each wind observation prior to compositing and all cyclones are rotated to a common heading.

MOTROT–VORT : Wind vector in the MOTROT coordinate system that results after the symmetrical mean tangential wind for each radial band (VORT) has been removed.

MSLP : Minimum Sea-Level Pressure measured at the surface by dropsonde or at 700 mb by aircraft.

NAT : From NATural; a cylindrical earth-relative coordinate system which is concentric with the center of the tropical cyclone.

OCS : Outer Core Wind Strength; the area–weighted average tangential wind speed calculated relative to the moving cyclone from four–radial leg missions extending through the region of the outer core from 1° to 2.5° radius.

OUTER CORE : The region of the tropical cyclone from 1° to 2.5° radius.

RESIDUAL WIND ($\vec{V}_{Res}$) : $\vec{V}_T$ (MOTROT–VORT) + $\vec{V}_R$ (MOTROT)= V_T (asym.) + V_R (MOTROT). Wind field values obtained after symmetric tangential winds and the mean cyclone motion vector have been removed.

RMW : Radius of Maximum Wind speed.

ROT : Rotation; signifiying that wind observations in cylindrical coordinates have been rotated prior to compositing so that data for all storms are adjusted to correspond to a common storm heading, in this case toward the top of the figure.

V_R : Radial wind speed.

V_T : Tangential wind speed

V_T (MOTROT-VORT) : V_T (MOTROT) - V_T (VORT)= V_T (asym.). The asymmetric tangential wind vector in the cyclone-relative coordinate system that results after the mean vortex has been removed.

V_T (VORT) : The symmetrical mean tangential wind speeds around the cyclone vortex. This wind varies with radius.

Chapter 1

INTRODUCTION

Tropical cyclones worldwide account for nearly 65% of deaths resulting from natural disasters (Anthes, 1982). For all their destructive power, the damaging winds of tropical cyclones have yet to be accurately documented or forecast. Research aircraft have routinely flown into tropical cyclones since 1947 for the express purpose of obtaining measurements of core conditions. However, these measurements have not been effectively used for describing details of the manner in which core region (0-2.5 ° radius) winds change during a cyclone's life cycle. Other larger scale (beyond 2° radius) structural studies, accomplished primarily through rawinsonde composites, have not been able to relate changes of core region winds with changes in the outer-region. Hence, wind field changes which occur within the 0-2.5 ° radius during the lifetime of a cyclone are poorly understood. This study focuses on the evolution of 700 mb wind fields of tropical cyclones in the Northwest Pacific by analyzing aircraft observations of these cyclones from development to decay.

An adequate cyclone forecast must specify expected changes in the wind profile and where the entire vortex will move in time. Forecasts of motion are as crucial as forecasts of structural change. For example, whereas the average growth of a typhoon's radius of damaging (25 ms^{-1}) winds during its development is 80 km per day (Weatherford and Gray, 1988b), errors in the cyclone's forecast position average 230 km over the same 24-hour period (Matsumoto, 1984). Reasons for the position forecast errors include inadequate measurements of the current which steers the cyclone. Greater knowledge of the background wind fields can shed light not only on future cyclone track changes, but also on the manner in which the environment interacts with the cyclone during its life cycle. This study provides more insight into the steering current of tropical cyclones within the 2.5° radius region and how this interior steering current relates to actual cyclone motions.

1.1 Background Information on the Wind Structure of Tropical Cyclones

Over the last 30 years, the inner core wind fields (< 1° radius) of tropical cyclones in the Atlantic have been investigated by operational and research aircraft and most of what has been learned from aircraft research is the result of case studies of various Atlantic hurricanes. A partial listing of these studies includes the following: Daisy and Helene (Riehl and Malkus, 1961; Colon et al., 1961, 1964); Cleo (LaSeur and Hawkins, 1963); Ella, Janice and Dora (Sheets, 1967a,b; 1968); Debbie and Hilda (Hawkins and Rubsam, 1968a,b, 1971); and Allen, David, Anita and Frederic (Jorgensen, 1984a,b). Also, Shea and Gray (1973), Gray and Shea (1973), and Gray (1962, 1965, 1967) combined many of these case studies to obtain a more general view of the inner core wind structure of hurricanes as well as the variability from storm to storm.

However, because of the sparseness of outer radius (> 1° radius) reconnaissance information, little has been done to relate observations of the cyclone's inner core region to conditions in the adjoining outer core (1 to 2.5° radius). Although Merrill (1984) showed that, in general, Atlantic cyclones are smaller than Pacific cyclones, many Pacific cyclones are as small as those typically found in the Atlantic (Arakawa, 1950). For this reason, the wind field characteristics of Pacific cyclones, classified according to size, should adequately approximate those of cyclones found in other tropical ocean basins.

Studies of outer core structure using reconnaissance aircraft data are few. Hughes (1952) was the first to study the cyclone's 0 to 4° region. His study on the average wind profiles of 13 mature typhoons presented the first aircraft measurements of the low-level wind profile of the mean typhoon. His verification of strong inflow in the typhoon boundary layer had great impact on later theoretical speculation on the nature of the physical processes of tropical cyclones. However, state-of-the-art in wind measuring during that time (late 1940s) was primitive by present standards and Hughes' wind measurements were based on various visual estimates of the sea state. Therefore, a degree of subjective uncertainty in these wind estimates was always present.

Subsequent to Hughes' study, Weatherford and Gray (1988a, b) undertook the task of relating the cyclone's inner (0-1°) and outer (1-2.5°) core winds using wind data obtained with more accurate measuring equipment. They found a high degree of variability between the cyclone's inner core maximum winds and the radius of gale force winds in the outer core. They were also able to show that cyclones with comparatively small eyes and similar central pressure had smaller radii of gale-force winds and weaker winds throughout the outer core. For the first time the entire wind profile, from the radius of maximum winds to the radius of gale force winds, was depicted for cyclones of different intensities and eye sizes.

From the late 1970's until the present, the main objective of hurricane research flights in the Atlantic has been the study of the hurricane's finer-scale convective processes. Studies by Willoughby, et al. (1982), Barnes, et al. (1983), Jorgensen (1984a,b), Frank (1984), Marks and Houze (1987), and Barnes and Stossmeister (1987) have revealed much about the convective and mesoscale processes of hurricanes. The later studies improved upon the snapshot depictions of hurricane wind fields which were common from the 1950's through the 1970's by following changes on a mesoscale time frame (ie., changes on the order of an hour to a few hours). Nevertheless, these studies still lacked depictions of the tropical cyclone's wind field through its outer core (1-2.5° radius) for periods longer than one day.

The question of structural evolution of winds on time scales beyond one day was examined by Dunn (1951) who suggested four stages of cyclone development; 1) formative, 2) immaturity, 3) maturity, and 4) decay. Colon et al. (1963) verified that wind profiles of individual cyclones differ considerably from case to case. Based on this premise, Colon classified the evolution of tropical cyclone winds into two types: 1) a small, intense–type of wind evolution and, 2) a large-diffuse type of wind evolution. The problem with this depiction lay in the data sample which did not extend beyond the inner core and thus did not sample the radius of gale-force winds and included only 9 hurricanes, most of which were observed for only one day. The typical lifetime of a typhoon is 7.5 days with a maximum of about 15 days. Therefore, although Colon et al's. study did alert tropical meteorologists to the variable nature of cyclones, it also fell far short of describing the full evolution of the wind field from beginning to end.

Although these early life cycle studies provided useful patterns of the general wind fields given the limited data sample, it was unlikely that a handful of cases could adequately describe all cyclones. It is felt that a large number of randomly selected cases, each individually followed throughout their lifetimes, might provide a more complete description of the cyclone's wind field. Only then can different cyclones be categorized and compared for similarities.

This study attempts to fill the gap in our present knowledge of the wind evolution of tropical cyclones by focusing on the 700 mb winds, primarily from the center to 3°, (occasionally out to 4°) and thereby capturing the wind field throughout the life cycle of the cyclone. In addition, once the mean vortex is removed from the wind field and all cyclones are oriented to a common directional heading, the resulting background wind field can be examined for indications of systematic steering current and cyclone motion differences.

1.2 Focus of this Study

Operational reconnaissance flights in the northwestern Pacific Ocean were routinely flown every 12 hours from the center to 4° radius and from genesis to decay for nearly all cyclones. Five years of these flight observations (1980-84), representing 750 aircraft missions into 101 tropical cyclones were processed and analyzed. The present study explores changes of the 700 mb wind field evident in both the mean vortex and the 700 mb steering current of the tropical cyclone, from just past genesis until cyclone decay.

A description of the data used and the manner in which they were processed is presented in Chapter 2. Chapter 3 examines the basic steady-state structure of tropical cyclone winds when stratified by intensity and by the strength of outer core. Chapter 4

Chapter 2

DATA REDUCTION PROCEDURES

The principal goal of this research was to describe the evolution of the 700 mb wind structure of tropical cyclones throughout their life cycle. To achieve this goal, a large number of tropical cyclones were observed. The data used for this study encompassed over 750 aircraft reconnaissance missions into 101 named tropical cyclones that traversed the northwestern Pacific ocean basin during the 5-year period of 1980 to 1984. The tracks of these 101 cyclones are shown in Fig. 2.1. This data set was an expanded version of a three year flight data set used in a prior study by the author. Two additional years (1983 and 1984) of data were processed in order to obtain a more representative sample of the typical changes occurring during the typhoon's lifetime.

2.1 Scope of the Flight Missions

Aircraft reconnaissance missions were designed to track and measure all Pacific cyclones from genesis to decay. A wide range of storm intensities, locations, and headings were sampled. Only data for 700 mb were processed so that comparable and consistent results could be obtained. Hence, boundary level missions which were generally flown at 300 meters elevation into tropical depressions during the development stage of the vortex, are not included. No other attempt was made to exclude data for specific cyclone intensity classes. Because all other categories of cyclones were sampled as they naturally occurred, the data set was ideal for study of the cyclone's life cycle.

Restrictions imposed upon these operationally-designed reconnaissance flights prohibited missions over land, within 100 nautical miles of the People's Republic and China and Vietnam and north of 35° latitude. However, because flights were taken every 12

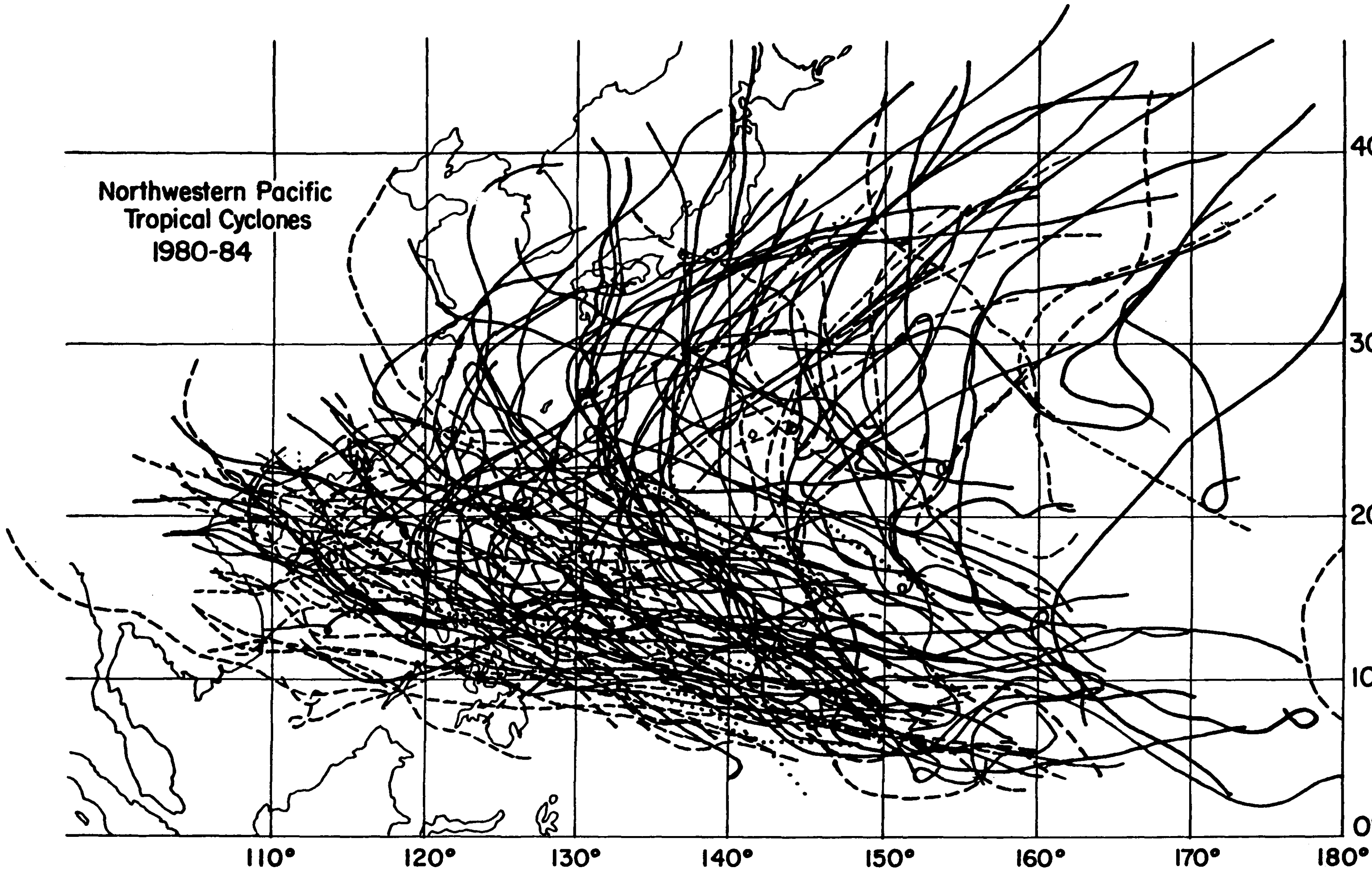

Figure 2.1: Northwestern Pacific tropical cyclone tracks for the 101 cases of 1980-84 used in the present study. Solid lines are the paths of the cyclone while a typhoon and dashed lines denote the tracks of the cyclones' tropical storm stage.

hours on nearly all cyclones in the northwest Pacific, very extensive data were available and the restrictions did not limit the analysis. Data extended outward to 450 km from the storm center (typically beyond the radius of gale-force winds) throughout the life of the cyclone and missions penetrated the center of the storms four times a day. Typical flight tracks consisted of radial (entry-exit) at 700 mb passes from the center to 2.5 degrees latitude, and 2 entry-exit passes to 4 degrees (Fig. 2.2). This flight track provided information every .5° along each radial leg inside 2.5°. In order to provide the forecaster with information on the cyclone prior to the 00 and 12Z GMT forecast times, flight data sampling typically spanned the 4-hour periods centered on 0900 and 2100 GMT (often 1800 and 0600 local time, respectively). Total flight time per mission typically lasted 10 (or 8-12) hours.

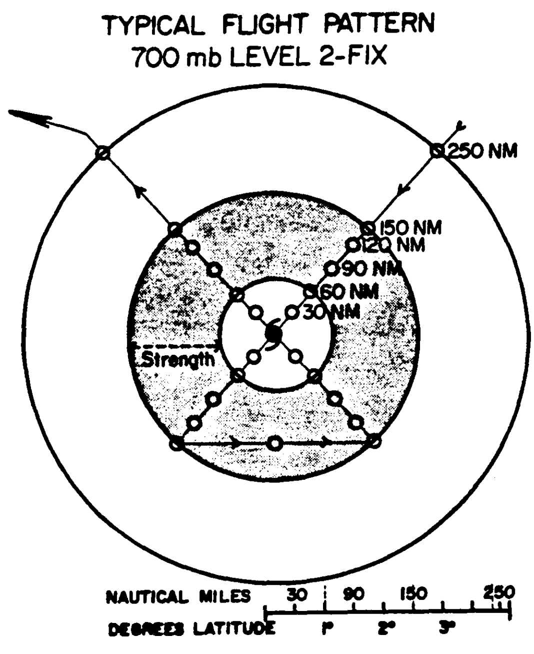

Figure 2.2: Typical 700 mb flight pattern for a single mission into a tropical cyclone. Circles denote required observation positions taken every .5° (55 km), with four additional observations taken at the radius of maximum wind. The shaded region marks the outer core (1° to 2.5° radial band) while the unshaded inner core is defined as the region inside 1° radius.

The flight missions afforded a substantial data set as shown in Fig. 2.3 for the relative frequency of observations for three cyclone intensity classes. Two-thirds of all the cyclones in this study developed into typhoons. The average life span of tropical cyclones which developed into typhoons was 7.5 days while that for systems which only developed into tropical storms was 4.5 days. The longest lived cyclone in this data set was Typhoon Pamela of 1982 which traversed the Pacific for 16 days.

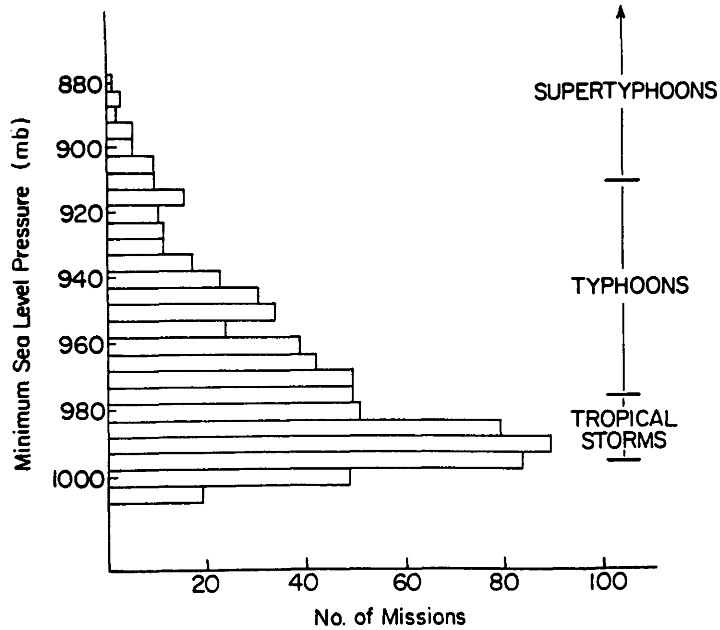

Figure 2.3: Histogram showing the aircraft observed frequency of MSLP (Minimum Sea Level Pressure) for overwater tropical cyclones of the northwestern Pacific from 1980 to 1984.

2.2 Data Navigation

All composite analyses are done in a cylindrical coordinate system which, for the purposes of compositing data, is always centered over the typhoon. This cylindrical system may be referred to as either the NAT, MOT, or ROT system, depending on the type of analysis to be done. Although the coordinate system moves with the storms in that all composited data are positioned radially relative to the storm center, completely unadjusted wind observations (ie., as measured) appear only in the NAT or natural coordinates. Wind data in MOT (as in MOTION) coordinates have been adjusted by subtracting the current mean motion vector of the typhoon from individual wind observations prior to compositing. The resultant wind data after this adjustment reveal the flow relative to the cyclone. Wind observations in ROT coordinates have been rotated azimuthally (both position and direction) prior to compositing so that observations for each cyclone are analyzed relative to a common heading; in this case toward the north which is always toward the top of these figures. Combining the latter two definitions, wind data in a MOTROT representation will have been adjusted for the relative motion of the cyclones and rotated so that relative motion for all storm systems included in a composite analysis is directed toward the north. In the cyclone-relative MOTROT coordinate system, one can detect the 700 mb environment through which the cyclone moves.

The process of navigating each observation to either NAT, MOT, ROT, or MOTROT coordinates were important steps. Basically the procedure involved using the Best Track center position data provided by the Joint Typhoon Warning Center (JTWC) and interpolating through time to obtain a smooth and reliable cyclone track. Aircraft observations were then obtained relative to both the fixed and moving cyclone center. Additional details of the data navigation are given in Weatherford (1985) and Weatherford and Gray (1988a).

2.3 Compositing Method

The five-year data set included 101 cyclones which was sufficient to allow several composite stratifications to be made with full data coverage in all octants of the cyclone. Examples of the data coverage for two such stratifications are shown in Fig. 2.4 for cyclones with medium-sized eyes and in Fig. 2.5 for cyclones undergoing rapid intensification (defined as a decrease of MSLP of 42 $mb\ d^{-1}$). Although the data coverage represented in Fig. 2.5 was the least dense of all stratifications attempted, the supply of observations was ample for the analyses.

The design of the composite grid, shown in Fig. 2.6, was based in part on the spatial distribution of data. Observations were typically taken every 0.5° (or 55 km) out to 275 km, and then less frequently out to 460 km. Figure 2.7 shows a larger grid, encompassing a 4° (440 km) radius with the total data count for all missions shown in each grid box.

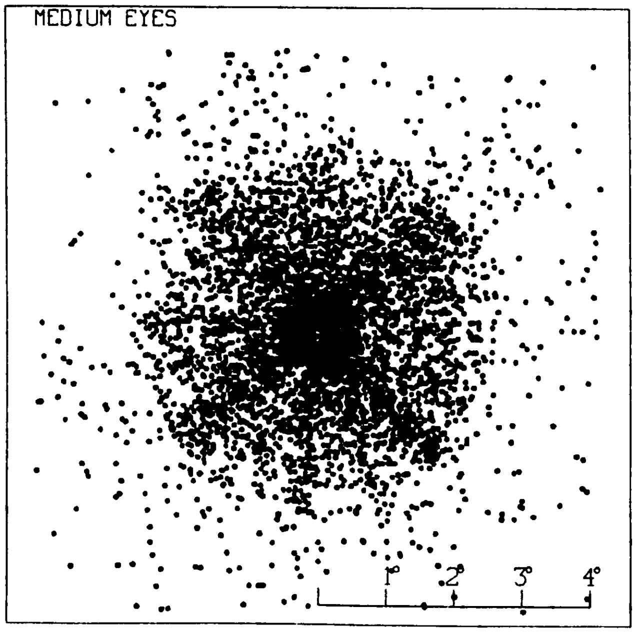

Figure 2.4: Locations of data points of a composite of all aircraft missions flown into tropical cyclones with medium eyes (diameters ranging from 28 to 55 km).

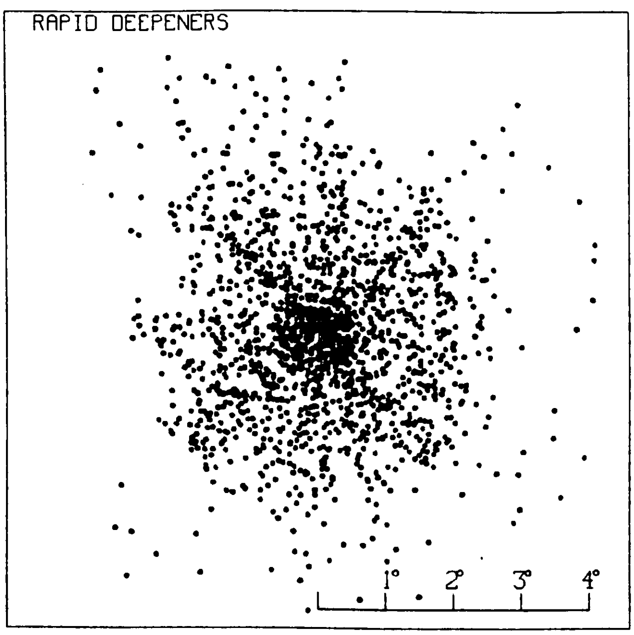

Figure 2.5: Data point distribution for a composite of all flight missions into cyclones undergoing rapid deepening of MSLP ($\geq$ 42 mb per day).

Notice that the density of data drops off significantly beyond 2.5° (275 km). The grid used for the analyses in this study extends only as far as 2.5°, as shown in the example in Fig. 2.8 for the tangential winds of extreme typhoons. Although, in general, there were not enough data points for plan view depictions beyond 2.5°, azimuthally-averaged composites allowed approximate radial depictions of wind, moisture, and vorticity fields to extend out to 4° radius.

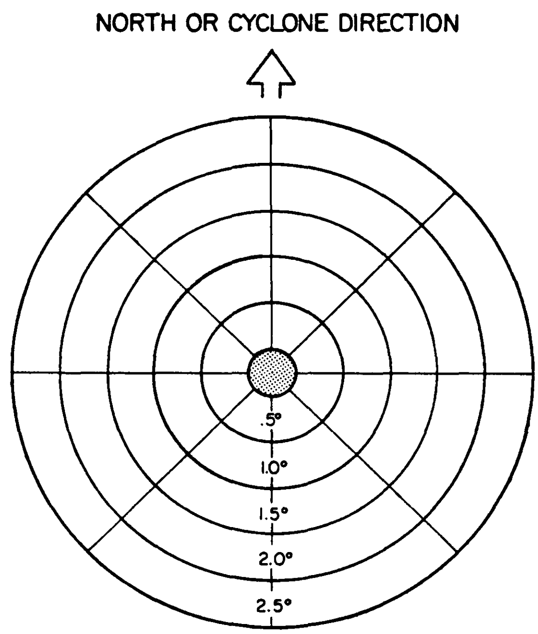

Figure 2.6: Composite grid used in plan-view analyses of asymmetries of cyclones utilizing aircraft observations from .25° to 2.5° radius. Observations which fall in the shaded region from the center to .25° are not composited. The arrow points to the cyclone's motion heading in the cyclone-relative MOTROT coordinate system.

Once the composite grid was specified, data averaging could commence. All data points within each 0.5° radial band and octant grid sector were averaged and assumed to represent the center point of the grid sector. This procedure worked well in providing spatially-balanced averages in that observations were scattered rather evenly throughout each sector due to inherent discrepancies between the anticipated (forecast) and actual locations of storm centers. Note the distribution of the radial flight tracks for all missions into typhoon Wynne in Fig. 2.9.

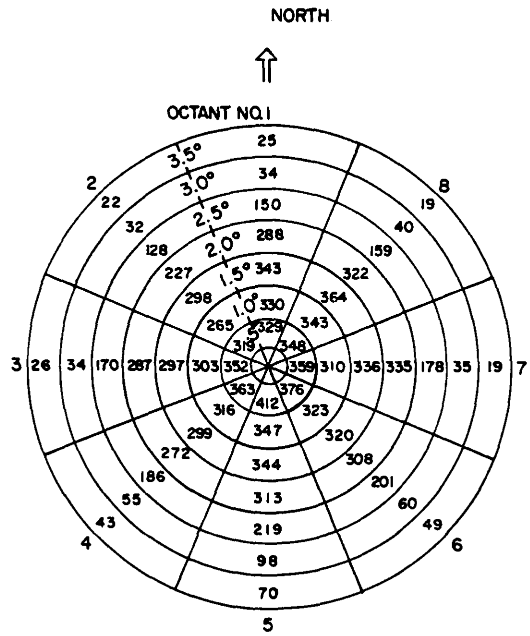

Figure 2.7: Frequency of observations falling into each grid sector for all missions into tropical cyclones.

Data points that lay within 28 km of the storm center were not plotted because of the rapidly changing wind fields. Obviously, averaging maximum (eyewall) wind speeds with light-and-variable winds within the eye would result in misrepresentative values. Thus, the composite grid extended from .25° (28 km) to 2.5° radius (278 km), with all data falling within each 0.5° octant sector being averaged to single grid point values. Maximum wind speeds were then estimated for purposes of comparison but these estimates were not included in the plan views. This composite grid will be used throughout this paper in both the NAT and MOTROT coordinate systems to focus on the asymmetries in both earth-relative and the cyclone-relative coordinates.

2.4 Estimates of the Vortex-averaged Maximum Wind and Normalized Wind Profiles

The maximum wind and the radius of maximum wind (RMW) are established indices for characterizing the strength and size of tropical cyclones. The accuracy of our measurements for these two parameters was frequently compromised when heavy rainfall attenuated the signal of the doppler wind equipment. These problems necessitated the

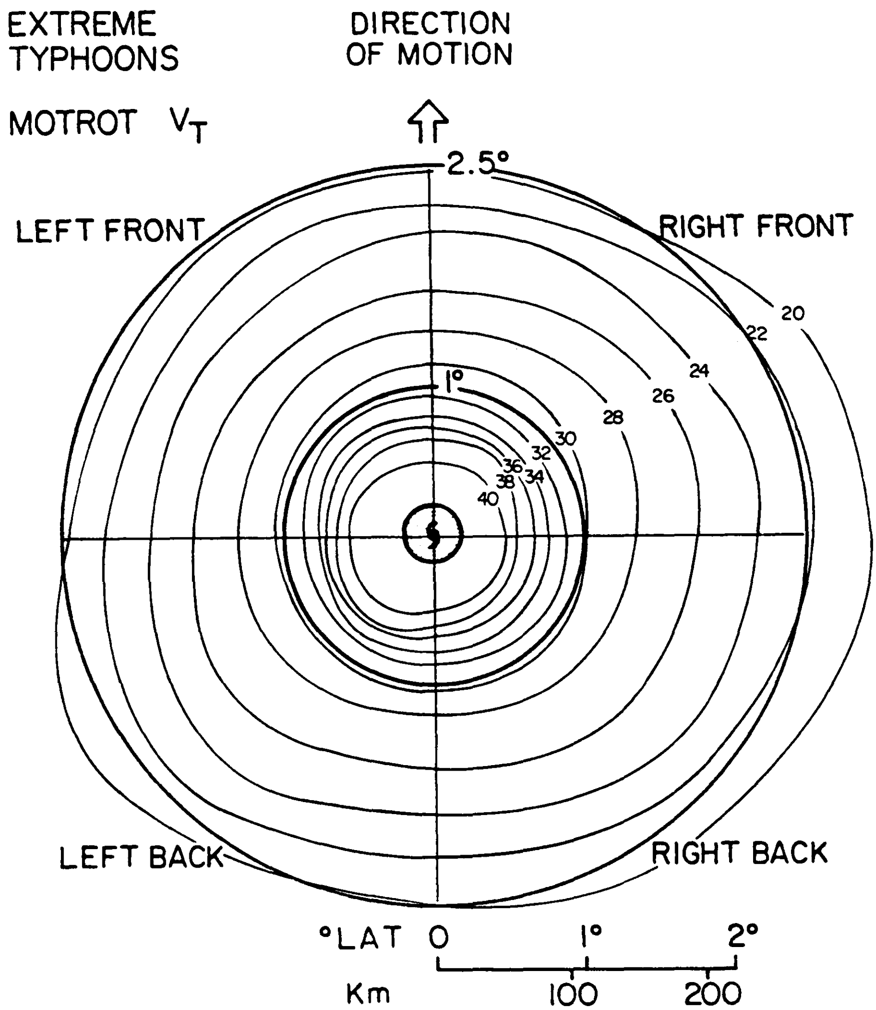

Figure 2.8: Plan view composite showing the distribution of the tangential wind speeds (isotachs) for extreme typhoons (MSLP $\leq$ 920 mb). (Units in ms^{-1}).

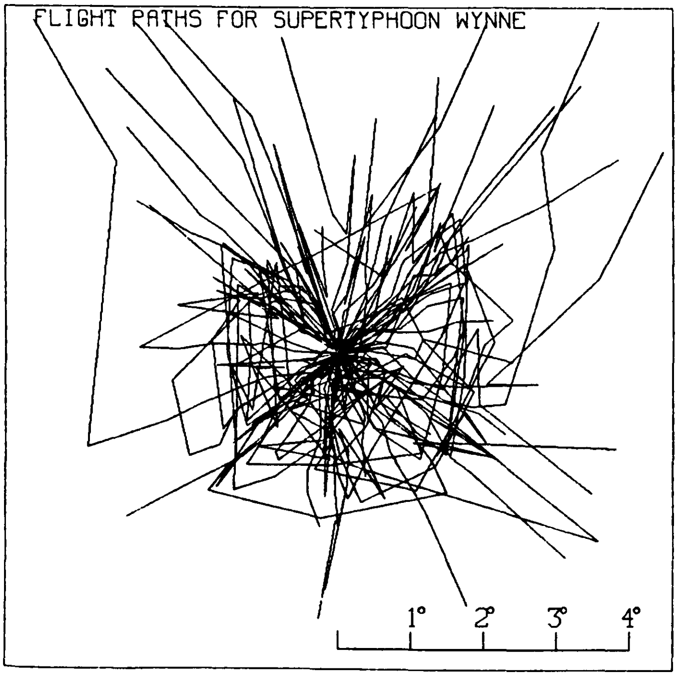

Figure 2.9: Flight paths for all missions flown into typhoon Wynne (1980).

application of a systematic procedure for specifying the maximum wind and RMW for all missions using the borader scale measurements of the wind and pressure profiles. Though important to the study, details of the testing and refinement of these procedures entail an extended digression which is presented in Appendix C. This Appendix also contains a brief description of efforts to use the data sets to devise a normalized wind profile. If successful, this procedure would have permitted the specification of the main features of the cyclone wind profile as a function of the maximum wind and RMW.

Chapter 3

THE MEAN BASIC STATE WIND STRUCTURE OF TROPICAL CYCLONES

Before considering time varying processes associated with the typical life cycle of a tropical cyclone, the mean basic state of the cyclone's structural features must first be defined. Allowing that the mean typhoon encompasses a broad range of intensities, (ie. wind speeds from 33 ms^{-1} to 80 ms^{-1}), we define three typhoon sub-classes, along with the mean tropical depression and the mean tropical storm to depict the full range of intensities which tropical cyclones attain.

Several acronyms which are used repeatedly throughout the following chapters are defined as follows:

MSLP : Minimum Sea- Level Pressure. A measure of cyclone intensity obtained either directly by dropsonde equipment, or by extrapolation from 700 mb flight level. MSLP is the best available intensity measure in lieu of direct measurements of the maximum wind speed.

OCS : Outer Core Wind Strength. An area-weighted average of tangential wind speeds from 1 to 2.5 degrees radius. OCS provides a conservative measure of the outer core for comparison with inner core MSLP. As was shown by Weatherford and Gray (1988b), the OCS correlates highly (.91) with the radius of gale-force winds.

RMW : Radius of Maximum Wind speed.

3.1 The Mean Typhoon

Characteristics of a conceptual "mean typhoon" were obtained as the averages of composited data for 358 typhoon reconnaissance missions. The mean typhoon in the western Pacific basin is positioned at approximately 20°N latitude and 135°E longitude, moves at an average speed of 5 ms^{-1} towards the NNW (330 degrees) with an average MSLP of 945 mb and an OCS of 22 ms^{-1}. Figure 3.1 shows the azimuthally-averaged tangential and radial wind fields of the mean typhoon. Note that radial inflow occurs at 700 mb within approximately 150 km of the storm center and that data inside 28 km are <u>not</u> averaged, resulting in a data void region near the center. Inflow at 700 mb is concentrated in the cyclone's inner core region where convection is densely packed. The average estimated maximum wind speed at the RMW was obtained using procedures outlined by Holland (1983) (see Appendix C).

The natural coordinate (NAT) plan view of the mean typhoon in Fig. 3.2 reveals asymmetric features in the mean radial winds. The environmental steering flow at 700 mb in this analysis is from South to North, implying that the average typhoon lies about even with the axis of the 700 mb subtropical ridge. Frank (1977) found a similar position relative to the ridge for the mean steady-state typhoon when viewed on a larger scale perspective delineated by composited rawinsonde reports. The 700 mb current in Fig. 3.2 is flowing at 4 ms^{-1} while the mean typhoon moves at a faster speed of 5 ms^{-1}. Notice also that the mean typhoon moves at a heading of 330° while the 700 mb current is directed towards 350°. Thus, at radii of up to 2.5°, the mean typhoon moves faster and to the left of its 700 mb environment in a fashion quite similar to that observed from rawinsonde compositing at radii of 3-7° by Frank and Gray (1980) and Chan and Gray (1982). This finding implies that the inner 2.5° radius belt also reflects the environmental steering current and will be discussed in greater detail in Chapter 4.

Background asymmetries of mean tangential winds are isolated and shown in Fig. 3.3, using the cyclone-relative coordinate system. In this moving (MOT) coordinate framework, the cyclone's motion and mean tangential vortex winds (VORT) have been sub-

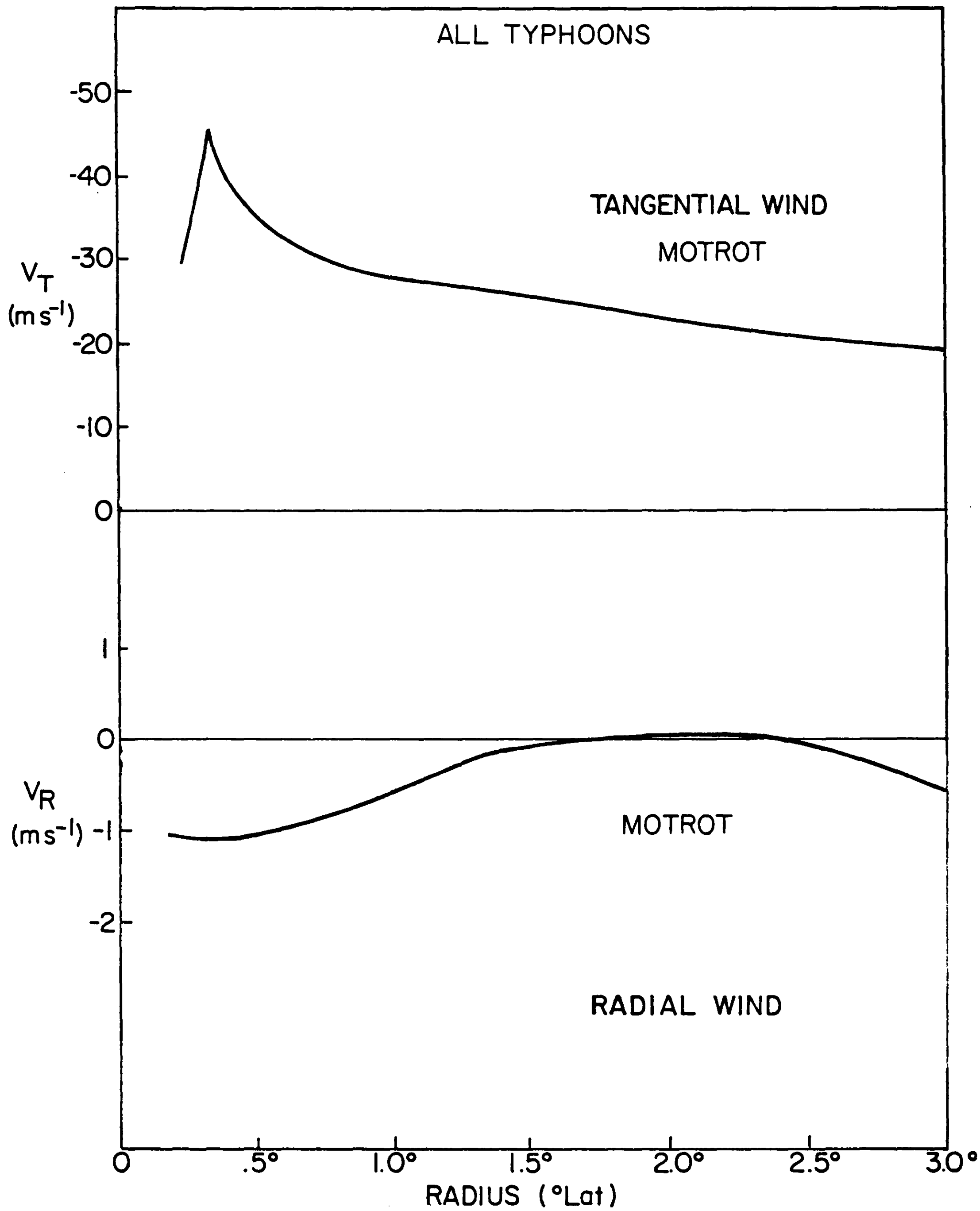

Figure 3.1: Radial profiles of azimuthally-averaged tangential (V_t) and radial (V_r) wind fields for the mean typhoon at 700 mb. All values are in ms^{-1} with positive radial wind denoting outflow.

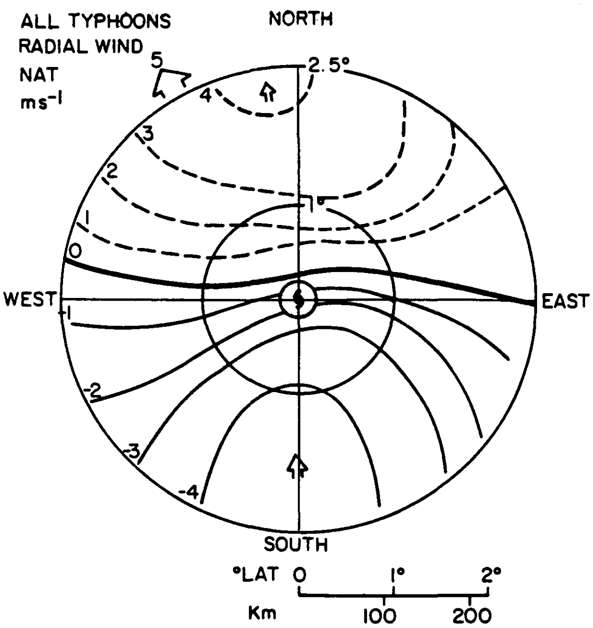

Figure 3.2: Plan-view analysis of the mean 700 mb radial wind speed in NAT coordinates. Mean cyclone motion and speed (ms^{-1}) are shown by arrow on the rim. Solid curves denote inflow and dashed curves outflow.

tracted from all winds and the individual cyclone headings have been rotated (ROT) to a common forward direction (hence, MOTROT—VORT). The mean asymmetries of the tangential winds shown in Fig. 3.3 reveal a slight maximum in the left-rear quadrant and a minimum in the right front quadrant.

Figure 3.3 and all subsequent plan views show the .25-2.5° radius region which is usually outside the zone of maximum winds. Because maximum winds in the .25-2.5° region are smoothed by the grid averaging process, these results do not consider asymmetries of the maximum wind.

3.2 Methodology of the MOTROT-VORT Depiction of Asymmetries

The MOTROT-VORT coordinate transformation represented in Fig. 3.3 has been devised for the purpose of more clearly showing the asymmetric features of composited cyclone data. All wind vectors are in the cyclone-relative (MOTROT) coordinate system with the mean vortex (VORT) removed. To remove the mean vortex, the symmetrically–averaged tangential wind speed profile is calculated for all radial bands. This profile,

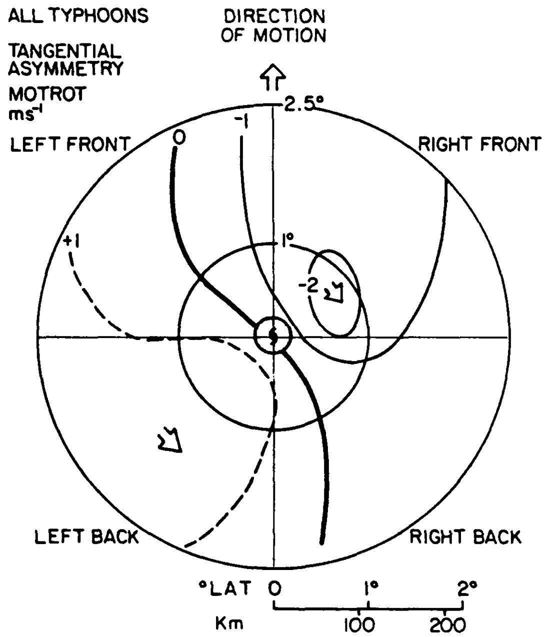

Figure 3.3: Plan-view analysis of the asymmetrical structure of the mean tangential wind field $\vec{V}_{T(asym)}$ at 700 mb in MOTROT-VORT coordinates. Solid curves denote tangential wind decrease, while dashed curves denote an increase.

$\vec{V}_{T(VORT)}$, is then subtracted from the tangential wind speeds of each grid box. When the mean vortex is removed, any asymmetric structure of the background wind field can be readily observed. The following definitions further clarify the procedure.

Tangential Asymmetric Windfield:

$$\vec{V}_{T(asym)} = \vec{V}_{T\,MOTROT-VORT} = \vec{V}_{T_{MOTROT}} - \vec{V}_{T\,VORT}$$

Radial Wind:

$$= \vec{V}_{R_{MOTROT}}$$

Total Residual Wind:

$$\vec{V}_{Res} = \vec{V}_T\ (asym.) + \vec{V}_{R_{MOTROT}}$$

$$\vec{V}_{Res} = \vec{V}_{T_{MOTROT\,-\,VORT}} + \vec{V}_{R_{MOTROT}}$$

The radial wind field of the mean typhoon in the MOTROT system is shown in Fig. 3.4. A general radial flowthrough can be observed moving from left-front to right-rear. When the MOTROT radial winds of Fig. 3.4 are vectorially combined with the asymmetric tangential wind field in Fig. 3.3 the total residual wind field is obtained as shown in Fig. 3.5. This residual 700 mb current is observed to flow through both the inner and outer core regions of the typhoon. Hence, this analysis shows that the average typhoon moves both to the left of and faster than the 700 mb environmental wind in which it is embedded. Because the cyclone's speed of motion exceeds that of the 700 mb flow, a region of maximum residual wind occurs on the left side and a minimum wind field occurs on the right side.

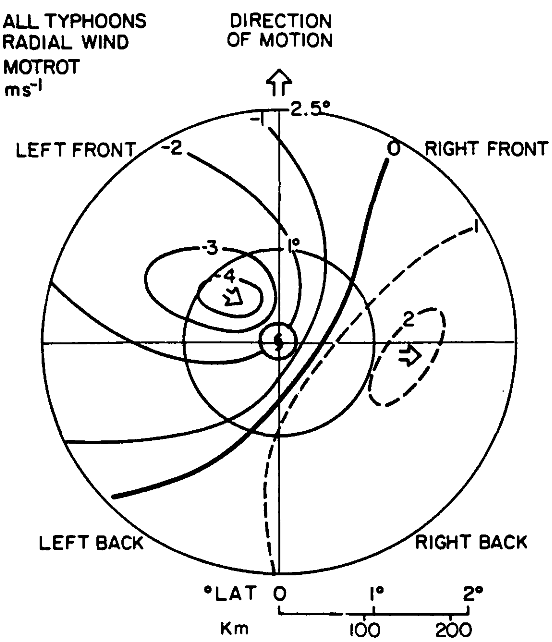

Figure 3.4: Plan-view analysis for the 700 mb radial wind field in MOTROT coordinates $\vec{V}_{R_{MOTROT}}$ for the mean typhoon. Solid curves denote inflow and dashed curves outflow.

3.3 Intensity Classes

An advantage afforded by the large number of missions flown during the 5-year study period is that data are sufficient to allow the mean typhoon to be stratified for intensity sub-classes to isolate differences associated with varying levels of cyclone intensity. Missions flown into typhoons, tropical storms, and tropical depressions are all included in the data sample. The number of missions for each intensity class generally reflects the natural frequency of each class with the exception of tropical depressions which were usually flown

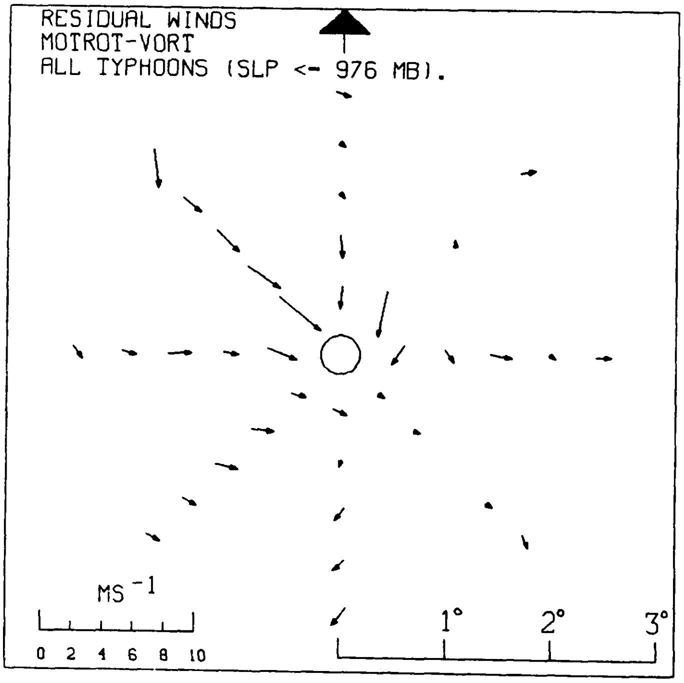

Figure 3.5: Plan view analysis for the 700 mb residual wind field $\vec{V}_{Res}$ of the mean typhoon which incorporates both the radial and asymmetrical tangential wind vectors in MOTROT-VORT coordinates. The bold arrow at the top marks the cyclone's motion heading. Vector lengths are proportional to speed as shown in the lower left corner.

at levels below 700 mb. The data set does not include low-level missions into early-stage depressions and missions into developing depressions are included only if the depression eventually became a tropical storm. The MSLP and number of missions for the three typhoon intensity classes plus tropical storms and depressions are as follows:

EXTREME TYPHOON MSLP $\leq$ 920 mb, 59 MISSIONS

INTERMEDIATE TYPHOON MSLP 920-950 mb, 113 MISSIONS

MINIMAL TYPHOON MSLP 950-976 mb, 205 MISSIONS

TROPICAL STORM MSLP 976-996 mb, 329 MISSIONS

TROPICAL DEPRESSION MSLP $\geq$ 996 mb, 91 MISSIONS

Table 3.1 gives the average statistical properties for each cyclone intensity class. All three typhoon classes were situated at similar average positions and heading in the same approximate direction with the same speed, indicating that all typhoon subclasses were embedded in the same average steering current. Tropical storms and depressions were situated at lower average latitudes and headed in a more westerly direction than were the average typhoon classes. Note that the tropical depressions included in this data set were well developed with MSLP near 998 mb and average maximum wind speeds of 13 ms^{-1}.

Table 3.1: Average statistics for cyclones of different intensity class by latitude (°N), longitude (°E), speed of motion (ms^{-1}), cyclone heading (degrees), MSLP (mb), Outer Core Wind Strength (OCS 1-2 1/2° radius ms^{-1}), and maximum wind speed (Holland estimate ms^{-1}).

INTENSITY CLASS	LAT	LONG	SPEED	HEADING	MSLP	OCS	MAX WIND
EXTREME TYPHOON	19°	133°	5	325	892	25	56
INTERMEDIATE TYPHOON	20°	135°	5	330	938	23	48
MINIMAL TYPHOON	21°	137°	6	327	964	21	37
TROPICAL STORM	17°	137°	5	310	988	14	23
TROPICAL DEPRESSION	15°	139°	6	290	998	9	13

Classifying tropical cyclones by intensity allows for more detailed analyses of the symmetrical wind fields than were provided by the mean typhoon alone. The mean tangential wind profiles in Fig. 3.6 show a relatively flat wind field for the average tropical depression. These profiles increased with storm intensity, albeit much more rapidly near the center than in the outer core. Notice that the RMW contracts with increasing intensity, thereby concentrating momentum in the inner core. Notice also that in contrast to the inner core winds, the tangential wind at 3° radius is nearly the same for the extreme, intermediate, and minimal typhoons.

Tropical storms show the least 700 mb inflow of all intensity classes in Fig. 3.6 and the intermediate typhoon exhibit the most. Such inflow appears to build as the cyclone intensifies. Tropical depressions were observed to have outflow at 700 mb, apparently reflecting the undeveloped nature of this early stage. Aside from the tropical depression, the 700 mb inflow appears to be concentrated in the inner core. Mean radial profiles of relative vorticity shown in Fig. 3.7 also indicate a concentration of tangential winds in the inner core. Note the more rapid increase of vorticity for the inner core as opposed to the outer core. This concentration of wind intensity is also reflected in the change in the 700 mb divergence field shown in Fig. 3.8.

The radial distribution of dewpoint temperatures in Fig. 3.9 show significantly rising 700 mb moisture with increasing intensity class. This association reflects the higher equivalent potential temperature (θ_e) and greater convection of more intense cyclones. Although the pressure falls throughout the inner 3° of the cyclone, it generally contributes only 10% to the moisture increase. Also, relative humidity (not shown) increases with increasing intensity, implying a greater surface flux of moisture to the 700 mb level following vigorous convection.

To more thoroughly investigate the concentration of winds in the inner core, a comparison of the wind and pressure accelerations was made for each 0.5° radial band using the symmetrical radial equation of motion in cylindrical coordinates or:

$$\frac{dV_R}{dt} = (\frac{\overline{V_T^{\,2}}}{R} + f\bar{V}_T) - g\frac{\partial Z}{\partial r})_p + F_R \tag{3.1}$$

where

$$\frac{dV_R}{dt} = \frac{\partial V_R}{\partial t} + V_R\frac{\partial V_R}{\partial r} + \omega\frac{\partial V_R}{\partial p},$$

and

$$F_R = radial\ friction$$

Assuming a steady state frictionless flow and neglecting radial and vertical advection, this equation can be expressed in the more familiar gradient wind form as:

$$(\frac{\overline{V_T^2}}{R} + f\bar{V}_T) = g(\frac{\partial Z}{\partial R})_p \tag{3.2}$$

The implications of friction and radial advection might be tested through an evaluation of the right vs. the left hand sides of this Eq. 3.2. Figure 3.10 shows the ratio of the wind term $(\overline{V_T^2}/R + f\bar{V}_T)$ to pressure gradient term $g(\frac{\partial Z}{\partial P})_p$. Note that in these

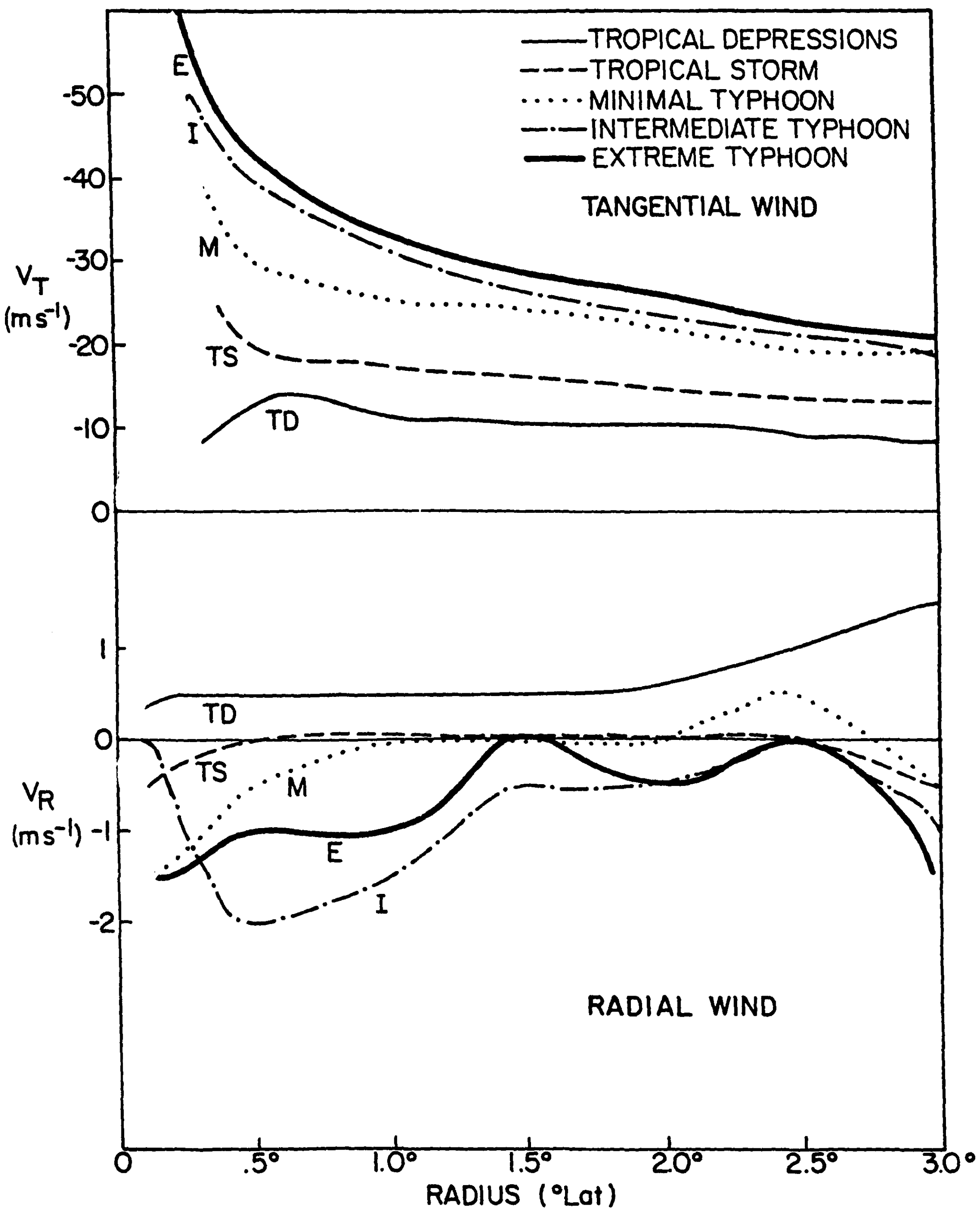

Figure 3.6: Radial profiles of azimuthally-averaged 700 mb tangential (V_t) and radial (V_r) wind fields for the five classes of tropical cyclone as defined in the text.

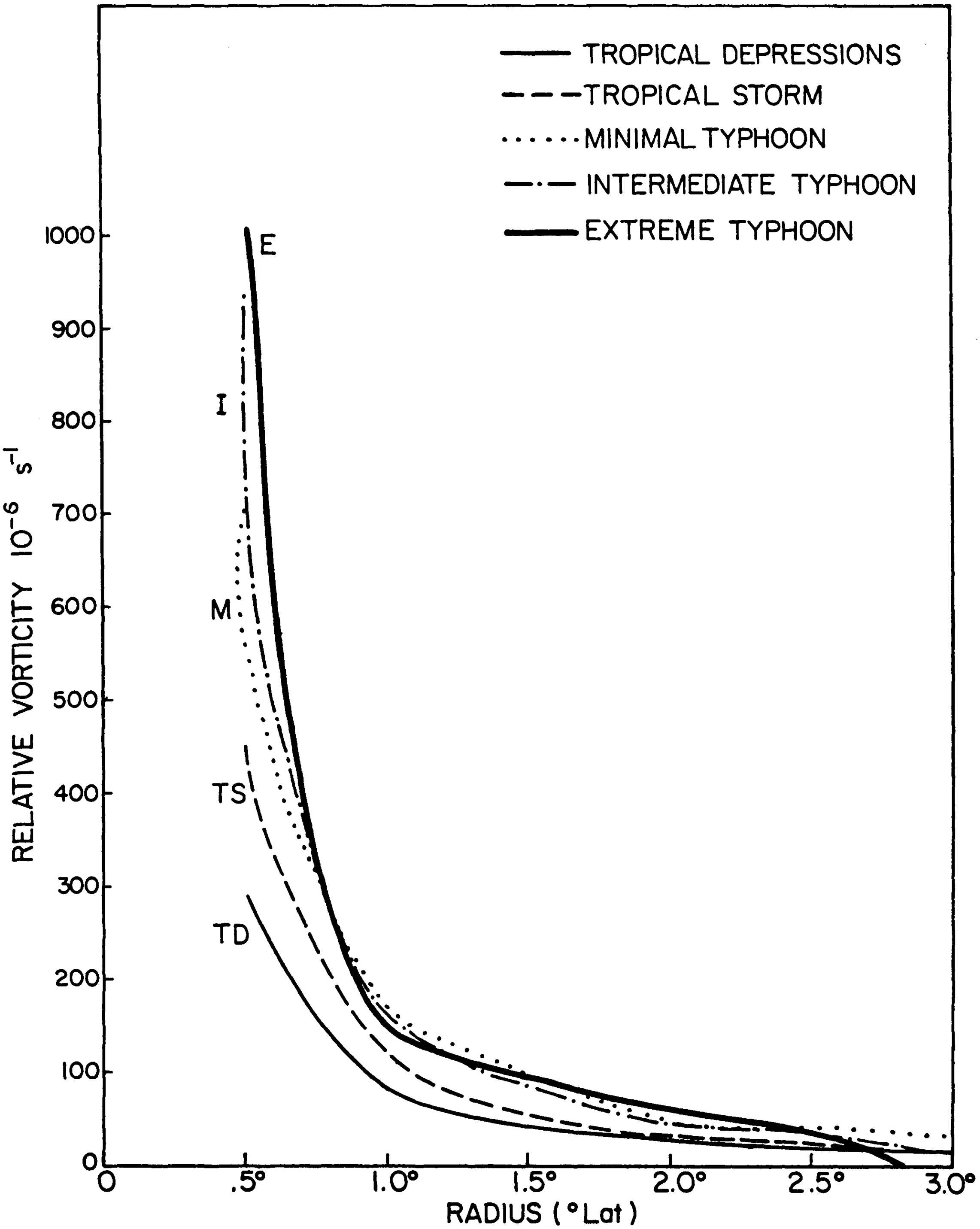

Figure 3.7: Radial profiles of azimuthally-averaged relative vorticity fields for each of the five classes of tropical cyclone at 700 mb.

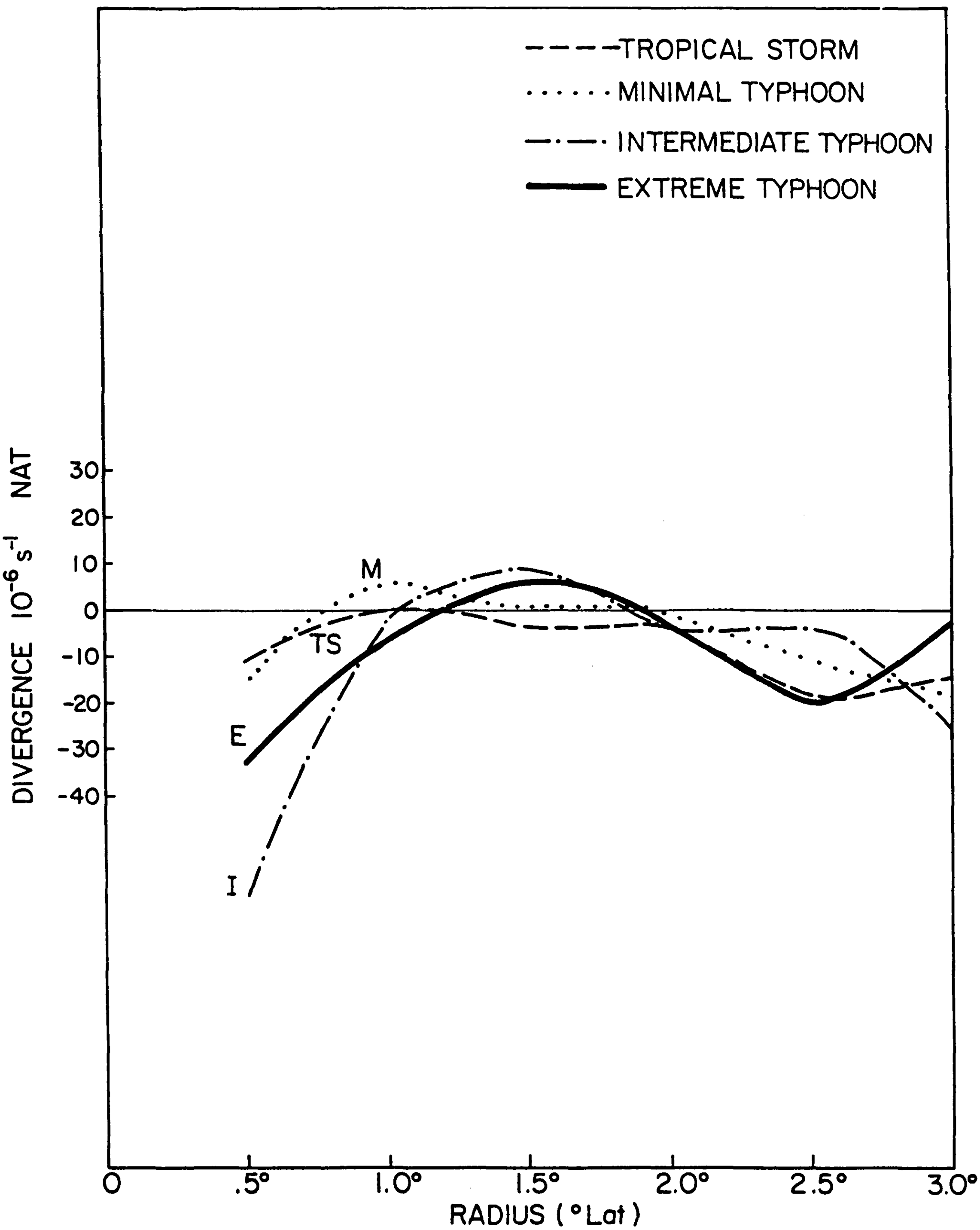

Figure 3.8: Radial profiles of azimuthally-averaged divergence fields for four different tropical cyclone intensity classes at 700 mb.

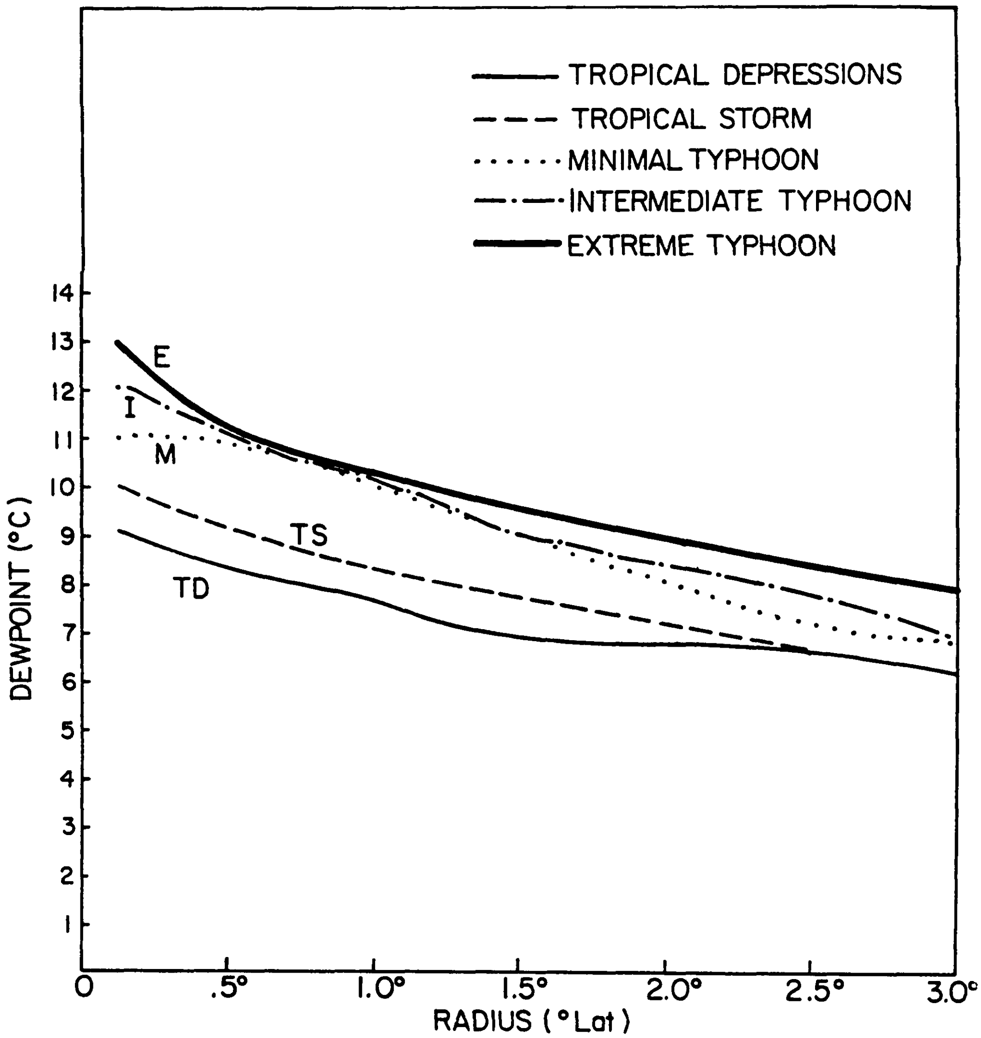

Figure 3.9: Radial profiles of azimuthally-averaged dewpoint temperature fields at the 700 mb level for each of the five classes of tropical cyclone.

analyses, all individual values of tangential wind speed are squared before averaging. In general, pressure accelerations in Fig. 3.10 are noticably greater than the wind accelerations, especially for the more intense typhoons. Part of this imbalance may be due to a small systematic correction for water motion. The Doppler wind measuring equipment used here measures wind relative to the sea surface. It has been previously estimated (as discussed by Gray and Shea, 1973) that Doppler wind may read 3-5 percent too low. A correction of 5 percent for water motion would reduce these imbalances by about 10 percent. Radial ($V_R \frac{\partial V_R}{\partial r}$) and vertical ($\omega \frac{\partial V_R}{\partial p}$) advection by the mean flow may also account for a small part of this imbalance. An analyses of this possible Doppler wind correction and of the advective terms in Eq. 3.1 in combination is not large enough, however, to fully account for these observed gradient wind imbalances. It is likely that cumulus-scale mixing processes are also involved and that cumulus convective momentum transports also make a significant contribution to this imbalance. Gray (1967) has previously hypothesized that in the lower levels of hurricanes (below 500-600 mb), radially directed friction acts outward to offset a stronger inward directed pressure acceleration. This 700 mb level radial friction is likely a consequence of convectively induced vertical transport of negative radial momentum ($\overline{V_R' \omega'}$) which increases with height. Ascending negative radial eddy momentum (V_R') from the typhoon's boundary layer is advected upward more rapidly at middle levels than at low levels. This difference causes a stronger vertical eddy flux ($V_R' \omega'$) and a stronger cumulus induced stress ($\tau_{RP} = \frac{\overline{V_R' \omega'}}{g}$) at middle levels than that which occurs at the top of the inflow layer. The resulting vertical stress gradient causes a divergence of negative radial momentum by the unresolved cumulus exchange processes.

These gradient wind imbalance observations appear to lend support to Gray's hypothesis of cumulus induced radial friction. It is noted that Gray and Shea (1973) also observed sub-gradient winds in Atlantic hurricanes at radii beyond the radius of maximum wind of (0.4-1.0° radius) for sea surface Doppler wind increases of up to 5 percent.

It is to be expected that if inward directed boundary level air is advected in cumulus clouds to middle levels, that a significant radial stress might result. Figure 3.6 shows

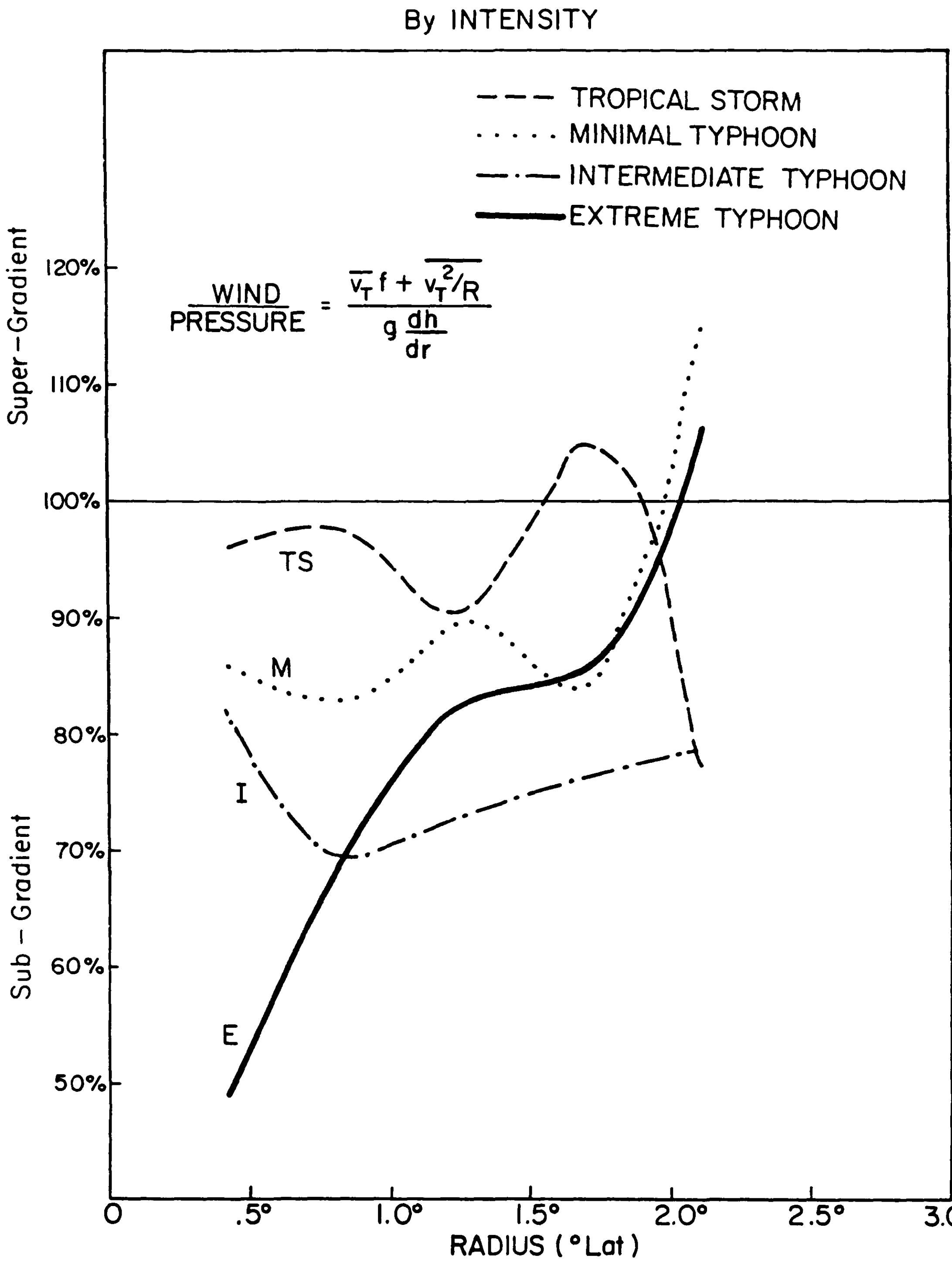

Figure 3.10: Radial profiles of azimuthally-averaged ratio of 700 mb wind to pressure gradient fields (Coriolis + centrifugal forces/pressure gradient) for four different tropical cyclone intensity classes.

that typhoon intensity cyclones had inward directed radial winds at 700 mb. It is to be expected that this type of cumulus radial frictional component becomes larger with increasing typhoon strength.

3.4 700 mb Flow in Relation to Cyclone Intensity

We next investigate differences in the asymmetric winds of cyclones for different intensity classes. Analyses of mean radial winds in NAT coordinates for each intensity class are shown in Figs. 3.11a-e. These results suggest that the speed of tropical cyclones relative to the 700 mb environment decreases as the intensity of the cyclones becomes greater. Recalling from Table 3.1 that the mean absolute speed of these cyclone classes changes little with intensity, it can be seen in Fig. 3.11e that the most intense cyclones move at about the same velocity (ie. 5 ms^{-1}) as the 0-2.5° maximum radial currents. Presumably, this association has to do with the character of the steering current above the 700 mb level of more intense cyclones. Although the average vertical wind structure is unknown, the lesser motion relative to the environment for intense cyclones implies an environment with less vertical shear.

Another rendering of these same data, but in the MOTROT system, is shown in Fig. 3.12a-e. The resultant environmental flowthrough for the more intense cyclones in these analyses is from left to right only. Hence, the more intense the cyclone, the more closely the 700 mb level MOTROT data approximated the parallel component of the en.ironment (Fig. 3.13) and the less well they approximated the perpendicular component, as shown in Fig. 3.14. The extreme typhoon reflects only a lateral (leftward) 700 mb drift. Also notable in the MOTROT radial wind data in Fig. 3.12 is the appreciable inner core convergence for the mean typhoons, but not for the mean tropical storms or depressions. Flowthrough for the weaker systems did not appear to be absorbed as much in the inner core. Evidently, inward convergence in the inner core environment increases with cyclone intensity.

Total asymmetric wind fields in MOTROT-VORT coordinates are shown in Figs. 3.15a-e. Tropical depressions, tropical storms and minimal typhoons all show a positive

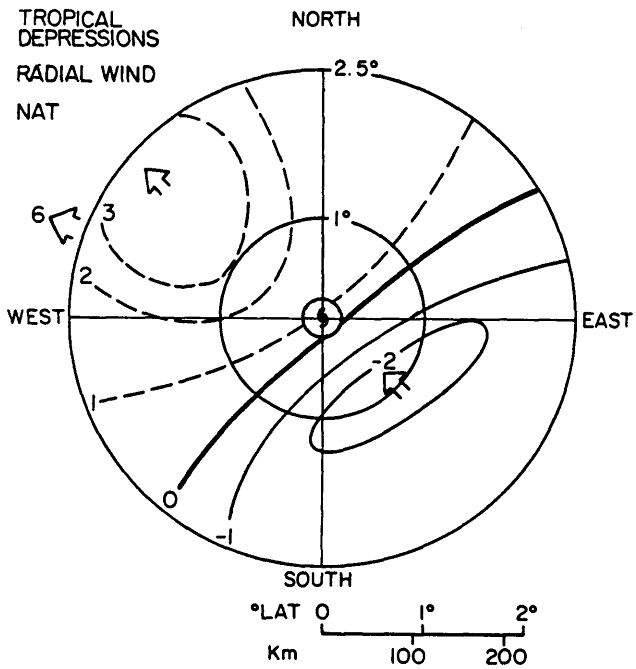

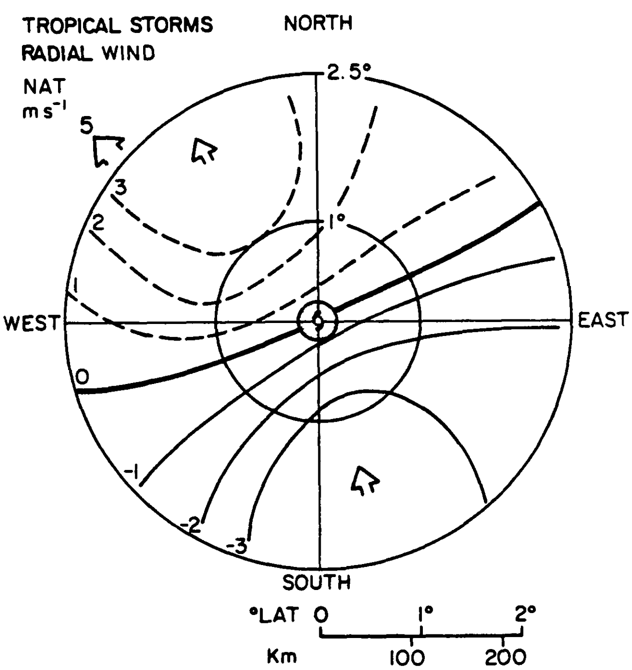

Figure 3.11: a-e. Plan-view analysis of the radial wind field in NAT coordinates for a) tropical depressions, b) tropical storms, c) minimal typhoons, d) intermediate typhoons, and e) extreme typhoons. Mean motion and speed (ms^{-1}) for each composite are shown by arrow on the rim.

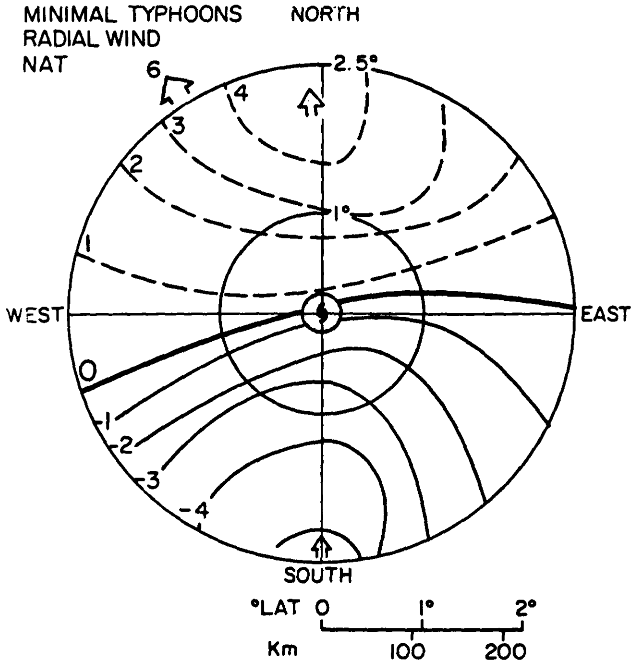

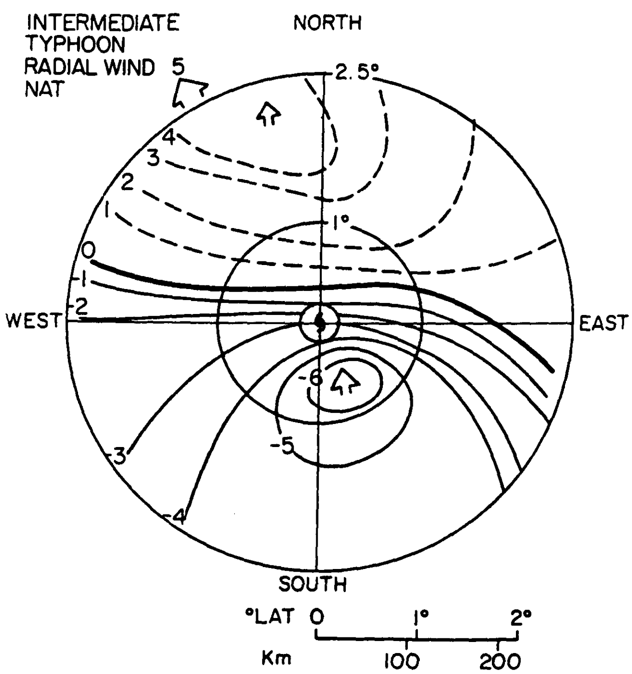

Figure 3.11: a-e. Continued.

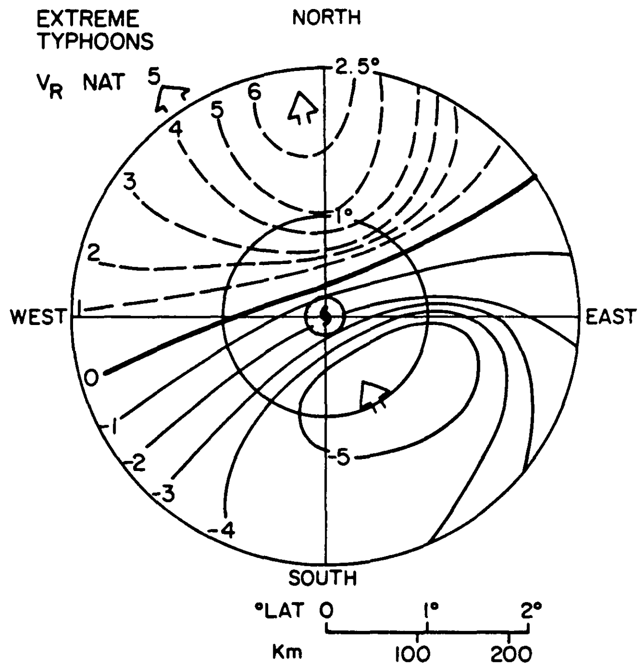

Figure 3.11: a-e. Continued.

tangential flowthrough component in the lower-left quadrant and a negative component in the front-right portion of the cyclone. Since the contribution of the steering current near the surface is likely to be less than at 700 mb, this tangential asymmetry is probably more pronounced near the surface. Thus, MOTROT-VORT winds at the surface are likely to have a larger natural maximum on the lower-left quadrant than shown here for the 700 mb level. Also, the more intense cyclones are noticeably less asymmetric as shown by the nearly symmetric intermediate and extreme typhoon classes (Figs. 3.15e,f). It appears that the more resistant a cyclone is to 0-2.5° parallel wind flowthrough, the more intense it becomes.

The residual wind fields of Fig. 3.16a-e indicate that flowthrough is oriented primarily from front to back in tropical depressions but from left to right in the more intense typhoons. Other important features in Fig. 3.16 include intensity related differences in the symmetry of the cyclone's inner regions which are presumably due to more vigorous convection in the more intense cyclones. Note in Fig. 3.16a how the 700 mb environment appears to flow through the depression, seemingly unaware that a cyclone exists. This

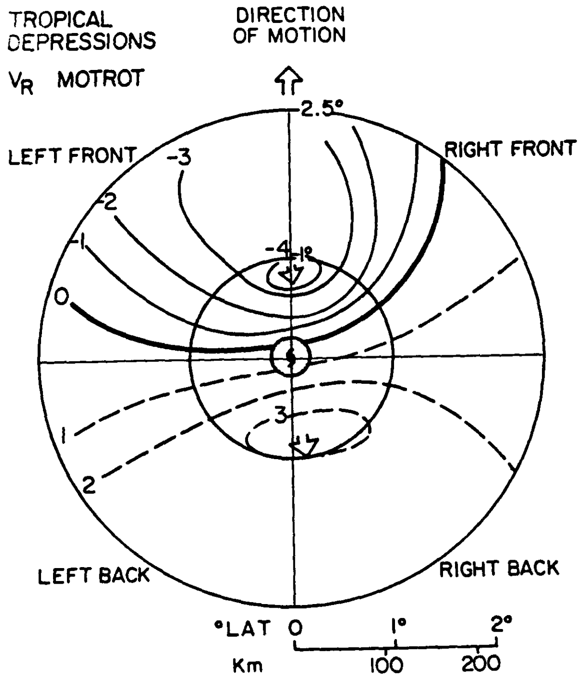

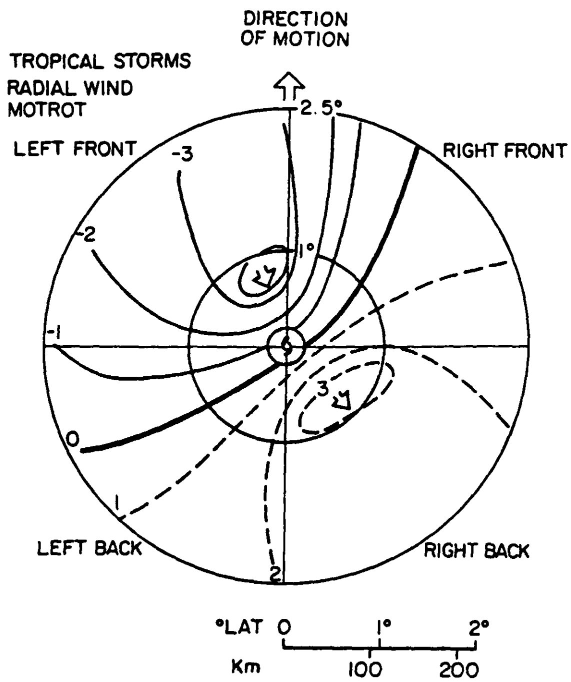

Figure 3.12: a-e. Plan-view analysis of the radial wind field (ms^{-1}) in MOTROT coordinates for a) tropical depressions, b) tropical storms, c) minimal typhoons, d) intermediate typhoons, and e) extreme typhoons.

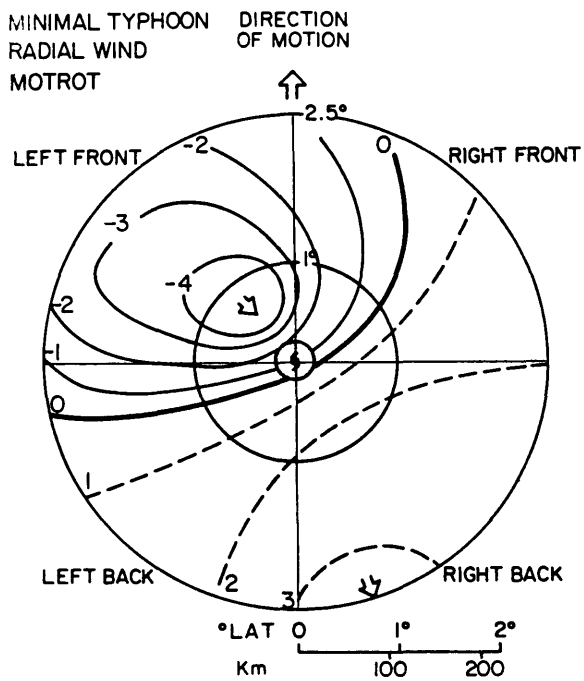

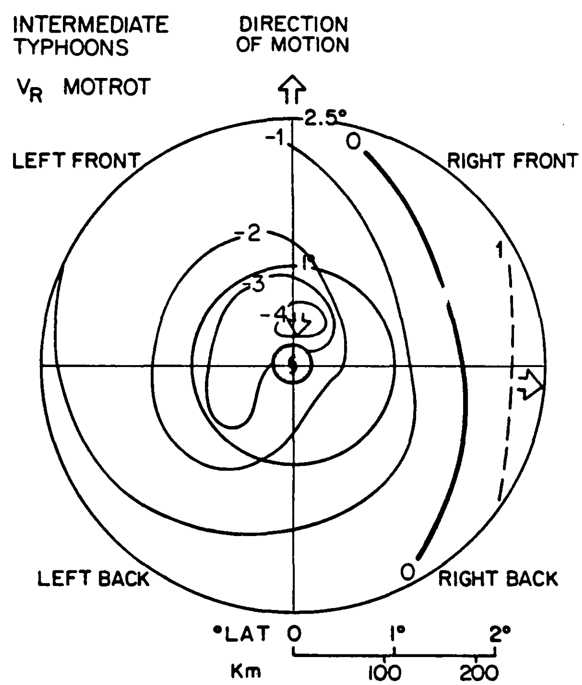

Figure 3.12: a-e. Continued.

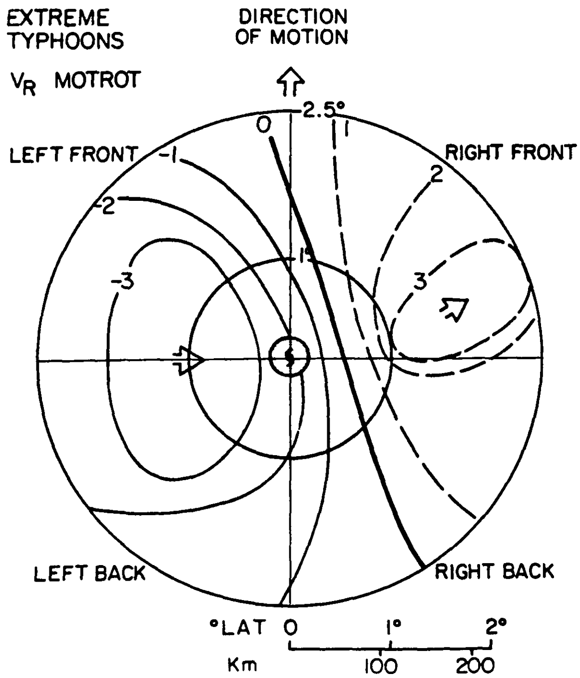

Figure 3.12: a-e. Continued.

flow contrasts with that of the intermediate typhoon wherein 700 mb air is drawn into the inner core from all quadrants. Once again it is obvious that 700 mb flowthrough decreases with increasing intensity. Only the most intense typhoons (intermediate and extreme) exhibit a 700 mb flow channel coming from the equatorial region.

3.5 Stratification by Outer Core Wind Strength (OCS)

As was discussed in a previous paper (Weatherford and Gray, 1988b) MSLP and OCS are not closely correlated. Also, a tropical forecaster frequently will not have information on the center of an approaching tropical cyclone but may obtain some data for conditions in the outer regions. Moreover, as a cyclone approaches land areas, it is the outer core winds which cause the initial damage to structures and disrupt normal societal activities. The greatest OCS value observed in the 5-year study period was 37 ms^{-1}, for Supertyphoon Forrest of 1983. Focusing on the outer core, cyclones were stratified by weak, medium, and strong outer core winds, regardless of the intensity of the inner core. The OCS classes are defined as follows:

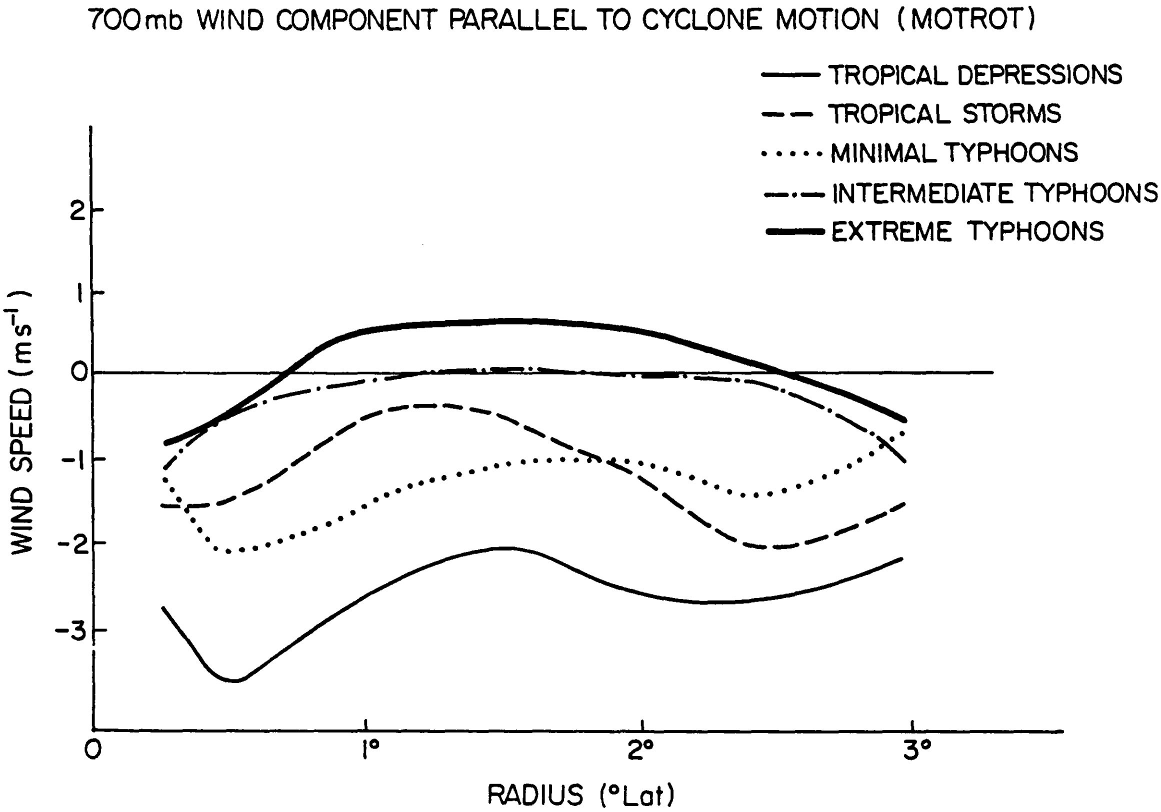

Figure 3.13: Radial profiles of azimuthally-averaged components of the 700 mb wind current parallel to the cyclone's direction of motion for: tropical depressions, tropical storms, minimal typhoons, intermediate typhoons, and extreme typhoons. Negative values (ms^{-1}) imply the cyclone is moving faster than the 700 mb stream.

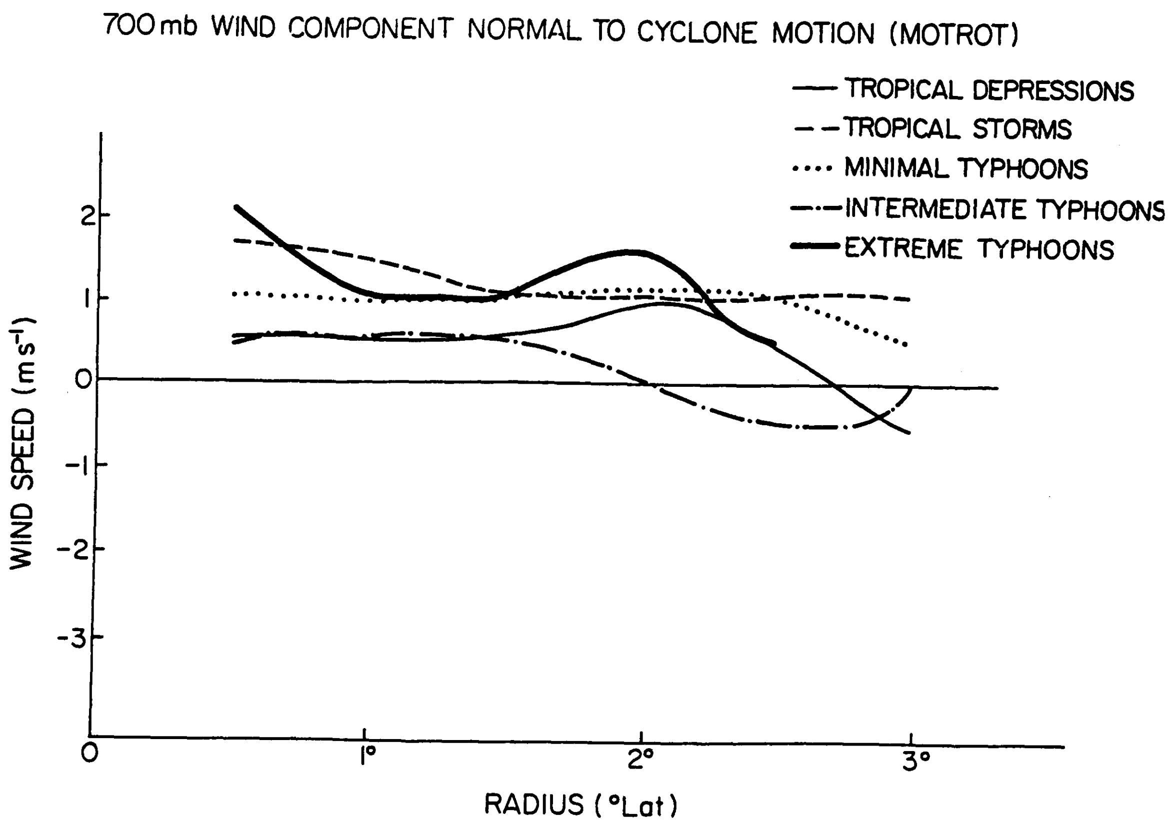

Figure 3.14: Radial profiles of azimuthally-averaged components of the 700 mb wind current which are normal to the cyclone's direction of motion for: tropical depressions, tropical storms, minimal typhoons, intermediate typhoons, and extreme typhoons. Positive values (ms^{-1}) imply the cyclone is moving to the left of the 700 mb stream.

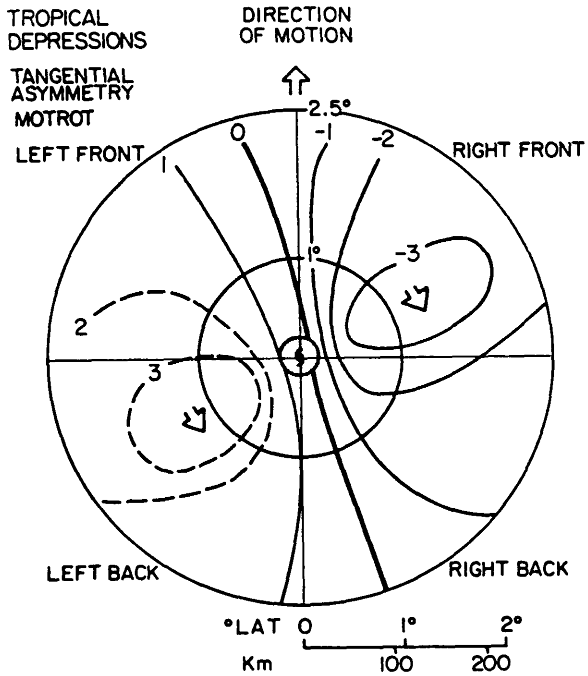

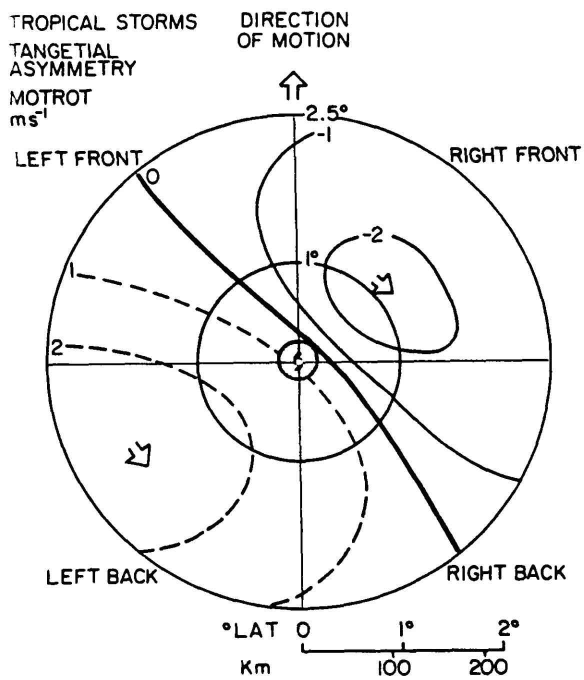

Figure 3.15: a-e. Plan-view analysis of the tangential asymmetries of the tangential wind field at 700 mb for a) tropical depressions, b) tropical storms, c) minimal typhoons, d) intermediate typhoons, and e) extreme typhoons in MOTROT-VORT coordinates. Solid curves denote values lower than the mean while dashed curves denote values greater than the mean. Values are in ms^{-1}.

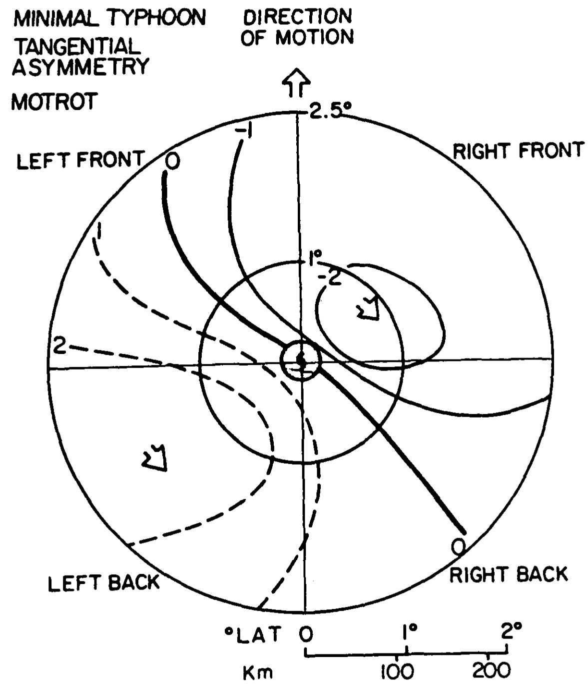

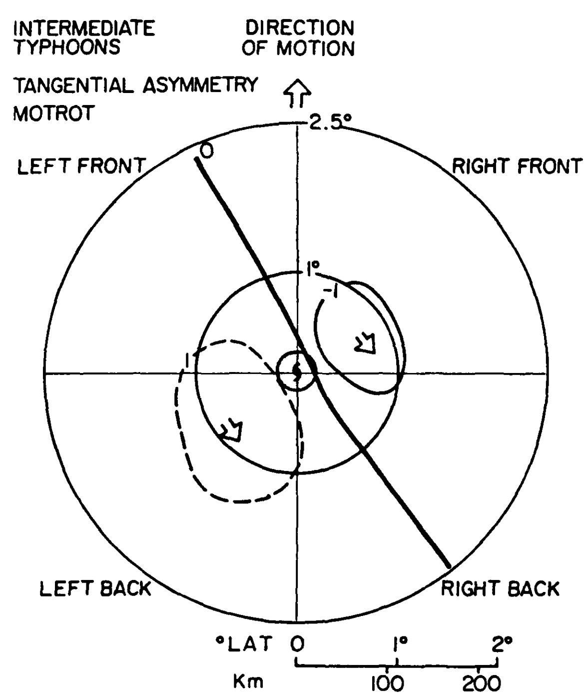

Figure 3.15: a-e. Continued.

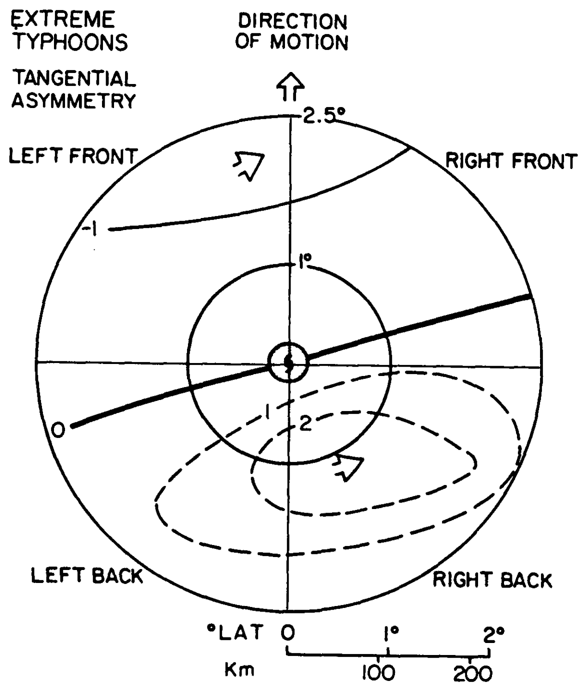

Figure 3.15: a-e. Continued.

WEAK OUTER CORE WIND: 0 TO 13 ms^{-1} 407 MISSIONS

MEDIUM OUTER CORE WIND: 13 TO 23 ms^{-1} 260 MISSIONS

STRONG OUTER CORE WIND: OVER 23 ms^{-1} 135 MISSIONS

Table 3.2 shows the average position, motion, MSLP, OCS, and maximum wind speed for the mean cyclone in each OCS class. All of the OCS stratified classes move at the same average speed of $5ms^{-1}$. Although the average strength of the outer core winds is approximately one-half that of the maximum wind speed, it was shown by Weatherford and Gray (1988b) that there is substantial variability of the ratio of inner to outer core wind speeds.

Damage potential is closely related to the total kinetic energy of the cyclone which, for a given storm, is proportional to the wind speed squared. Therefore, although the average OCS of the strong cyclones is only 2.7 times that of the weak cyclones, the average damage

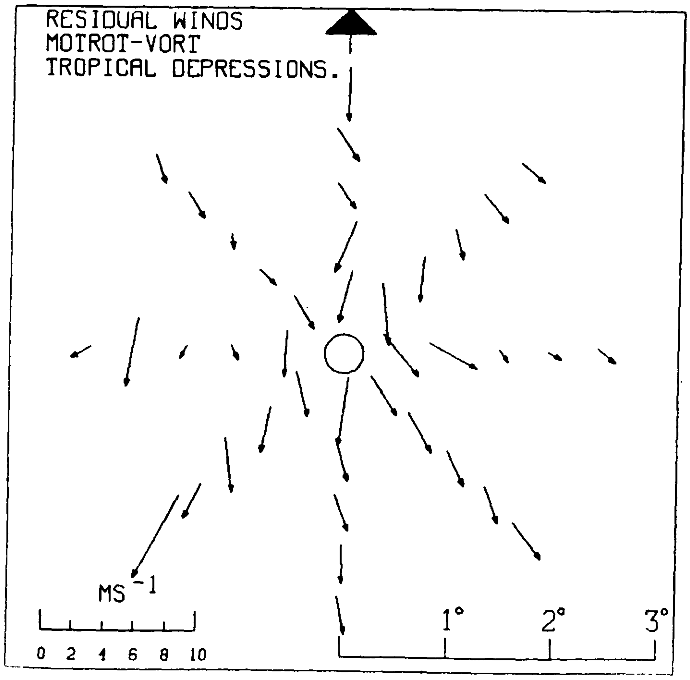

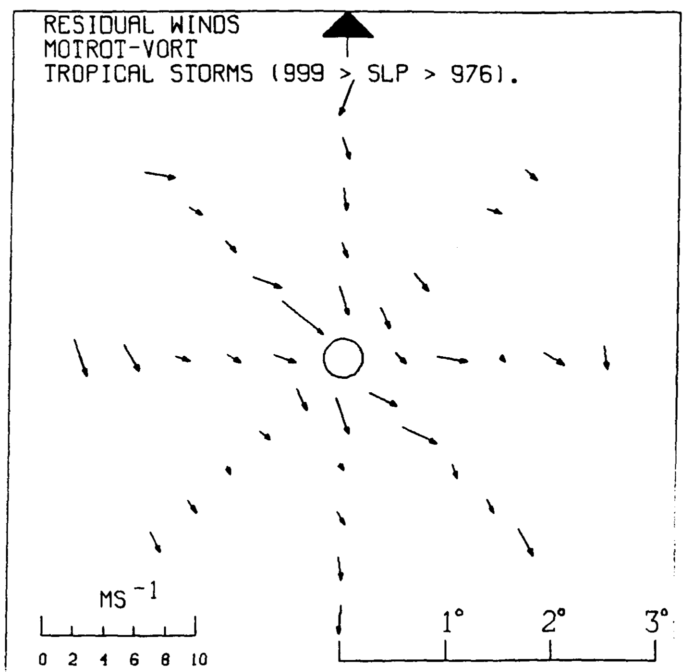

Figure 3.16: a-e. Plan-view analysis of the 700 mb residual wind field for a) Tropical Depressions, b) Tropical Storms, c) Minimal Typhoons, d) Intermediate Typhoons and e) Extreme Typhoons. These analyses incorporate both the radial and asymmetrical tangential wind vectors in MOTROT-VORT coordinates. The bold arrow marks the cyclone's motion heading. Vector lengths are proportional to wind speed as shown in the lower left.

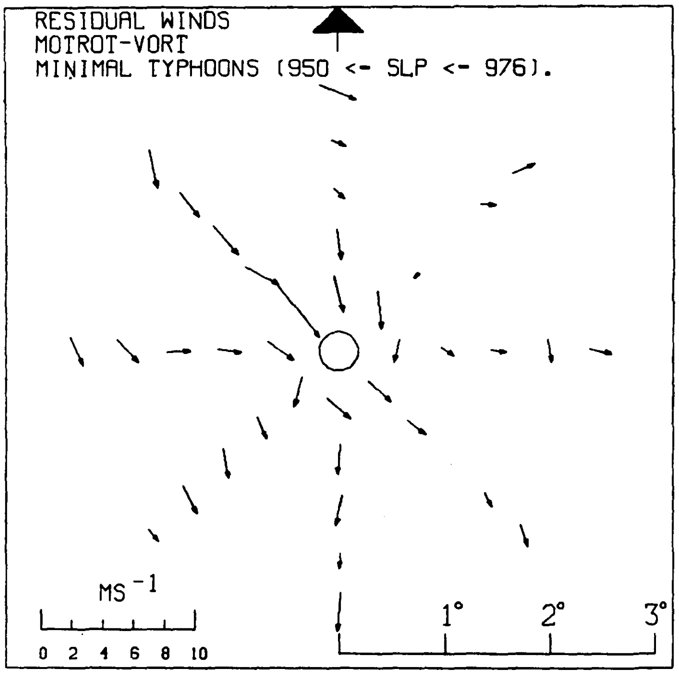

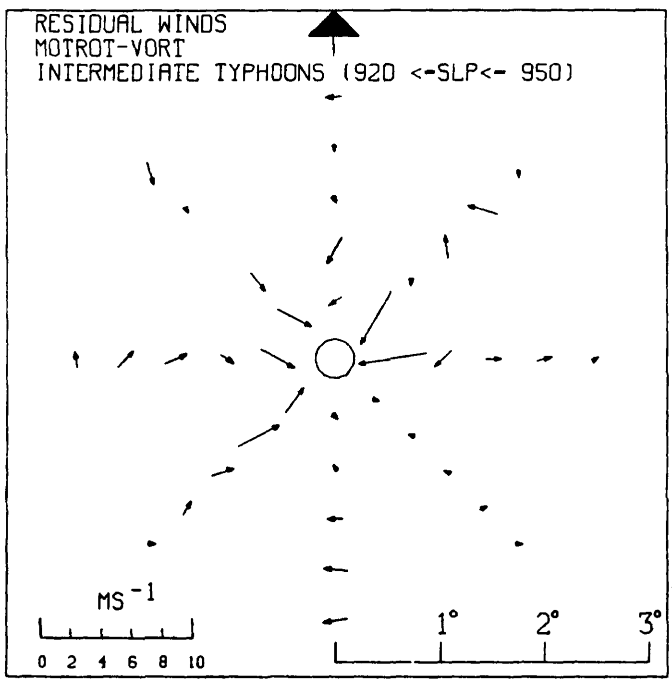

Figure 3.16: a-e. Continued.

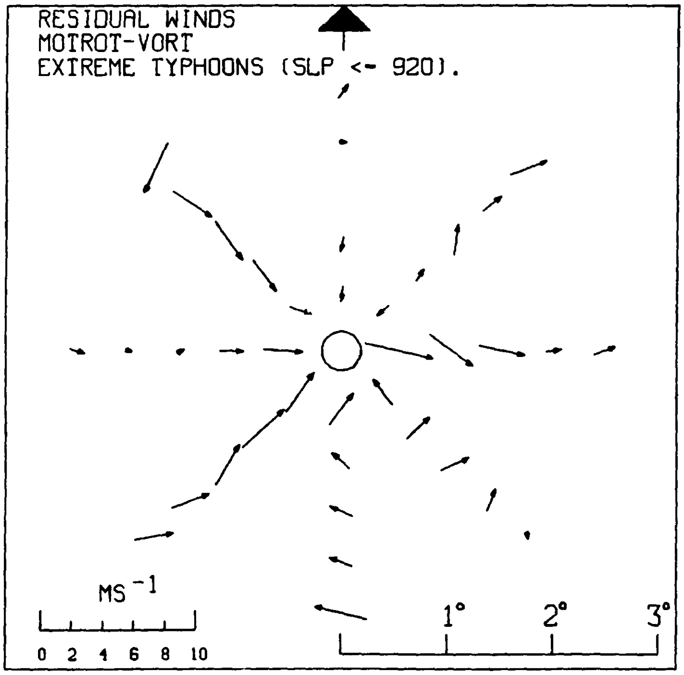

Figure 3.16: a-e. Continued.

Table 3.2: Average values of position, motion, intensity, and OCS for each OCS class.

OCS CLASS	LAT.	LONG.	HEADING	SPEED (ms^{-1})	MSLP (mb)	MAX WIND (ms^{-1})	OCS (ms^{-1})
WEAK	17°	137°	310°	5	980	20	10
MEDIUM	18°	136°	315°	5	964	35	18
STRONG	23°	134°	345°	5	941	45	27

potential is 7.3 times greater for the strong systems and up to 14 times greater for the strongest individual case observed in the data set.

Aside from the outer core strength values themselves, the biggest difference associated with the OCS stratification is for moisture. Figure 3.17 shows that the average dewpoint temperatures of strong OCS cases significantly exceed those of the other two cases. Figure 3.18 shows the radial distribution of the difference between mixing ratios of strong and weak OCS systems, revealing 10 to 30 percent greater values for the strong class. The moisture differences become larger as one moves closer to the cyclone center. There are two effects which probably combine to create the 700 mb moisture differences in Figs. 3.17 and 3.18. For the same underlying sea surface temperatures, lower 700 mb heights of the strong OCS systems can account for roughly 10 percent of the observed mixing ratio increase. More importantly, stronger boundary layer winds induce a more vigorous surface energy and moisture exchange which can be brought up through the 700 mb level within convective cells. The increase of moisture at 700 mb cannot be due to horizontal advection from outside the vortex because the external environment typically does not have these high moisture values. Increased moisture values out to 3° radius for cyclones with greater OCS are likely to be due to increased convection in the stronger outer core areas. This implies heavier rainfall and hence, potential flood problems for large OCS systems, regardless of the MSLP or maximum inner core winds.

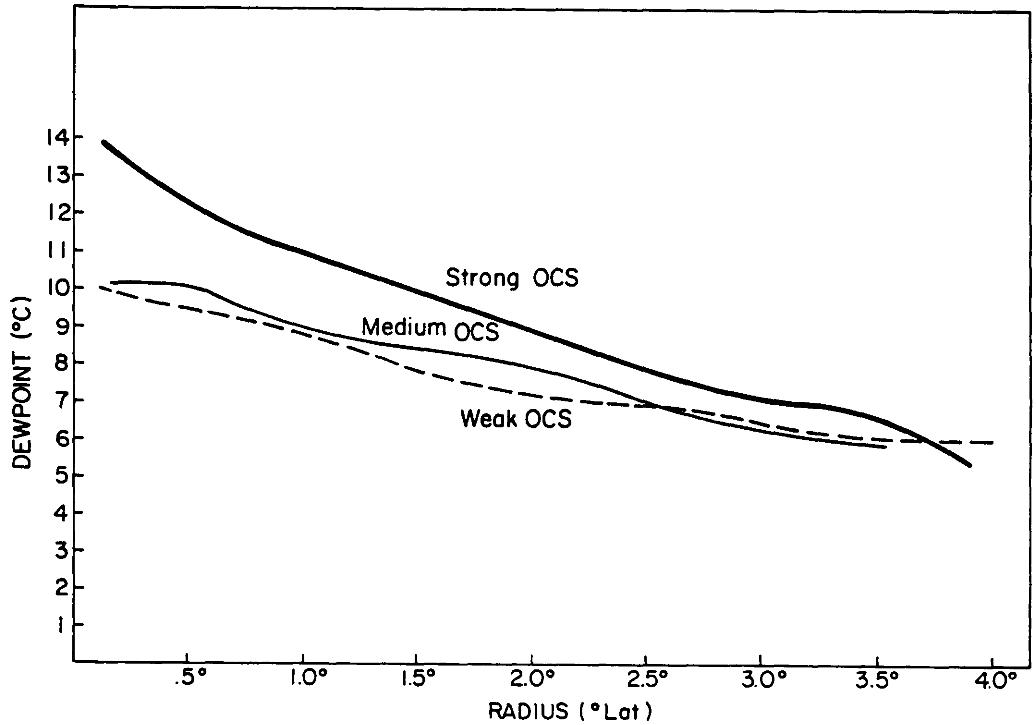

Figure 3.17: Radial profiles of azimuthally-averaged dewpoint temperatures for the three classes of OCS at the 700 mb level.

NAT coordinate analyses for the three OCS classes in Fig. 3.19 suggest that the 700 mb environment may flow slightly faster for the strong OCS class, but with little convergence in the inner core. An interesting phenomenon in Fig. 3.19 is that the greater

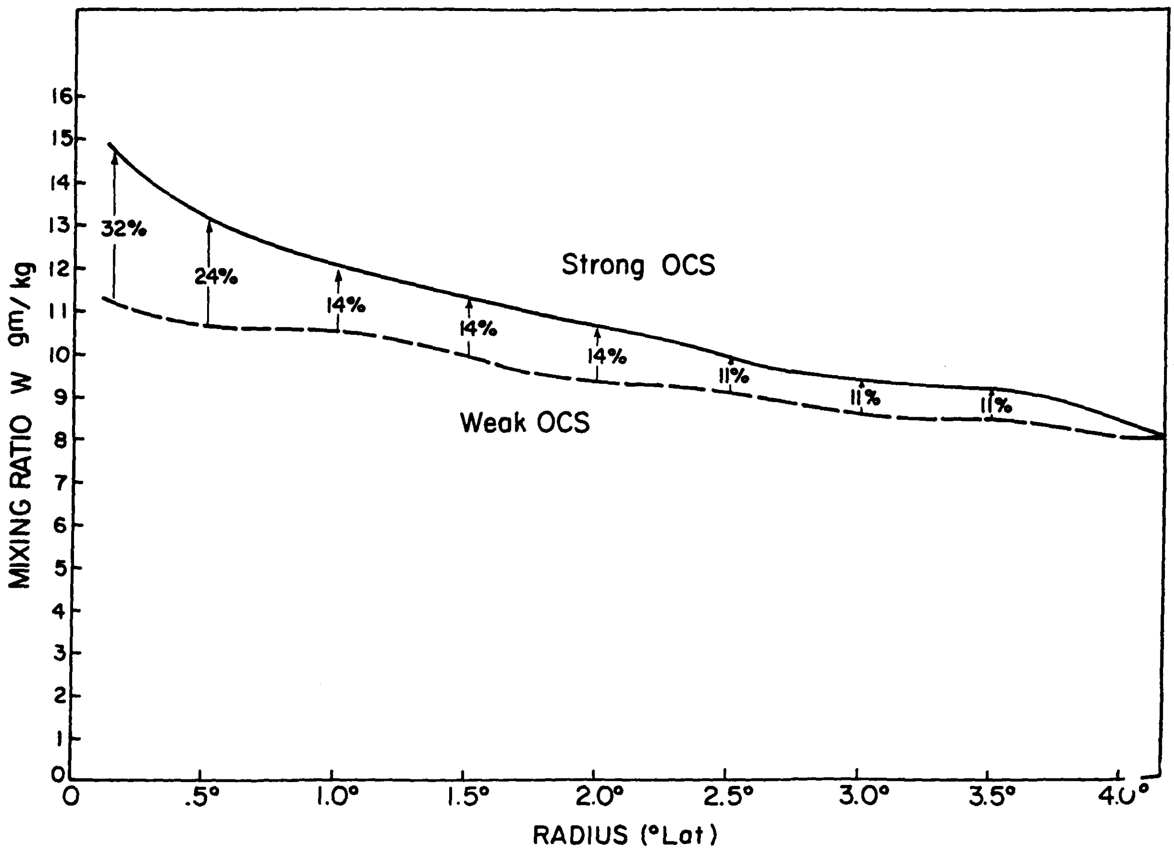

Figure 3.18: Radial profiles of azimuthally-averaged mixing ratios for the three classes of OCS at the 700 mb level.

the OCS, the greater the leftward drift of the vortex. Inspection of Figs. 3.19a-c shows that the environmental flow was directed toward 330° for weak systems, toward 340° for medium systems, and toward 23° for the strong systems. When the cyclones' average headings and motions were subtracted from these estimates, the resulting leftward drift angles were 20° for weak, 25° for medium, and 38° for strong OCS systems. These results support the belief that the Beta-effect causes a more pronounced drift for systems encompassing a larger area (De Maria, 1985). Apparently the stronger outer core winds advect more earth-vorticity by way of the vorticity term:

$$v\delta f/\delta y \tag{3.3}$$

The Radial wind fields in MOTROT coordinates (Figs. 3.20a-c) reveal inflow and convergence of environmental air for medium and strong OCS cyclones but not for the weak case. The inflow values are also relatively large in relation to outflow for the medium and strong OCS cases but are essentially equal for weak cyclones. These differences imply that, unlike weak systems, strong outer core systems advect environmental air inward at 700 mb, then upward through convection near the core to a higher level, following Willoughby, et al. (1984). Cyclones with weak OCS values generally had weaker intensity values as well and mostly included tropical storms which did not show significant inflow at 700 mb.

When the symmetric tangential wind or VORT was removed to obtain the MOTROT-VORT representation, (see Figs. 3.21a-c) flowthrough became less apparent for stronger OCS cyclones. More symmetric tangential wind fields and more detached or shielded inner-core circulations also appeared for the strong OCS systems. These differences are also evident in the residual flowthrough shown in Figs. 3.22a-c. In general, weaker OCS systems had stronger residual wind fields on the lower left side of the cyclone and weaker wind fields on the upper right. The medium OCS composite appears to accept more environmental air from the left-front than passes through to the opposite side. Finally, the strong OCS composite allows the least outer core air to enter the inner core. Hence, the strong OCS case provided the sturdiest shield against environmental effects.

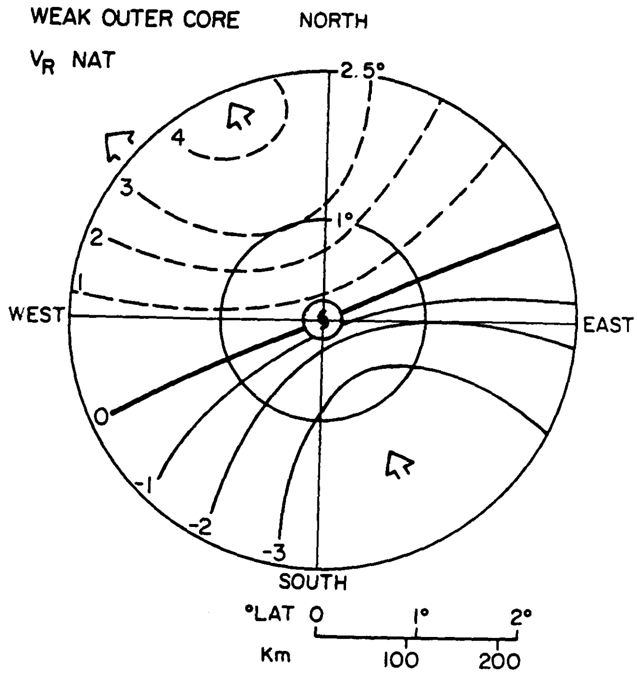

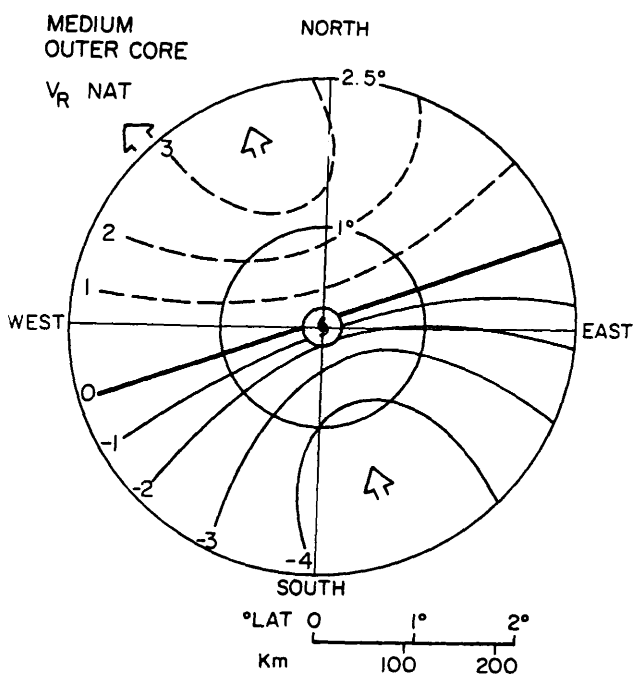

Figure 3.19: a-c. Plan-view analyses of the radial wind in NAT coordinates for a) weak OCS, b) medium OCS, and c) strong OCS. Mean motion and speed of the composites (ms^{-1}) are shown by arrow on the rim.

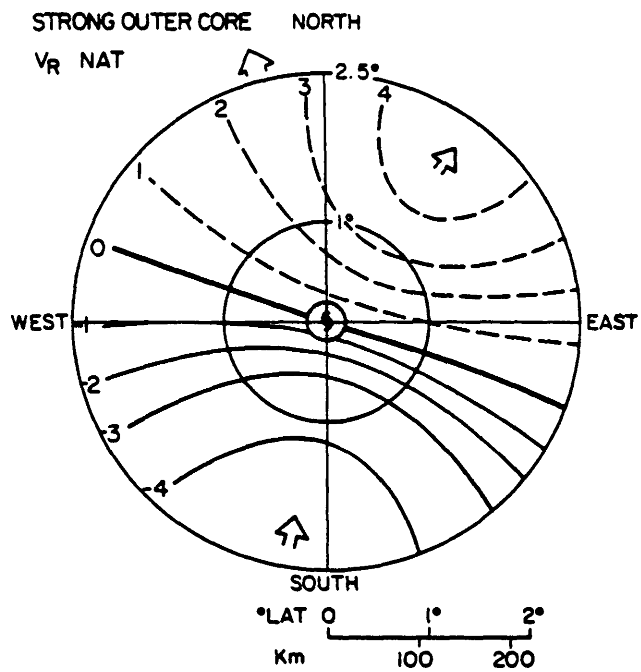

Figure 3.19: a-c. Continued.

In summary, it appears that the strength of the outer core is proportional to Beta-effect displacements and to the moisture content of the air at 700 mb. A new and fundamental observation is that the cyclone's basic steering current can be observed within the inner core circulation. This observation is not consistent with the concept of the inner core as a rigid inner gyre, unaffected, by its environment. Although a shielding effect gradually appears with strengthening winds, residual winds still appear throughout the cyclone, even for the strongest cases. The ways in which differing environments affect cyclones are examined in the next chapter.

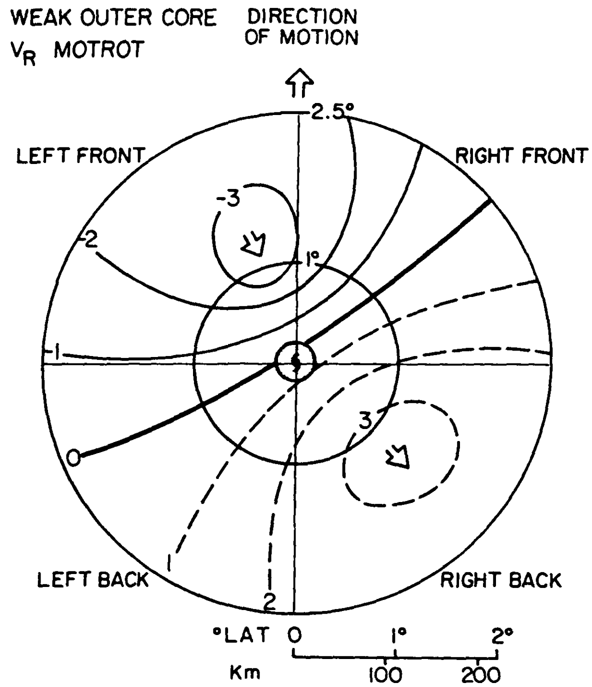

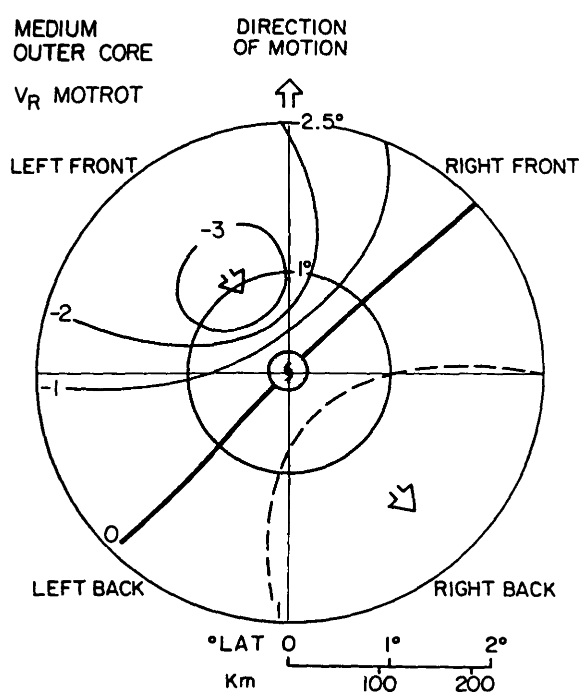

Figure 3.20: a-c. Plan-view analyses of the radial wind in MOTROT coordinates for a) weak OCS, b) medium OCS, and c) strong OCS. Values are in ms^{-1}.

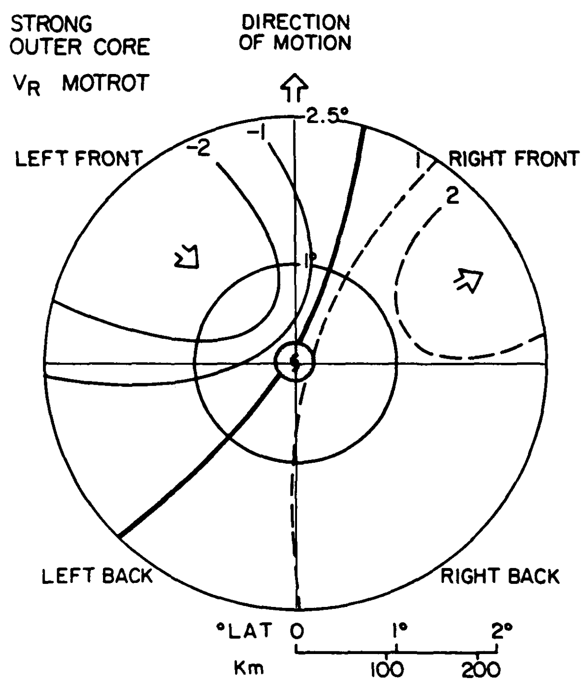

Figure 3.20: a-c. Continued.

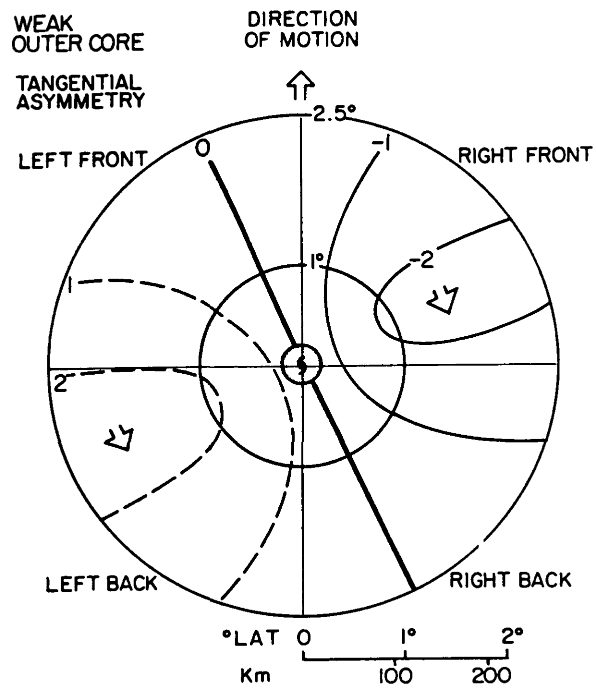

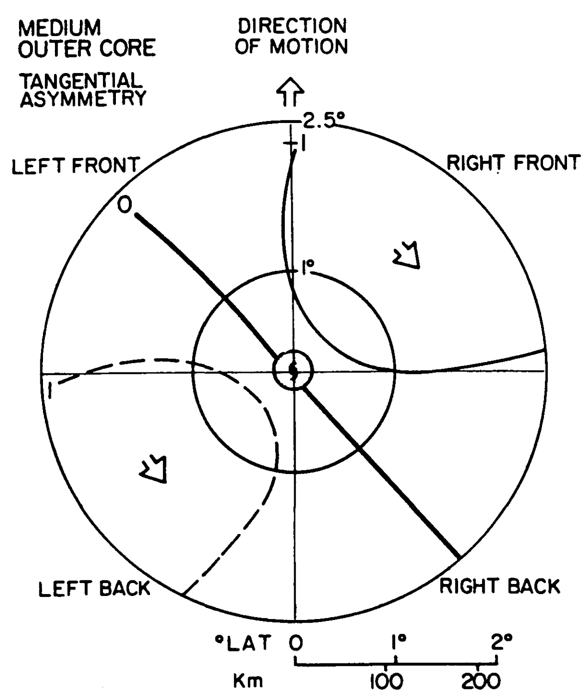

Figure 3.21: a-c. Plan-view analyses of the asymmetrical structure of the tangential wind field at 700 mb for a) weak OCS, b) medium OCS and c) strong OCS in MOTROT-VORT coordinates. Solid curves denote tangential wind decrease while dashed curves denote increased speed. Values are in ms^{-1}.

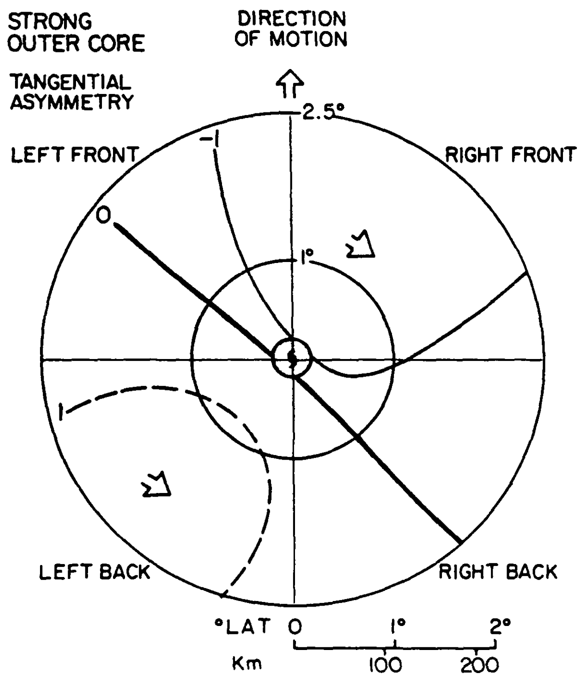

Figure 3.21: a-c. Continued.

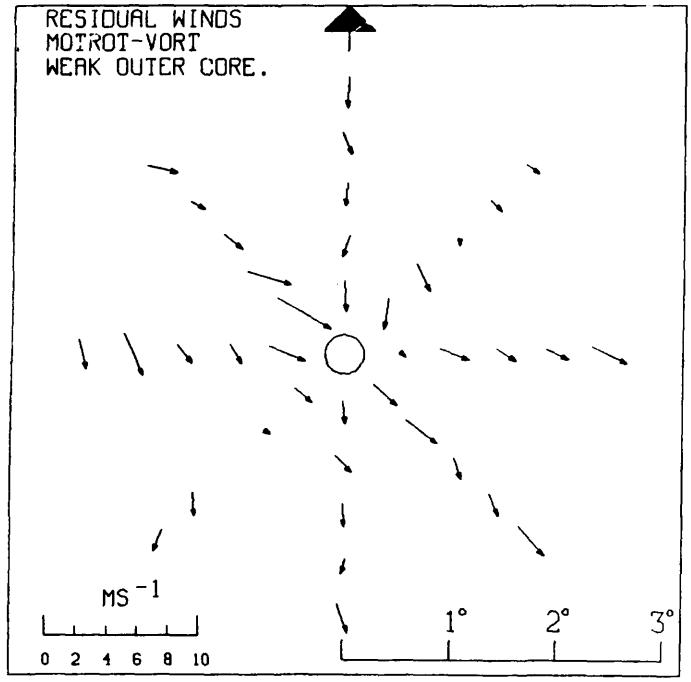

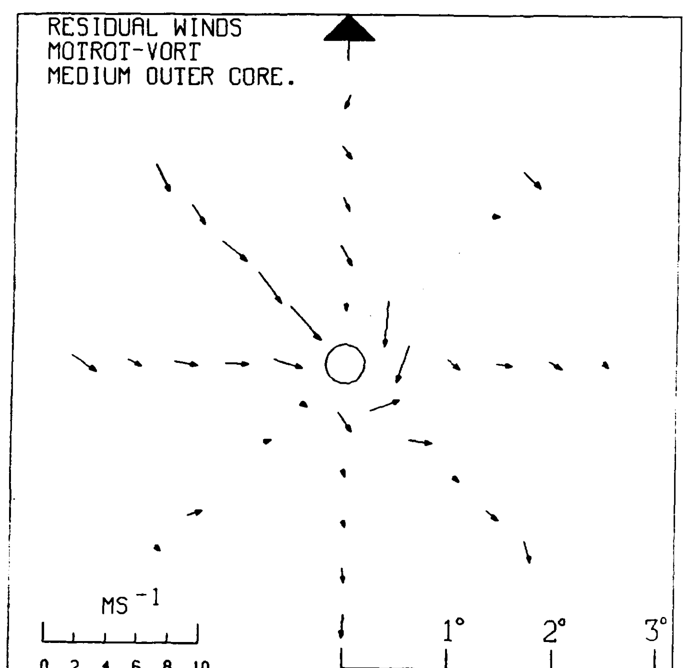

Figure 3.22: a-c. Plan-view analyses of the 700 mb residual wind field which incorporates both the radial and asymmetrical tangential wind vectors in MOTROT-VORT coordinates for a) weak OCS, b) medium OCS and c) strong OCS. The bold arrow marks the cyclones' direction of motion. Vector lengths denote speeds as shown in the lower left corner.

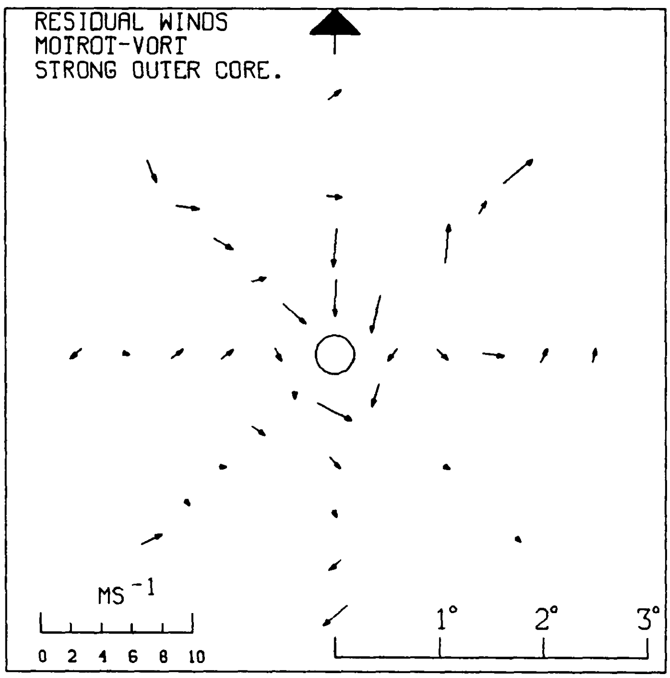

Figure 3.22: a-c. Continued.

Chapter 4

THE 700 MB INTERIOR STEERING CURRENT

The movement of tropical cyclones is largely controlled by the environmental steering current in which they are embedded. Although large scale flow patterns are easily detected on a day-to-day basis, factors governing smaller scale meanders are not. These meanders may determine when the cyclone is going to recurve, when will it loop around a minor circle while remaining on the same general course and, in general, when a 12-hour change in course may or may not indicate movements over the next few days. The meandering portion of the steering current near the cyclone often can not be detected by the synoptic observational network. A large portion of these close-in winds are due to the vortex flow itself. By removing the mean cyclone vortex from composited wind field data, the interior background wind field can be examined to reveal the nature of the close-in steering current. This residual wind field reflects both the interior (.25 to 2.5° radius) 700 mb steering current and its interaction with the central vortex. In this chapter we examine variations in this vortex–subtracted wind field as a function of cyclone heading, speed, and latitude.

4.1 The Steering Current

Several important questions concern the relationship between the motions of tropical cyclones and the interior, .25° to 2.5° radius 700 mb wind fields. Although the deep layer steering current between 850 to 300 mb is superior values for the single 700 mb level, the flow at the 700 mb level is known to closely approximate the deep-layer mean flow (George, 1975; George and Gray, 1976). Xu and Gray (1982) found that in the 5-7° radius region, the 700-500 mb level correlates most closely with cyclone motion. Here we examine data for the 700 mb interior region to see if they are involved with cyclone steering or if this region is shielded from the environment which controls its movements.

During the active (July through November) portion of the cyclone season, the dominant flow pattern steers cyclones around the mid-level subtropical ridge. Cyclones south of the ridge move westward (Fig. 4.1) in the typical zonal tropospheric flow of this region. The mean tropospheric winds represented in Fig. 4.1 were obtained from 21 years of rawinsonde observations. These observations were composited out to 15° radius of the position of all tropical cyclone formation cases, but for the environment one year before and one year after each formation event, as described in Lee, 1986e. Note that these easterly winds typically increase with height and that the mean 850-300 mb steering current is stronger than the 700 mb component. The mean layer current thus moves the cyclone vortex faster than the 700 mb winds would indicate and the vortex must experience flowthrough from front to back at the 700 mb level when south of the subtropical ridge. Cyclones north of the ridge typically have a significant westerly component, as shown in Fig. 4.2. The 850 to 300 mb mean zonal steering current in this region is again greater than the zonal wind at 700 mb. One should also expect that cyclones north of the subtropical ridge would experience front to rear environmental flow-through at 700 mb.

4.2 Tropical Cyclones Stratified by Latitude

Tropical cyclones of the northwestern Pacific generally exist in the latitude belt from 5° to 40° North latitude (see Fig. 2.1). Within this belt, cyclones may reside south of, on, and north of the ridge axis during their lifetime. As can be inferred from Fig. 4.3, the most intense tropical cyclones reach maximum intensity in the latitude belt from 15° to 25° and typically fill north of 25°. We shall stratify cyclones for the latitude belts between 5-15°, 15-25°, and north of 25° to provide a general separation of cyclone positions into zones which are south of, on and north of the mid-level ridge axis. This stratification yields the following data distribution:

Low-Tropical Latitudes 5 – 15° **North** 275 MISSIONS

Mid-Tropical Latitudes 15 – 25° **North** 388 MISSIONS

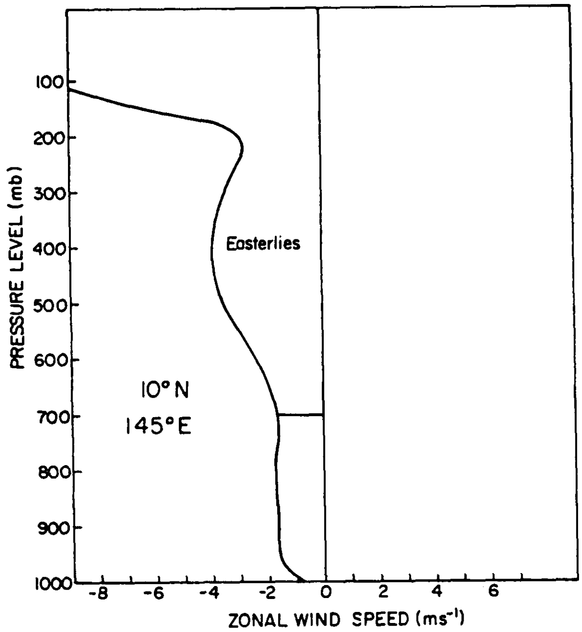

Figure 4.1: Vertical profile of the mean zonal wind for the tropical troposphere at 10° north, 145° east, derived from 21 years of rawinsonde composites. Values are in ms^{-1}.

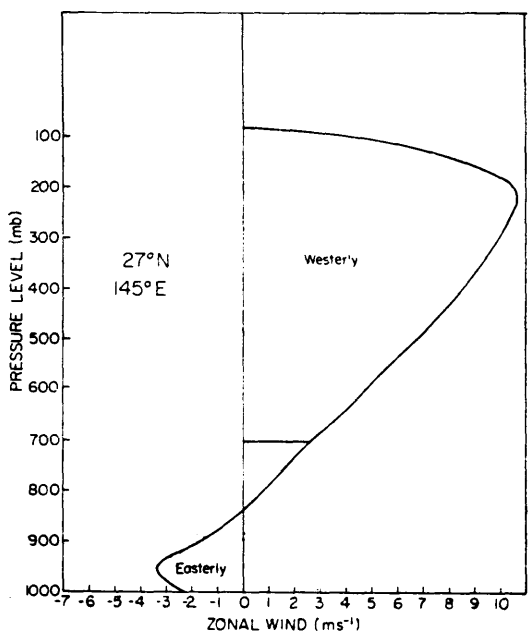

Figure 4.2: Vertical profiles of the mean zonal wind for the tropical troposphere at 27° north, and 145° east, derived from 21 years of rawinsonde composites. Values are in ms^{-1}.

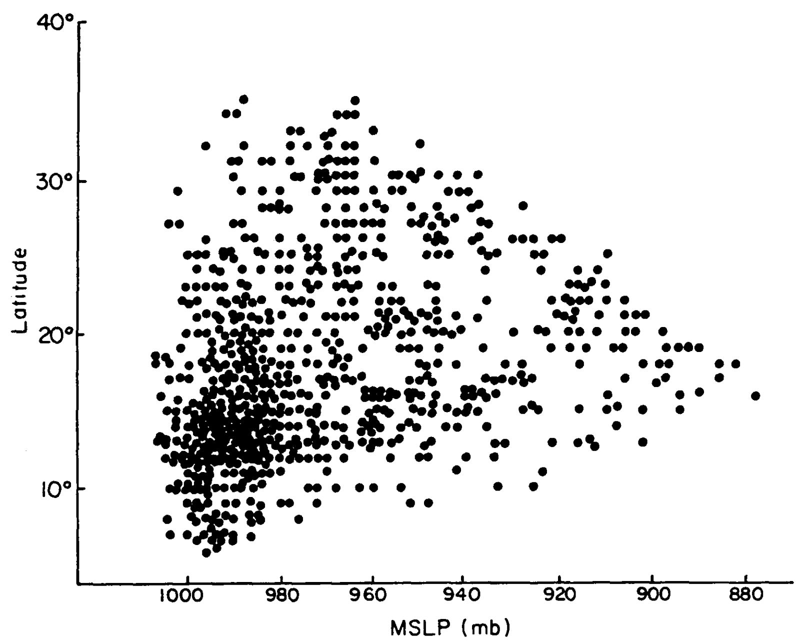

Figure 4.3: Scatter diagram of the latitudes of cyclone centers versus MSLP for the 750 missions included in this data set.

High-Tropical Latitudes 25 – 35° North 134 MISSIONS

Although aircraft data were limited to areas south of 35°N, the data are adequate for describing cyclones north of the subtropical ridge. Table 4.1 shows the average position, motion, intensity, and OCS for each cyclone latitude stratification. Systems in the mid (15-25°) and higher tropics (> 25°) had similar average maximum winds but very different outer core wind strengths. The stronger OCS values of the high-tropics storms reflect the fact that cyclones generally reach maximum intensity as they moved past the ridge axis, but do not attain their strongest outer core speeds until reaching higher-tropical latitudes. Systems in the lower-latitude belt (5-15°) had generally weaker inner and outer cores.

Plan-view depictions of mean cyclones stratified by latitude belt are shown in Figs. 4.4a-c. These NAT coordinate figures show the 700 mb interior radial wind flow for each latitude class. The 700 mb current can be observed flowing toward the northwest, north, and northeast for the south of, on, and north of ridge composites, respectively. What is not apparent in these figures is any evidence of the Solitary Eddy Solution (SES) as

Table 4.1: Average of position, heading and speed of motion, MSLP, maximum wind speed (Holland estimate), and OCS.

LATITUDE CLASS	LAT.	LONG.	HEADING	SPEED (ms^{-1})	MAX WIND (ms^{-1})	MSLP (mb)	OCS (ms^{-1})
LOW-TROPICS	12°	138°	295°	5	27	979	15
MID-TROPICS	20°	133°	320°	5	35	961	19
HIGH-TROPICS	29°	141°	360°	7	35	963	24

described by Flierl et al., (1980) for which the environmental flow moves around but not through the vortex. The mean cyclone for all three latitude classes is moving faster than the 700 mb interior flow and approximately 30° to the left of the flow. The question of why cyclones move left of the mean steering current has been examined previously by George and Gray (1976) and Gray (1977) and has been attributed to the Beta effect described by Holland (1983) and Chan (1984) (see below, section 4.3).

Figures 4.5a-c show the 700 mb radial wind field in MOTROT coordinates. In each case, the 0 to 2.5° interior radial winds flow from the left front to the right rear, directly across the cyclone. Given this front to back flow-through in the MOTROT coordinate system, one would expect a weaker tangential wind asymmetry on the right side and stronger asymmetry on the left as is observed for all cases shown in Figs. 4.6a-c.

As described in Chapter 3, combining the radial and tangential components yields the residual wind shown in Figs. 4.7a-c. The greatest inner core residual wind convergence occurs in the lower tropics cyclones (Fig. 4.7a). Some convergence of the residual wind also occurs in the mid-tropics (Fig. 4.7b) whereas a general divergence of residual winds prevail at higher latitudes (Fig. 4.7c). The inner cores of the higher-tropical systems allows 700 mb environmental air to pass directly through. As with the weaker OCS cyclones described in section 3.5, this observation is counter to the concept of the typhoon as a relatively rigid vortex embedded in a moving stream with momentum impingement at the edges only. These data indicate that the cyclone's steering current extends to near the radius of maximum winds. Whether this current penetrates the Stationary Band Complex (SBC) as

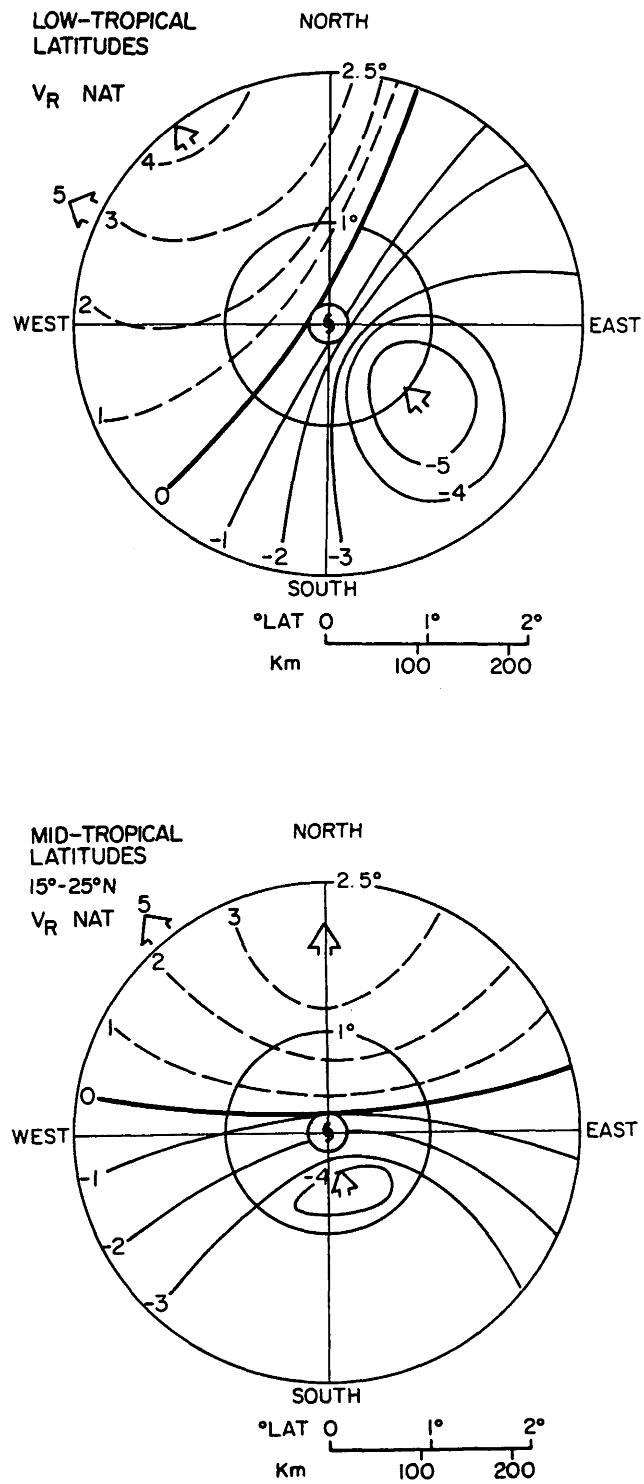

Figure 4.4: a-c. Plan-view analyses of the mean 700 mb radial wind field (V_r) in ms^{-1} in NAT coordinates for a) low-tropical latitudes, b) mid-tropical latitudes, and c) high-tropical latitudes. Arrow on the rim depicts mean cyclone motion.

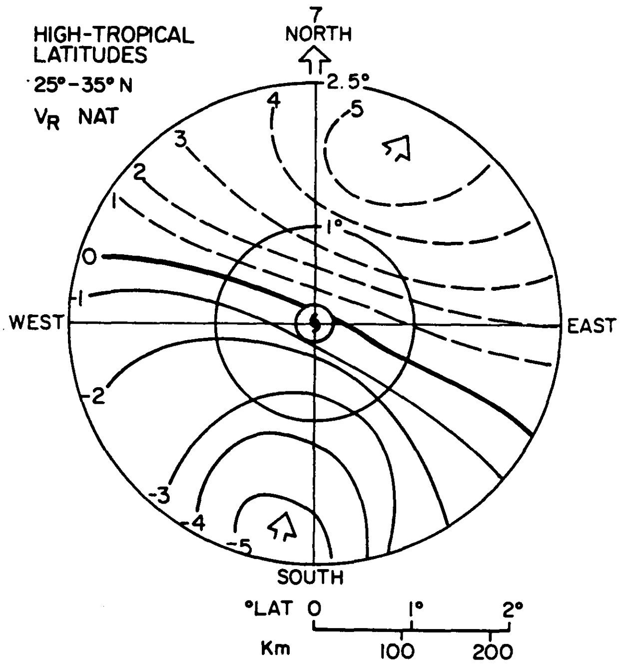

Figure 4.4: a-c. Continued.

defined by Willoughby, et al. (1984) cannot be resolved with certainty because information on feeder bands were not obtained. However, Willoughby, et al.'s study showed that the SBC resided 80 to 120 km from the center. Their main contention was that a 'spinning top' regime existed within the SBC zone, through which environmental air did not penetrate. Figures 4.7a-c show that environmental air does appear to pass through the vortex to areas well inside the 80 to 120 km zone. If this region were shielded from outside air, these figures would show either no flow, or light and variable flow within 80 to 120 km of the storm center.

4.3 Stratification by Cyclone Heading

While stratification by latitude band tends to depict these general heading classes (ie., Table 4.1), stratification of the data by flow direction is also helpful. Cyclone heading stratifications include the following:

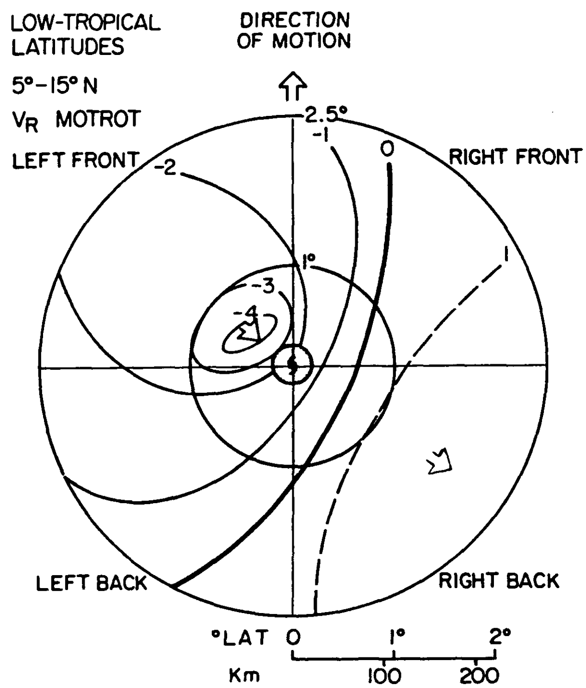

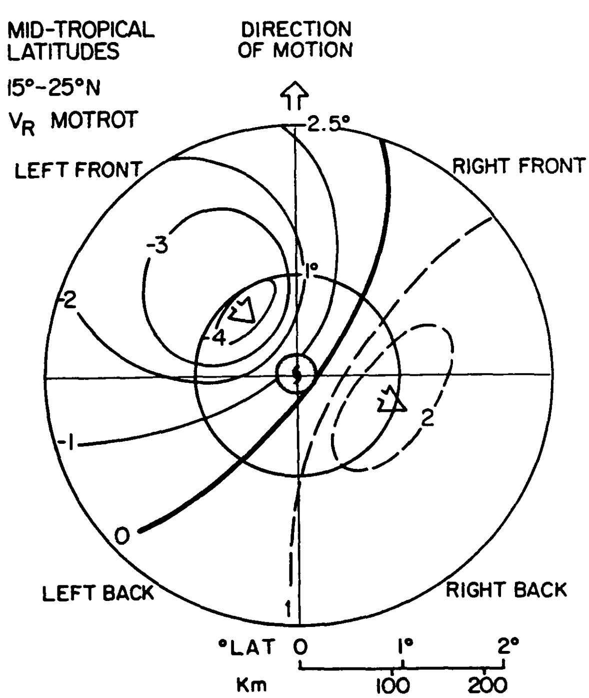

Figure 4.5: a-c. Plan-view analyses of the mean 700 mb radial wind field (V_r) in ms^{-1} in MOTROT coordinates for a) low-tropical latitude, b) mid-tropical latitude, and c) high-tropical latitude cyclones.

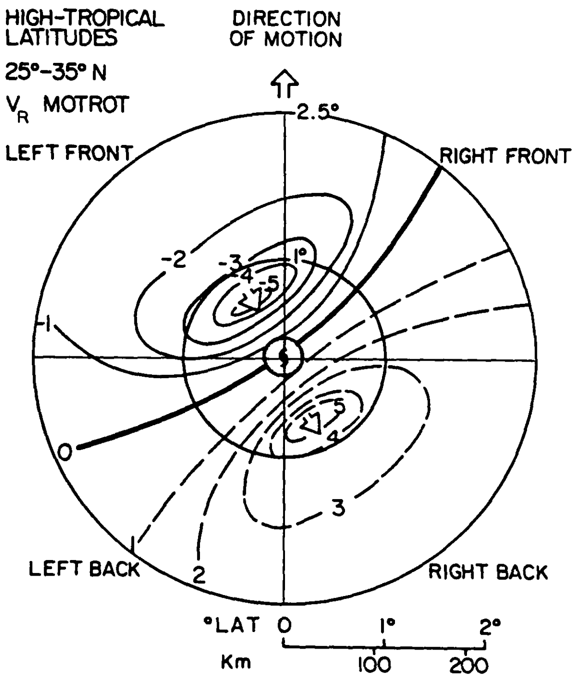

Figure 4.5: a-c. Continued.

HEADING CLASS	RANGE	NO. OF MISSIONS
SOUTHWEST	180° – 265°	66
WEST	250° – 290°	207
NORTH	330° – 30°	176
EAST	30° – 120°	87

Notice that there are a significant number of cyclones moving to the southwest. Southwest headings are atypical in that these cyclones move very slowly and in more erratic paths, as seen for the later stages of Typhoon Faye in Fig. 4.8. We include this southwest class to allow additional study of the Beta-effect. Table 4.2 gives the average position, motion, intensity, and OCS values for each heading class. Cyclones moving northward appear to slow down under the influence of a reduced steering current and then speed up again when north of the ridge. Eastward-moving cyclones have slightly stronger OCS values but weaker intensities than their northward-moving counterparts.

Plan-view depictions of radial winds in NAT coordinates are shown for the heading stratification in Figs. 4.9a-d. Once again, it can be seen that each cyclone class moves to the left of the mean 700 mb steering current. Following Holland (1983), a cyclonically

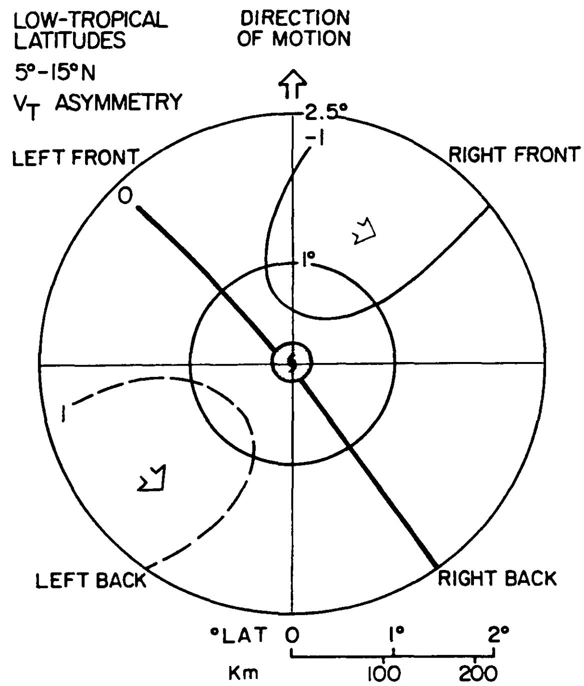

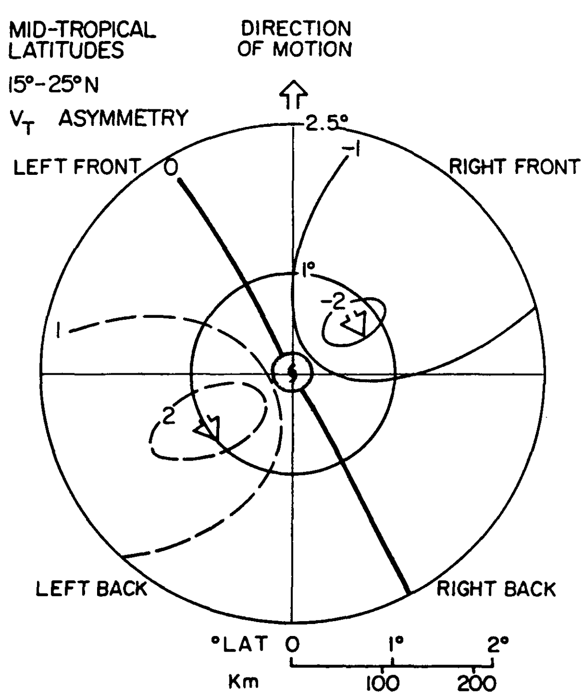

Figure 4.6: a-c. Plan-view analyses of the 700 mb tangential asymmetry pattern in ms^{-1} and in MOTROT-VORT coordinates in which the mean vortex has been removed for a) low-tropical latitudes, b) mid-tropical latitudes, and c) high-tropical latitudes.

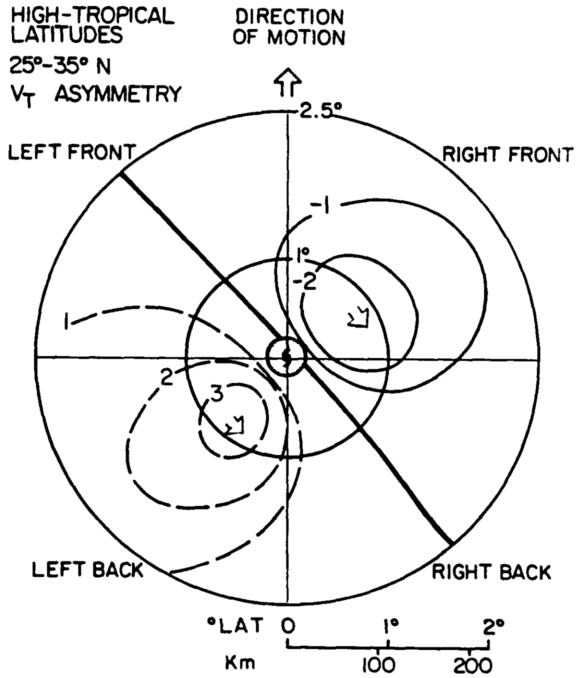

Figure 4.6: a-c. Continued.

Table 4.2: Average values of position, heading, speed of motion, maximum wind speed (Holland estimate), MSLP, and OCS for each cyclone heading of motion class.

HEAD	LAT.	LONG.	HEAD	SPEED (ms^{-1})	MAX WIND (ms^{-1})	MSLP (mb)	MSLP CHANGE (mb/d)	OCS (ms^{-1})
Southwest	17°	138°	240°	4	27	980	0	14
West	15°	136°	275°	6	28	975	- 10	15
North	22°	138°	360°	5	36	959	0	21
East	24°	136°	45°	6	34	966	+ 5	22

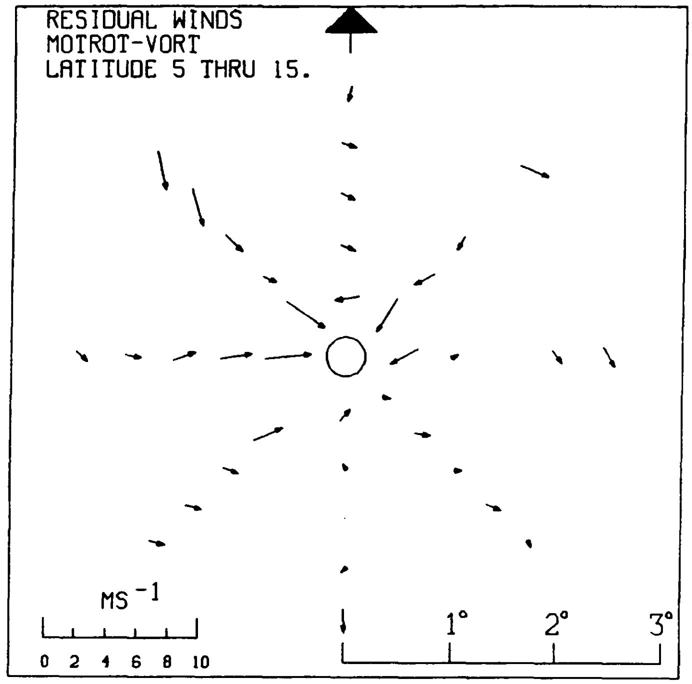

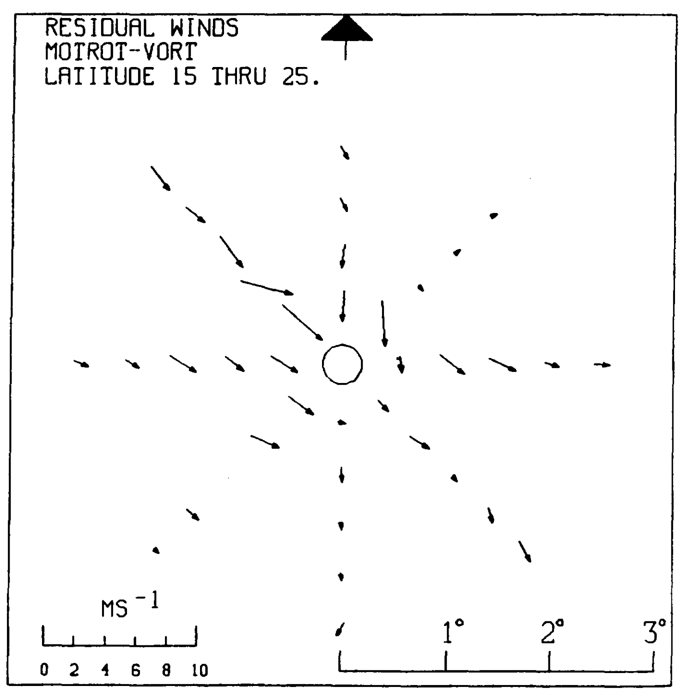

Figure 4.7: a-c. Plan-view analyses of latitudinally stratified residual wind field flow-through pattern in MOTROT-VORT coordinates with the bold arrow denoting the cyclone motion heading. Values are in ms^{-1} with arrow length implying speed as shown in the lower left corner. The classes are: a) low-tropical latitudes, b) mid-tropical latitudes, and c) high-tropical latitudes.

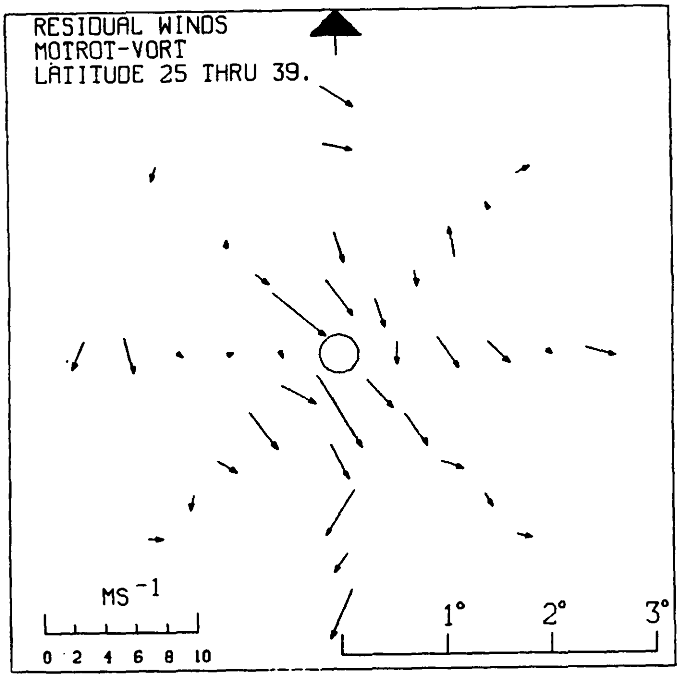

Figure 4.7: a-c. Continued.

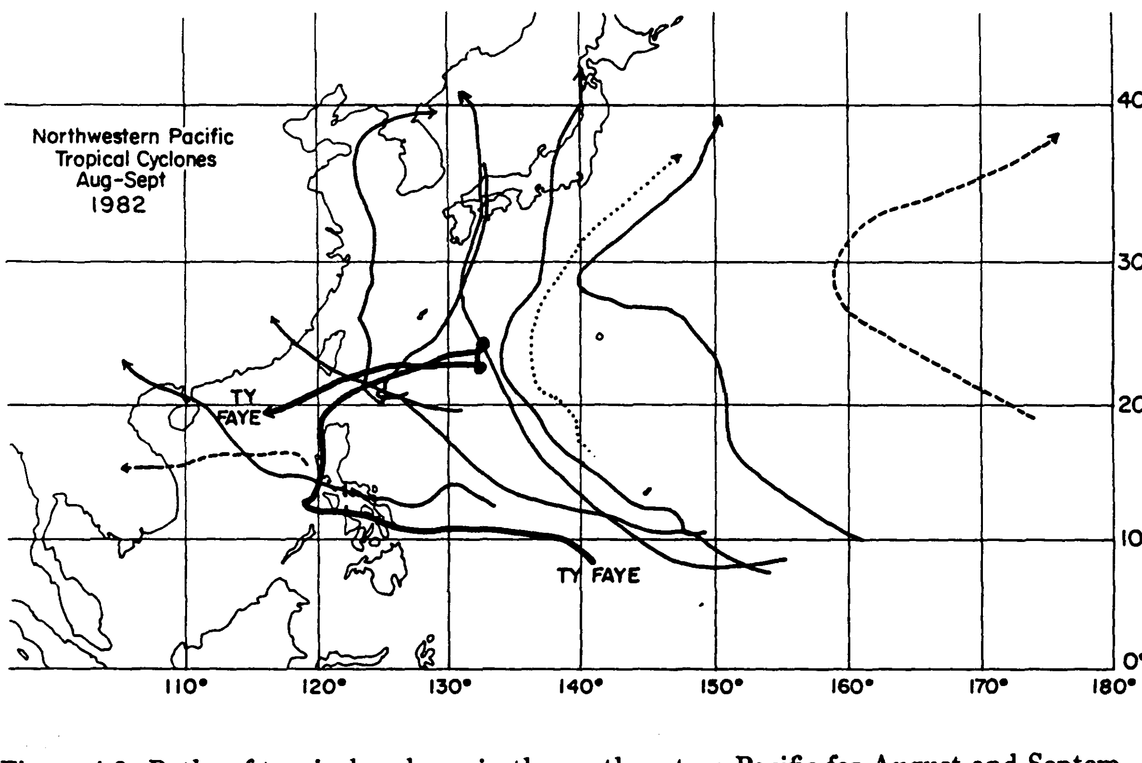

Figure 4.8: Paths of tropical cyclones in the northwestern Pacific for August and September 1982.

rotating vortex of typhoon scale would advect higher earth-vorticity (the Beta-effect) on the cyclone's west side while lower earth-vorticity on its east side. Assuming the vortex is moving toward the region of maximum vorticity advection, the cyclone would appear to move to the left of its steering current. However, this left-drift effect should only work for cyclones embedded in a northward flowing environment on an east-west axis. Cyclones in an environmental current that is flowing south of an east-west axis should be deflected right of the steering flow. It was hoped that the 66 cases of southwest heading cyclones would provide some new insight on this latter case. However, as Fig. 4.9a shows, those cyclones which moved towards the southwest were embedded in an environment which, on average, was moving west northwest, and thus were still in a left-drift regime. Consequently, right-drift motion was not observed with the 1980-84 composited cyclones. The few cases which headed southeast or south were undergoing a looping pattern and thus were not considered to be under the influence of a dominant steering current. An interesting feature of the southwest moving cyclones is that they were in a markedly slower environment and yet show the greatest leftward drift (nearly 85°).

When viewed in the MOTROT coordinate system (Figs. 4.10a-d), all cases were observed to move faster than the 700 mb environment. Thus, to some extent the cyclones entrained the 700 mb environment that they moved into. An interesting departure from this generalization was for the case of eastward moving cyclones. Note in Fig. 4.10d that the flow-through which normally entered from the left-front and exited the right-back, prevailed only in the lower-left portion of the system with a different regime on the upper-right of this figure. This peculiar pattern is more clearly illustrated in the analyses of tangential asymmetries (Figs. 4.11a-c). The one-wave asymmetry pattern observed in cyclones embedded in a left-drift environment shows up well for cyclones heading either southwest, west, or north when viewed in the MOTROT-VORT system. However, east-heading cyclones (Fig. 4.11d) deviate from the one-wave asymmetry pattern and reveal a two-wave pattern dominating the residual tangential wind field. What appears to occur in this case is that the 700 mb current entering the cyclone from the left-front affects only

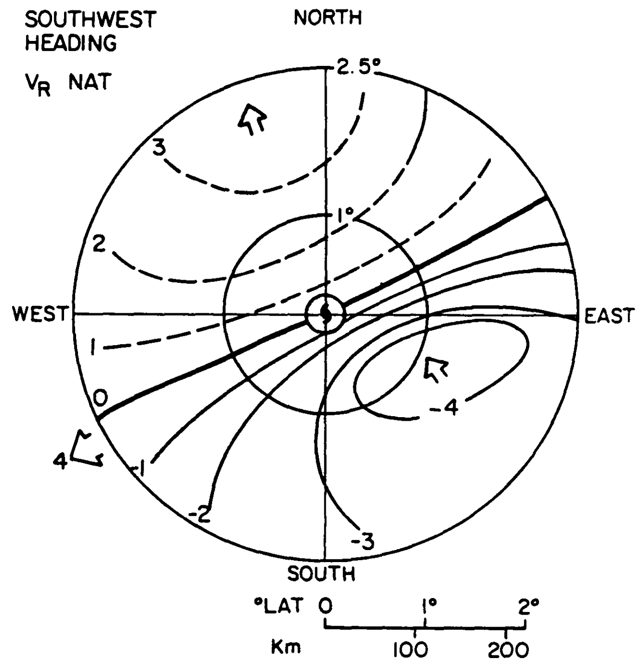

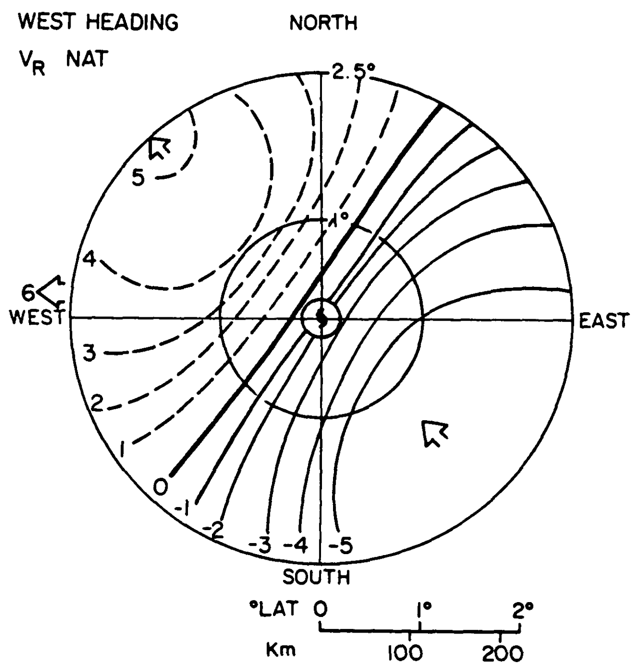

Figure 4.9: a-d. Plan-view analyses of heading stratified radial wind field (V_r) in ms^{-1} in NAT coordinates for the four cyclone headings of a) southwest, b) west, c) north, and d) east. Arrow on exterior rim denotes the mean cyclone motion.

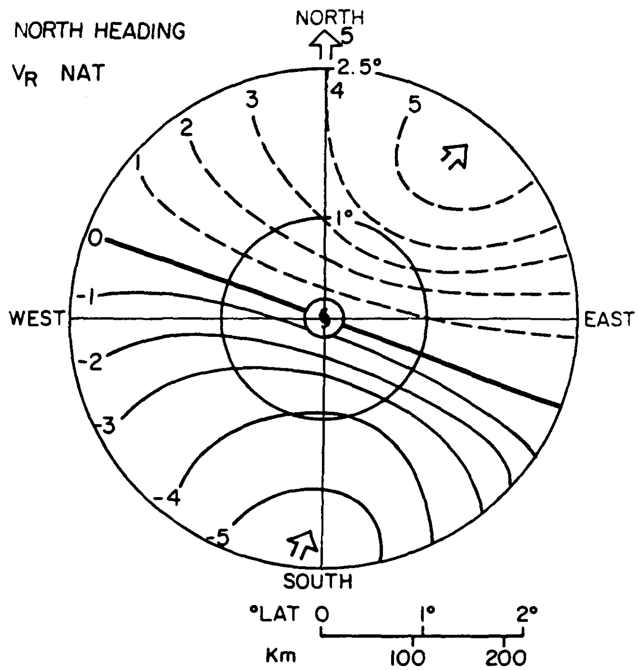

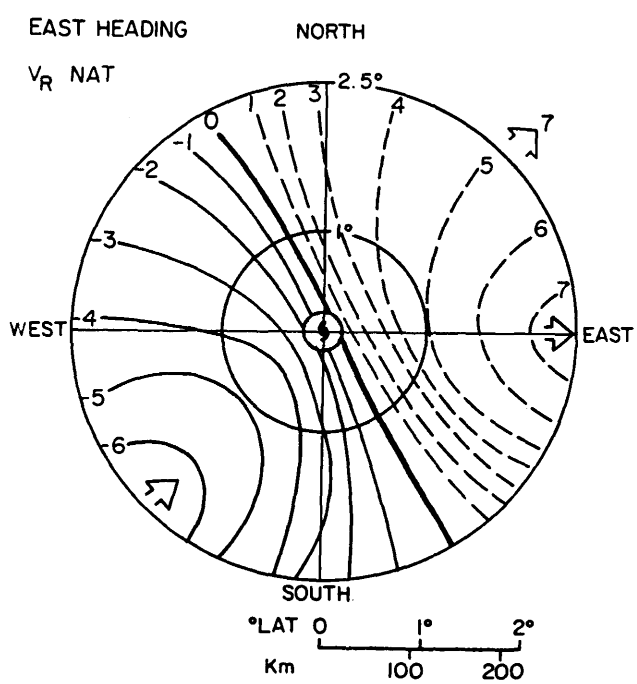

Figure 4.9: a-d. Continued.

the back portion of the storm, indicative of cyclones which are moving faster and to the left of the 700 mb environment. However, the front right portion of the cyclone, exhibits flow-through entering from the right, as shown conceptually in Fig. 4.12. East-heading cyclones are, on average, situated on a bend in the 700 mb current as the stream curves around the subtropical ridge. Presumably, the cyclone encounters increasingly westerly shear when rounding the bend as the 700 mb wind field becomes stronger and more westerly. At this time we can only speculate that the atypical flow pattern in the upper right of Fig. 4.11d may then be due entirely to horizontal shear at 700 mb as the cyclone approaches increasingly westerly flow to the north.

4.4 Stratification by Cyclone Speed

In addition to stratifying cyclone data by latitude and by heading, it is important to compare cyclones of differing speeds. Although average speed of motion for tropical cyclones in the data set was 5 ms^{-1}, individual values varied from 0 to 26 ms^{-1} as shown in Fig. 4.13. Therefore, an additional environmental effect to be considered includes possible differences between rapidly and slowly moving cyclones. The approach is to contrast those cases which depart significantly from the average and which are classified as follows:

SPEED CLASS	RANGE OF SPEEDS	NO. OF MISSIONS
FAST CYCLONES	$\geq 7.5 ms^{-1}$	137
SLOW CYCLONES	$\leq 2.5 ms^{-1}$	154

Average properties of the slow and fast moving composites are shown in Table 4.3. Both sets of storms have roughly the same inner and outer core wind structure and have average characteristics similar to those of minimal typhoons (see Table 3.1). Hence, differences between the two groups do not appear to reside within their basic structure. The fast moving cyclones tend to be somewhat north and east of the slow movers but are heading in essentially the same direction. It is surprising that the average latitude values are so similar in that it was expected that the faster moving cyclones would, in general, be caught up in the westerly jetstream north of 30°. Thus, it appears that some cyclones move much faster than others at similar latitudes but within very different steering environments.

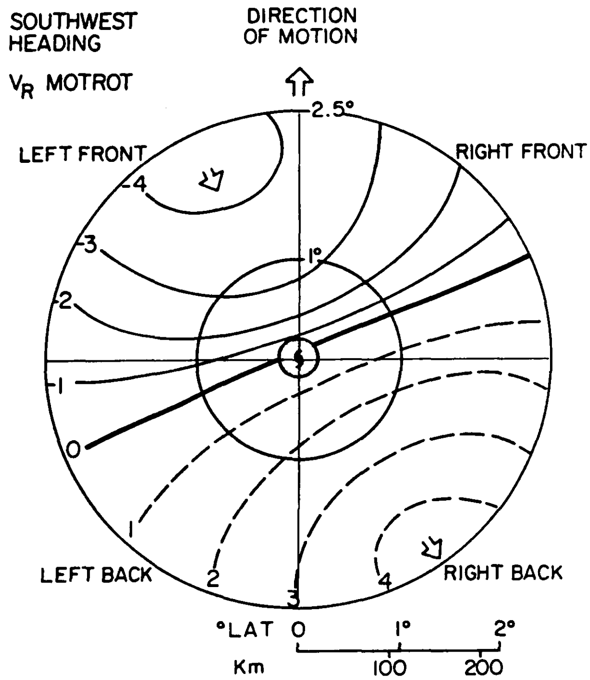

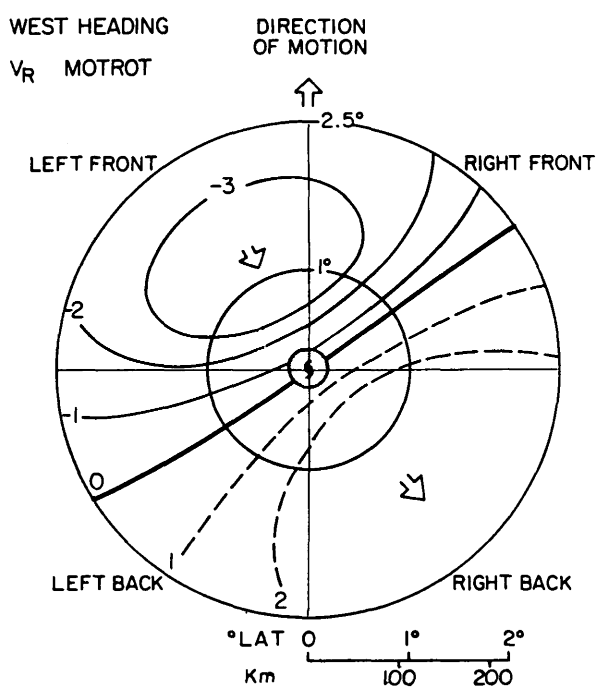

Figure 4.10: a-d. Plan-view analyses of heading stratified radial wind fields (V_r) in ms^{-1} in MOTROT coordinates for the four cyclone headings of a) southwest, b) west, c) north, and d) east.

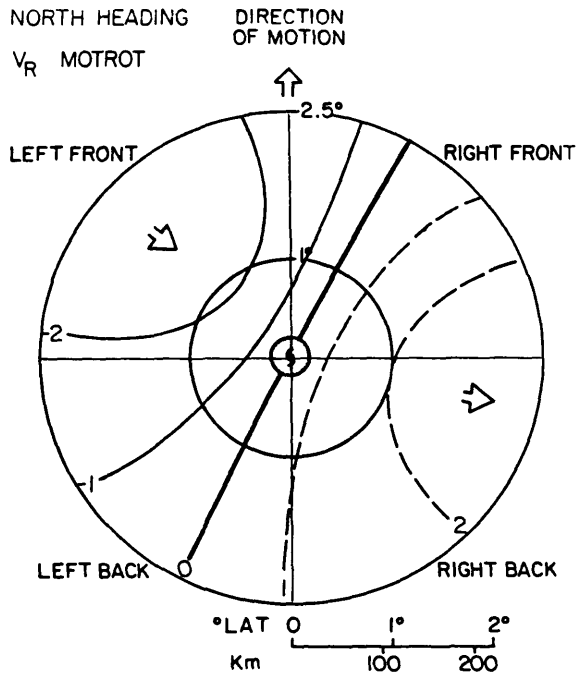

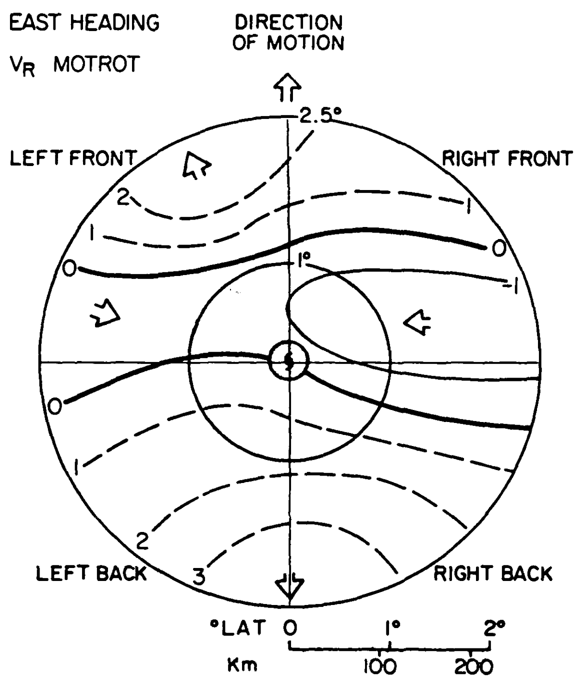

Figure 4.10: a-d. Continued.

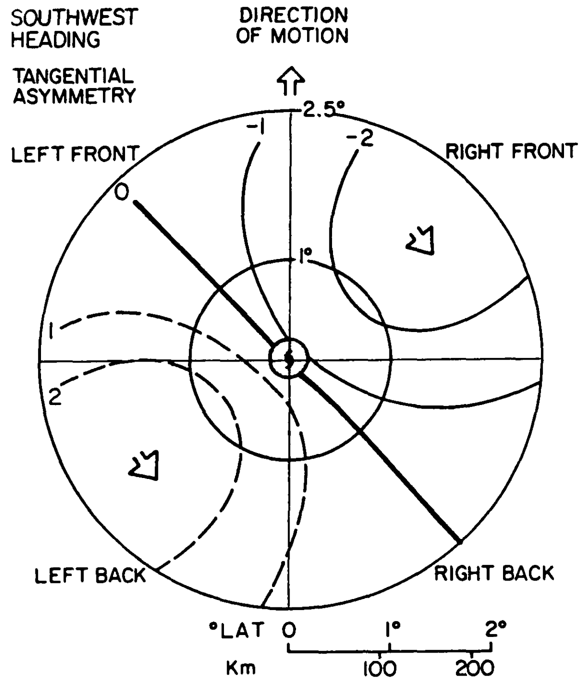

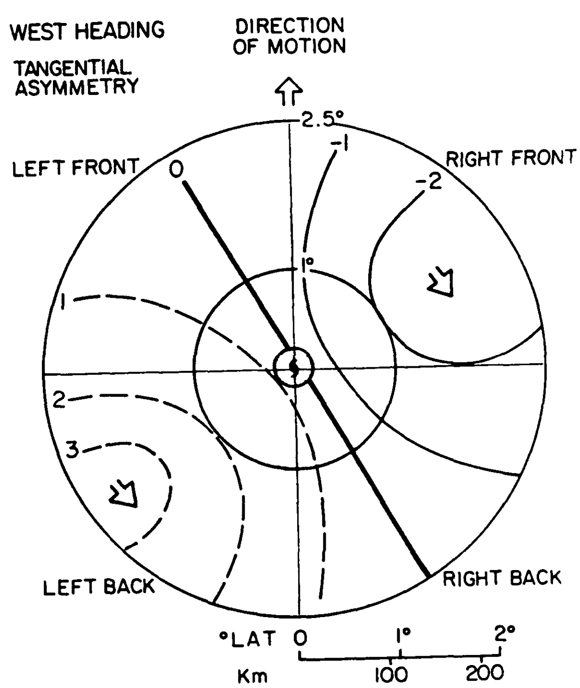

Figure 4.11: a-d. Plan-view analyses of heading stratified tangential asymmetry patterns in ms^{-1} in MOTROT-VORT coordinates for the four cyclone headings of a) southwest, b) west, c) north, and d) east.

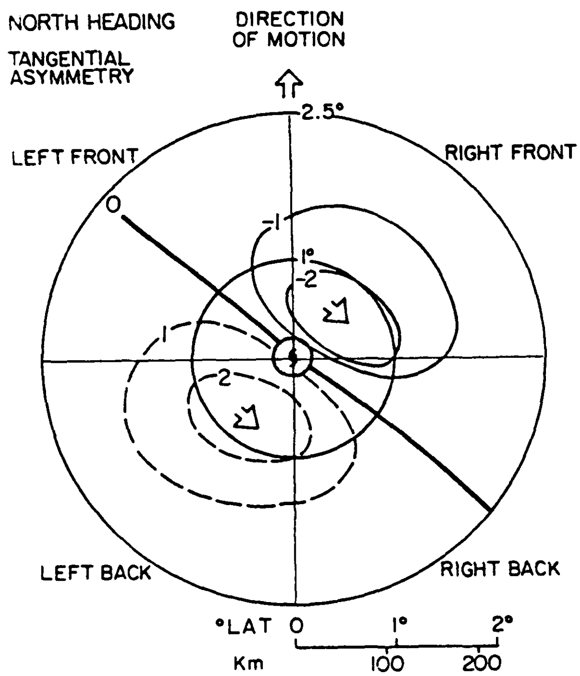

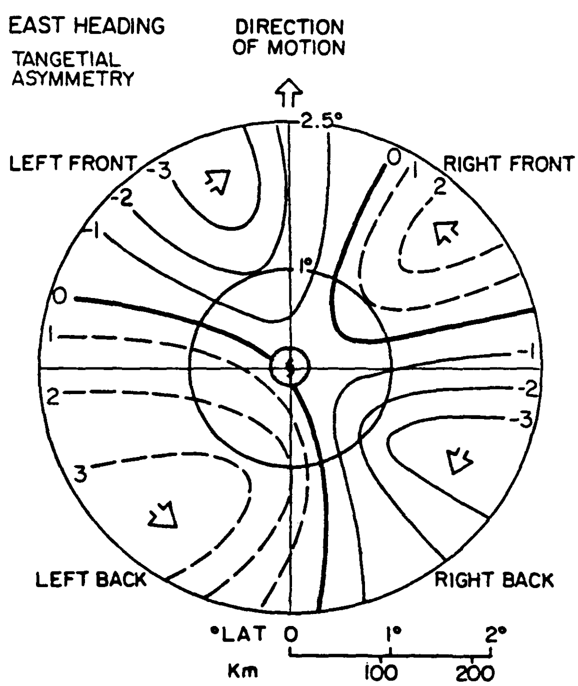

Figure 4.11: a-d. Continued.

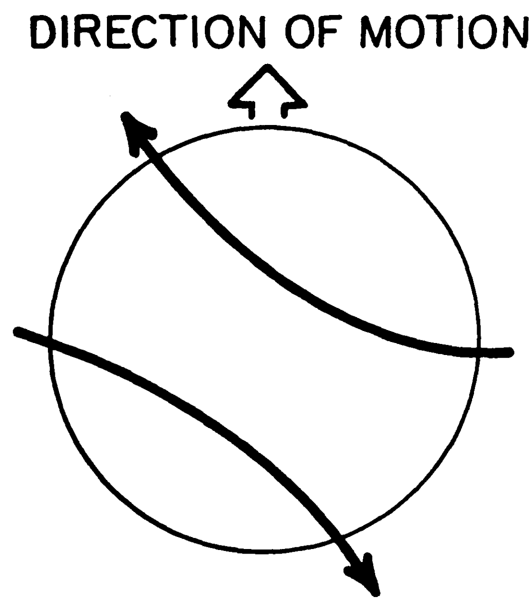

Figure 4.12: Schematic illustration of the environmental flow-through pattern observed in eastward-moving cyclones in the MOTROT-VORT system.

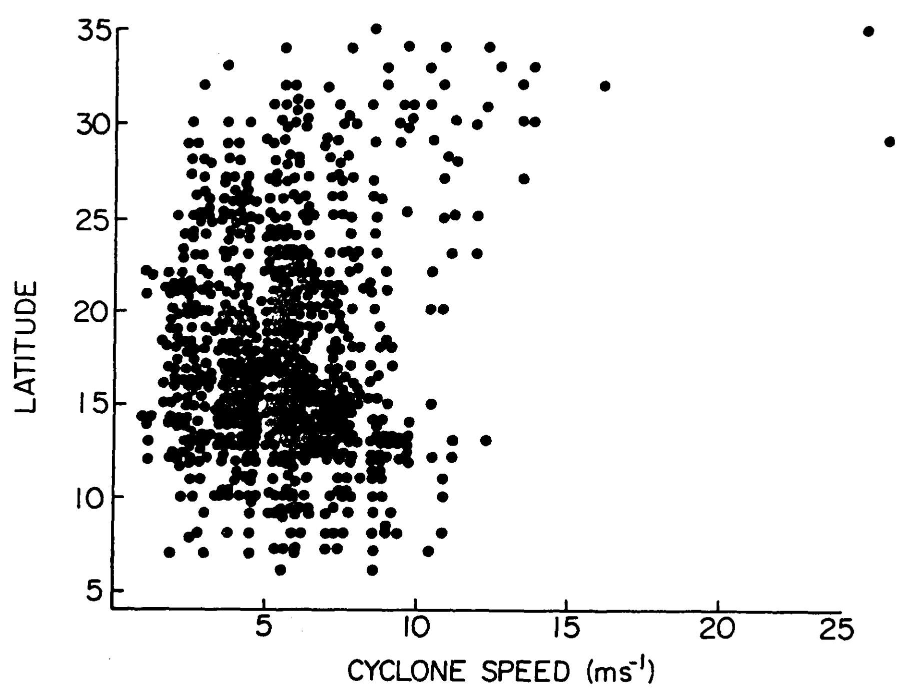

Figure 4.13: Scatter diagram of cyclone latitude versus speed of motion.

Table 4.3: Average positions, motion, MSLP, maximum wind speeds, and OCS values for the speed classes of fast and slow.

SPEED CLASS	LAT.	LONG.	HEAD	SPEED (ms^{-1})	MSLP (mb)	MAX WIND (ms^{-1})	OCS (ms^{-1})
FAST MOVERS	20°	139°	330°	9	972	30	19
SLOW MOVERS	18°	134°	320°	2	969	32	18

The 700 mb environmental current is roughly proportional to the peripheral radial wind maxima in the plan-view depictions of Figs. 4.14a-b. Although the 700 mb current is flowing approximately twice as fast for the fast movers as for the slow movers, this difference cannot account for the four-fold speed difference between these two classes. Evidently, the environment at higher levels (above the 700 mb level) must be moving faster to explain the rapid motion of the fast cyclone class. The NAT coordinate plan-view in Fig. 4.14b suggest that the fast-moving cyclones lie close to the axis of the subtropical ridge, as evidenced by the northward heading of the 700 mb flow. The slow-moving cyclones, whose 700 mb flow is moving northeastward, must then tend to occur slightly to the north of the ridge, even though they are at lower latitudes. This combination of motion and latitude for the slow movers is indicative of early and late season cyclones when the ridge axis lies farther south. Notice that the slow-moving cyclones drift 70° to the left of the mean 700 mb current whereas the fast-moving cyclones move roughly 30° to the left. The greater leftward drift for the slow cyclones supports contentions of the Beta-effect argument that cyclones will move towards the region of greatest vorticity advection. In this case, the slower the steering current, the greater the relative role of the planetary vorticity advection for total motion.

When viewed in the MOTROT system (Figs. 4.15a-b), the 700 mb flow-through is shown to be drastically reduced for the slow movers as compared to fast movers. Consequently, this difference implies that advection at 700 mb was smaller for the slow movers. This flow-through manifests itself in both speed classes as a one-wave asymmetry pattern resulting in higher winds on the left-back quadrant (Figs. 4.16a-b). The fast movers show

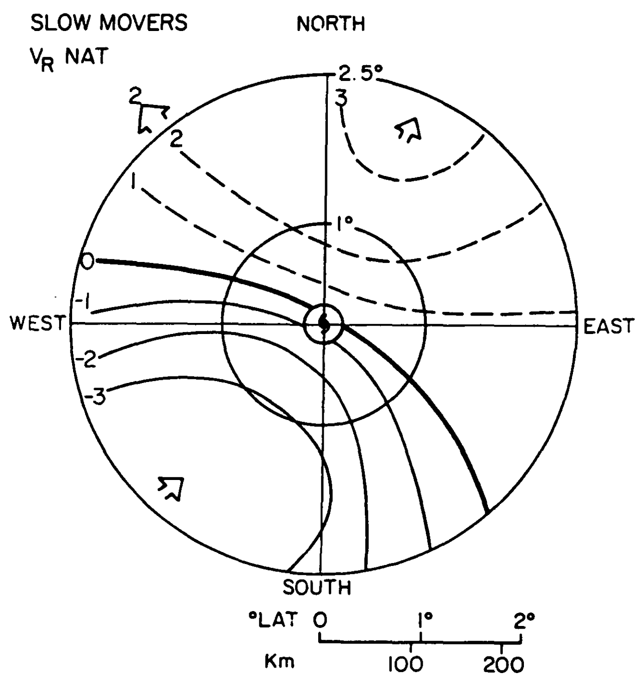

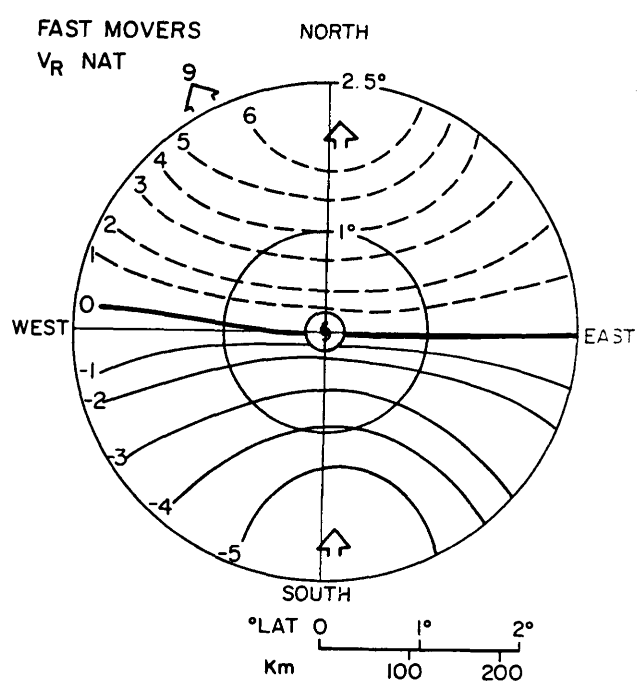

Figure 4.14: a-b. Plan-view analyses of speed stratified radial wind fields (V_r) in ms^{-1} in NAT coordinates for slow moving cyclones (less than 2.5 ms^{-1}) and fast moving cyclones (speed greater than 7.5 ms^{-1}). Arrow on rim denotes mean direction of cyclone motion.

this asymmetry much farther out from the inner core than the slow movers. This increased flow-through shows up in the residual wind field (MOTROT-VORT coordinates) in Figs. 4.17a-b. Although both classes have the average characteristics of minimal typhoons, the slow movers reflect little flow-through at 700 mb. In contrast, the flow-through pattern of the fast movers seems to pass through with little energy being absorbed in the inner core.

The cyclone speed most conducive to rapid intensification is approximately 5 ms^{-1}, as shown by Weatherford and Gray (1987a). The average slow storm in this study did not change in intensity with no observed mean MSLP change for either the prior or subsequent 12 hour periods. The fast movers, on the other hand, tended to deepen slightly at an average rate of 3 $mb\ d^{-1}$. However, neither the slower nor faster speeds appear to be clearly associated with the deepening process. This question of intensity change, although intimately connected with the environment, is addressed directly in the next chapter as cyclones are stratified by phases of their life cycle.

4.5 Discussion

The 700 mb steering current has been shown to flow directly through the tropical cyclone vortex. This observation is counter to the concept of the cyclone core area as a rigid vortex embedded in a stream which impinges only on its outer edges. Apparently, the steering current penetrates the vortex and influences it from its center, as well as from its fringes and our concept of cyclone motion must therefore include steering of the eyewall. This observation also emphasizes the usefulness of inner core flight data for describing the inner-core steering current. When the mean vortex is removed from the wind data, much of the residual wind field is comprised of the steering current itself. The remaining portion of the residual wind field reveals vortex-environment interactions. In the previous chapter it was noted that the more intense the cyclone, the greater the tendency for environmental air to be drawn toward the center of the vortex. Although the residual steering current was shown to penetrate the inner core region, the extent to which the center of the cyclone was shielded from environmental air was proportional to the strength of the vortex and the relative contribution of the steering current to the total wind field decreased with

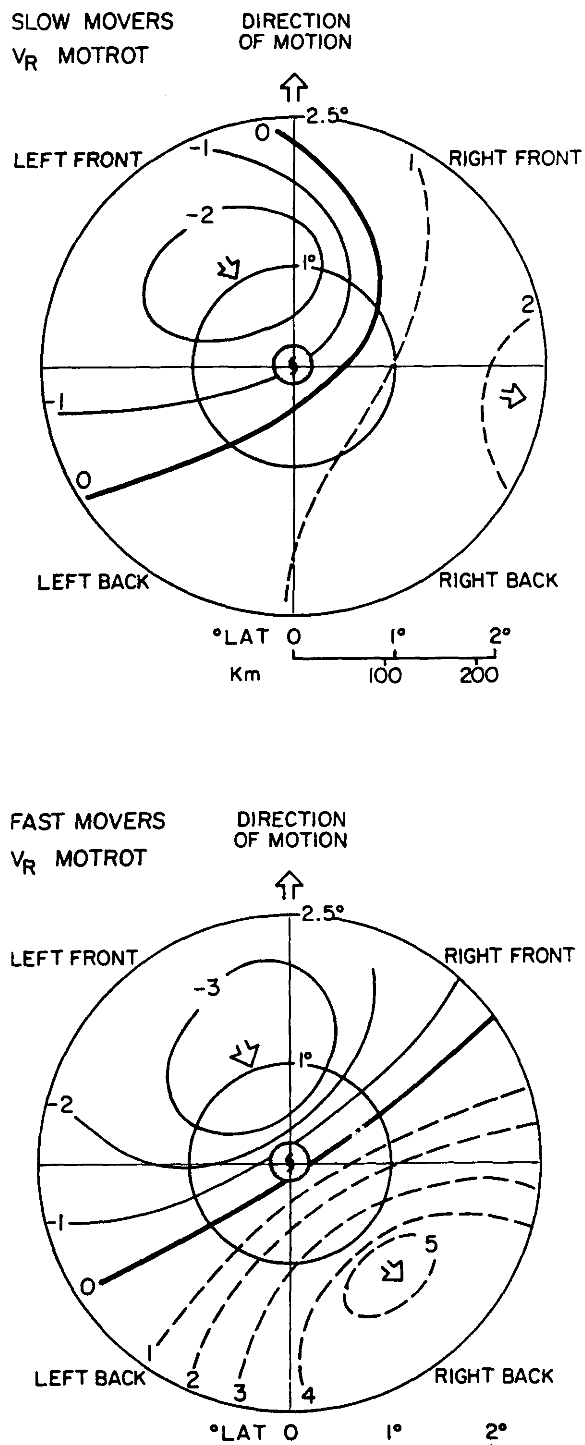

Figure 4.15: a-b. Plan-view analyses of speed stratified radial wind fields (V_r) in ms^{-1} in MOTROT coordinates for slow moving cyclones (less than 2.5 ms^{-1}) and fast moving cyclones (speed greater than 7.5 ms^{-1}).

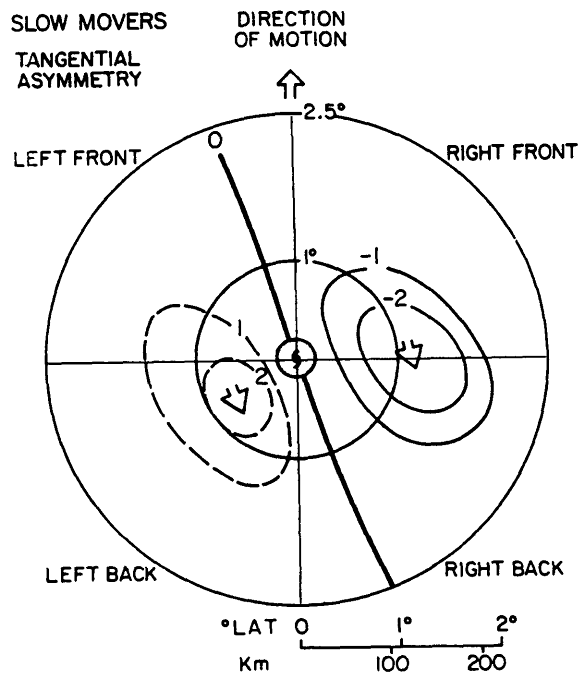

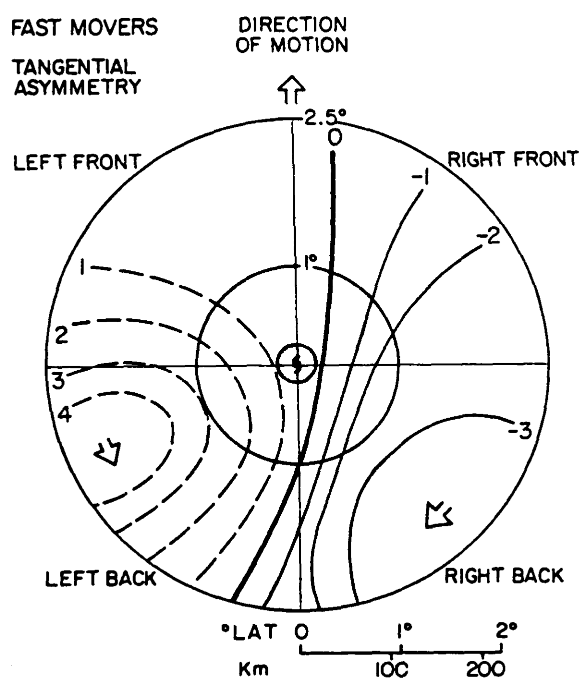

Figure 4.16: a-b. Plan-view analyses of speed stratified tangential wind asymmetry patterns in ms^{-1} in MOTROT-VORT coordinates for slow moving (less than 2.5 ms^{-1}) and fast moving cyclones (speed greater than 7.5 ms^{-1}).

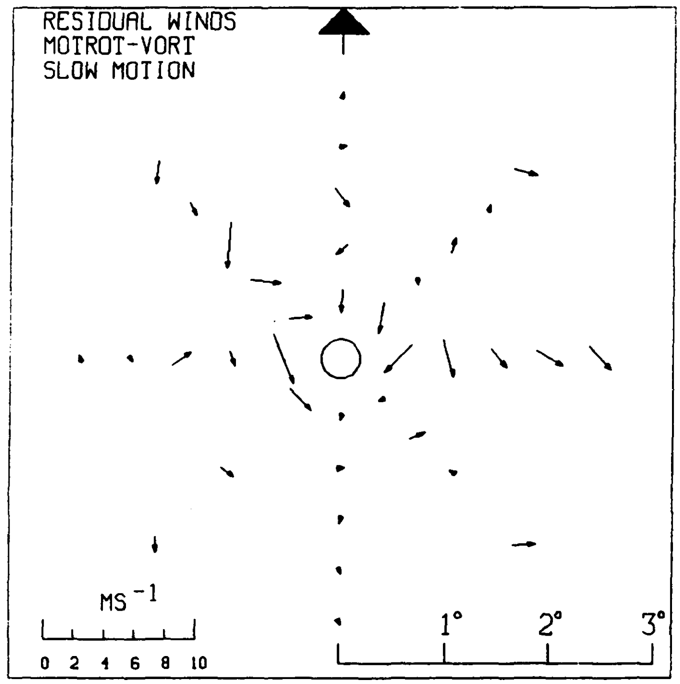

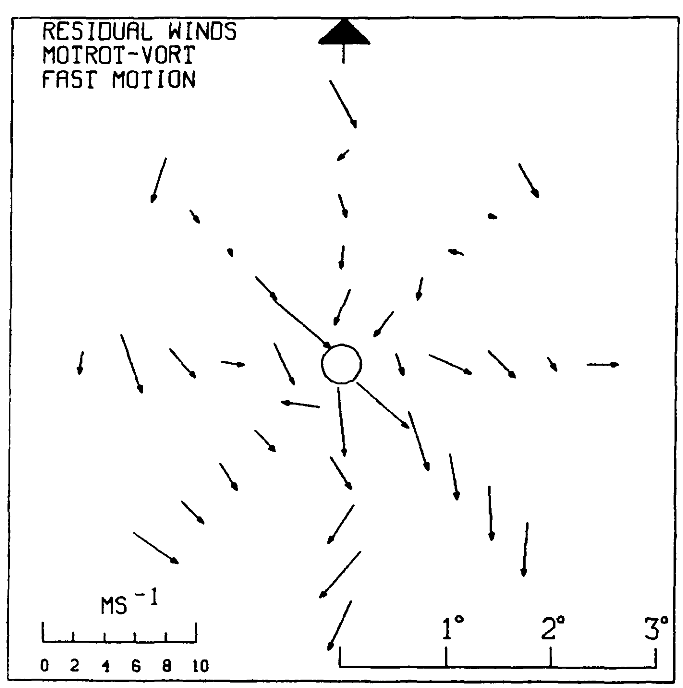

Figure 4.17: a-b. Plan-view analyses of the mean 700 mb residual wind field in MOTROT-VORT coordinates with the bold arrow denoting the mean cyclone motion heading. Values are in ms^{-1} with arrow length is proportional to wind speed with scale as shown in the lower left corner. The classes are a) slow moving cyclones (speed less than 2.5 ms^{-1}) and b) fast moving cyclones (speed greater than 7.5 ms^{-1}).

increasing storm intensity. However, this shielding effect was not total, but increased rather gradually with both increasing intensity and strength.

A vortex which is not fully shielded from its larger scale steering current will entrain air with the lower potential temperatures characteristic of the outer, low-level regions. This continual low-level ventilation implies that the composition of the environment into which the cyclone is moving is likely to be intimately related to its future intensity potential.

Chapter 5

THE LIFE CYCLE OF THE TROPICAL CYCLONE

If tropical cyclones are carefully followed throughout their life cycle, distinct patterns of development and decay can be observed. These patterns of change can assist the forecaster in predicting the future of a tropical cyclone's wind field. Therefore, the focus of this chapter is to describe the typical life cycle of tropical cyclones so that their changing wind fields can be better understood and forecast.

Changes occur most rapidly near the center of a tropical cyclone, as in the case of Supertyphoon Forrest (1983), which exhibited a MSLP drop of 92 mb in one day. However, wind changes well away from the center can also be important as shown by Weatherford and Gray (1988b) who describe the damaging wind radius of Typhoon Owen (25 ms^{-1}) which expanded 188 km in a twelve-hour period.

The tropical cyclone's life cycle is traditionally defined by the time variation of its central pressure. Typically, central pressure falls slowly during the depression and tropical storm stages but intensifies rapidly through the typhoon stage. Steady state periods have been observed to occur throughout the deepening and filling process and are more likely to occur in weaker cyclones. Of the nearly 800 missions included in this data set, 44 percent were intensifying cyclones, 33 percent were steady state systems and 23 percent were filling systems. Whereas the intensification period was typically prolonged, the filling process was often swift, especially if the cyclone moved over land or took on extra-tropical characteristics.

5.1 Stages of Intensity

Typhoons undergo changes of intensity in several different ways. Some intensify slowly while others do so very rapidly. Some reach supertyphoon intensity and remain there for days (Fig. 5.1) while others only briefly touch on such intensities before weakening (Fig. 5.2). In order to more clearly describe these trends and isolate their characteristic patterns, we decompose the cyclone life cycle into five distinct stages as shown in Fig. 5.3.

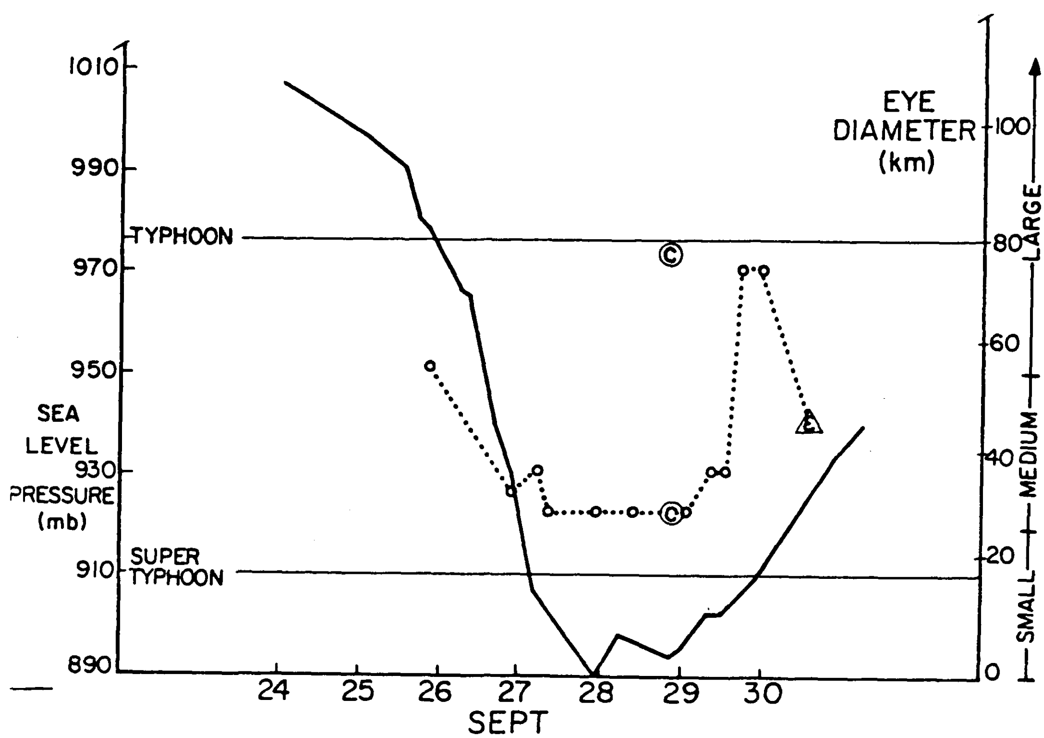

Figure 5.1: The evolution of the central pressure (solid line) and eye diameter (dashed line) in Supertyphoon Elsie. More information for the interpretation of this figure is provided in Appendix A.

Those tropical cyclones that achieved considerable intensity and resided over water throughout their lifetime exhibit all five of the major stages common to the life cycle of tropical cyclones. Twenty-nine such typhoons which intensified below 930 mb and displayed complete life cycles were chosen for study. Particular attention was directed to excluding cyclones making landfall so that the effects of diminished moisture supply

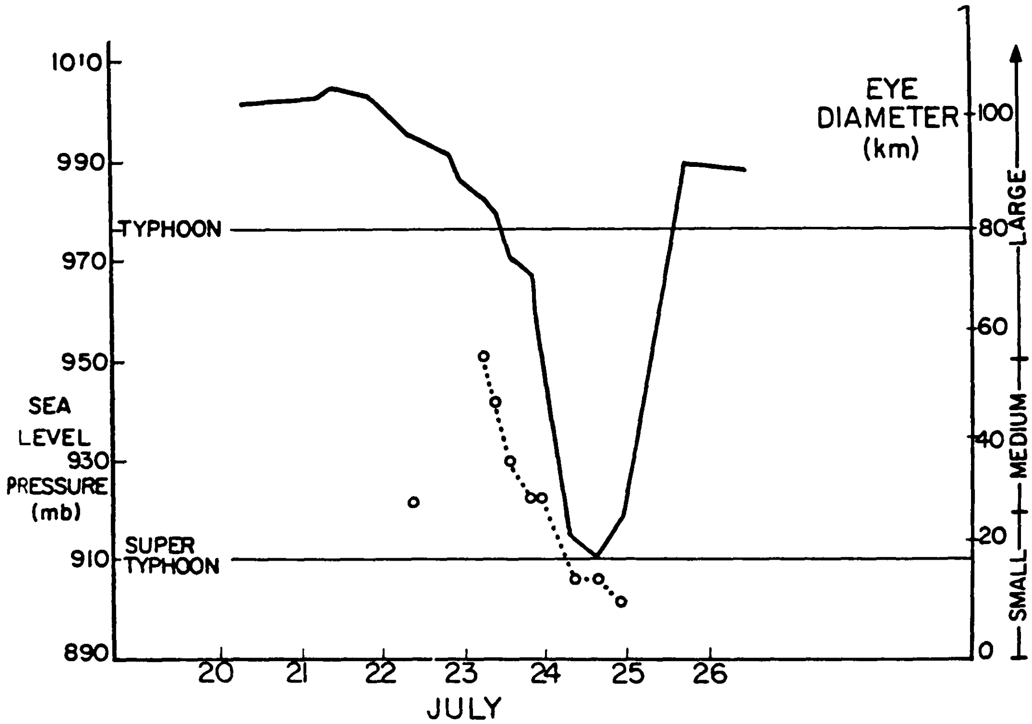

Figure 5.2: The evolution of the central pressure (solid line) and eye diameter (dashed) in Supertyphoon Kim.

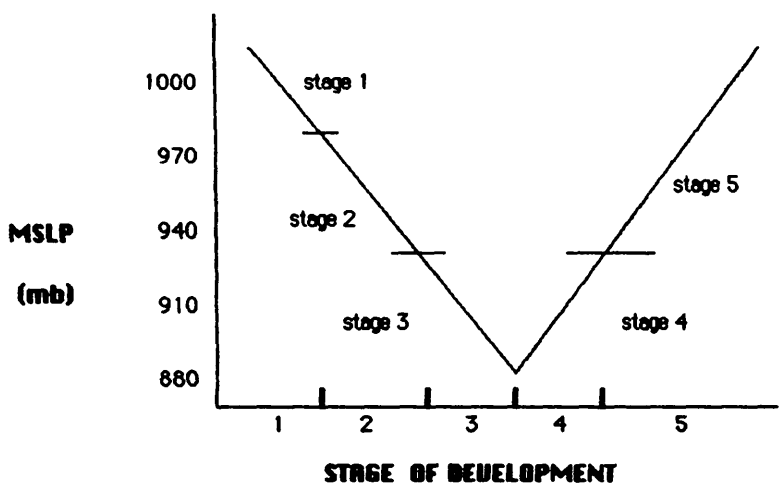

Figure 5.3: Conceptual rendering of the five-stage life cycle of a tropical cyclone. Rates of intensification are not drawn to scale.

and increased friction would not alter the results. The five typical life cycle stages are as follows:

STAGE	MSLP RANGE	NO. OF MISSIONS
1 - INTENSIFYING TROPICAL STORM	998 - 976 mb	102
2 - INTENSIFYING LEAST TYPHOON	976 - 930 mb	97
3 - INTENSIFYING INTENSE TYPHOON	930 - 870 mb	49
4 - FILLING INTENSE TYPHOON	870 - 930 mb	57
5 - FILLING LEAST TYPHOON	930 - 976 mb	68

A characteristic sequence of changes was observed to occur as tropical cyclones intensify. As indicated in Table 5.1, tropical cyclones generally move northwestward as they intensify, then recurve to the east and fill. Notice how these intense typhoons gain intensity rather quickly but (barring landfall) fill much more slowly. Notice also that typhoons in Stage 3 were, on average, deepening at an average rate of $42mb\ d^{-1}$, while in Stage 4, they were filling at a rate of about $14mb\ d^{-1}$.

Appendix A shows details of the time variation of MSLP, 700 mb OCS, eye temperature, and radar eye diameters for the life cycles of 47 cyclones. One can see from these life cycle data that those cyclones which attain maximum intensity values below 930 mb, did so in a comparatively rapid fashion. These data reinforce the observation by Holliday and Thompson (1979) that gradual deepening to extreme intensities is rare. Cyclones which did not reach MSLP values of 930 mb, and were thus not included in this subset, showed much slower rates of intensification during their typhoon stage. Because the cyclones which were included in this subset were required to attain MSLP's of 930 mb, the values for Stages 1 through 5 in Table 5.1 are biased toward rapid deepeners. Because changes occurred so rapidly in this sample, the MSLP change of Table 5.1 was given for 12-hour rather than full-day increments. This shorter time interval served the purpose of better associating changes of MSLP with changes of the Outer Core Wind Strength (OCS).

The greatest OCS values occurred during the filling (Stages 4 or 5), rather than during the stage of greatest intensity (Stage 3). Notice the much higher MSLP in Stage 5 (959 mb) than in Stage 3 (914 mb) for the same average OCS; however, the ratio of the maximum wind to the OCS is 2.4 in Stage 3 but only 1.6 in Stage 5. This difference implies that during intensification, inner core maximum winds increase at a faster rate than do winds in the outer core.

Table 5.1: Averages of latitude, longitude, cyclone heading and speed of motion, MSLP and its change, and OCS for each life cycle stage.

STAGE	LAT.	LONG.	HEAD	SPEED ms^{-1}	MSLP mb	MSLP CHANGE mb/12 hr	MAX WIND ms^{-1}	OCS ms^{-1}
1	13°	143°	290°	5	989	- 5	22	14
2	16°	137°	305°	5	955	-11	41	20
3	17°	134°	310°	5	914	-23	56	23
4	21°	132°	335°	5	922	+ 7	52	27
5	24°	132°	345°	6	959	+10	39	23

5.1.1 Azimuthally-averaged properties

Changes in the tangential wind profile from the center out to 3° as the cyclone passes through the stages of its life cycle are shown in Fig. 5.4. Although cyclones begin their intensification (Stage 1) with a rather flat horizontal wind profile, inner core winds intensify more rapidly than outer core winds through Stages 2 and 3. During Stage 4 filling, inner core winds decrease rapidly while outer core winds continue to strengthen. In Stage 5, the entire wind field decreases with the inner core decreasing more rapidly than the outer core. This cycle results in a relatively flat Stage 5 wind profile, albeit at a much higher outer-core wind strength than in Stage 1. These observations show that the radius of gale force winds is much greater during the filling stage than in the deepening stage for cyclones with the same MSLP.

Figure 5.5 shows that relative vorticity remains concentrated near the center during all stages of development, despite large variations in OCS. Nevertheless, in the 1 to 2° radius region, vorticity values in Stage 5 are nearly double those of the more intense Stage 3. Notice also that the outer core vorticity fields are nearly equal for the three intensifying Stages (1, 2, and 3), but become much larger during the filling Stages (4 and 5). Because the vorticity provides the dominant contribution to inertial stability, the outer core is only

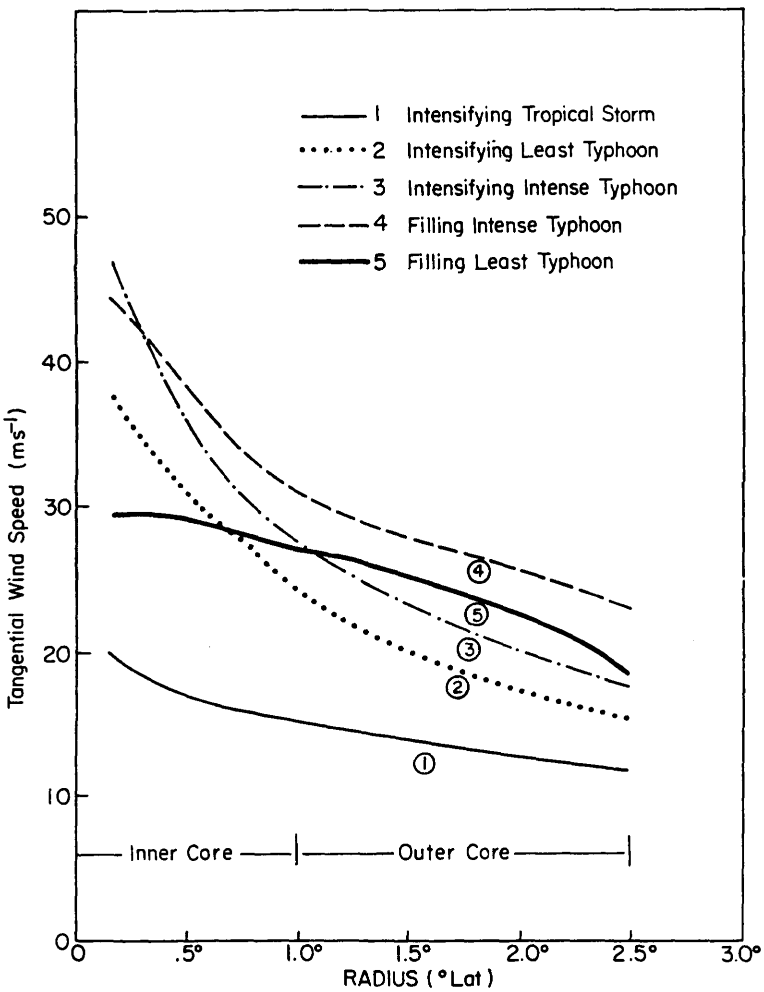

Figure 5.4: Radial profile of average 700 mb tangential wind fields for the five stages of a tropical cyclone's life cycle.

slightly more resistant to radial motions in the intense Stage 3 than in the earlier Stage 1. However, the inertial stability of the outer core is generally twice as great in Stage 4 as in Stage 3, even though MSLP and maximum winds have diminished. Following inertial stability arguments, it may be assumed that radial inflow is less able to penetrate into the cyclone's inner core during Stage 4 than during Stage 3. Consequently, the cyclone in Stage 4 becomes less intense and inflow is forced upward at larger radii during the decaying state.

The moisture fields for these five life cycle stages have also been examined. As outer core winds increase, outer core convection should also increase resulting in increased moisture in the 700 mb outer-core. Figure 5.6 shows that relative humidity values are highest during Stage 4 which also exhibits the strongest outer core wind field (Table 5.1), even though the central pressures are filling.

5.1.2 Residual Core Wind Field by Cyclone Stage

Cyclones undergoing rapid intensity changes distort the residual wind field far more than the relatively steady state cases shown in the previous chapters. Figures 5.7a-e show the interior background wind field (MOTROT–VORT) for each of the five stages of the cyclone's life cycle. Apparently, the cyclone forms from the inside out, interacting with its environment as it forms. The residual wind field shows progressively greater distortion with each stage. In Stage 1 (Fig. 5.7a) the environment is seen to flow from the front-left to the right-back and is relatively undistorted by the vortex except that less of the 700 mb current exits than enters the storm area (evidently retained in the intensifying inner core). However, as the storm intensified, a clear channel from the higher θ_e of the equator appeared (see stages 2, 3, and 4).

5.2 Variations of Tangential Wind Profiles

The tangential wind fields of tropical cyclones generally follow three basic patterns of change which are shown in Table 5.2 and in Fig. 5.8. Phase 1 in Fig. 5.8 is the intensification period during which winds of both the inner and outer cores gather momentum.

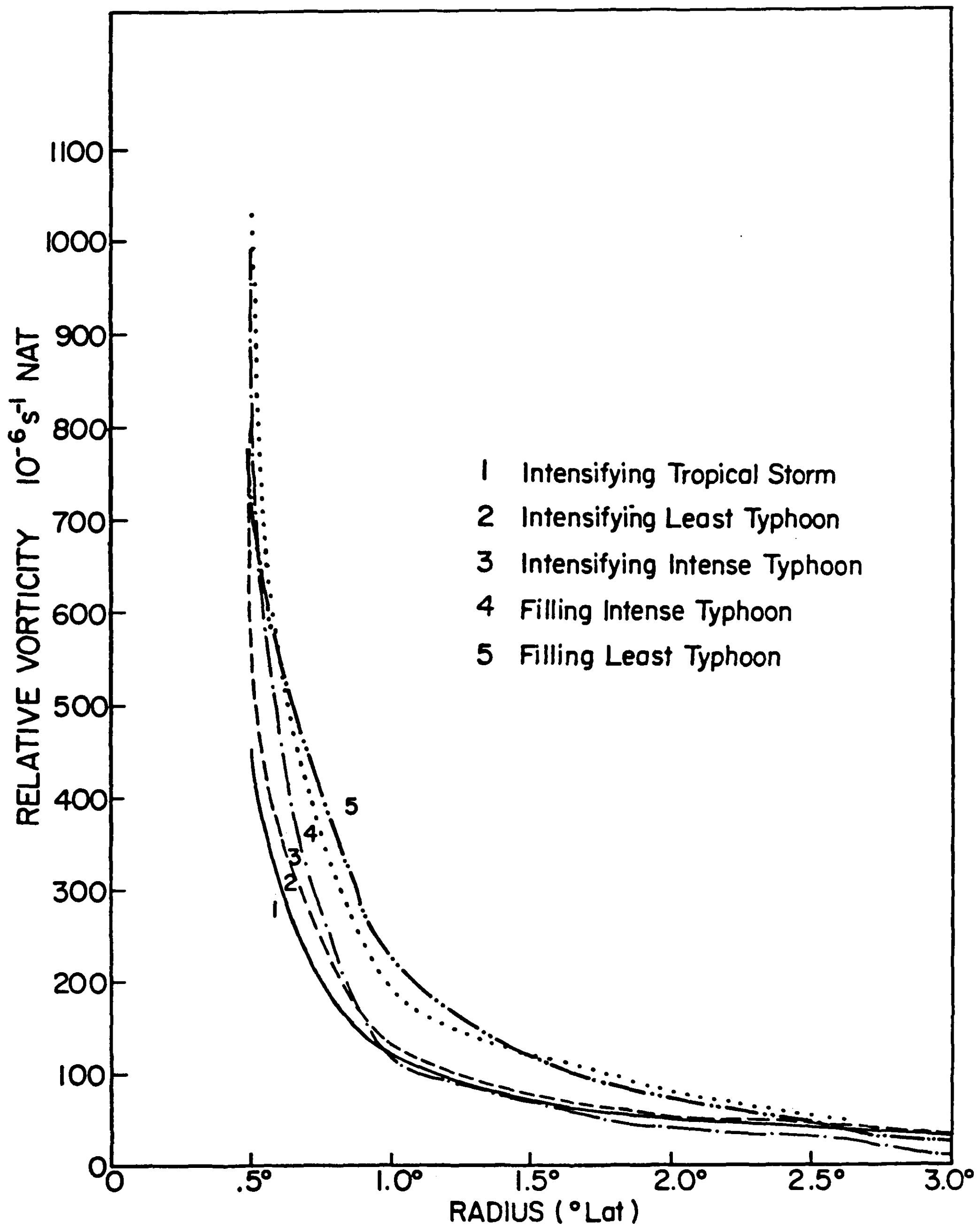

Figure 5.5: Radial profiles of vorticity fields at 700 mb for the five stages of a tropical cyclone's life cycle.

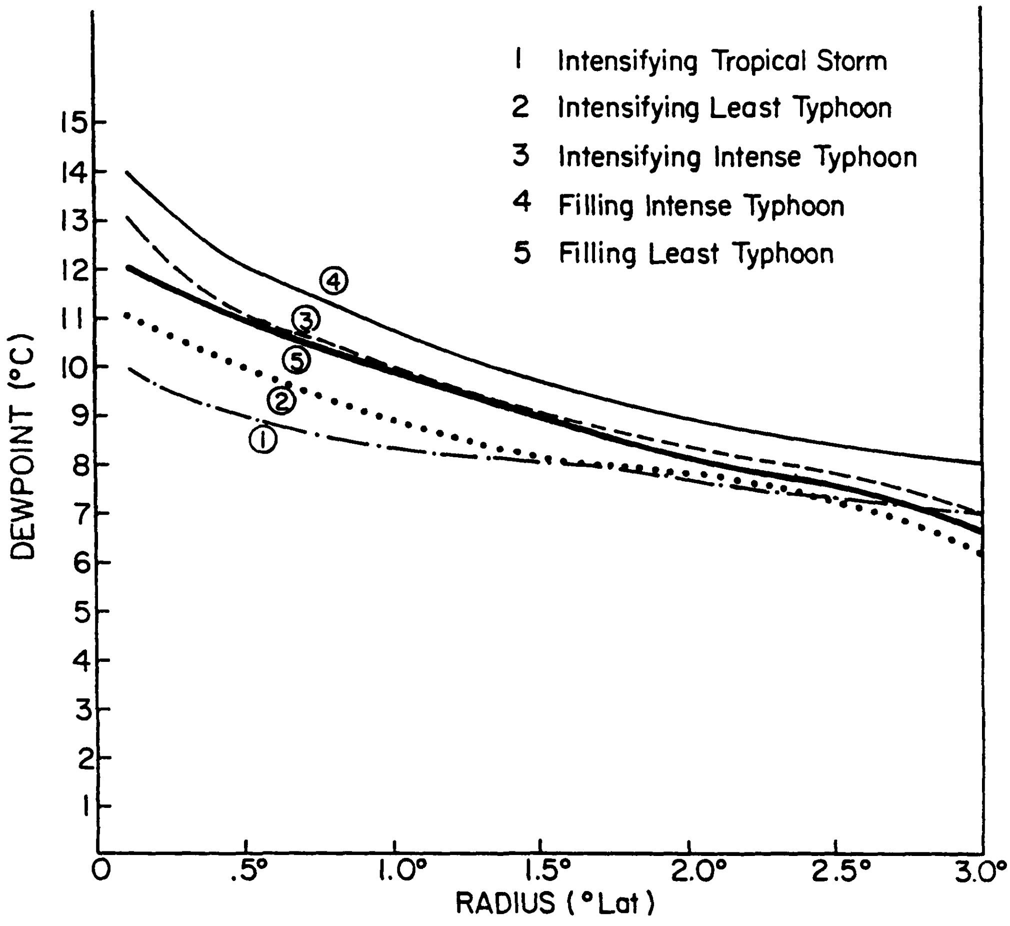

Figure 5.6: Radial profiles of the mean dewpoint temperature field at 700 mb for the five stages of a tropical cyclone's life cycle.

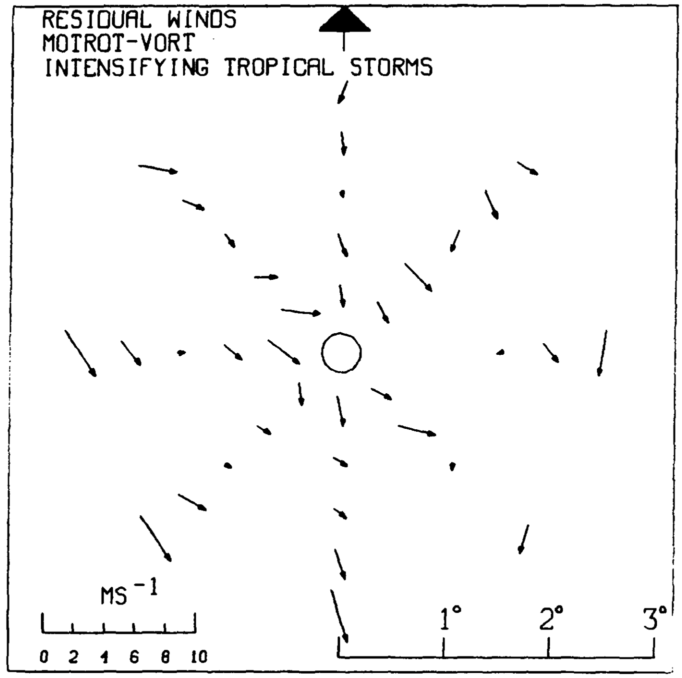

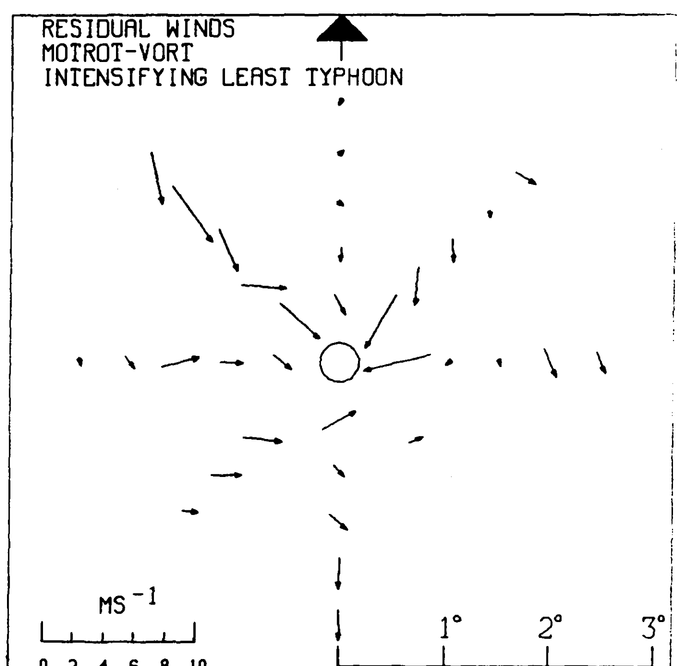

Figure 5.7: a-e. Plan-view analyses of the mean 700 mb residual wind field or MOTROT-VORT wind stratified for the five phase cyclone life cycle. The arrow on the rim denotes the cyclone heading. Values are in ms^{-1} with arrow length specifying speed as shown in the lower left corner.

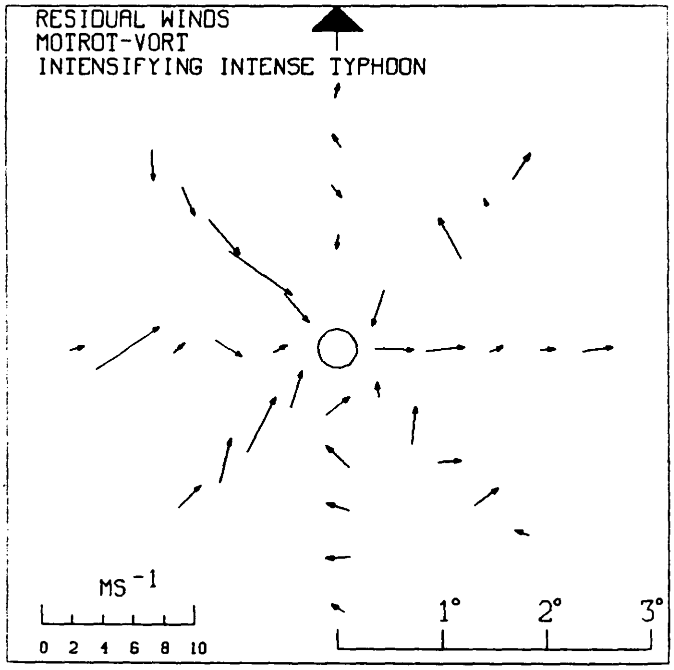

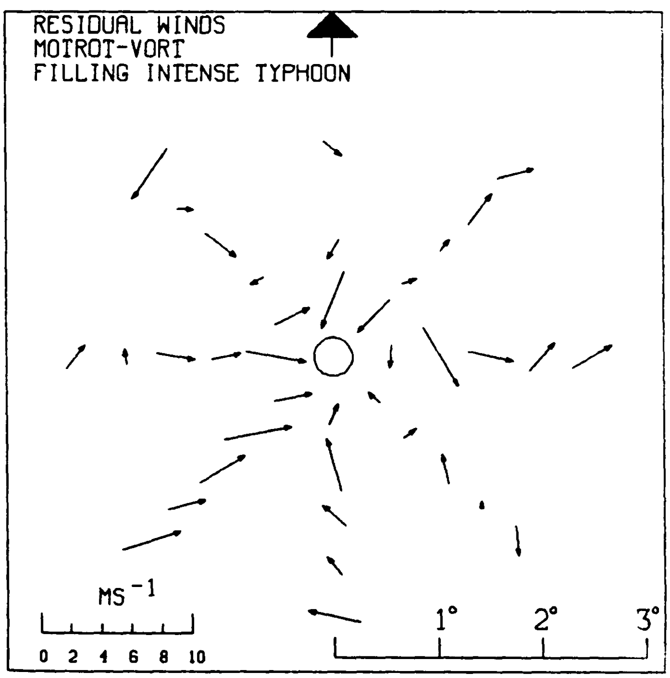

Figure 5.7: a-e. Continued.

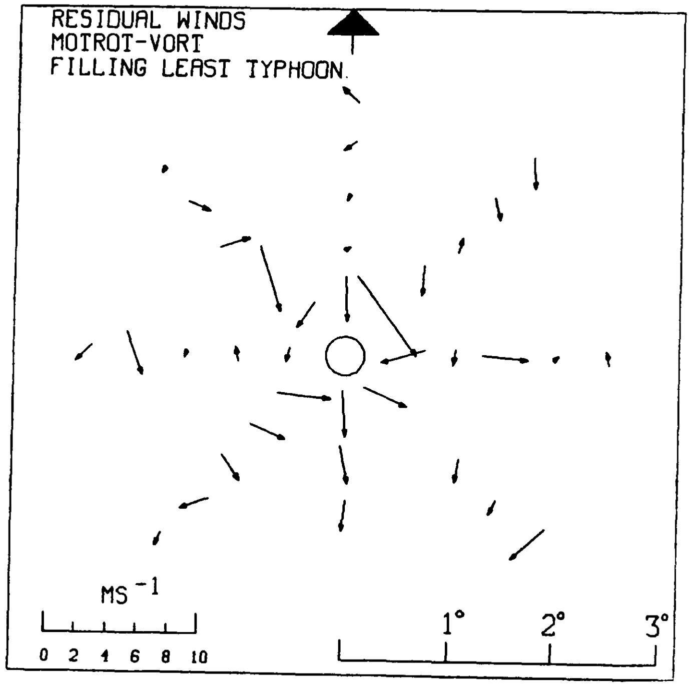

Figure 5.7: a-e. Continued.

It was observed that maximum winds in the inner core increased at an average rate of 7.5 ms^{-1}/d as opposed to outer core winds which increased at 2.5 ms^{-1}/d. Evidently, the vortex concentrates momentum close to the center during this intensifying phase. Although the average changes shown in Fig. 5.8 typically occurred over a period of four days, shorter-term changes were quite variable. Weatherford and Gray (1988b), for example noted that over a period of 12 hours, outer core winds might remain unchanged while inner core winds increase rapidly. Subsequently, the outer core winds were generally observed to follow the inner core by strengthening as well.

Once a cyclone passes maximum intensity and begins to fill, it may enter phase 2 or, it may go directly to phase 3. In the former, phase 2 case, the outer core continues to strengthen at the same rate of 2.5 ms^{-1} while the inner core weakens somewhat. If the cyclone progresses immediately to phase 3, the outer core weakens in conjunction with the inner core. Notice from Fig. 5.9 that the later the phase, the less penetration of the center by the radial inflow.

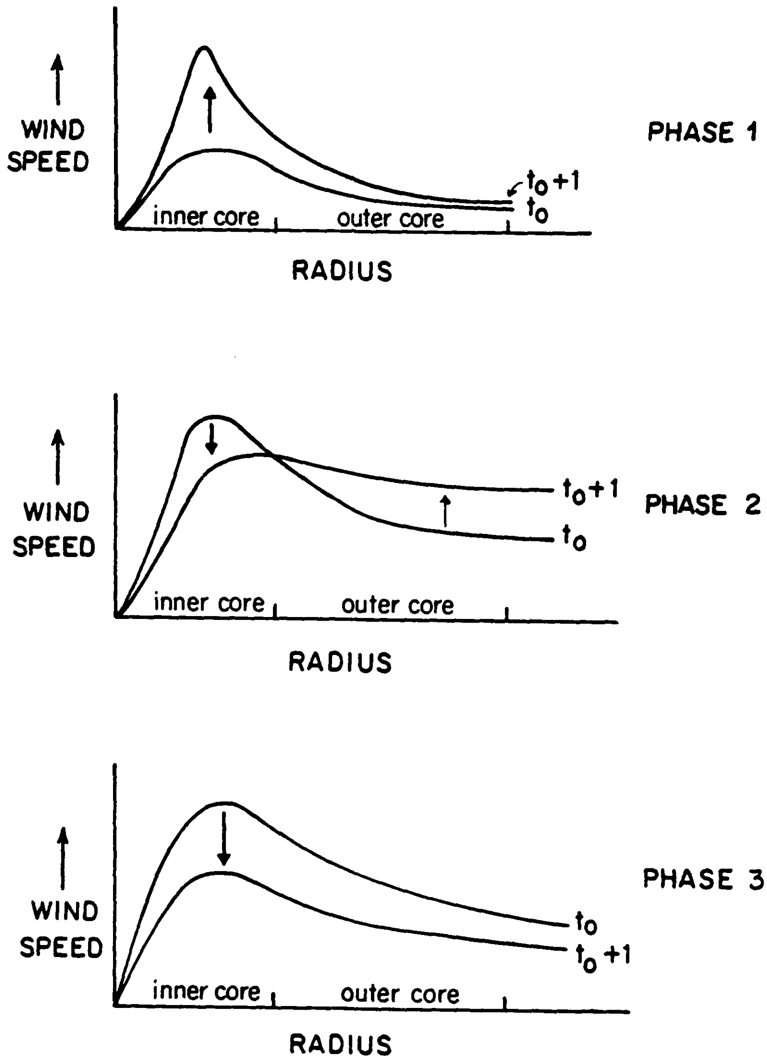

Figure 5.8: Schematic of the three phase life cycle of cyclone wind profiles: In phase 1 the inner core intensifies as the outer core strengthens; phase 2, inner core fills as the outer core strengthens; phase 3, the inner core fills as the outer core weakens.

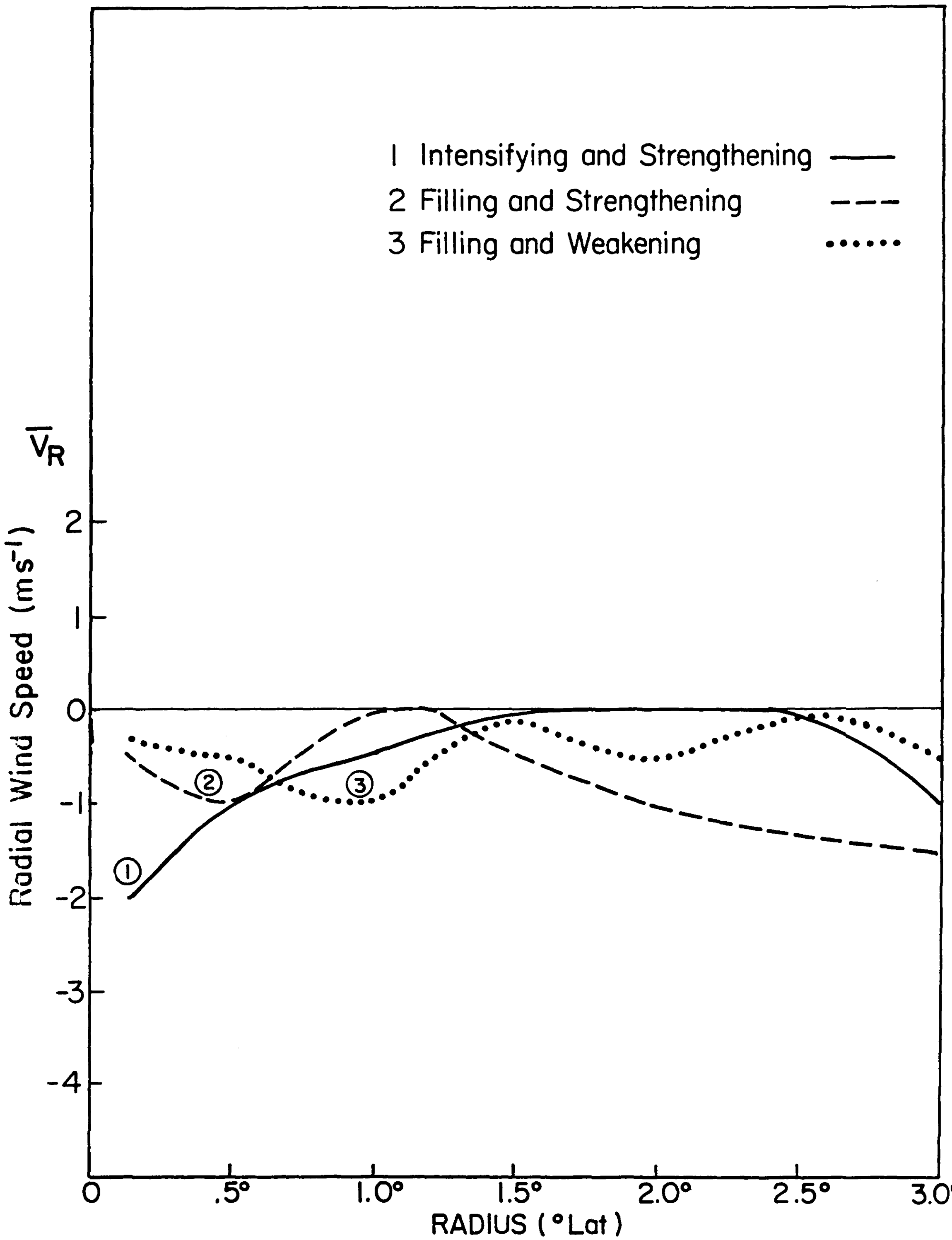

Figure 5.9: Radial profiles of azimuthally-averaged radial wind profiles for the three typical cyclone life cycles.

Table 5.2: Average positions, cyclone headings and speeds, MSLP, MSLP 24-hour changes, maximum wind speeds, and outer core strengths for three phase life cycle wherein 1 = intensifying and strengthening, 2 = filling and strengthening, 3 = filling and weakening.

PHASE	LAT.	LONG.	HEAD	SPEED ms^{-1}	MSLP mb	MSLP CHANGE mb/12 hr	MAX WIND ms^{-1}	OCS ms^{-1}
1	17°	136°	310°	5	953	-23	40	20
2	20°	135°	335°	5	939	+14	44	25
3	21°	133°	330°	5	967	+17	34	19

Generally, phase 1 was observed to last an average of four days while phase 2 lasted just one day and phase 3 lasted an average of two days. Some cyclones reached multiple MSLP maxima, as in the case of Supertyphoon Abby (see Appendix A). There appears to be a MSLP cutoff of 955 mb which governs whether a filling cyclone will begin to weaken (phase 3) or continue to strengthen (phase 2). It was also observed that the faster a cyclone fills, the lower the MSLP at which the outer core begins to weaken. As will be covered in the next chapter, this latter association correlates well with the disappearance of the eye.

A fourth theoretically possible wind profile phase can occur wherein the inner core intensifies at the expense of the outer core; a situation wherein the cyclone is simultaneously intensifying and weakening. No cases with this type of change were observed except for those storms whose outer cores had moved over land. In these cases, increased surface friction weakened the outer core while the center briefly intensified. Supertyphoon Kim exhibited this effect when its center intensified to 909 mb while its outer core was over Luzon Island. Although this fourth type of change has been discounted for the developed cyclone, the cases studied here did not address the question of genesis for which this fourth type of change may be a possibility.

5.3 Comparative Properties of Deepening versus Filling Cyclones

Useful comparisons can be made between the 700 mb wind fields of cyclones which are in the process of intensifying versus cyclones which are filling. To isolate the differences between these deepeners and fillers, two subsets of 235 missions each were chosen. These two sets of mission data bore the same average MSLP so that the observed difference would not necessarily be due to differences of intensity. Table 5.3 lists the average characteristics for each set. The most notable difference in these values is the stronger OCS of the filling systems. This difference was not due to an expansion of the radius of maximum wind since the average eyewall diameters of both classes was 40 km. Figure 5.10 shows the increased OCS extending from near the center to 3°. Note also in Fig. 5.10 that the wind curves in this figure cross over near the center of the cyclone with the intensifying systems having the higher maximum winds. In Fig. 5.11, there is nearly 50 percent more relative vorticity at 2° radius in the filling systems as in the intensifying systems. Following inertial stability arguments, there will be more resistence to inflow at this level for filling cyclones due to their stronger outer core structure, as can be seen in Fig. 5.12. Given the same central pressure, the stronger outer core of the filling cyclones exerted twice the inertial stiffness as the deepeners. High levels of inertial stability prevent low-level momentum from reaching the inner core of filling systems by restricting the inner radius to which inflow can penetrate. As shown in Fig. 5.13, there is approximately 50 percent more Kinetic Energy in the outer core of filling systems, implying greater momentum loss due to friction and greater outer core damage potential for filling versus intensifying cyclones. There is also more likely to be rain in the outer core of a cyclone that is past its maximum intensity.

It appears that intensifying tropical cyclones sow the seeds of their own subsequent weakening by gradually building up outer core circulations which then inhibit inflow from reaching the region of highest convective efficiency in the inner core. Notice in Fig. 5.14 that once the OCS value passes a threshold of approximately 20 ms^{-1}, it becomes less likely that rapid inner core pressure drop will continue. As a result of these effects we do not see typhoons attain intensities much below 870 mb, nor would we expect to.

The advective processes which concentrate energy in the inner core interact in a non-linear fashion and it is presumed that the faster they occur, the deeper the cyclone may

Table 5.3: Averages of position, cyclone motion, intensity, intensity change, and OCS for cases before and after minimum SLPA (maximum intensity).

± MAX INT.	LAT.	LONG.	HEAD	SPEED ms^{-1}	MSLP mb	MSLP CHANGE $mb\, d^{-1}$	MAX WIND ms^{-1}	OCS ms^{-1}
Before Max	16°	137°	310°	5	956	-21	42	19
After Max	22°	133°	340°	5	956	+ 12	41	23

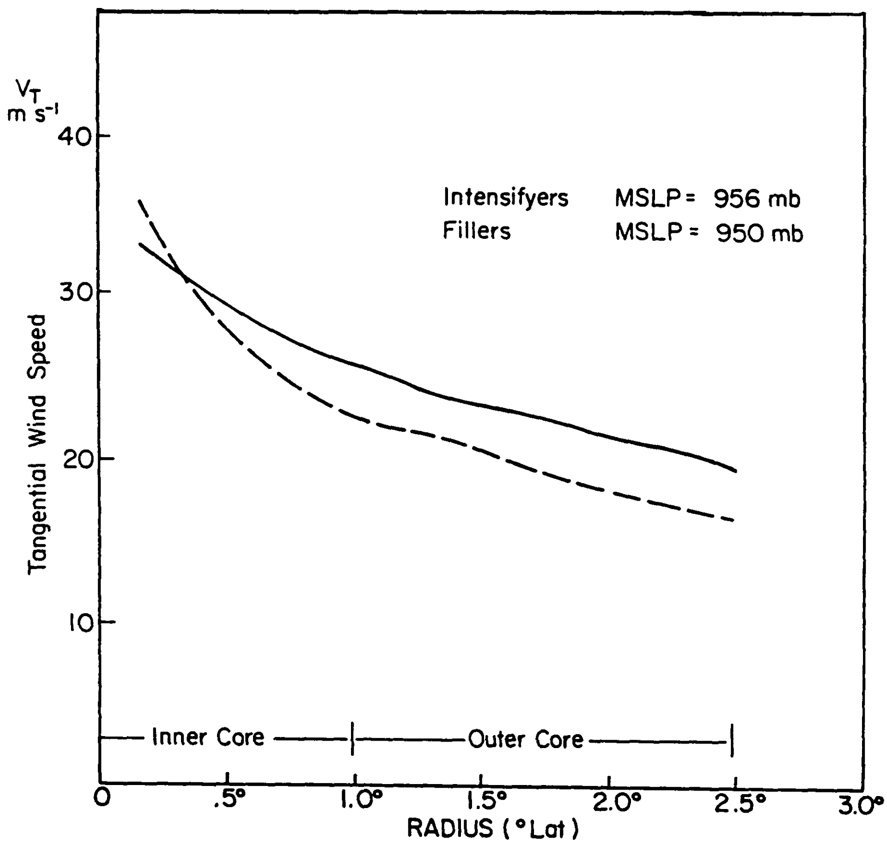

Figure 5.10: Radial profiles of azimuthally-averaged tangential winds for intensifying (dashed) and filling (solid) cyclones of the same MSLP.

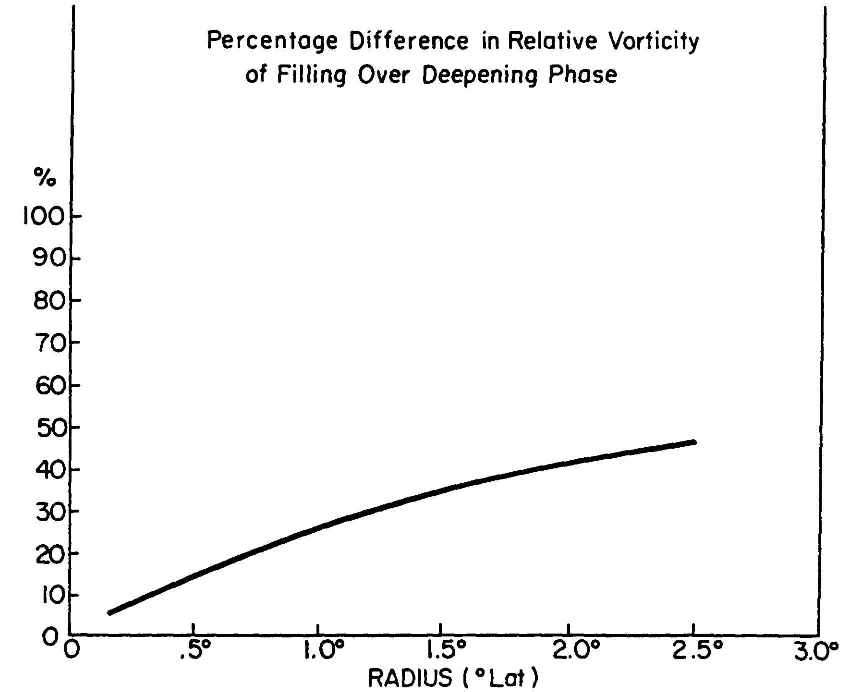

Figure 5.11: Radial profiles of the difference in percent between the relative vorticity fields of filling minus intensifying cyclones for the same mean MSLP of 956 mb.

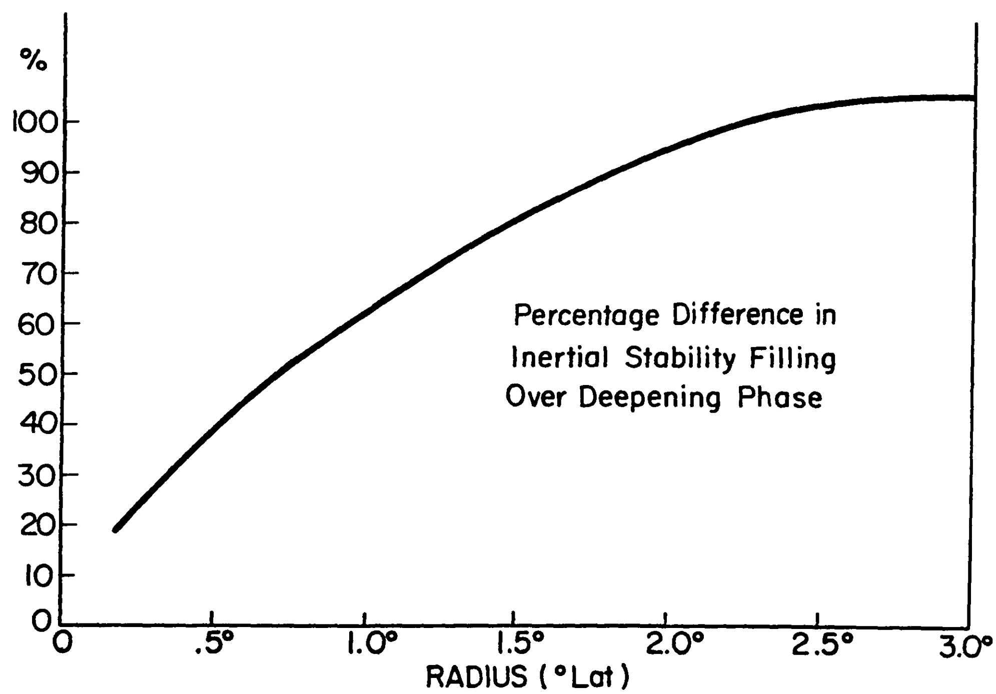

Figure 5.12: Radial profiles of the difference in percent between the inertial stability fields of filling minus intensifying cyclones of the same mean MSLP of 956 mb.

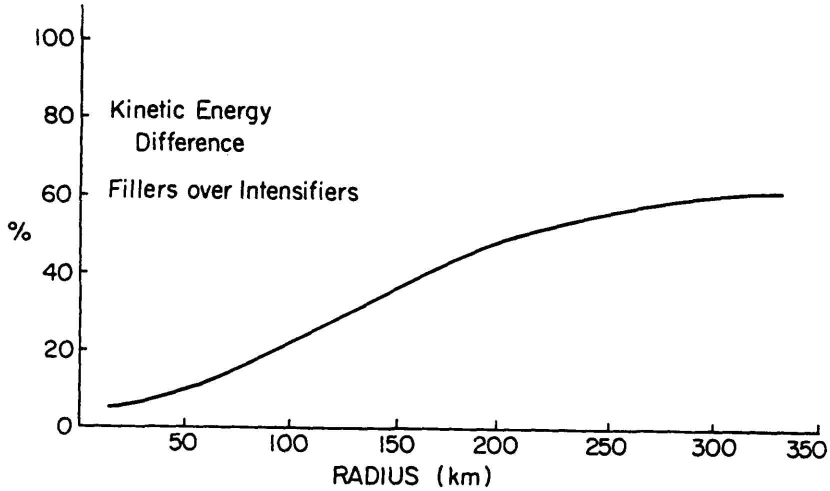

Figure 5.13: Radial profile of the difference in percent between the kinetic energy fields of filling minus intensifying of the same mean MSLP of 956 mb.

become. The rate at which a cyclone can intensify varies significantly from cyclone to cyclone and is the focus of the next section.

5.4 Differences Between Rapid versus Slowly Deepening Cyclones

"Rapid deepeners" were defined by Holliday and Thompson (1979) as cyclones undergoing a rate of intensification of 42 mb per day or greater. This exceptional rate of intensification was observed in roughly 15 percent of the cyclones in the northwestern Pacific. Improved knowledge of the circumstances that preceded these exceptional rates of intensification is quite important to the forecaster. For example, Supertyphoon Forrest of 1983 was a tropical storm one day and a supertyphoon the next; nearly tripling the intensity of its maximum winds in 24 hours. By contrast, "slow deepeners" as defined here, intensify at less than 9 mb per day.

Significant differences were observed for the averaged properties of storms in these two deepening rate classes. Table 5.4 lists the average of position, motion, intensity, and OCS for each class. There were 20 cyclones which were observed to deepen rapidly, providing 81 missions for analysis. Slow deepeners were more abundant, affording 200 missions. The most notable difference in the data in Table 5.4 is that rapid deepeners tended to occur farther south and had a more westerly heading than their slowly deepening counterparts.

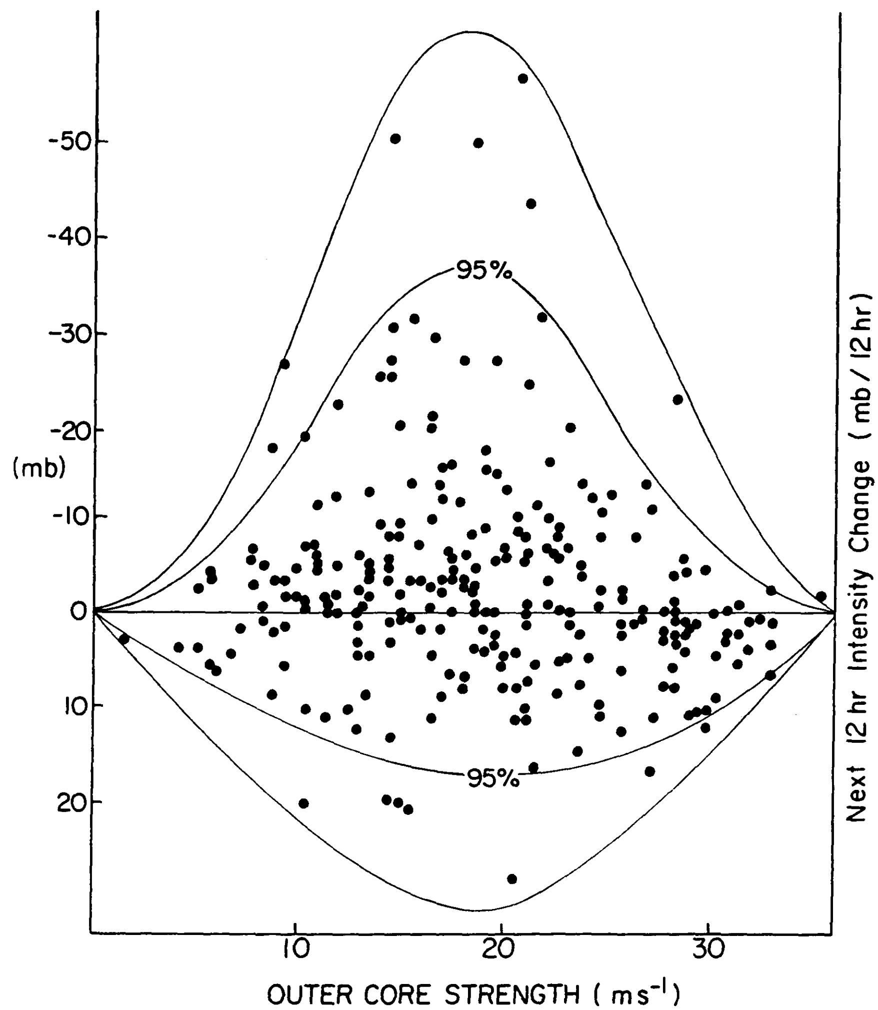

Figure 5.14: Scatter diagram showing the relationship between OCS and intensity change during the subsequent twelve hours.

It is also important to note the large difference in mean MSLP occurring for the same average OCS value. The relationship between MSLP and OCS for both classes is shown in Fig. 5.15.

Table 5.4: Averages of position, heading and speed of the cyclone center, MSLP, maximum wind and OCS for rapid and slow deepeners.

RATE OF INCREASE	LAT.	LONG.	HEAD	SPEED ms^{-1}	MSLP mb	MAX WIND ms^{-1}	OCS ms^{-1}
RAPID DEEPENING	15°	136°	303°	5	945	44	18
SLOW DEEPENING	19°	137°	320°	5	971	31	18

Differences in the maximum wind relative to the OCS may be the key to distinguishing between these two cases. For rapid deepeners, the OCS value was 40 percent of the maximum wind speed, whereas for slow deepeners the OCS to maximum wind ratio was approximately 60 percent. The inner-core wind field of the rapid deepeners was also observed to increase more rapidly near the center than did that of the slow deepeners. Outer core winds of both classes strengthened at about the same rate. Apparently, as shown in Fig. 5.15, the inner core processes of rapid deepeners concentrate momentum more effectively than in the slow deepeners. Another clue for detecting rapid deepeners during the tropical storm stage lies with the appearance of its eye which is examined in detail in the next chapter.

5.5 Discussion

Wind profiles of tropical cyclones typically follow a three phase sequence of changes during their life cycle. Phase 1 is the intensification phase in which the wind field gathers momentum and strengthens from the center out to 3° radius. The inner core is observed to increase at a more rapid rate than the outer core as the cyclone concentrates its momentum near the center. There is no evidence of outer core weakening while the inner

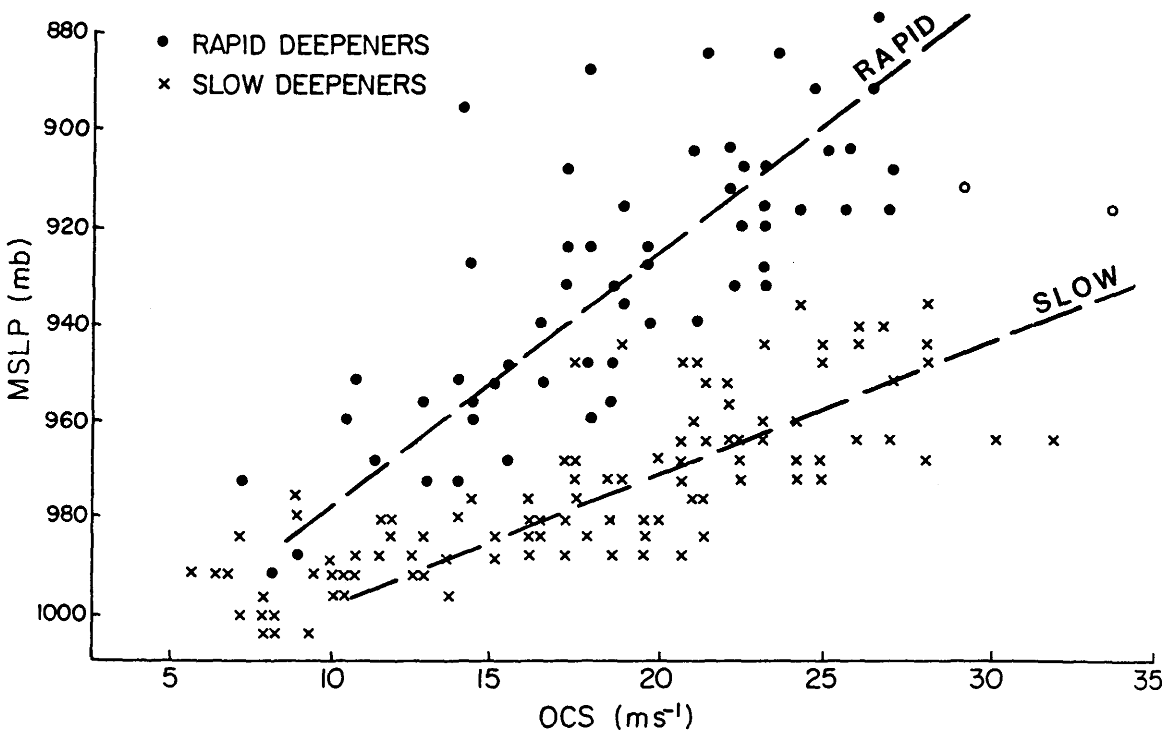

Figure 5.15: Scatter diagram of intensity (MSLP) versus OCS for rapid deepeners (denoted by circles and defined as an MSLP drop of $42mb\ d^{-1}$) and for slow deepeners (denoted by X's and defined as an MSLP drop of less than $10mb\ d^{-1}$).

core intensifies. Once past maximum intensity, the cyclone's center begins to fill while outer core winds may either continue to increase (generally for typhoons of MSLP lower than 955 mb), or begin to decrease (typically cyclones with MSLP higher than 955 mb).

There is cause to suspect that a strong outer core may restrain internal changes of the cyclone's inner core. Willoughby (1979), Schubert and Hack (1982), and Shapiro and Willoughby (1982) have applied Elliasen's (1951) balanced vortex model to hurricanes in order to relate the effects of inertial stability on intensity change. Holland and Merrill (1984) applied these results to observations of Australian region cyclones and observed that the strength of the low-level wind flow has a definite constraining effect on further intensity changes. Since it is inner core convection which must be energized in order to efficiently convert latent heat energy into kinetic energy for futher intensification (Hack and Schubert, 1986), this outer core constraint on the inner core is observed. Filling typhoons generally exhibited twice the outer core inertial stability of deepening typhoons with the same central pressures. This stability is likely to greatly inhibit momentum from reaching the region of greatest energy efficiency near the storm center and filling then commences. Since the behavior of the eyewall is a key factor in the intensification process, it is the focus of the next chapter.

Chapter 6

THE EYE AND THE WIND FIELD

The eye of the tropical cyclone is one of the most dramatic features seen by satellite, radar, or by direct observation. The most striking aspect of the eye includes multiple convective cells packed tightly together in a ring and delineated by a sharp clear region in the center.

It is the eye of the storm which immediately draws the attention of tropical forecasters, for in addition to being so vivid, it is within the eyewall itself that the typhoon's strongest winds are located. This is also where the energetics are most powerful, and where the author encountered the worst turbulence while flying through typhoons. Little has been done to document the basic features of the eye and its changes as typhoons develop and decay. Thus, the focus of this chapter is to describe the characteristics of the eye throughout the life cycle of the tropical cyclone and to relate these characteristics to other structural features of the cyclone.

6.1 Measurements of the Eye

During the five typhoon seasons of 1980-84 in which flights were made into 101 cyclones, 668 sets of eye observations were reported. Spot measurements were generally taken for two to three hours per mission with missions flown every 12 hours. Thus a nine to ten-hour data void period would usually precede the next sighting of an eye which prevented analyses of short-term fluctuations of time varying properties. The data did, however, allow general trends of eye size to be examined. Therefore, if a typhoon exhibited a continuous eye, it would normally be observed four times a day.

An eyewall was reported if it encompassed at least 50 percent of the center and was distinctly separate from spiralling feeder bands of convection. All measurements were taken by the on-board mission director who viewed the eye on an APN-59 3-cm radar from flight level. In this study, the flight level was usually 700 mb or roughly 3000 m, but occasionally, while in an early-stage tropical storm, observations were made as low as 300 m. Although only measurements of the 700 mb wind field are used in this study, those rare low-level missions in which an eye was observed were also used to obtain supplemental data on the life cycle of the eye. Objective measurements were made of the diameter(s) of the eye as depicted in Fig. 6.1. If the eye was circular, one diameter measurement was recorded; if concentric, two eye diameters were recorded; if elliptical the diameters across both the major and minor axes and their orientation were recorded.

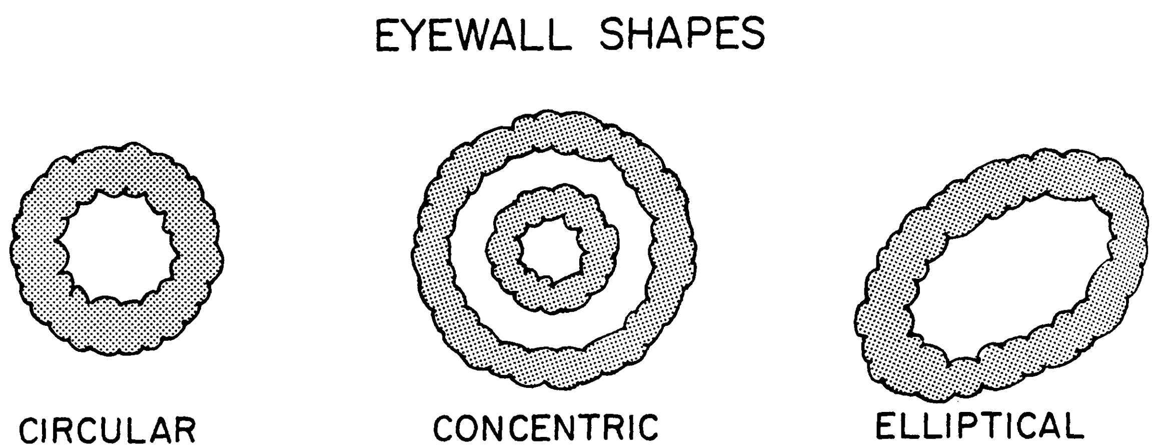

Figure 6.1: Schematic illustration of the three observed types of eyewalls.

In addition to recording the size of the eye, subjective observations were made of how much of the eye was encompassed by an eyewall, of the wall clouds appearance, density, thickness and its relative "stadium" or "fishbowl" aspect as illustrated in Fig. 6.2. The latter descriptions were obtained in only the most intense cases in which the inner region was cloud-free above the boundary layer due to powerful subsidence. In less intense cyclones, the area within the eye was often scattered with clouds which were too diffuse to be observed on radar but nevertheless inhibited observations of the eye. These clouds extended from the surface to the tropopause and rendered an obscured visual depiction.

Even in the most intense typhoons wherein the eye was clear above 1,500 meters, there were always clouds covering most of the surface. These clouds indicated that the subsidence did not penetrate through the boundary layer convergence, thereby allowing positive vertical forcing of the moist, near surface air.

After all eye reports were compiled, life cycle patterns of the eye were examined and compared with other structural features. The diameter of the eye varied from 7 to 220 km and averaged 42 km as shown in Fig. 6.3. In order to contrast differences between eyes of various sizes, observations were classified into four size groups; small eyes (0 to 28 km), medium eyes (28 to 55 km), large eyes (greater than 55 km) and cyclones exhibiting no eye. Cyclones over water exhibit an eye about 50 percent of the time with the greater probability of an eye associated with cyclones of greater intensity. The medium size eye class was defined so that it equally bounded the average observed diameter and comprised the class with the greatest number of sightings. Storms with significantly smaller or larger eyes were classified such that appreciable differences were observed between the mean sizes for each class. Results plotted in Fig. 6.3 show how eye size varies with intensity and how small eyes are observed in storms of all intensity values. The correlation between eye size and MSLP for the data shown in Fig. 6.3 is -0.09, signifying a definite lack of association.

6.2 The General Behavior of the Eye

The typical behavior of the eye followed a pattern of contracting as a cyclone intensified and expanding as the cyclone filled. This pattern has been alluded to previously by Jordan (1961) and will be examined in greater detail here. Although size fluctuations were observed on time scales of 3 to 12 hours, this general pattern was observed when the size of the eye was smoothed over time. A caveat that accompanies this observation is that small-scale fluctuations of short duration are to be expected and that if the eye has expanded in 3 hours, one cannot say with certainty that the central pressure has risen. Furthermore, for the most intense cyclones, there is a period of time during which the eye attains a certain minimum size, even though the central pressure continues to fall. Thus changes of eye size and MSLP do not necessarily occur simultaneously.

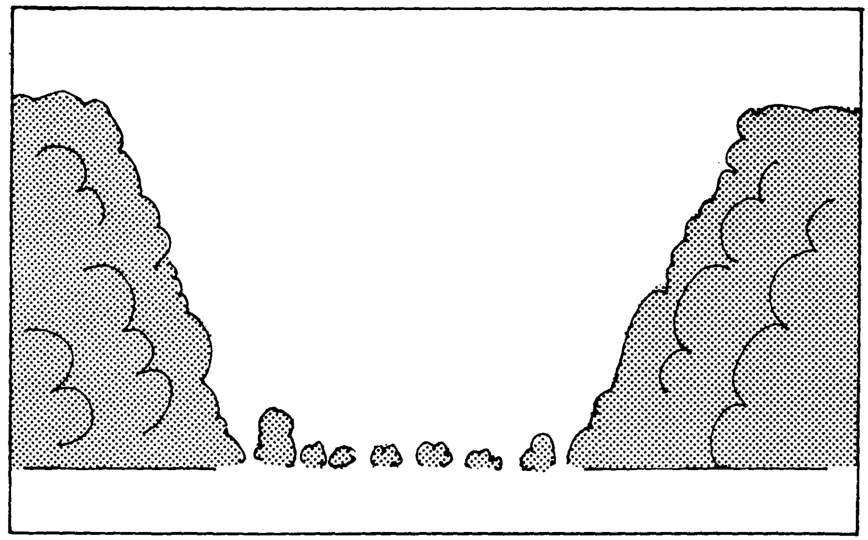

Stadium Effect

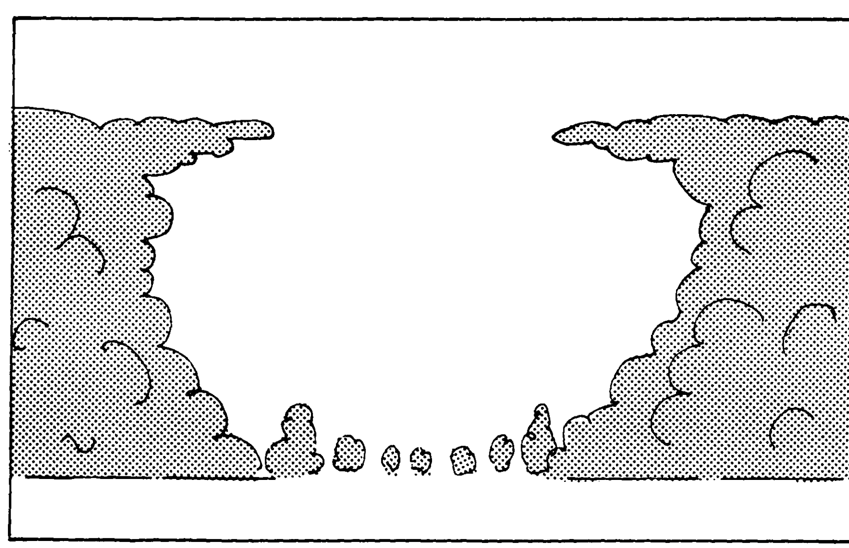

Fishbowl Effect

Figure 6.2: Schematic illustration of the stadium and fishbowl effects of the eyewall as viewed from the WC—130 aircraft.

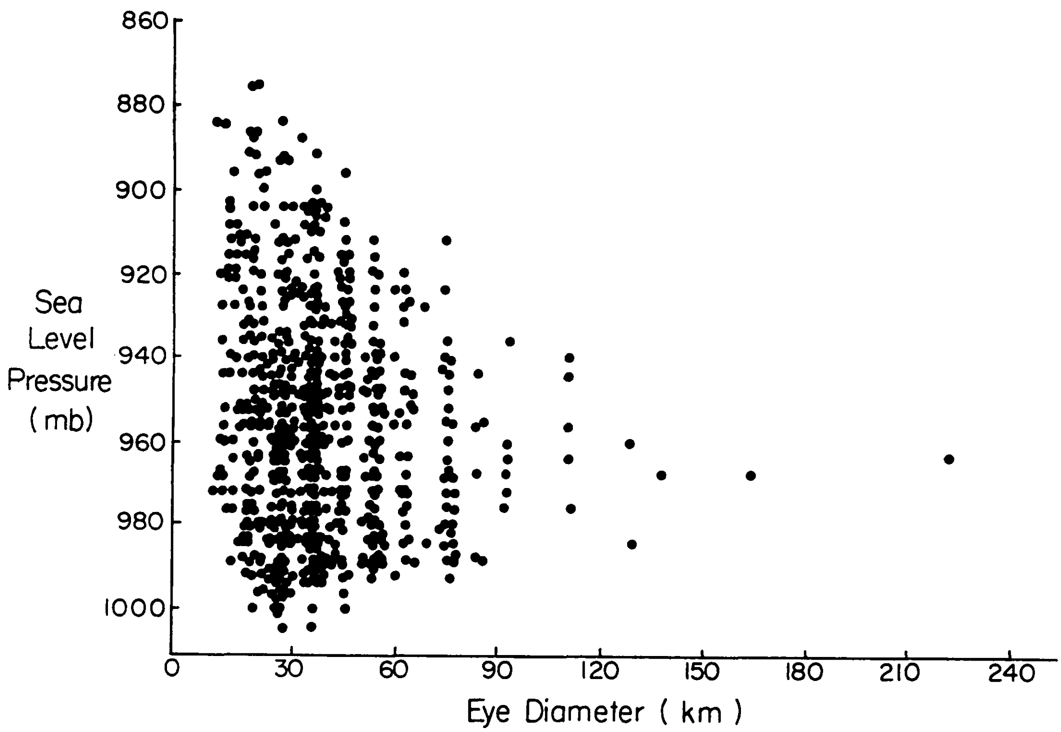

Figure 6.3: Scatter diagram of MSLP versus eye diameter.

Cyclic diurnal changes in eye diameter were not observed in the 700 mb aircraft radar data. Zehr (1987) has shown significant diurnal variations in the area of coldest cloud tops in the inner core of some of the cyclones used in this data set. Together these observations imply that changes in the strength of convection occur independently of changes in the 700 mb diameter of the eyewall in a diurnal sense.

6.3 The Initial Development of the Eye

Detailed observations of the circumstances attending the initial development of the eye have not been reported in the scientific literature. A number of important questions relating to the development of the eye need to be examined. Considerations include the developmental characteristics of eyes for rapid versus slowly deepening cyclones, the implications of concentric, circular and eliptical eyes and the circumstances relating to the disappearance of the eye.

Three-fourths of the cyclones examined in this study produced an eyewall. When an eyewall formed, the average initial appearance of the eye at 982 mb ($\pm$ 10 mb) paralleled the cyclones' approach to typhoon intensity. Cyclones in the northwestern Pacific are designated typhoons when their MSLP reaches 976 mb which, following Atkinson and Holliday (1977), is the pressure value associated with 64 kt surface winds (33 ms^{-1}). Cases which deviated significantly from the average include Typhoon Ellen of 1983 which developed an eye at an intensity of 1000 mb, while at the opposite extreme, Typhoon Betty of 1980 which did not obtain an eye until its MSLP reached 951 mb. It is interesting to note that Ellen's initial eye was small while Betty's was comparatively large. This apparent dependence of the initial size of the eye on the MSLP at which it first appears seemed to be a common feature in all cases (Table 6.1).

Table 6.1: Average and standard deviation of MSLP and total number of cyclones whose initial appearance of an eye corresponded to a small, medium, or large eye as defined above.

EYE CLASS	MSLP	STANDARD DEVIATION	NO. OF CYCLONES
SMALL	988 mb	$\pm$ 10 mb	17
MEDIUM	982 mb	$\pm$ 10 mb	45
LARGE	979 mb	$\pm$ 9 mb	15

6.3.1 Elliptical Eyes

Elliptical eyes generally appeared in either the early stages or in the late, filing stages of the cyclone. The initial eye was often elliptical and became more circular with increasing intensity. Elliptical eyes were typically poorly organized and changed diameter rapidly; an average 9 km every twelve hours, as opposed to circular eyes which expanded or contracted an average of only 2 km/12 hr. Fewer elliptical eyes were found during intense stages. Evidently, the cyclone, in transforming its central cloud fields into an eyewall, only gradually forms a circular eye. In the early, less intense stages, the cyclone exhibits large changes in size and forms odd shapes. One might wonder if the cyclone is in search of a configuration of maximum efficiency as it concentrates its convection into an eye during this initial stage.

6.3.2 Rapid Deepeners

Cyclones which deepened at a rate of 42 $mb\ d^{-1}$ or greater developed an eye at an average MSLP of 985 mb, as opposed to and average of 980 mb for all other storms. Rapid deepeners not only tended to form an eye earlier but also tended to develop a smaller eye. This tendency was likely due to non-linear advective processes which act to more rapidly concentrate energy into the core of rapid deepeners than for the other cyclones. Recall that the outer core tends to strengthen at a relatively constant rate of 2.5 ms^{-1}/d throughout the intensification period. Therefore, the earlier an eye formed, the weaker and less inertially stable was the outer core through which the momentum passed and hence, the easier it was to concentrate momentum near the center. It is important to note that rapid deepeners usually began their rapid intensification period when the eye appeared and that the average initial eye diameter was 40 km, as opposed to 50 km for all other storms, exclusive of rapid deepeners. The rapid deepening phase ended with a considerably reduced eye diameter which was on average 20 km. Thus, rapid deepeners had a head start in their intensification process and could often be identified while still tropical storms by the relatively early (985 mb) development of an eye.

For the great majority of cyclones, the initial development of the eye occurred during the tropical storm stage which, following Atkinson and Holliday (1977), corresponded to maximum winds of 27 ms^{-1} (53 knots) for rapid deepeners and an average of 30 ms^{-1} for all others. The mean OCS value concurrent with eye development of rapid deepeners was 10 ms^{-1}, hence at a time when the cyclone's inertial stability was low and allowed more rapid import of moisture through inflow processes. Although these differences in the wind field help explain the processes by which rapid deepeners form, they are unlikely to be easily detected by the forecaster. What can be observed by the forecaster is the earlier appearance of the eyewall, assuming reliable eye and central pressure information can be obtained.

6.3.3 Early vs. Late Initial Eye Appearance

To further clarify the temporal development of the eye, a study was done of cyclones with comparatively early versus late eye development. Cyclones were grouped according to whether or not an eye was present when the MSLP of the developing storms fell to 987 mb, which was the average MSLP at which eyes first appeared. Rapidly deepening cyclones and cyclones forming an eye at higher MSLP's fell into the early class, while those whose eye formed at pressures lower than 987 mb fell into the late class. Table 6.2 lists average properties for each class. Note that cyclones showing an eye early in their development were generally farther southeast than the other storms whereas maximum wind speeds were the same and OCS values were weaker. The difference in the OCS values appears to be significant and supports inertial stability arguments of cyclone intensification. The ease with which a cyclone can import momentum through the outer core and near the center is vital to its further capacity to intensify. Notice from Fig. 6.4 that the relative vorticity of late eye-appearing cyclones is 50 percent higher, corresponding to double the inertial stability and thus putting a stronger constraint on the radial inflow.

Table 6.2: Averages of position, cyclone motion, intensity, intensity change, and OCS for cyclones in which the eye appeared early vs. those whose eye appeared late in their development.

EYE APPEAR-ANCE	LAT.	LONG.	HEAD	SPEED	MAX WIND	MSLP	MSLP CHANGE	OCS
				ms^{-1}	ms^{-1}	mb	$mb\ d^{-1}$	ms^{-1}
EARLY	14°	141°	290°	6	24	987	- 10	11
LATE	17°	138°	315°	5	24	987	-7	14

The inflow processes which are vital to a cyclones development delineate the differences between the early and late developing eyes. Figure 6.5 shows the azimuthally-averaged radial winds after the cyclone's motion has been removed. Cyclones forming eyes early had significantly greater inflow within 150 km of the center. Notice from the plan-view depictions of residual winds in Figs. 6.6a and b, how much the near environ-

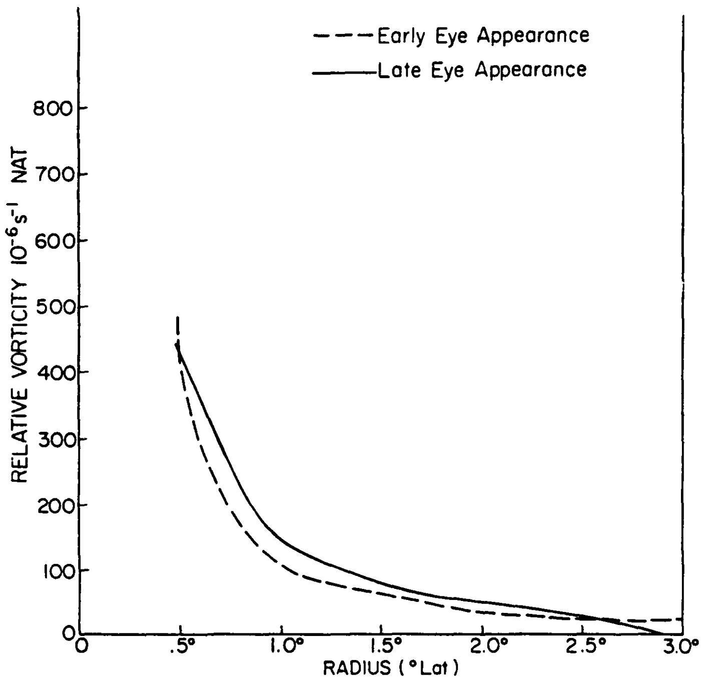

Figure 6.4: Radial profiles of azimuthally-averaged vorticity fields for early versus late eye-forming cyclones.

ment was drawn into those cyclones which developed eyes earlier than other cyclones. The divergence patterns in Fig. 6.7 also show a concentration of flow close to the center during this early stage of intensification.

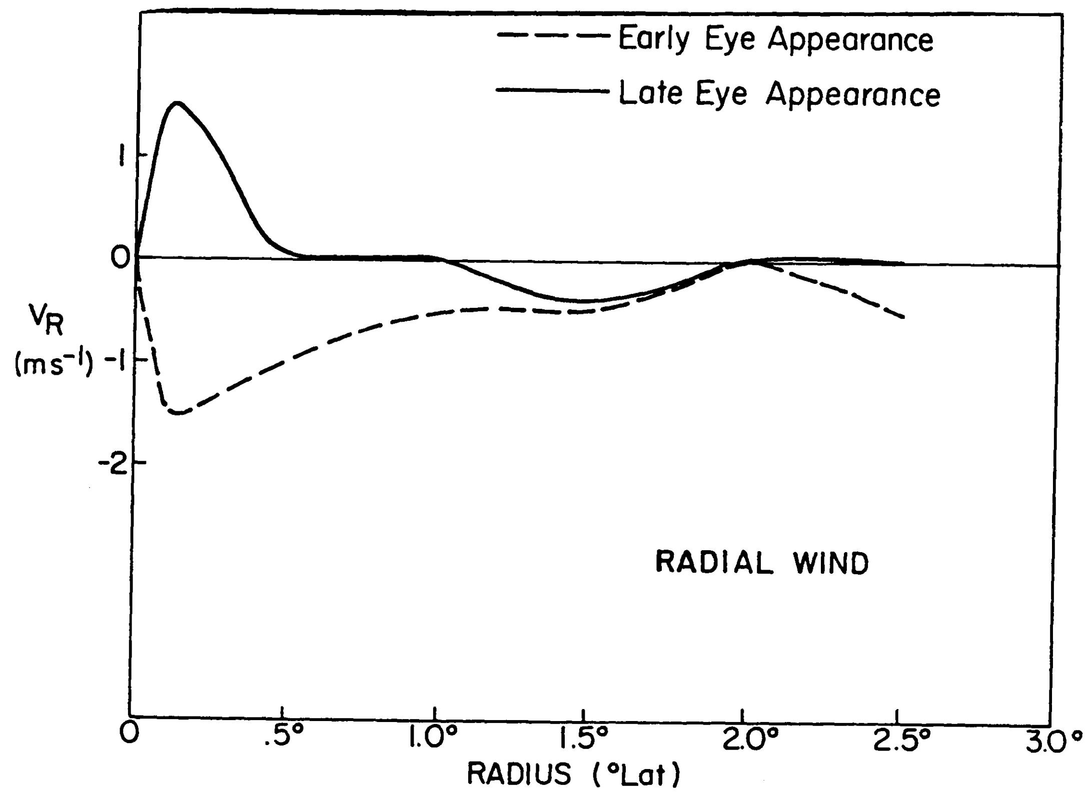

Figure 6.5: Radial profiles of azimuthally-averaged radial wind fields in MOT coordinates for early versus late eye-forming cyclones.

6.4 The Eye During Intensification

The presence of an eye signals that a cyclone has begun to rapidly concentrate energy into its core and intensification usually speeds up, regardless of the initial eye size. Prior to the initial appearance of the eye, cyclones intensify at an average rate of 8 $mb\ d^{-1}$. Once the eye forms, this rate increases by 250 percent to 20 $mb\ d^{-1}$ for cases still in the tropical storm stage. The average intensification rate throughout the entire deepening period for cyclones with eyes is 24 $mb\ d^{-1}$. Recall that rapidly deepening cyclones generally obtain an eye early in their development, thereby gaining an initial advantage in concentrating energy more quickly into the inner core while the outer core was still relatively weak.

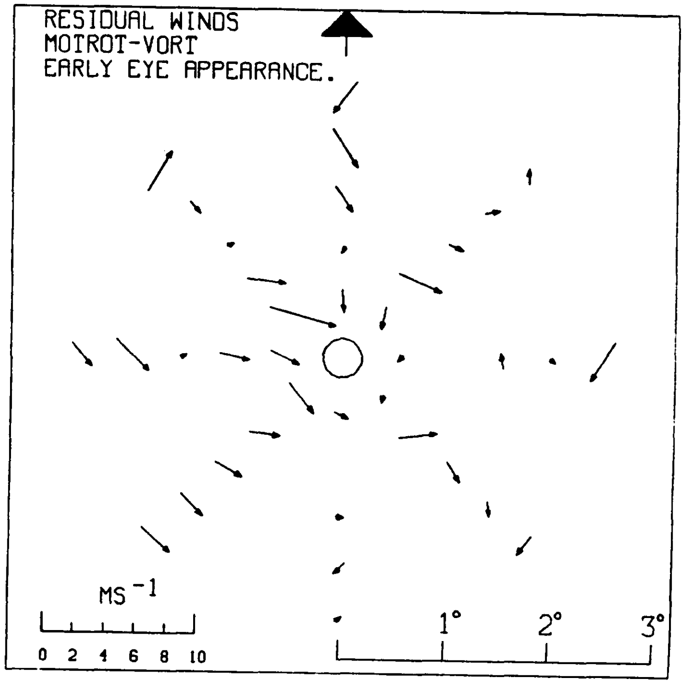

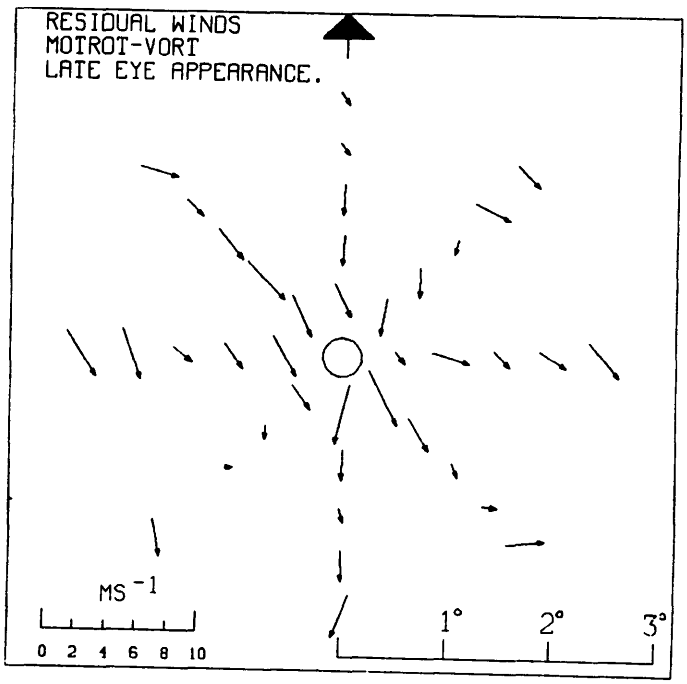

Figure 6.6: a-b. Plan-view analyses of the mean 700 mb residual wind field for early-eye versus late-eye cyclones in MOTROT-VORT coordinates with the arrow on the rim denoting the cyclone heading of motion. Values are in ms^{-1} with arrow length implying speed as shown in the lower left corner.

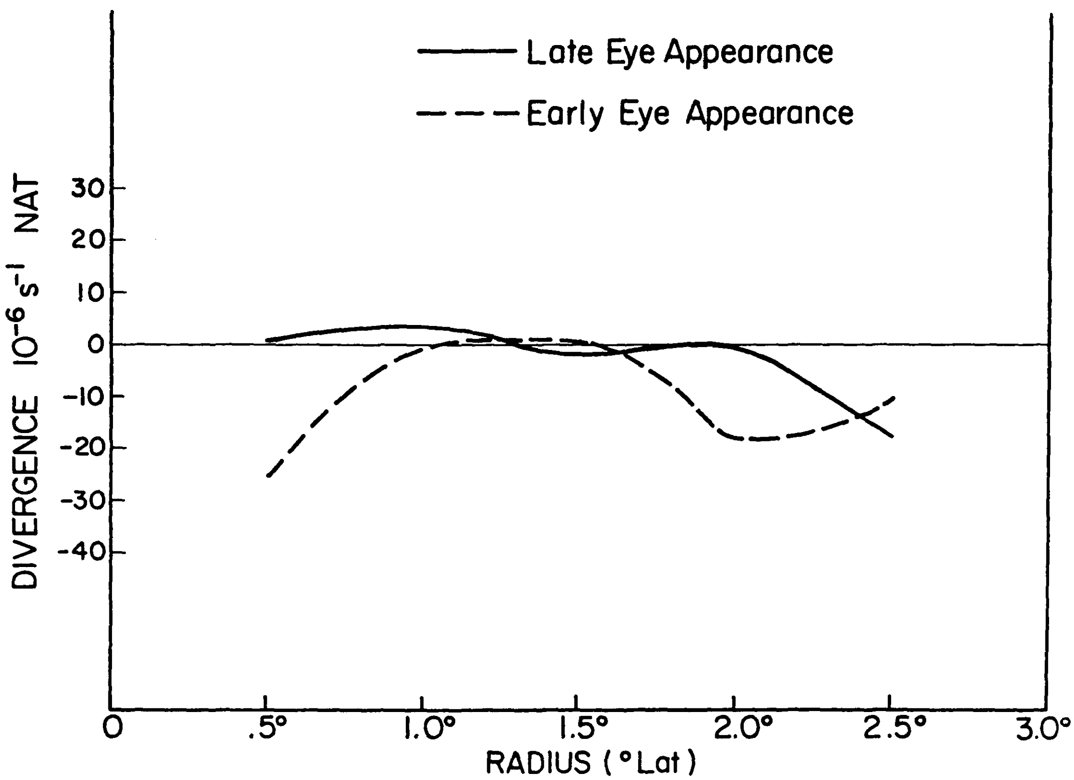

Figure 6.7: Radial profiles of the divergence fields for early versus late eye forming cyclones.

Eyes usually contracted while deepening, regardless of the rate of deepening or of the initial size of the eye. Appendix A provides many examples of changing eye size with increasing cyclone intensity. Whereas some cyclones initially formed a large eye and showed sizable contractions, those cyclones with small initial eyes, and hence with much less room to contract, showed only slight changes in size. Evidently there is a minimum size which a cyclone eye can attain which varies for each case. However, when a cyclone attains maximum intensity, it also usually exhibits its smallest eye at the same time. The smallest eyes observed in this study were 7 km across for Typhoons Dinah of 1980 and Gay of 1981. Further intensification with no additional contraction lasted a few days in some instances, as in the case of Supertyphoon Forrest of 1983. It was during this steady state period that concentric eyes tended to appear.

6.5 Concentric Eyes

Observations of concentric eyes were relatively rare, occurring for only four percent of all sightings but which occurred in 16 percent of all cyclones. Concentric eyes were only observed for cyclones which had MSLP pressures lower than 945 mb and occurred an average of three days after the initial eye sighting. Changes that preceded or followed the observation of a concentric eye on timescales shorter than 9-10 hours are unknown because of the data void period between aircraft missions. A few typhoons exhibited concentric eyes for two consecutive missions, but in no case were they documented to persist for more than 15 hours. Concentric eyes are thus observed to last for only a fraction of a day. Good examples of concentric eyes include the cases of Supertyphoons Wynne (1980) and Vanessa (1984) in Appendix A.

Concentric eye diameters averaged 20 km for the inner eye and 55 km for the outer eye, as compared to the average eye diameter for all observations of 42 km. The average MSLP for concentric sightings was 925 mb, with a highest value of 946 mb and lowest of 886 mb. In general, concentric eyes appeared when an intense typhoon was in the process of switching from a deepening to a filling stage. Thirty percent of the concentric eye observations were in deepening typhoons, 20 percent occurred when MSLP had bottomed out and was steady, and 50 percent were observed in filling typhoons. All were circular for both the inner and outer eyewalls.

Willoughby *et al.* (1982) focused on the concentric eye cycle using the example of the very intense Hurricane Allen of 1980, and concluded that the appearance of concentric eyes preceded an intensification period. Evidently, cyclones can, and do intensify without concentric eyes, but whether intensification follows the cycle proposed by Willoughby *et al.*, cannot be proven with the coarse time resolution of this data set.

6.6 Eye Characteristics During Cyclone Filling

The eyewall generally expands while filling and becomes diffuse so that it can no longer be recognized as an eye. On average, a cyclone which is filling over water loses its eye at approximately 954 mb. However, Supertyphoon Wynne (1980) lost its eye while over water at a rather intense value of 927 mb. This was the lowest pressure for eye disappearance observed in this data set and is in notable contrast to the MSLP at which the eye first appeared (980 mb).

Cyclones lose their eyes at the same time that they stop strengthening which, on average, has been observed to occur at 955 mb. Figure 6.8 shows time variation of the height field for Supertyphoon Abby at 0.5° intervals from the center in order to illustrate these effects more clearly. Notice how the outer core height field continued to lower for six days after the height at the center began to rise on August 8. The outer core (2.0° radius) heights started rising after Abby lost its eye on August 15 (Fig. 6.9). Therefore, even though a cyclone's central pressure is filling, as long as an eye exists, momentum continues to be advected through the outer core towards the eyewall and thereby strengthening the outer core. Once the eye disappears however, the outer core begins to weaken as well, marking the beginning of the decay of the entire vortex.

6.7 Eye Characteristics Related to Core Winds

Eye size classifications along with the number of sightings in each class are defined as follows:

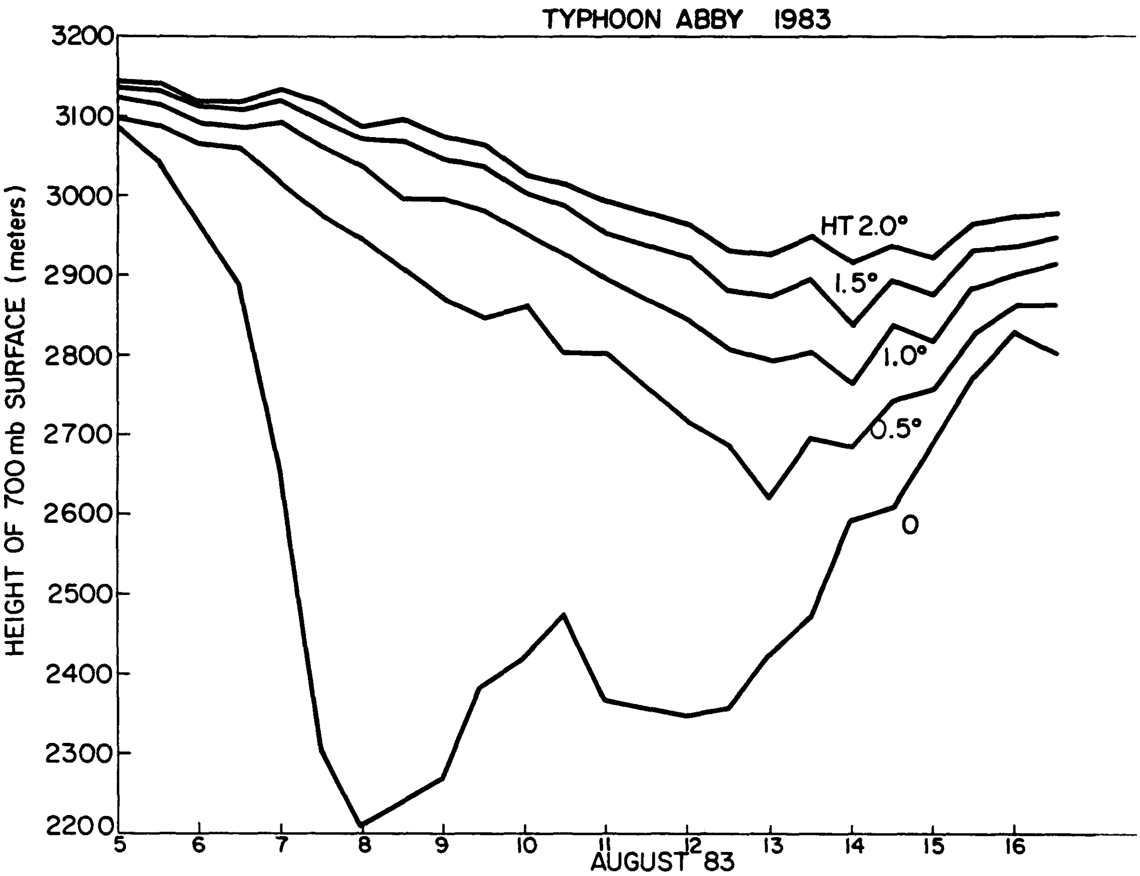

Figure 6.8: The series of 700 mb height profiles versus time at the center (0°), .5°, 1.0°, 1.5° and 2.0° for Supertyphoon Abby.

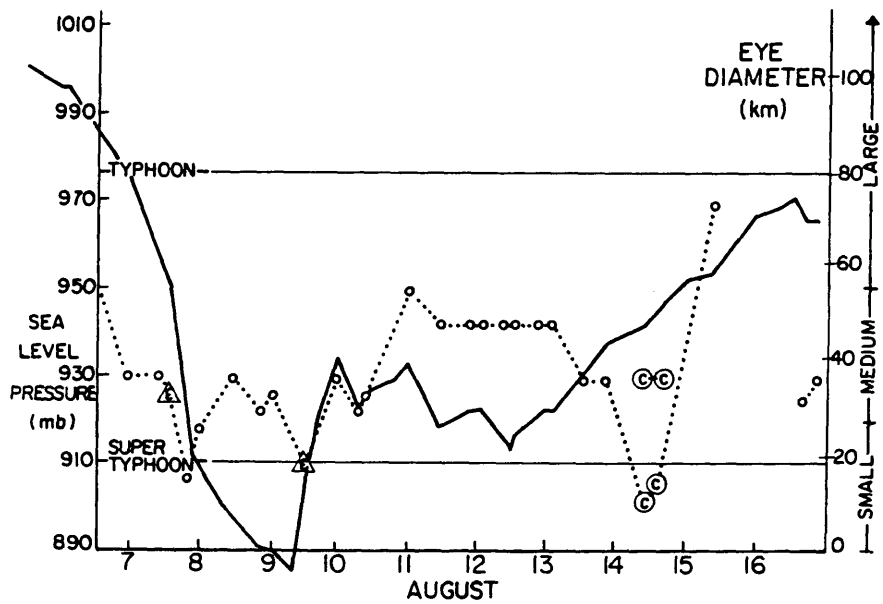

Figure 6.9: Evolution of MSLP and eye diameter versus time for Supertyphoon Abby.

EYE CLASS	RANGE OF DIAMETERS	NO. OF SIGHTINGS
SMALL EYE	< 28 km	164
MEDIUM EYE	28 to 55 km	411
LARGE EYE	> 55 km	91
NO EYE	—	755

Smaller eyes tended to show a greater concentration of drying and subsiding core region (< 2.5°) air. Table 6.3 shows the average values of various parameters for each eye class. All classes lie in the same average geographical location and have similar mean values for forward speed, direction, and intensity. Notice however, the differences in the OCS values. From Table 6.3 it can be seen that the smaller the eye, the greater the intensity and yet, the <u>weaker</u> the outer core. The weaker outer core probably contributes to the greater inward penetration of inflow air to the inner core. For instance, at 100 km, the average inertial stability of large eye cyclones was double that of small eye storms. Thus, subtle differences in the magnitude of the wind could provide significantly different forcings on radial motions.

Analyses of height field data by eye-size class provides further support to the contention that cyclones with smaller eyes have more focused energy and momentum gradients

Table 6.3: Average characteristics of eyes by size class.

EYE CLASS	LAT.	LONG.	HEAD	SPEED	MAX WIND	MSLP	MSLP CHANGE	OCS
				ms^{-1}	ms^{-1}	mb	$mb\,d^{-1}$	ms^{-1}
SMALL	17°	137°	315°	5	42	951	- 16	19
MEDIUM	18°	135°	317°	5	42	955	-10	20
LARGE	19°	137°	318°	5	41	961	-2	22
NO	19°	137°	320°	6	27	985	-1	16

near the center. The 700 mb height profile data in Fig. 6.10 have been scaled relative to central pressure and environmental values following Eq. 6.1.

$$ht_s = (ht_r - ht_c)/(ht_\infty - ht_c) \tag{6.1}$$

where ht_s is the scaled value, ht_r = the height at radius r, ht_c = the height at the center, and ht_∞ = the height well away from the storm (3130 m). A scaled height of 100 percent equalled the height of the environment, ht_∞. This analysis shows where height gradients tend to be most concentrated within the cyclone. Thus, in the Fig. 6.10 one can see that, as expected the height gradient is concentrated near the center for the small eye-class cyclones.

6.7.1 Eye Size Related to Interior Wind Fields

Figures 6.11a-d show 700 mb radial wind fields in the NAT coordinate system for cyclones with eyes of various size. Few asymmetric differences are found. Generally the cyclones are embedded in similar 700 mb steering currents, regardless of eye size. This also is the case when viewed in the MOTROT coordinate system, as shown in Figs. 6.12a-d. Radial winds are observed to flow through the cyclone at 700 mb from the left-front to right-back. Differences are found in the residual wind field when both radial and tangential components are combined as in Figs. 6.13a-d. The residual winds show distinct inner core concentrations for the small and medium eye classes in contrast to general flowthrough for the cyclones without eyes. Notice in Fig. 6.13d that eyeless cyclones generally reflect

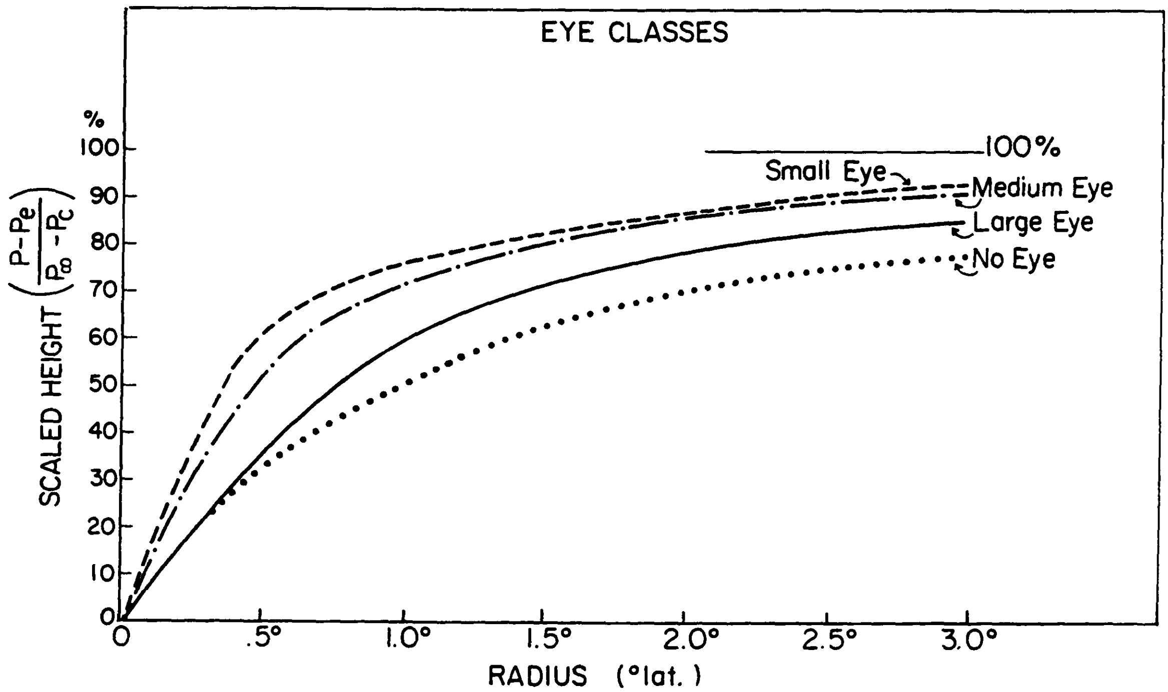

Figure 6.10: The 700 mb height field for the four cases of eye size where heights scaled by the factor: $(h_r - h_c)/(h_\infty - h_c)$.

the 700 mb steering current. Once an eye exists however, more of the steering current is drawn into the center with less flow through to the other side.

6.8 The Temperature of the Eye

Analysis of the inner temperature of a cyclone can provide clues concerning the intensity. The temperature within the eye of a tropical cyclone is an indirect indication of the strength of vertical motion in the eyewall convection which, in turn, induces subsidence warming within the eye. In general, the stronger the eye-wall convection, the warmer the temperatures within the eye. Whereas the average temperature at 700 mb in the Tropics is 10° C, the highest eye zone 700 mb temperature in this data set was 31° C in Supertyphoon Vanessa of 1984. Air temperatures this warm are not observed at 700 mb except in the eyes of intense tropical cyclones.

As shown in Fig. 6.14, eye temperatures generally increase with lower MSLP and are related to the shape and structure of the eyes. Temperatures inside concentric eyes

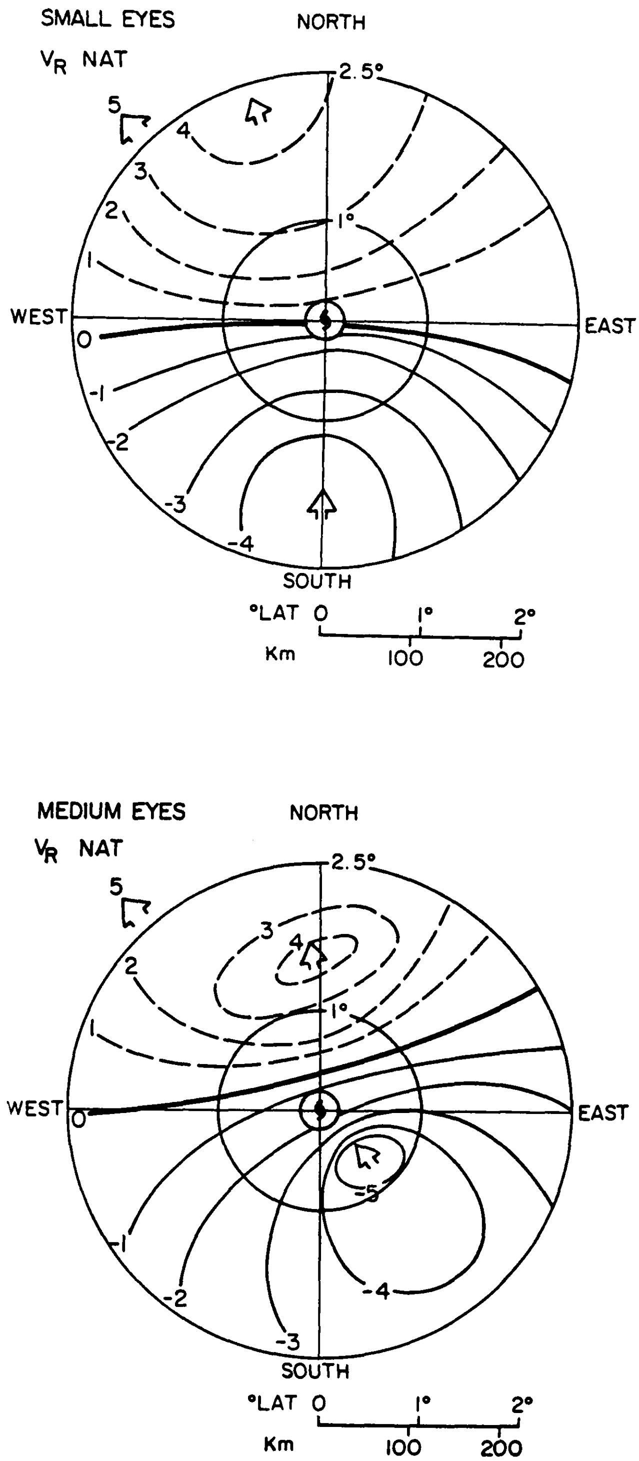

Figure 6.11: a-d. Plan-view depictions of the radial wind field (V_r) ms^{-1} in earth-relative coordinates (NAT) for the four eye size classes of a) small eye, b) medium eye, c) large eye and, d) no eye.

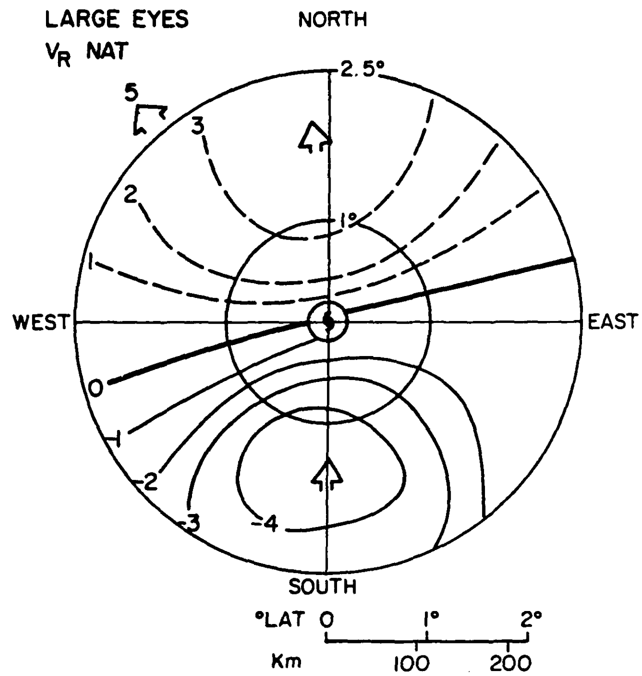

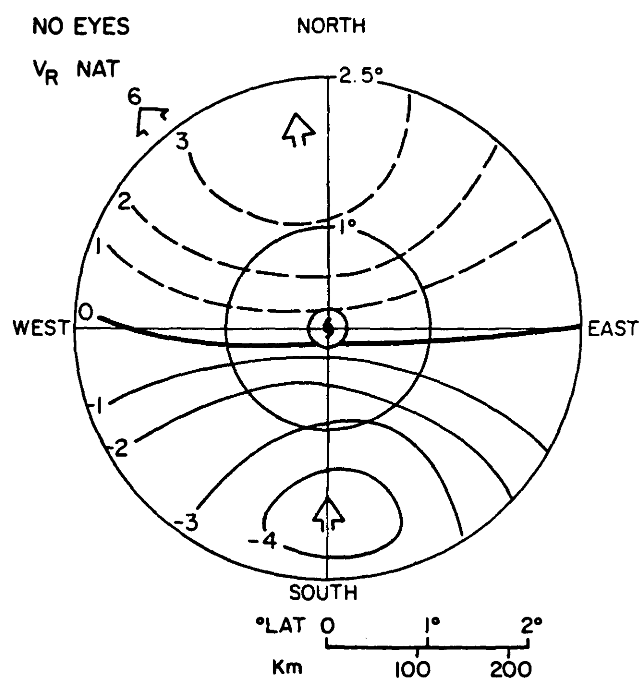

Figure 6.11: a-d. Continued.

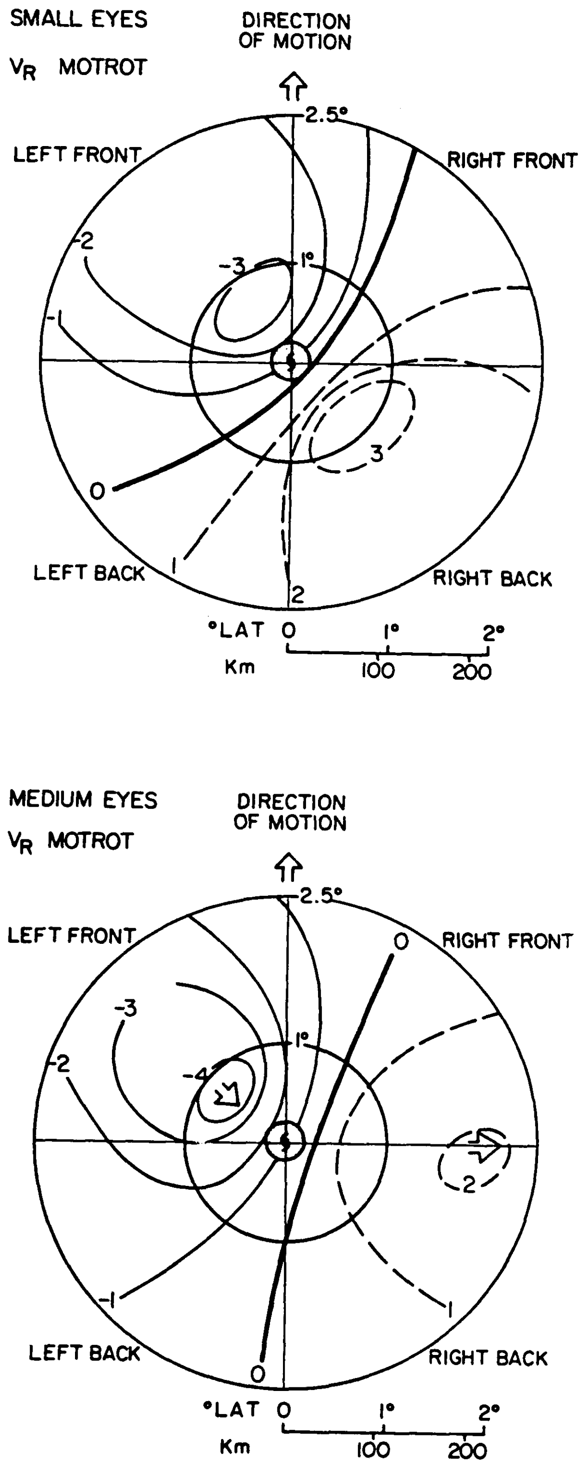

Figure 6.12: a-d. Plan-view depictions of the radial wind field (V_r) ms^{-1} in cyclone-relative coordinates (MOTROT) for the four eye size classes of a) small eye, b) medium eye, c) large eye and, d) no eye.

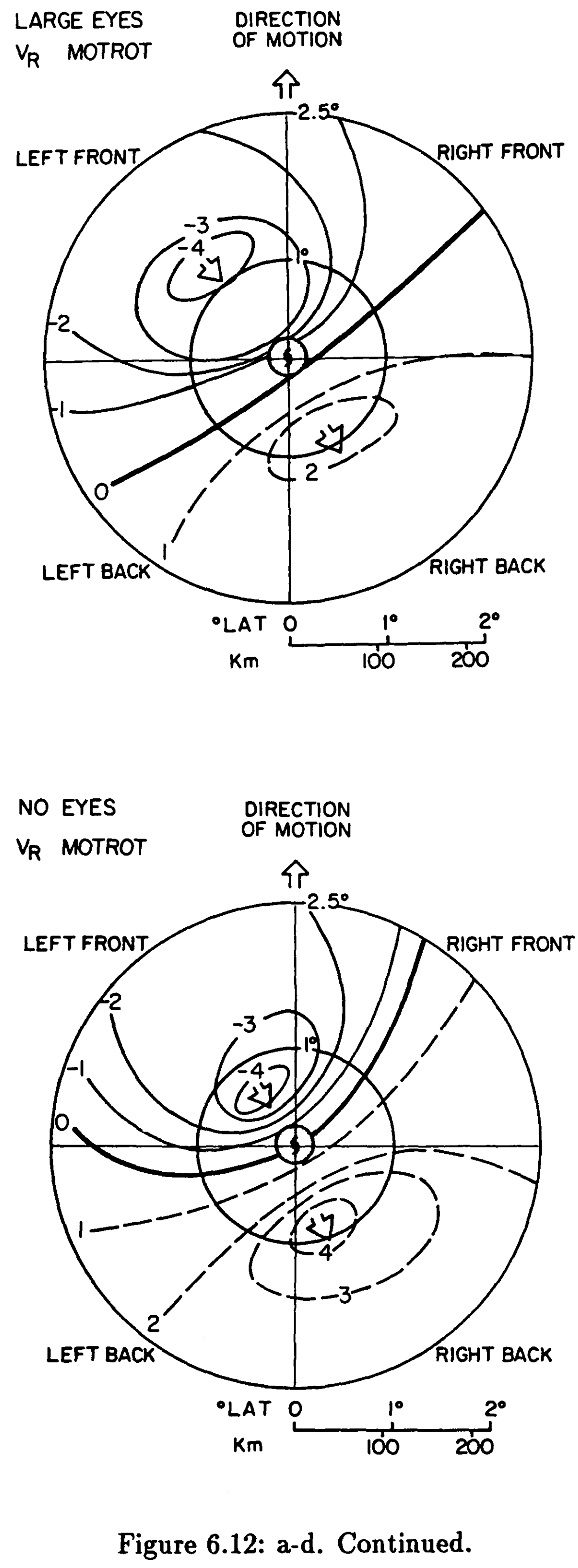

Figure 6.12: a-d. Continued.

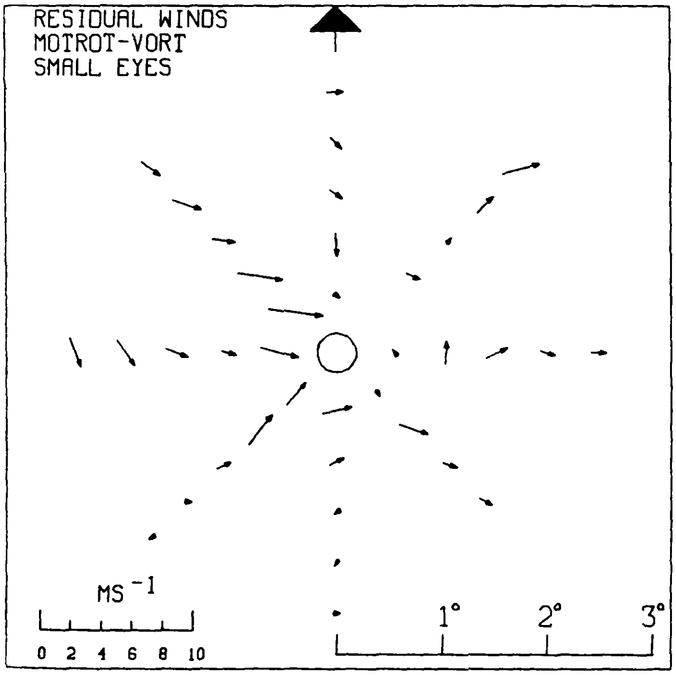

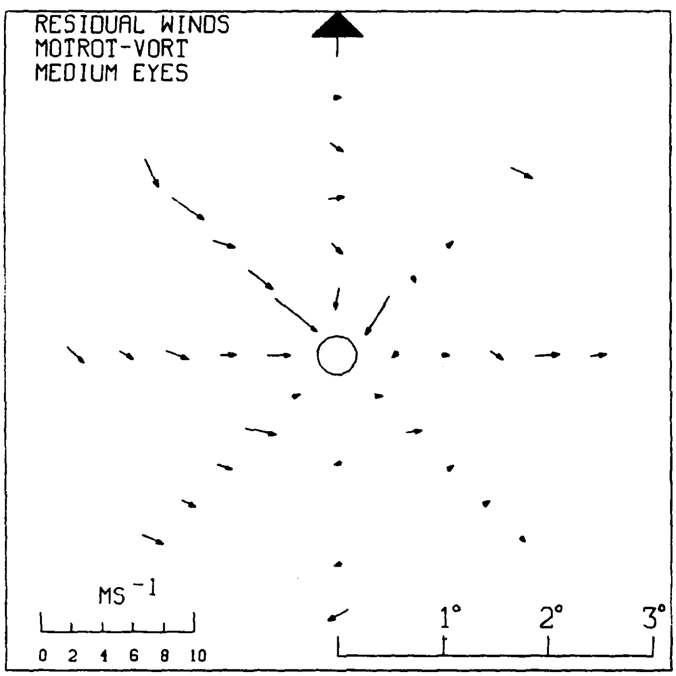

Figure 6.13: a-d. Plan-view depictions of the 700 mb residual wind field in MOTROT-VORT with the arrow on the rim denoting the cyclone's heading. Values are in ms^{-1} with arrow length representing speed as shown in the lower left corner. The four classes are a) small eye, b) medium eye, c) large eye and, d) no eye.

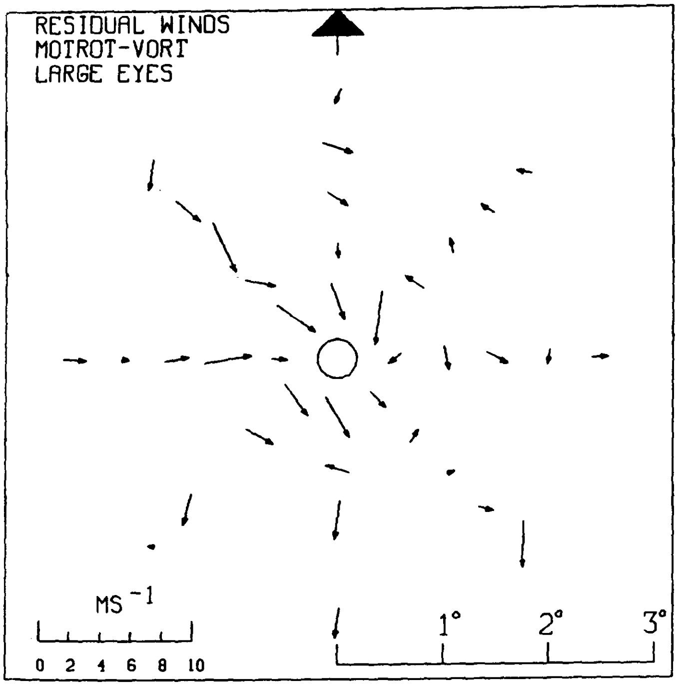

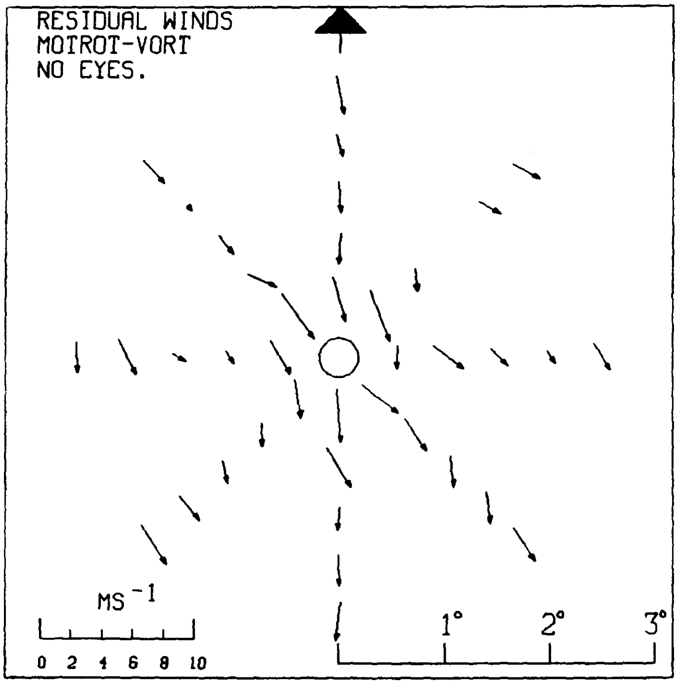

Figure 6.13: a-d. Continued.

were cooler than in either circular or elliptical eyes of the same intensity. Presumably, the comparatively cool concentric eyes are related to the cycle which Willoughby *et al.* (1977) discussed. When the inner eye contracts, evaporative cooling of the added moisture causes a lowering of temperatures.

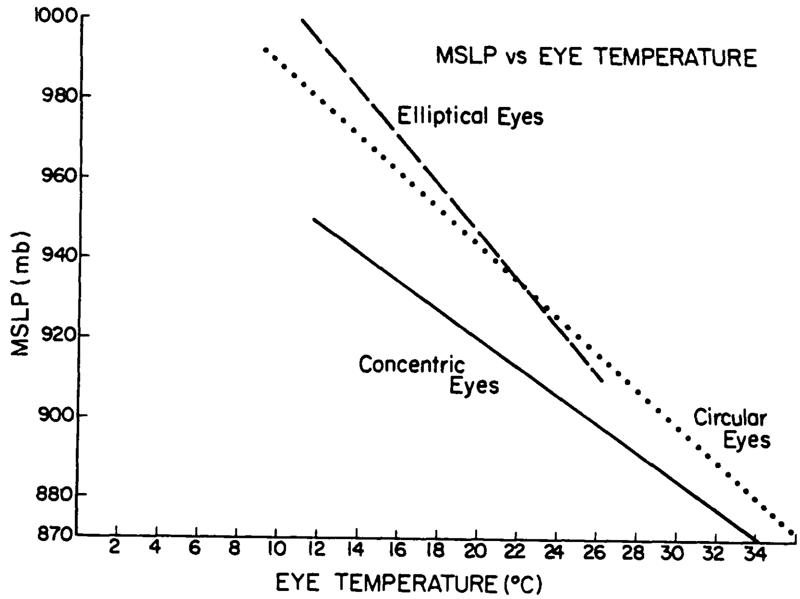

Figure 6.14: MSLP versus 700 mb inner eye temperature for elliptical, circular, and concentric eyewalls.

The temperature of the eye is not strictly a function of its intensity and character, but also of intensity change. Maximum eye temperatures were found to occur while cyclones were intensifying, rather than at maximum intensity or while filling. It is likely that the eyewall convection is most vigorous during intensification and that when the convective processes slow down, the intensification rate slows with it, resulting in lessened subsidence-forced warming and cooler central temperatures.

6.8.1 Equivalent Potential temperature

Equivalent potential temperature (θ_e) has been used at JTWC (on Guam) as a predictive index for cyclone intensity. Dunnavan (1981) devised a predictive scheme which attempted to identify those cyclones which would become relatively intense. His study indicated that when a cyclone's MSLP and θ_e curves intersected, as shown for September 22 in Fig. 6.15, a cyclone would either rapidly deepen or would at least reach a MSLP of 925 mb. Cyclones whose curves did not intersect were forecast to be slower deepeners.

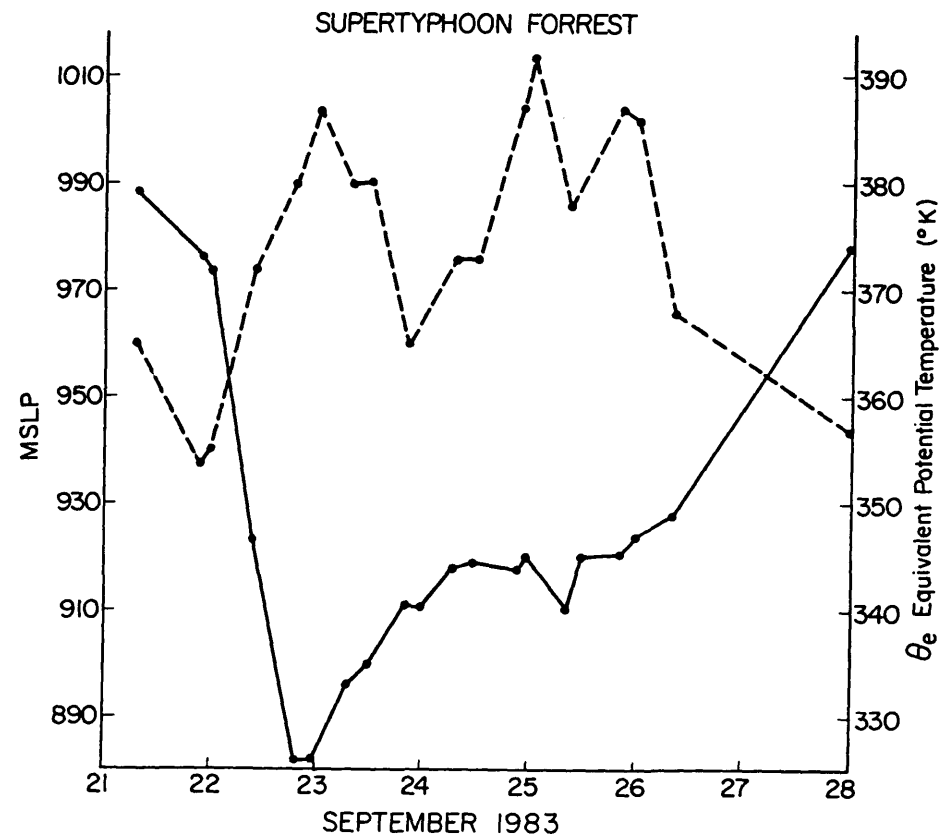

Figure 6.15: Evolution of MSLP and 700 mb equivalent potential temperature for Supertyphoon Forrest.

In order to test Dunnavan's hypothesis, all 101 cyclones of the 5-year data set were examined. Of these, 48 cases were identified wherein MSLP intersected θ_e. Ten percent of these intersecting cyclones made landfall within one day and further intensification could not be verified. Fifty-three percent followed Dunnavan's prediction of either rapidly deepening or reaching 925 mb. However, since this is a predictive scheme, lead time is an important factor in judging its usefulness. In thirteen percent of the cases the curves intersected without providing sufficient lead time to be useful. For the example of Supertyphoon Elsie (Fig. 6.16) it wasn't until Elsie hit 902 mb that the curve crossing was evident. Indeed, Elsie was already deepening rapidly well before the curves crossed. Also, not all typhoons exhibiting the curve intersection reached 925 mb or deepened rapidly. A full 38% of the intersecting cases were false alarms, as in the example of Typhoon Pamela in Fig. 6.17. The only feature common to all cyclones with intersecting MSLP and θ_e curves was that they did reach a MSLP of at least 950 mb, barring landfall within 12 hours, and thus at least developed into intermediate typhoons.

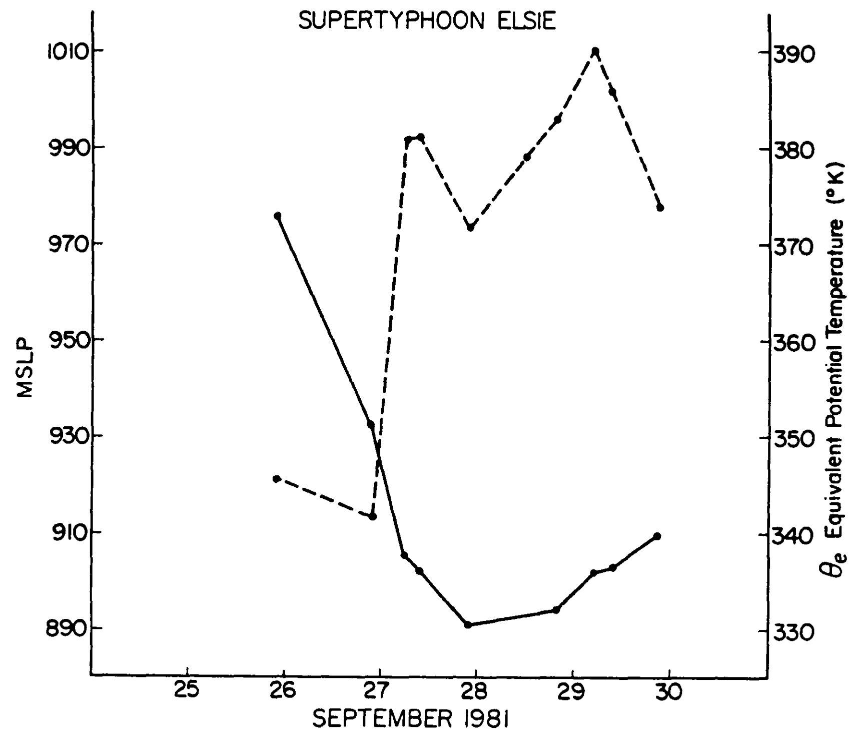

Figure 6.16: Evolution of MSLP and 700 mb equivalent potential temperature for Supertyphoon Elsie.

Of the cyclones whose curves did not cross, none ever attained MSLP values below 955 mb thus at best did not develop into minimal typhoons. However, this result may be due entirely to the design of the $\theta_e/MSLP$ grid. On average, the critical crossing point lies at 950 mb and 360° K. Hence, cyclones would typically have to reach at least 950 mb for the curves to intersect. Evidently, some cyclones reached 950 mb and intensified no further. Unfortunately for this predictive scheme, less than half of the qualifying cyclones actually intensified to 925 mb or deepened at a rate of 42 $mb\ d^{-1}$ with useful lead time.

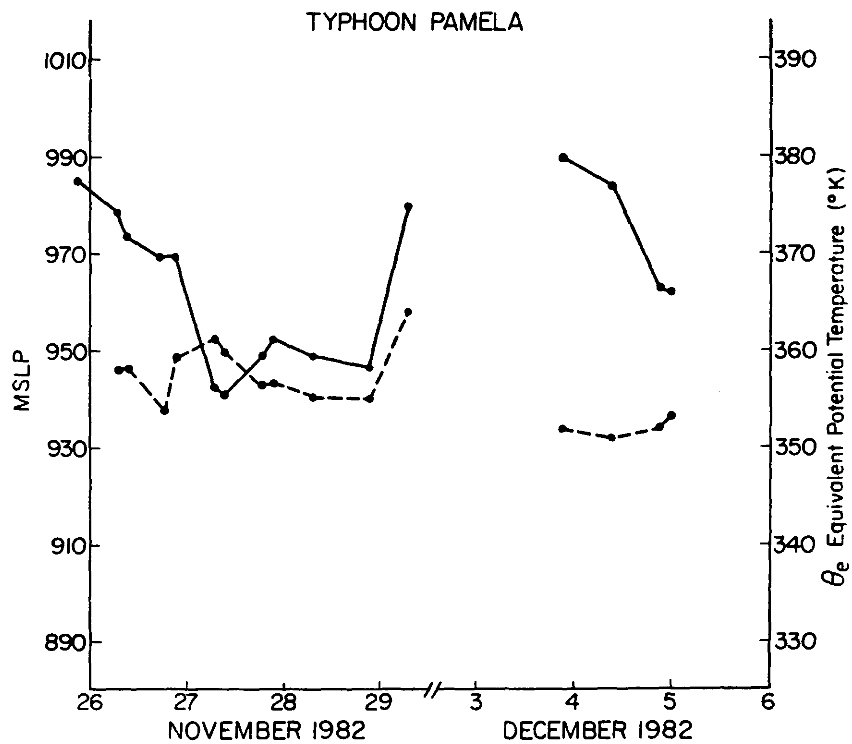

Figure 6.17: Evolution of MSLP and 700 mb equivalent potential temperature for Typhoon Pamela.

On the basis of these results, Dunnavan's predictive scheme does not appear to be a useful forecast tool.

Chapter 7

SUMMARY AND DISCUSSION

7.1 The Life Cycle of the Tropical Cyclone

The foregoing study has provided a broader understanding of the manner in which intensity changes occur in the tropical cyclones. In general, cyclones are observed to form from the center outward. Although inner core convection drives changes of intensity, the process is constrained in part by the strength of the adjoining outer core. A weak outer core provides comparatively easy access to the eyewall, while a strong outer core inhibits inflowing momentum and thereby depletes the supply of momentum to the inner core. These effects follow the typical cyclone life cycle as depicted in Fig. 7.1. In the phase 1 intensification period momentum gathers and strengthens 700 mb winds in the inner and outer cores. Although the entire 700 mb wind field builds, the inner core intensifies at a rate two to twenty times greater than outer core intensification. This concentration of momentum close to the cyclone center is much more efficient for intensification as measured in terms of surface pressure drop and maximum wind increase. This intensification process also causes an eyewall cloud to form, the appearance of which provides clues to further intensification.

Before the eye appears, the process of concentrating momentum into the inner core is slow. During this general tropical storm stage, intensification occurs at an average rate of 8 $mb\ d^{-1}$. This rate of intensification is equivalent to a maximum wind increase of about 5 ms^{-1} per day and a strengthening of the outer core (1-2.5° radius) an average of 2.5 ms^{-1} per day. Once the eye appears, usually about 987 mb, the rate of intensification increases by a factor of 250 percent, to about 20 $mb\ d^{-1}$. Evidently, the presence of an eye indicates that high momentum is being concentrated close to the center where energy

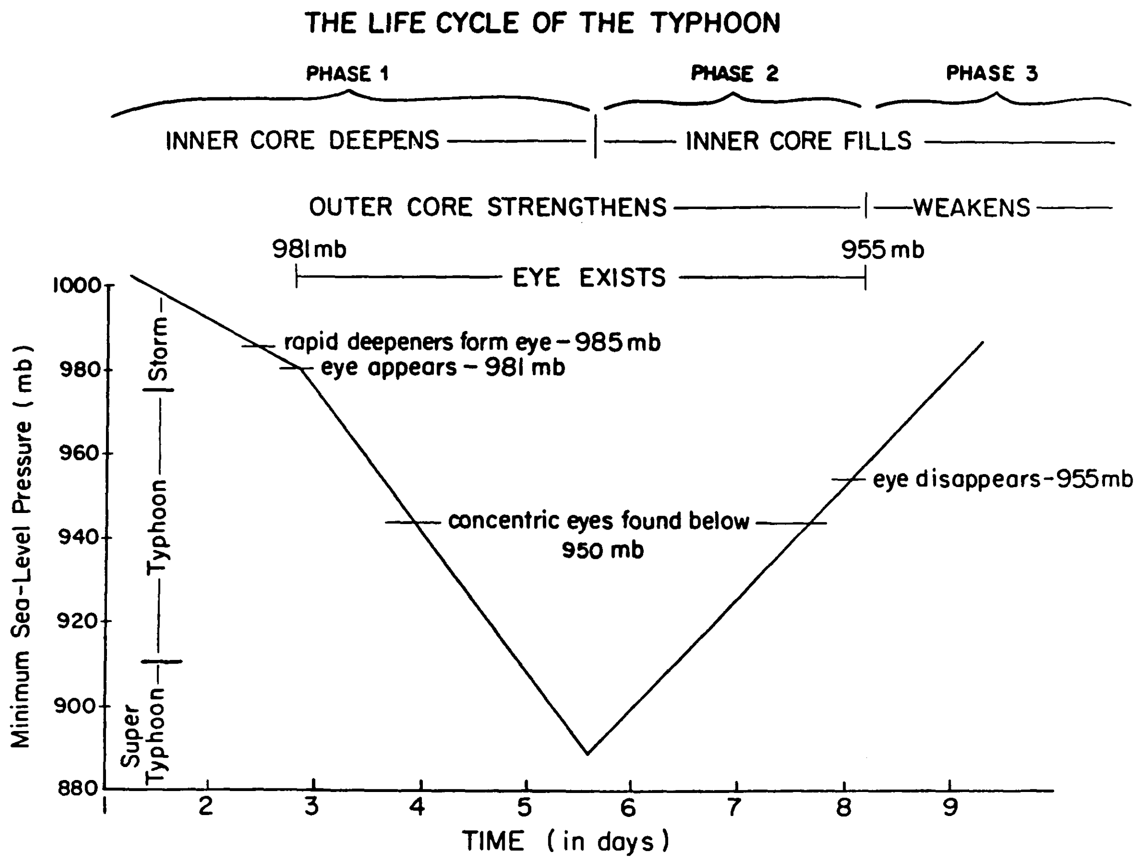

Figure 7.1: Conceptual rendering of the main events in the life cycle of a typical tropical cyclone.

conversions are most efficient. Rapidly deepening cyclones exhibit earlier eye formation, typically at 985 mb, and immediately begin deepening at a rate of 42 $mb\ d^{-1}$ or more. The most rapid rate of intensification for the five years studied was 92 $mb\ d^{-1}$ in Supertyphoon Forrest (1983) which first developed an eyewall at 988 mb. Hence in general, the earlier in a cyclone's development that an eye appears, the more rapidly it is likely to intensify.

This early-eye rapid-intensification relationship may be explained from reasoning derived from inertial stability theory. Since momentum must be advected into the eyewall, which is located in the inner core of the cyclone, then momentum must pass through the outer core region to get there. Observations reveal that inner core winds do not intensify at the expense of the outer core winds since the outer core is also observed to strengthen. Thus, when the eye forms before the outer core has strengthened, access to the eyewall is much easier for low-level inflowing air. Cyclones whose eyes form late typically do not reach intensities much below 930 mb, apparently due to the inertial stiffness of the outer core. Recall that in the Pacific, typhoons have reached intensities of 870 mb and that a full third of the cyclones which became typhoons reached intensities below 930 mb. Therefore, late-forming eyes suggest the cyclone will not deepen rapidly nor will it intensify into an extreme typhoon.

The filling process, in which the central pressure starts rising, does not necessarily imply the cyclone's outer core wind field is decaying. Indeed, onset of filling may coincide with a cyclone's period of greatest gale-force extent and strength of outer core winds. As long as an eye exists during the filling phase (generally at MSLP's lower than 955 mb), typhoons will continue to draw momentum through the outer core and continue to strengthen the winds in their outer cores. This is the phase 2 period in Fig. 7.1 during which the inner core winds are diminishing while the outer core winds are increasing. The eye expands during this time while filling of the inner core continues as inflowing air is less able to penetrate to the cyclone center. Recall how for the same central pressure, the inertial stability of the outer core is twice as large during the filling stage as in the deepening stage, thereby effectively stiffening the outer core to radial inflow. The expanding eye thus becomes less and less efficient and the central core fills.

Eyewalls are maintained for cyclones with MSLPs below 955 mb. The longer the cyclone spends in phase 2, the stronger outer-radius winds will be. It is important to realize that even though the center is filling in phase 2, the radius of damaging winds is still expanding as long as an eye exists. Therefore, if one has information on whether the central pressure is filling and if an eye exists, then forecasts of outer wind strength are likely to be far more accurate. In the case of Supertyphoon Abby, expansion of the eye occurred for 6 days after the MSLP started filling. This observation suggests that the cyclone reached its largest areal proportions while filling. Hence, forecasters should expect larger gale-force wind radii in the filling versus intensifying phase, given the same MSLP.

The eye is observed to disappear at about the same time as the outer core begins to weaken. This association is characteristic of the beginning of phase 3 in Fig. 7.1. Once the eye vanishes, the import of angular momentum that maintained the outer core ceases and the entire outer radius low-level wind field begins to decay. These effects are characteristic of cyclones which do not encounter landfall. Landfall would no doubt erode the wind field regardless of the appearance of an eye. Steady state periods may exist anywhere in the life cycle, however. The more intense the cyclone, the less likely it will encounter a period with no substantial intensity change.

Life cycle changes were described by Dvorak (1975) in terms of varying cloud field features as the cyclone's maximum winds progress in time. Without wind information for the cyclone's outer core region, the wind field away from the maximum wind zone was not analyzed with respect to cloud field changes. Since these outer winds are important as well, satellite and wind field comparisons are needed.

7.2 The 700 mb Interior Background Wind Field

Additional insight into the physical processes governing cyclone motion is obtained when the cyclone's motion and mean vortex are removed from the wind field. This residual (MOTROT-VORT) wind field clearly reflects the interaction between background winds and the vortex. Most notably, the cyclone's interior wind field shows a distinct 700 mb steering current passing through it. Apparently, the inner core vortex is not fully shielded from the outer core environment. The concept of a 'spinning top' embedded in a stream that impinges only on its outer edges cannot completely describe the motion of the cyclone. It is observed that the cyclone allows a continual flow to pass directly from its outer core through the vortex.

Tropical cyclones of the northwestern Pacific basin are observed to move faster and to the left of their 700 mb environment. Evidently, the reason for this relative motion is that the steering current is more heavily weighted to the stronger winds that lie in the upper troposphere. It is also observed that stronger winds in the outer core appear to cause a larger leftward deflection.

The effect of relatively fast motion and leftward drift of the cyclone is to induce an environmental flow-through, from left-front to right-back, in cyclone-relative coordinates. Thus, a natural, flowthrough-induced asymmetry is superimposed on the cyclone's 700 mb wind field with strongest tangential winds in the left quadrant. The environmental flow-through from left-front to right-back yields clues to the future intensity changes of the cyclone in that the cyclone is being fed at its lower levels by the new environment in to which it moves. Since it is in the low levels that the cyclone must obtain its moisture supply, what lies ahead on the cyclone's path is what will enhance or retard future development. More intense cyclones have more nearly symmetric tangential wind fields and channels of flow emanating from the equator. An unusual, two-wave asymmetry pattern appears for cyclones which are approaching the westerlies and a strongly sheared environment.

7.3 Future Research

The analysis of Northwestern Pacific flight data have provided a wealth of new information on the changing structure of tropical cyclones. The success of removing the mean vortex and cyclone motion vectors to reveal the 700 mb interior background wind field is especially pertinent to the motion question. Opportunities for learning more from these flight data are very promising. The flight data for 1985-86 have also been recently processed for future analysis in conjunction with satellite data.

Much has been learned from these flight data about the evolution of the tropical cyclone. Yet, as we learn more, additional questions are raised, especially in regard to interactions which occur between the vortex and its environment beyond 2.5° and changes that cloud fields reveal during the cyclone's life cycle. In order to answer these questions, the tropical project, headed by Professor William Gray, is already in the process of gathering and compiling the accompanying satellite pictures that match the 1980-84 aircraft reconnaissance data set. Additionally, the synoptic fields at many levels shall be studied in order to obtain clearer answers to the motion question. With inclusion of the 1985-86 flight data, a total of 150 named tropical cyclones will be available for analysis. (Recall that the reconnaissance information terminated in August 1987). This continuing study of the evolution of the tropical cyclone's wind field should enhance our understanding of this extremely hazardous phenomenon and thereby enable us to improve our tropical cyclone forecasts. It is important that this western Pacific reconnaissance data be studied in conjunction with the satellite information so that when the reconnaissance data are no longer available, we can make the best possible use of the satellite information alone.

Chapter 8

GENERAL FORECASTING RULES, OBSERVATIONS, AND SCIENTIFIC HIGHLIGHTS

The findings of this study provide the basis for improved understanding and forecasting of the process by which tropical cyclones develop and move. In this chapter, the highlights of this research have been summarized into three categories: scientific highlights, general observations, and forecasting rules. It is emphasized that these are only generalizations and exceptions to these statements will occur.

8.1 Scientific Highlights

1. Cyclones were observed to develop from the inner core outward and also to decay from the inner core outward.

2. As cyclones intensify, the inner-core wind fields outside the RMW at 700 mb become more subgradient, implying a greater role of cumulus friction.

3. As cyclones intensify, the 700 mb residual wind current appears to be increasingly drawn into the inner core.

4. Increasing inertial stability of the outer core causes greater resistence to inflow, thereby diminishing the transport of momentum to the inner core.

5. If an eye appears at a relatively high MSLP when the outer core is less resistant to radial inflow, angular momentum will concentrate rapidly in the inner core, enhancing the deepening process. The longer it takes a cyclone to form an eye, the more resistant the outer core becomes to radial inflow, thus repressing the deepening process.

6. The greater the OCS, the more the cyclone drifts leftward relative to the 700 mb current.

7. The more intense the cyclone, the more symmetric the tangential wind field.

8. The sooner an eye appears, the more rapid the deepening rate, and the more likely it is that a cyclone will become intense, if embedded in a moist environment.

9. Cyclone deepening and filling is much more rapid when an eye is present.

8.2 General Observations

1. Cyclones in the northwestern Pacific move faster than the low-level environmental flow and also tend to drift to the left.

2. The greater the OCS, the greater the leftward drift relative to the 700 mb 0-2.5° steering current.

3. After removing the cyclone motion from the observed wind field, there is a maximum tangential wind speed on the left-back quadrant and a minimum on the right-front of the cyclone.

4. The more intense the cyclone, the smaller the radius of maximum winds.

5. The more intense the cyclone, the more symmetric the tangential wind field.

6. The greater the OCS, the greater 700 mb moisture content out to four degrees radius.

7. Cyclones that move southwestward are unlikely to intensify and typically do not intensify much past tropical storm stage. These cyclones move more slowly and drift more to the left than the average cyclone.

8. Cyclones moving eastward are likely to fill and to exhibit a two-wave asymmetry in their tangential wind field.

9. More intense cyclones are less likely to undergo a steady state period for central pressure.

10. For cyclones which have intensified below 955 mb, the filling portion of their life cycle typically has lower maximum wind speeds but higher OCS values than were observed in the deepening phase at the same central pressure.

11. The eye generally contracts while deepening and expands while the cyclone fills. Brief exceptions to this rule are common however and a transient change in size does not necessarily imply a change in intensity.

12. The size of circular eyes is less variable than for elliptical eyes. Size fluctuations of elliptical eyes are 4 to 5 times that of circular eyes.

13. Elliptical eyes are commonly seen when the cyclone is first forming an eye and when the eye begins to disappear.

14. Concentric eyes appear on average at 925 mb and were not found above 950 mb.

15. Intense cyclones exhibit a channel of flow from the South, thus tapping into the high θ_e air near the equator.

8.3 General Forecasting Rules

1. Intensifying cyclones expand their gale-force wind radii at an average rate of 40 km/d. A filling cyclone will continue to expand at this rate as long as an eye is present.

2. The strength of the 1-2.5° radius OCS is, on average, half the value of the maximum wind speed. For an intensifying cyclone, when the OCS is less than half the maximum wind, expect more rapid deepening than normal. For an intensifying cyclone, when the OCS is more than half the maximum wind speed, expect slower than normal deepening.

3. The OCS generally increases at a rate of 2.5 ms^{-1}/d regardless of whether the cyclone fills or deepens, as long as an eye exists.

4. A developing cyclone intensifies at an average rate of 8 $mb\ d^{-1}$ before the appearance of an eye and at 20 $mb\ d^{-1}$ immediately after the eye appears.

5. During intensification, the eye typically appears at an average MSLP value of 980 mb and disappears at 955 mb during filling.

6. For cyclones which achieve MSLP's below 955 mb, the outer core does not begin to weaken until the eye disappears.

7. The sooner the eye appears, the more rapid the rate of deepening and the more intense the cyclone is likely to become.

8. Cyclones which deepen rapidly ($\geq 42\ mb\ d^{-1}$) have usually formed an eye when they reach a MSLP of 985 mb. This eye will characteristically be smaller than average (40 km for rapid deepeners vs. 50 km diameter for all cyclones).

9. The later the eye appears, the slower the deepening rate and less likely it is that the cyclone will become intense.

10. The more intense the cyclone, the more closely the 700 mb level approximates the speed of the steering current.

ACKNOWLEDGEMENTS

This study would not have been possible without the tremendous support of Professor William Gray who originally suggested this research topic. I thank him for allowing me to pursue this subject, while providing me with all the needed programming, clerical and data reduction support. I found that the many discussions with Professor Gray, Professor Wayne Schubert, Dr. Robert Merrill, Dr. Greg Holland and Professor George Young opened up new ideas to apply to the problems of the tropical cyclone. Many thanks go to Mr. John Scheaffer for manuscript editing and overall text improvement. Ms. Barbara Brumit was instrumental in solving many problems encountered in putting this paper together. Thanks also to Mr. Bill Thorson and Mr. Todd Massey for their valuable programming expertise, Ms. Judy Sorbie for drafting the figures and Ms. Patti Nimmo for her clerical help. Funding for this research was provided by the U.S. Air Force for tuition and living expenses, and the National Science Foundation/National Oceanic and Atmospheric Administration Grant Numbers ATM 8418204 and ATM 8720488 and the DE0306 DOD-NAVY-ONR- Office of Naval Research Grant No. N00014-87-K-0203.

REFERENCES

Anthes, R. A., 1974: The dynamics and energetics of mature tropical cyclones. *Rev. Geoph. and Space Physics*, 12, 495-521.

Anthes, R. A., 1982: Tropical cyclones, their evolution, structure and effects. *Meteor. Monographs*, Vol. *19*, AMS, 45 Beacon Street, Boston, MA, 02108, 208 pp.

Arakawa, 1950: Mame–taifu or midget typhoon. *Geophys. Mag.*, 23, 463-474.

Atkinson, G. D. and C. R. Holliday, 1977: Tropical cyclone minimum sea level pressure maximum sustained wind relationship for the western North Pacific. *Mon. Wea. Rev.*, 105, 421-427.

Barnes, G. M., E. J. Zipser, D. Jorgensen, and F. Marks, 1983: Mesoscale and convective structure of a hurricane rainband. *J. Atmos. Sci.*, 40, 2125-2137.

Barnes, G. M., and G. J. Stossmeister, 1987: The structure and decay of a rainband in Hurricane Irene. Submitted to *Mon. Wea. Rev.*.

Brown, K. M., and J. E. Dennis, 1972: Derivative free analogues of the Levenberg-Marquardt and Gauss algorithms for nonlinear least squares approximations. *Numerische Mathematik*, 18, 289-297.

Chan, J. C. L., 1984: An observational study of the physical processes responsible for tropical cyclone motion. *J. Atmos. Sci.*, Vol. 41, 6, 1036-1048.

Chan, J. C. and W. M. Gray, 1982: Tropical cyclone movement and surrounding flow relationships. *Mon. Wea. Rev.*, 110, 1354-1374.

Chan, J. C. and W. M. Gray, 1984: An observational study of the physical processes responsible for tropical cyclone motion. *J. Atmos. Sci.*, Vol. 41, 6,1036-1048.

Colon, J. A. and Staff, NHRP, 1961: On the structure of Hurricane Daisy (1958). NHRP Report No. 48, 102 pp.

Colon, J. A. and Staff, NHRP, 1963: On the evolution of the wind field during the life cyclone of tropical cyclones. NHRP Report No. 65, 36 pp.

Colon, J. A. and Staff, NHRP, 1964: On the structure of Hurricane Helene (1958). NHRP Report No. 72, 50 pp.

Depperman, C. E., 1947: Notes on the Origin and Structure of Philippine Typhoons. *Bull. Amer. Meteor. Soc.*, 9, 399-404.

DeMaria, M., 1985: Tropical cyclone motion in a nondivergent barotropic model. *Mon. Wea. Rev.*, 113, 1199-1210.

Dunn, 1951: Tropical cyclones. Compendium of Meteorology, American Meteorological Society, 45 Beacon St., Boston, MA, 02108, 887-901.

Dunnavan, G. M., 1983: An evaluation of 700 mb aircraft reconnaissance data for selected northwest Pacific tropical cyclones. M.S. Thesis, Naval Post Graduate School, Monterey, CA, 92 pp.

Dvorak, V. F., 1975: Tropical cyclone intensity analysis and forecasting from satellite imagery. *Mon. Wea. Rev.*, 103, 420-430.

Elliassen, A., 1951: Slow thermally or frictionally controlled motions in a circular vortex. *Astrophys. Norv.*, 5, 19-60.

Frank, W. M., 1977: The structure and energetics of the tropical cyclone I. Storm structure. *Mon. Wea. Rev.*, 105, 1119-1135.

Frank, W. M., and W. M. Gray, 1980: Radius and frequency of 15 m/s (30 kt) winds around tropical cyclones. *J. Appl. Meteor.*, 19 219-223.

Frank, W. M., 1984: Composite analysis of the core of Hurricane Frederick 1979. *Mon. Wea. Rev.*, 112, 2401-2420.

George, J. E. 1975: Tropical cyclone motion and surrounding parameter relationships. Dept. Atmos. Sci. Paper No. 241, Colo. State Univ., Fort Collins, CO, 105 pp.

George, J. E., and W. M. Gray, 1976: Tropical cyclone motion and surrounding parameter relationships. *J. Appl. Meteor.*, 15, 1252-1264.

Gray, W. M., 1962: On the balance of forces and radial accelerations in hurricanes. *Quart. J. Roy. Meteor. Soc.*, 88, 430-458.

Gray, W. M., 1965: Calculations of cumulus vertical draft velocities in hurricanes from aircraft observations. *J. Appl. Meteor.*, 4, 463- 474.

Gray, W. M., 1967: The mutual variation of wind, shear and baroclinicity in the cumulus convective atmosphere. *Mon. Wea. Rev.*, 95, 55-74.

Gray, W. M., 1977: Tropical disturbance to cyclone transformation. Paper presented at the 11th Technical Conference on Hurricanes and Tropical Meteorology, Dec. 13-16, Miami, FL, 27-34.

Gray, W. M., 1979: Hurricanes: their formation, structure, and likely role in the tropical cyclone. Meteorology over the Tropical Oceans. D. B. Shaw, Ed., *Roy. Meteor. Soc.*, 155-218.

Gray, W. M., 1981: Recent advances in tropical cyclone research from rawinsonde composite analysis. WMO Programme on Research in Tropical Meteorology. This report was prepared at the request of the WMO Commission for Atmospheric Science, Geneva, Switzerland, 407 pp.

Gray, W. M, and W. M. Frank, 1977: Tropical cyclone research by data compositing. US Navy Environmental Prediction Research Facility Report. Tech Paper No. 77-01.

Gray, W. M., and D. J. Shea, 1973: The hurricane's inner core region. II. Thermal stability and dynamic characteristics. *J. Atmos. Sci.*, 30, 1565-1576.

Hack, J. J., and W. H. Schubert, 1986: On the nonlinear response of atmopheric vortices to heating by organized cumulus convection. *J. Atmos. Sci.*, 43, 1559-1573.

Hawkins, H. F., 1962: Vertical wind profiles in hurricanes. NHRP Report No. 55, 16 pp.

Hawkins, H. F. and D. T. Rubsam, 1968a: Hurricane Hilda, 1964. I: Genesis, as revealed by satellite photographs conventional and aircraft data. *Mon. Wea. Rev.*, 96, 428-452.

Hawkins, H. F. and D. T. Rubsam, 1968b: Hurricane Hilda, 1964. II: Structure and budgets of the hurricane on October 1, 1964. *Mon. Wea. Rev.*, 96, 617-636.

Hawkins, H. F., 1971: Comparison of results of the Hurricane Debbie (1969) modification experiments with those from Rosenthal's numerical model simulation experiments. *Mon. Wea. Rev.*, 99, 427-434.

Hawkins, H. F. and S. M. Imbembo, 1976: The structure of a small intense hurricane—Inez 1966. *Mon. Wea. Rev.*, 104, 418-442.

Henderson, R. S., 1978: USAF Aerial Weather Reconnaissance using the Lockheed WC-130 Aircraft. *Bull. Amer. Meteor. Soc.*, 59, 1136- 1143.

Holland, G. J., 1980: An analytical model of the wind and pressure profiles in hurricanes. *Mon. Wea. Rev.*, 108, 8, 1212-1218.

Holland, G. J.,1983: Tropical cyclone motion: environmental interaction plus a beta effect. *J. Atmos. Sci.*, 40, 328-342.

Holland, G. J., and R. T. Merrill, 1984: On the dynamics of tropical cyclone structure changes. *Quart. J. Meteor. Soc.*, 110, 723-745.

Holliday, C. R., and A. H. Thompson, 1979: Climatological characteristics of rapidly intensifying typhoons. *Mon. Wea. Rev.*, 107, 1022-1034.

Hughes, L. A., 1952: On the low level wind structure of tropical cyclones. *J. Meteor.*, 9, 422-428.

Jilesnianski, C., 1973: A preliminary view of storm surges before and after storm modifications. NOAA Tech. Memo, ERL WMPO-3, 33 pp.

Jordan, C. L., 1961: Marked changes in the characteristics of the eye of intense typhoons between the deepening and filling stages. *J. Meteor.*, 15, 779-789.

Jordan, C. L., D. A. Hurt and C. A. Lowry, 1960: On the structure of Hurricane Daisy of 27 August 1958. *J. Meteor.*, 17, 337-348.

Jorgensen, D. P., 1984a: Mesoscale and convective scale characteristics of mature hurricanes. I. General observations by research aircraft. *J. Atmos. Sci.*, 41, 1268-1285.

Jorgensen, D. P., 1984b: Mesoscale and convective scale characteristics of mature hurricanes II. Inner core structure of hurricane Allen (1980). *J. Atmos. Sci.*, 41, 1287-1311.

LaSeur, N. E., and H. F. Hawkins, 1963: An analysis of Hurricane Cleo (1958) based on data from research reconnaissance aircraft. *Mon. Wea. Rev.*, 91, 694-709.

Lee, C.-S., 1984: The bulk effects of cumulus momentum transports in tropical cyclones. *J. Atmos. Sci.*, 41, 4, 590-603.

Lee, C.-S., 1986: An observational study of tropical cloud cluster evolution and cyclogenesis in the western north Pacific. Dept. of Atmos. Sci. Paper No. 403, Colo. State Univ., Ft. Collins, CO, 250 pp.

Lee, C.-S., 1989a: An observational study of tropical cloud cluster evolution and cyclogenesis in the western North Pacific: I: Background and evolution of non-genesis cloud clusters. Accepted by *J. Atmos. Sci.*, 46 (in press).

Lee, C.-S., 1989b: An observational study of tropical cloud cluster evolution and cyclogenesis in the western North Pacific: II: Evolution of genesis cloud clusters and comparison to non-genesis cases. Accepted by *J. Atmos. Sci.*, 46 (in press).

Lee, C.-S., 1989c: An observational study of tropical cloud cluster evolution and cyclogenesis in the western North Pacific: III: Moisture, energy, and angular momentum budget analysis. Submitted to *Mon. Wea. Rev.*

Levenberg, K., 1944: A Method for the solution of certain non-linear problems in least squares. *Quart. Appl. Math.*, 2, 164-168.

Marks, F. D., and R. A. Houze, 1987: Inner core structure of Hurricane Alicia from airborne Doppler radar observations. Submitted to *J. Atmos. Sci.*

Marquardt, D. W., 1963: An algorithm for least-squares estimation of nonlinear parameters. *J. Siam.*, 11.

Matsumoto, C. R., 1984: A statistical method for one- to three-day tropical cyclone track prediction. Dept. of Atmos. Sci. Paper No. 379, Colo. State Univ., Ft. Collins, CO, 80523, 201 pp.

Matsumoto, C. L., and W. M. Gray, 1986: A statistical method for one- to three-day tropical cyclone track prediction. Being submitted to *Mon. Wea. Rev.*

Merrill, R. T., 1984: A comparison of large and small tropical cyclones. *Mon. Wea. Rev.*, 112, 1408-1418.

Merrill, R. T., 1988a: Characteristics of the upper-tropospheric environmental flow around hurricanes. *J. Atmos. Sci.*, 45, 1665-1677.

Merrill, R. T., 1988b: Environmental influences on hurricane intensification. *J. Atmos. Sci.*, 45, 1678-1687.

Miller, B. I., 1958: On the maximum intensity of hurricanes. *J. Meteor.*, 15, 185-195.

Miller, B. I., 1958: The three dimensional wind structure around a tropical cyclone. NHRP Report No. 15, 41 pp.

Miller, B. I., 1962: On the momentum and energy balance of Hurricane Helene (1958). NHRP Report No. 53, 19 pp.

Powell, M. D., 1982: The transition of the Hurricane Frederick boundary-layer wind field from the open Gulf of Mexico to landfall. *Mon. Wea. Rev.*, 110, 1912-1932.

Ooyama, K., 1969: Numerical simulation of the life cycle of tropical cyclones. *J. Atmos. Sci.*, 26, 3-39.

Ooyama, K., 1982: Conceptual evolution of the theory and modeling of the tropical cyclone. *J. Meteor. Soc. Japan*, 60, 369-379.

Riehl, H., and J. Malkus, 1961: Some aspects of Hurricane Daisy, 1958. *Tellus*, 13, 181-213.

Schubert, W. H., and J. Hack, 1982: Inertial stability and tropical cyclone development. *J. Atmos. Sci.*, 39, 1687-1697.

Shapiro, L. J., and H. E. Willoughby, 1982: The response of balanced hurricanes to local sources of heat and momentum. *J. Atmos. Sci.*, 39, 378-394.

Shea, D. J., and W. M. Gray, 1973: The hurricane's inner core region. I. Symmetric and asymmetric structure. *J. Atmos. Sci.*, 30, 1544-1564.

Shea, D. J., and W. M. Gray, 1976: Data summary of NOAA's hurricane inner-core radial leg flight penetrations 1957-1967, and 1969. Dept. of Atmos. Sci. Paper No. 257, Colo. State Univ., Fort Collins, CO, 220 pp.

Sheets, R. C., 1967a: On the structure of Hurricane Janice (1958). NHRL Report No. 76, 38 pp.

Sheets, R. C., 1967b: On the structure of Hurricane Ella (1962). NHRL Report No. 77, 33 pp.

Sheets, R. C., 1968: On the structure of Hurricane Dora (1964). NHRL Report No. 83, 64 pp.

Weatherford, C. L., 1985: Typhoon structural variability. Dept. of Atmos. Sci. Paper No. 391, Colo. State Univ., Ft. Collins, CO, 80523, 77 pp.

Weatherford, C., and W. M. Gray, 1988a: Typhoon structure as revealed by aircraft reconnaissance: Part I: Data analysis and climatology. *Mon. Wea. Rev.*, Vol. 116, 5, 1032-1043.

Weatherford, C., and W. M. Gray, 1988b: Typhoon structure as revealed by aircraft reconnaissance: Part II: Structural variability. *Mon. Wea. Rev.*, Vol. 116, 5, 1044-1056.

Willoughby, H. E., 1978: A possible mechanism for the formation of hurricane rainbands. *J. Atmos. Sci.*, 35, 838-858.

Willoughby, H. E., 1979: Forced secondary circulations in hurricanes. *J. Geophys. Res.*, 84, 3173-3183.

Willoughby, H. E., J. A. Clos and M. G. Shoreibah, 1982: Concentric eye walls, secondary wind maxima, and the evolution of the hurricane vortex. *J. Atmos. Sci.*, 39, 395-411.

Willoughby, H. E., F. D. Marks, and R. J. Feinberg, 1984: Stationary and moving convective bands in hurricanes. *J. Atmos. Sci.*, 41, 3189-3211.

Zehr, R., 1987: The diurnal variation of deep convective clouds and cirrus with tropical cyclones. Paper presented at the 17th Technical Conference on Hurricanes and Tropical Meteorology, April 7-10, Miami, FL, 4 pp.

Appendix A

INDIVIDUAL CASE LIFE CYCLE PATTERNS

The cyclone life cycle patterns portrayed in the text of this paper were derived from the compositing of a large number of individual cases. In order to better document the variations typical of individual cases, the following typhoons have been depicted throughout the time during which aircraft reconnaissance observed their major features. Four fields are portrayed in each case; the eye temperature, OCS, MSLP, and eye diameter. The temperature of the eye (dashed curve) was taken at the warmest location at 700 mb. The largest value can be seen for Supertyphoon Vanessa who obtained 31°C. The OCS (upper solid curve) was an area-weighted average wind speed at 700 mb from 1° to 2.5° radius. The solid lower curve depicts the MSLP. Finally, the dotted curve portrays the diameter of the eyewall with the following shape codes superimposed on the plot: "E" enclosed by a triangle denotes an elliptical eye, "O" marks a circular eye, and "C" enclosed by a circle denotes concentric eyes with both diameters depicted.

TYPHOON DOM 1980

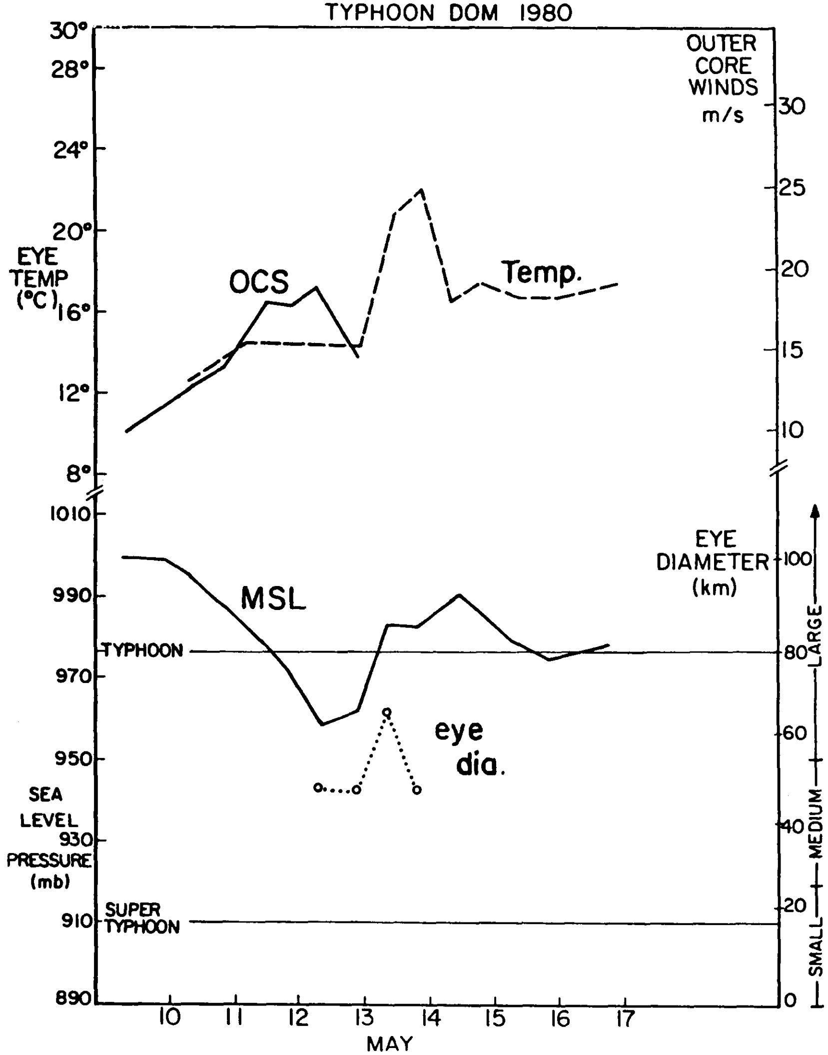

TYPHOON ELLEN 1980

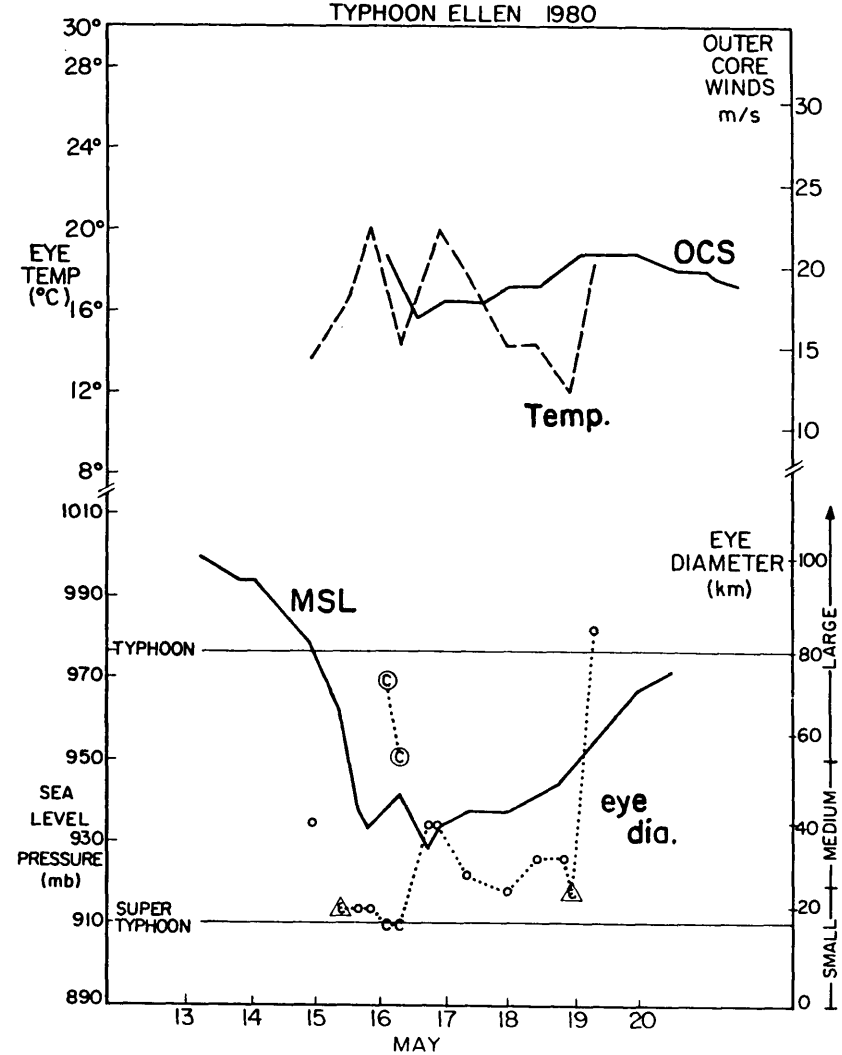

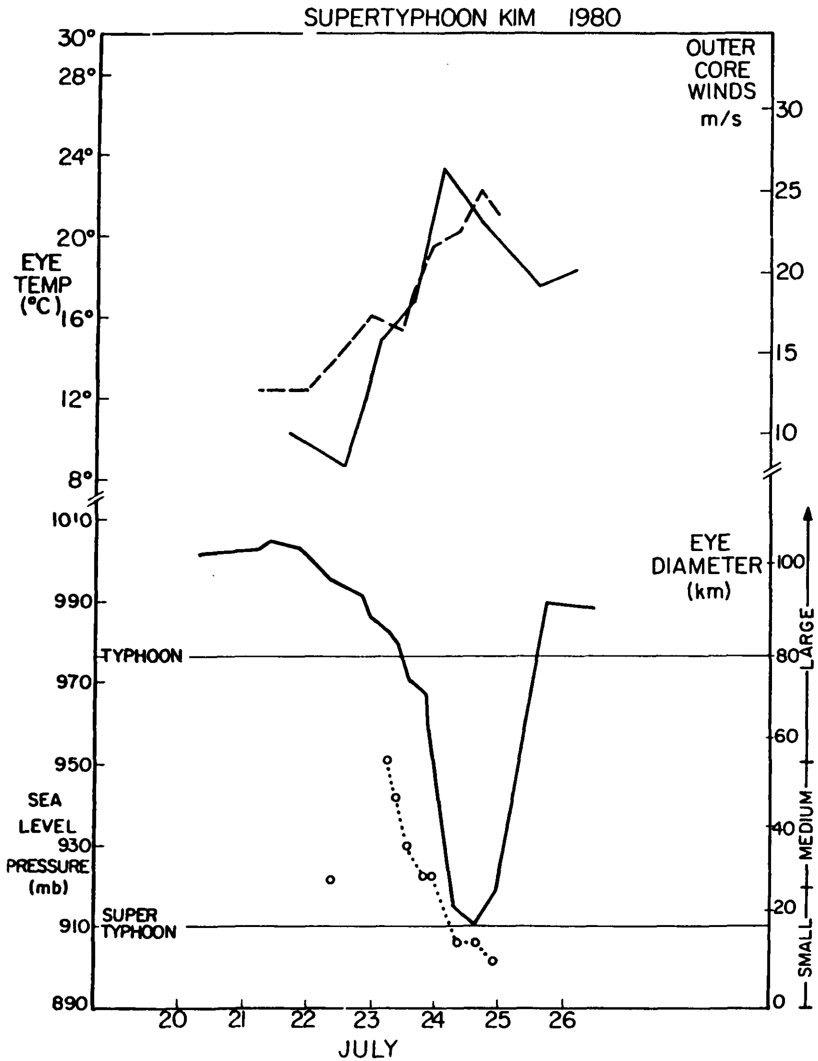
SUPERTYPHOON KIM 1980
OUTER CORE WINDS m/s
EYE TEMP (°C)
30°
28°
24°
20°
16°
12°
8°
30
25
20
15
10
EYE DIAMETER (km)
SEA LEVEL PRESSURE (mb)
1010
990
970
950
930
910
890
TYPHOON
SUPER TYPHOON
100
80
60
40
20
0
LARGE
MEDIUM
SMALL
20
21
22
23
24
25
26
JULY

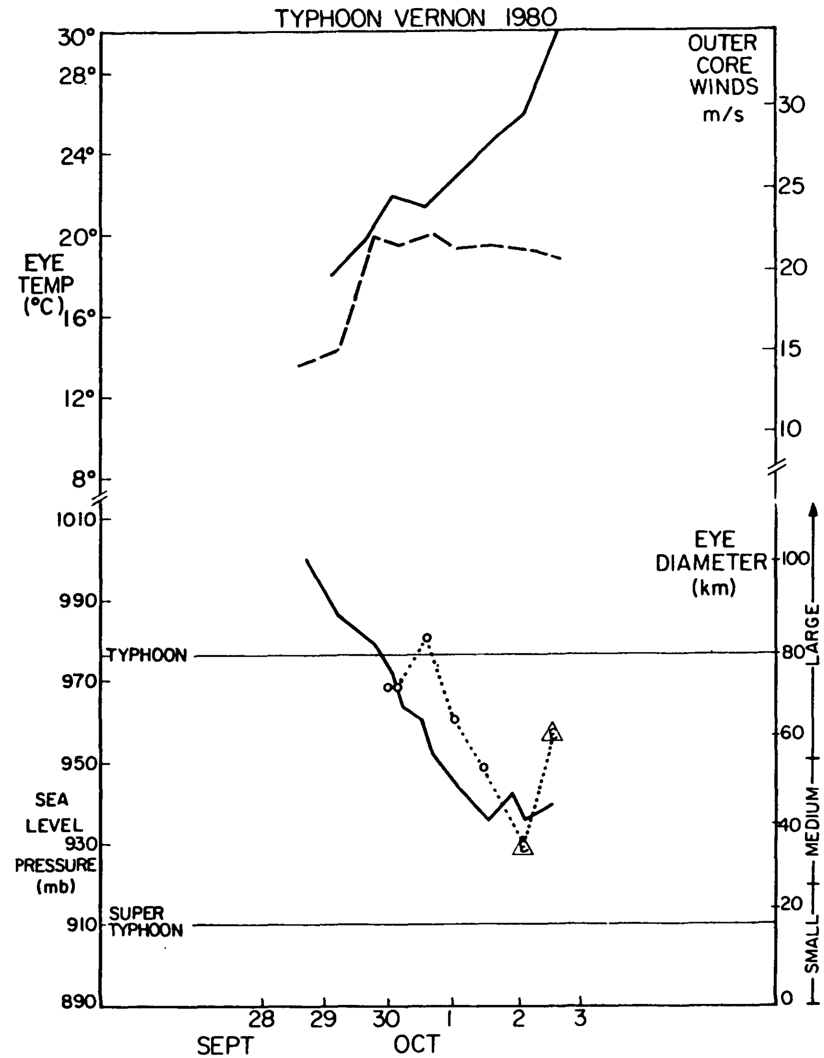
TYPHOON VERNON 1980
OUTER CORE WINDS m/s
EYE TEMP (°C)
30°
28°
24°
20°
16°
12°
8°
30
25
20
15
10
EYE DIAMETER (km)
SEA LEVEL PRESSURE (mb)
1010
990
970
950
930
910
890
TYPHOON
SUPER TYPHOON
100
80
60
40
20
0
LARGE
MEDIUM
SMALL
28
29
30
1
2
3
SEPT
OCT

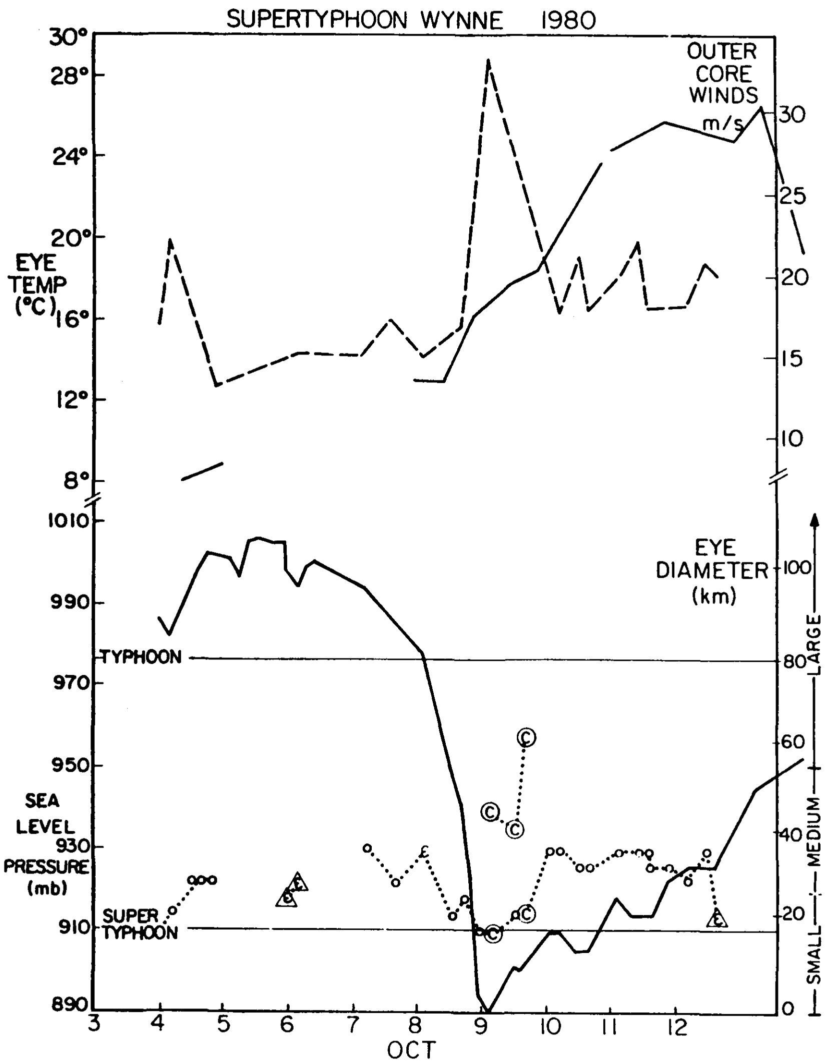
SUPERTYPHOON WYNNE 1980
EYE TEMP (°C)
OUTER CORE WINDS m/s
EYE DIAMETER (km)
SEA LEVEL PRESSURE (mb)
TYPHOON
SUPER TYPHOON
SMALL — MEDIUM — LARGE
OCT

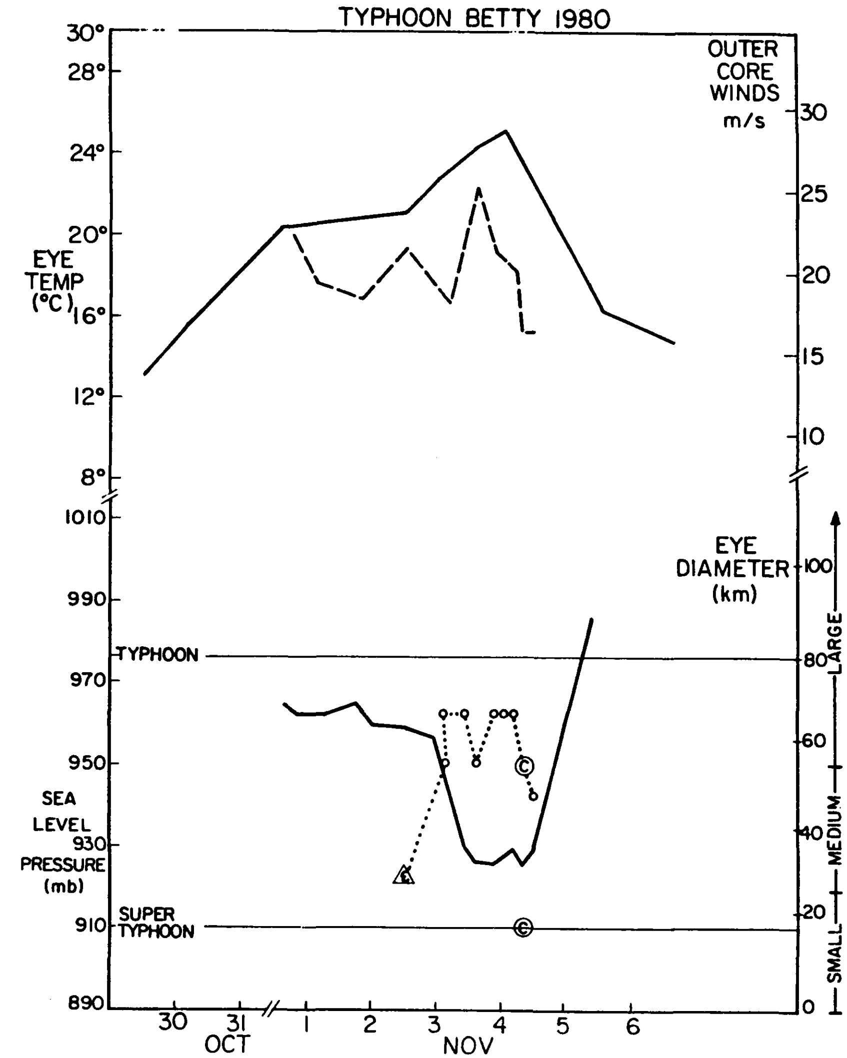
TYPHOON BETTY 1980
EYE TEMP (°C)
OUTER CORE WINDS m/s
EYE DIAMETER (km)
SEA LEVEL PRESSURE (mb)
TYPHOON
SUPER TYPHOON
SMALL — MEDIUM — LARGE
OCT
NOV

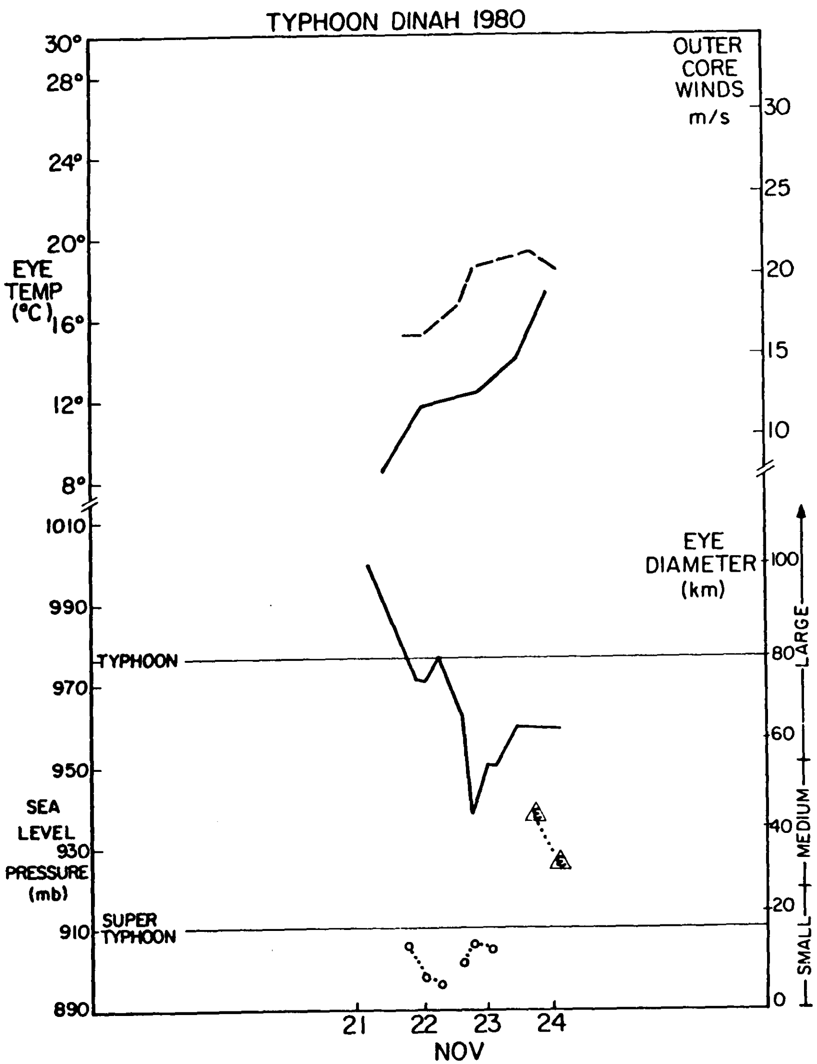
TYPHOON DINAH 1980
OUTER CORE WINDS m/s
EYE TEMP (°C)
30°
28°
24°
20°
16°
12°
8°
30
25
20
15
10
1010
990
970
950
930
910
890
SEA LEVEL PRESSURE (mb)
TYPHOON
SUPER TYPHOON
EYE DIAMETER (km)
100
80
60
40
20
0
LARGE
MEDIUM
SMALL
21
22
23
24
NOV

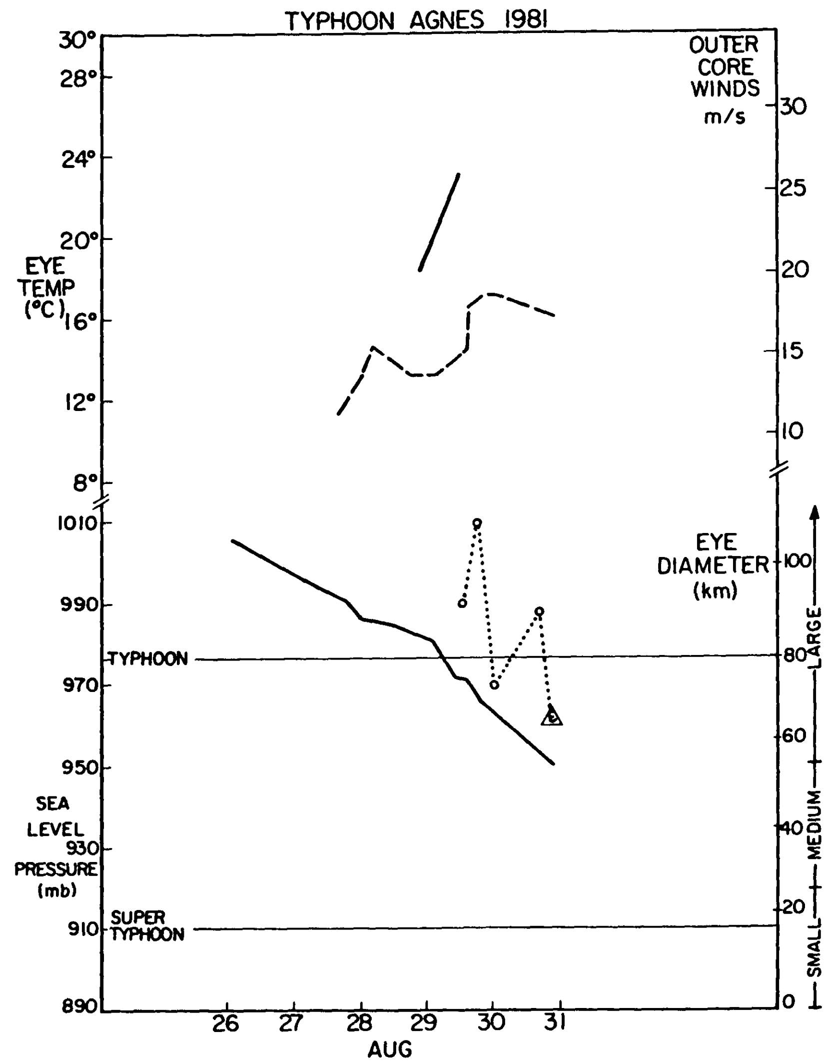
TYPHOON AGNES 1981
OUTER CORE WINDS m/s
EYE TEMP (°C)
30°
28°
24°
20°
16°
12°
8°
30
25
20
15
10
1010
990
970
950
930
910
890
SEA LEVEL PRESSURE (mb)
TYPHOON
SUPER TYPHOON
EYE DIAMETER (km)
100
80
60
40
20
0
LARGE
MEDIUM
SMALL
26
27
28
29
30
31
AUG

TYPHOON THAD 1981

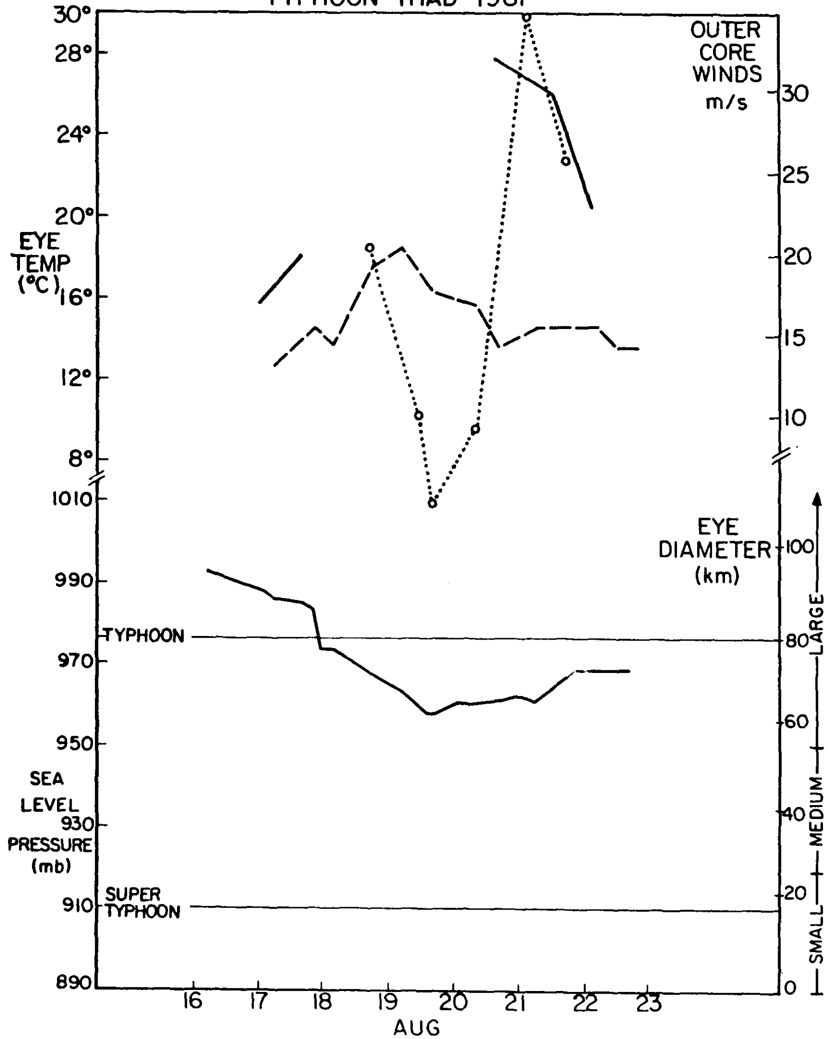

TYPHOON BILL 1981

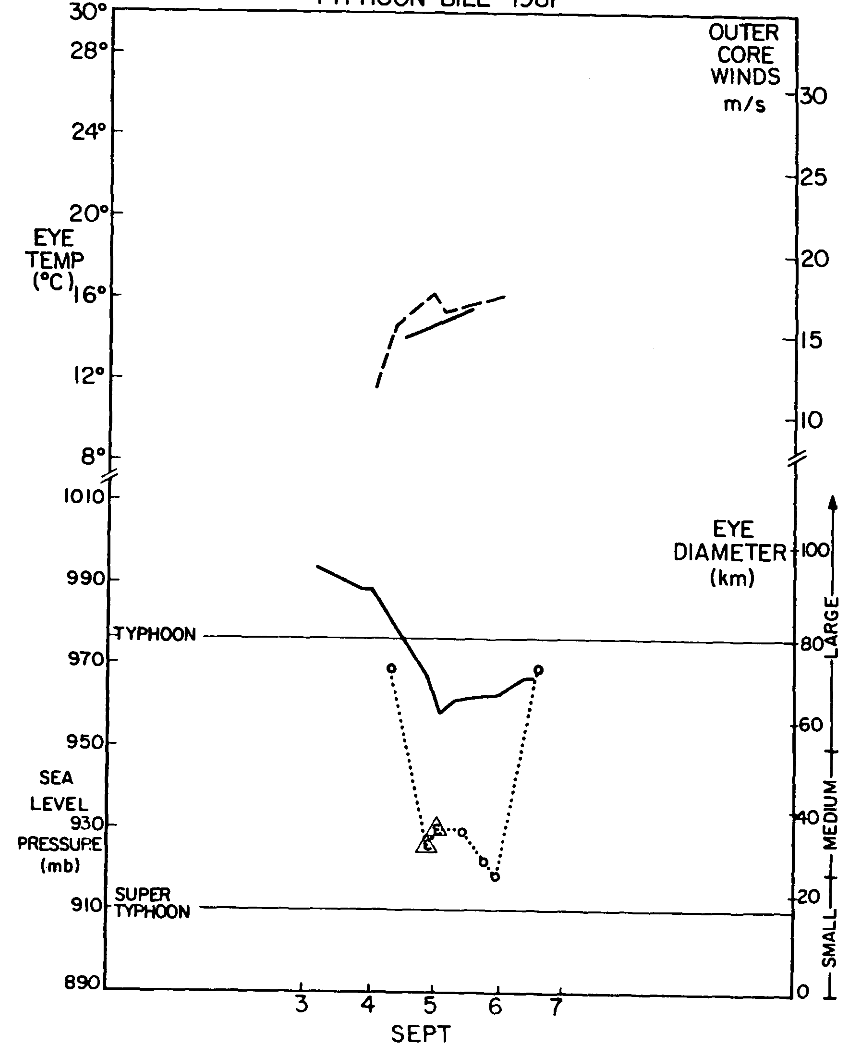

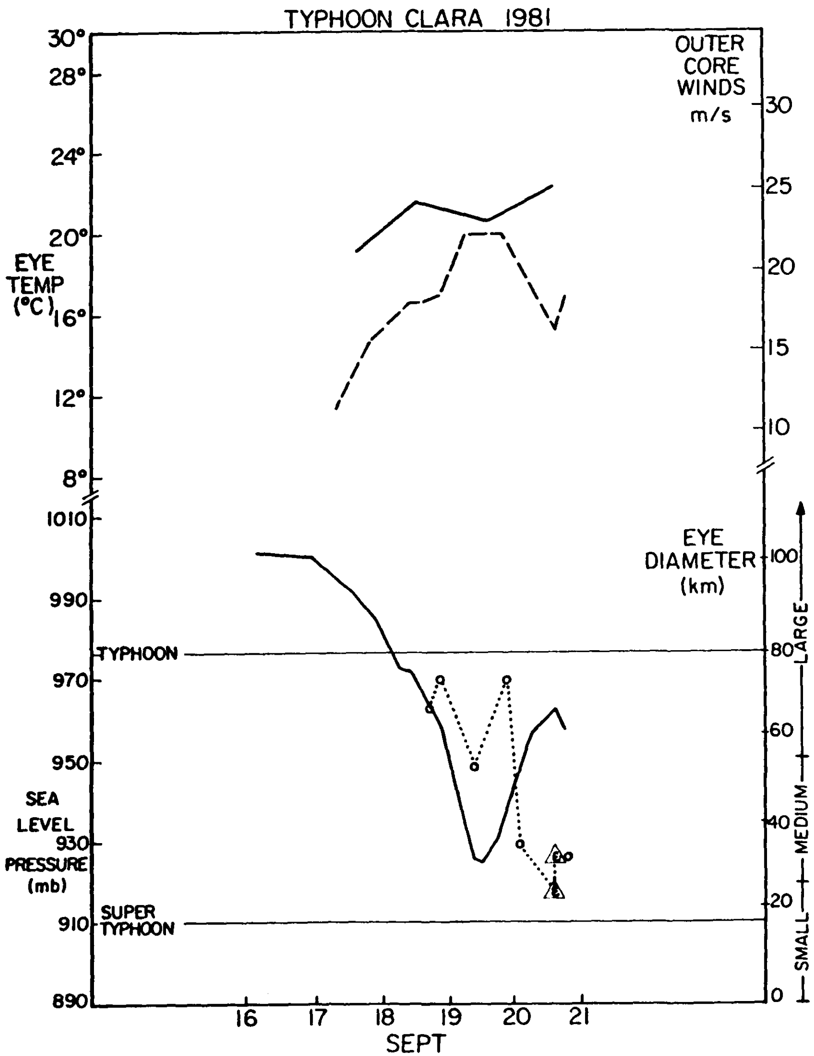
TYPHOON CLARA 1981
OUTER CORE WINDS m/s
EYE TEMP (°C)
EYE DIAMETER (km)
SEA LEVEL PRESSURE (mb)
TYPHOON
SUPER TYPHOON
LARGE
MEDIUM
SMALL
SEPT
30°
28°
24°
20°
16°
12°
8°
1010
990
970
950
930
910
890
30
25
20
15
10
100
80
60
40
20
0
16
17
18
19
20
21

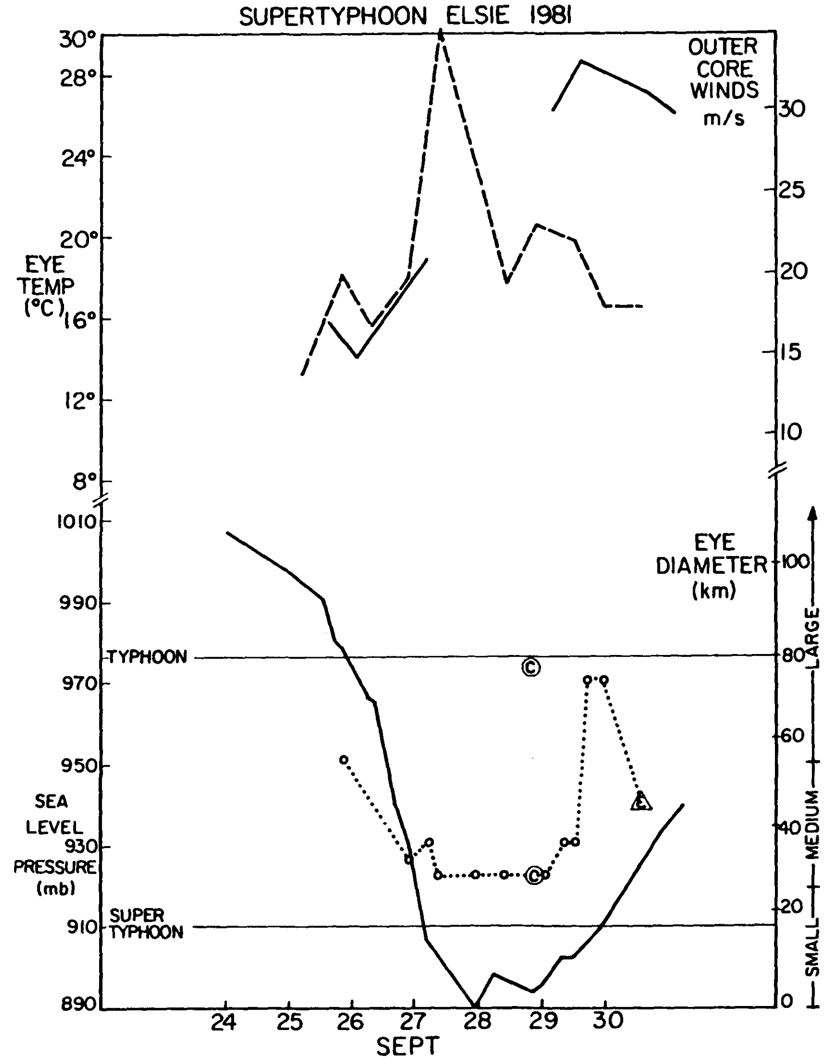
SUPERTYPHOON ELSIE 1981
OUTER CORE WINDS m/s
EYE TEMP (°C)
EYE DIAMETER (km)
SEA LEVEL PRESSURE (mb)
TYPHOON
SUPER TYPHOON
LARGE
MEDIUM
SMALL
SEPT
30°
28°
24°
20°
16°
12°
8°
1010
990
970
950
930
910
890
30
25
20
15
10
100
80
60
40
20
0
24
25
26
27
28
29
30

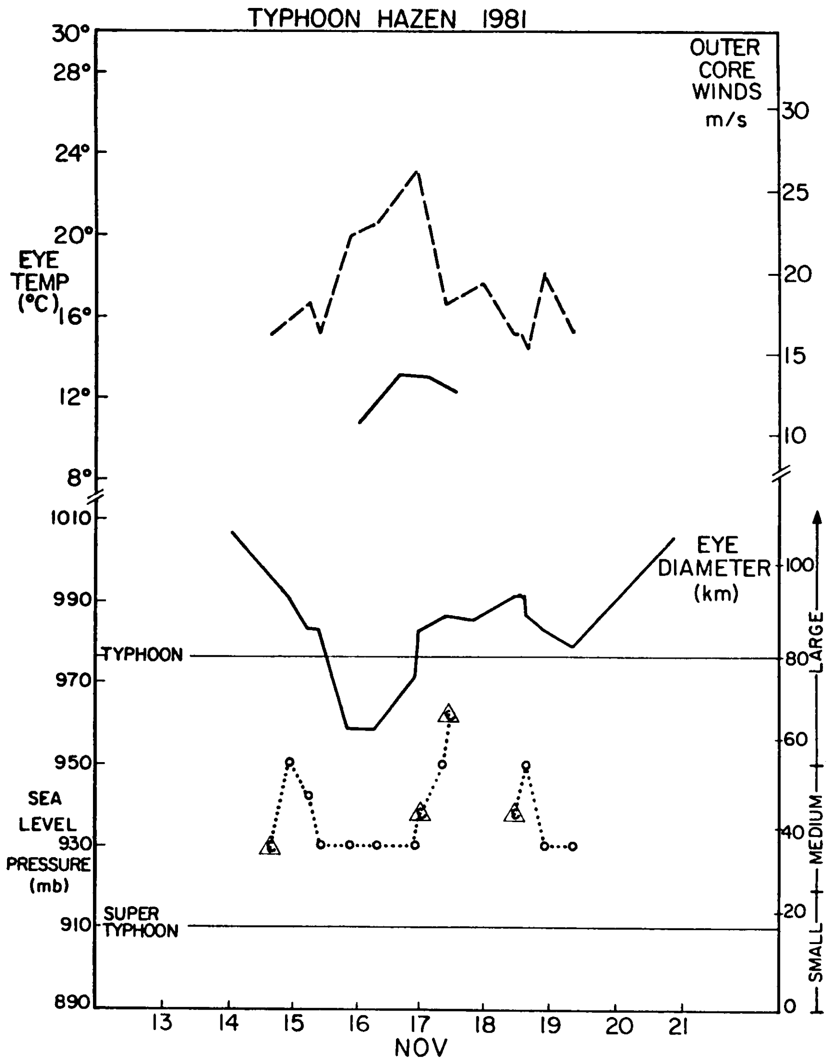
TYPHOON HAZEN 1981
EYE TEMP (°C)
OUTER CORE WINDS m/s
EYE DIAMETER (km)
SEA LEVEL PRESSURE (mb)
TYPHOON
SUPER TYPHOON
LARGE
MEDIUM
SMALL
NOV

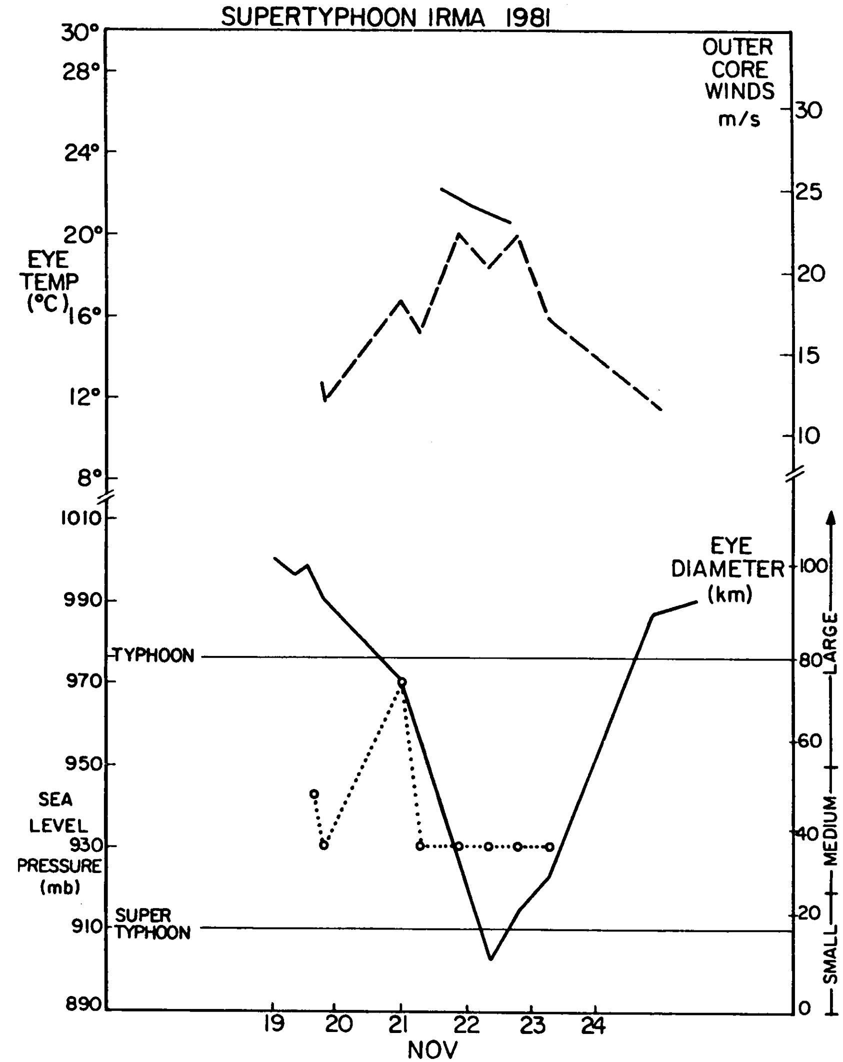
SUPERTYPHOON IRMA 1981
EYE TEMP (°C)
OUTER CORE WINDS m/s
EYE DIAMETER (km)
SEA LEVEL PRESSURE (mb)
TYPHOON
SUPER TYPHOON
LARGE
MEDIUM
SMALL
NOV

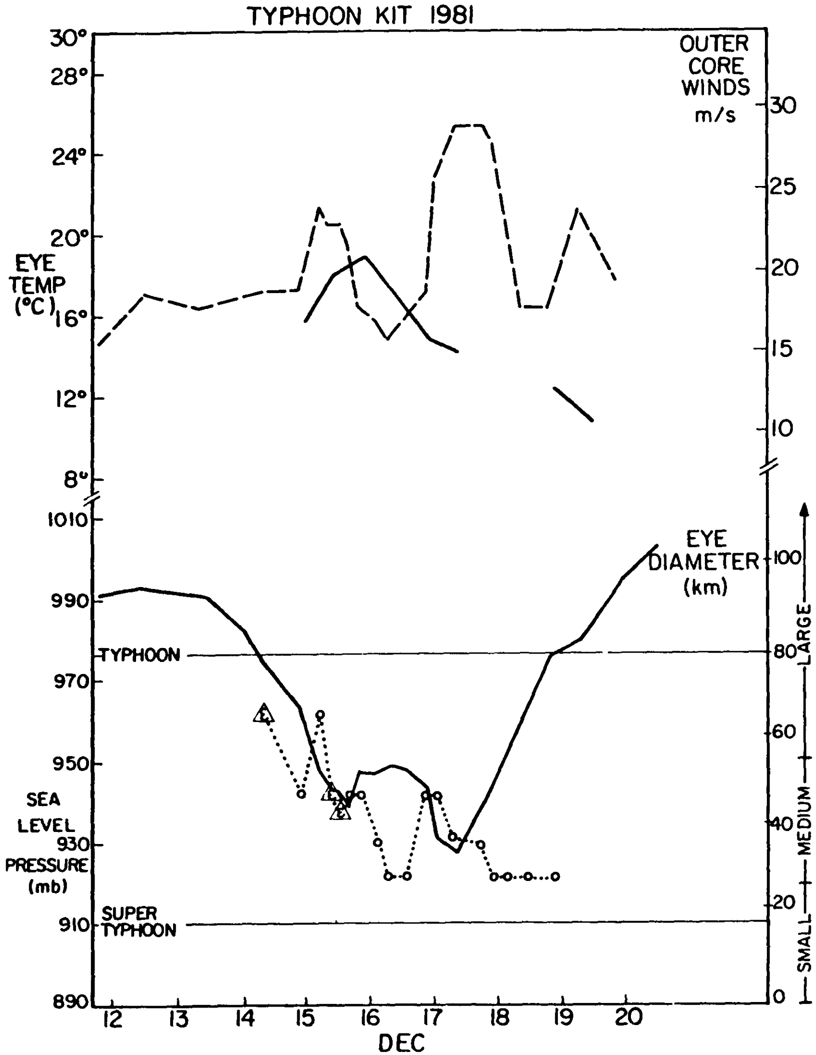
TYPHOON KIT 1981
OUTER CORE WINDS m/s
EYE TEMP (°C)
30° 28° 24° 20° 16° 12° 8°
30 25 20 15 10
1010 990 970 950 930 910 890
TYPHOON
SUPER TYPHOON
SEA LEVEL PRESSURE (mb)
EYE DIAMETER (km)
100 80 60 40 20 0
LARGE
MEDIUM
SMALL
12 13 14 15 16 17 18 19 20
DEC

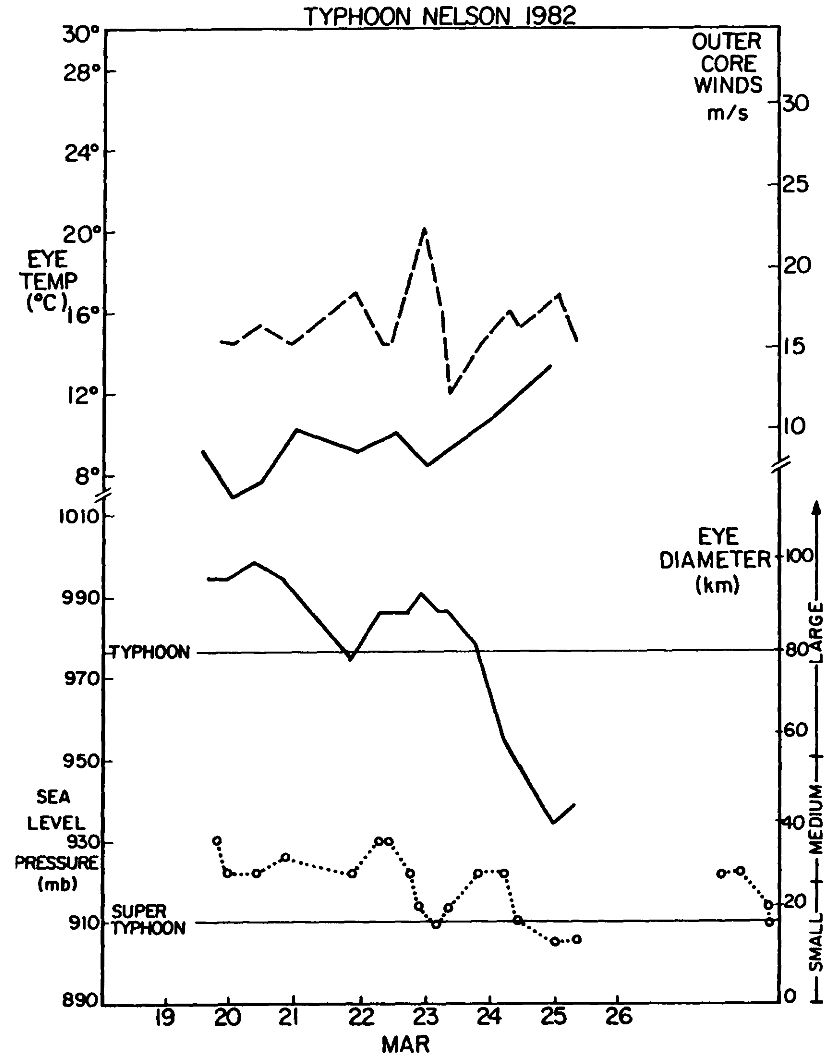
TYPHOON NELSON 1982
OUTER CORE WINDS m/s
EYE TEMP (°C)
30° 28° 24° 20° 16° 12° 8°
30 25 20 15 10
1010 990 970 950 930 910 890
TYPHOON
SUPER TYPHOON
SEA LEVEL PRESSURE (mb)
EYE DIAMETER (km)
100 80 60 40 20 0
LARGE
MEDIUM
SMALL
19 20 21 22 23 24 25 26
MAR

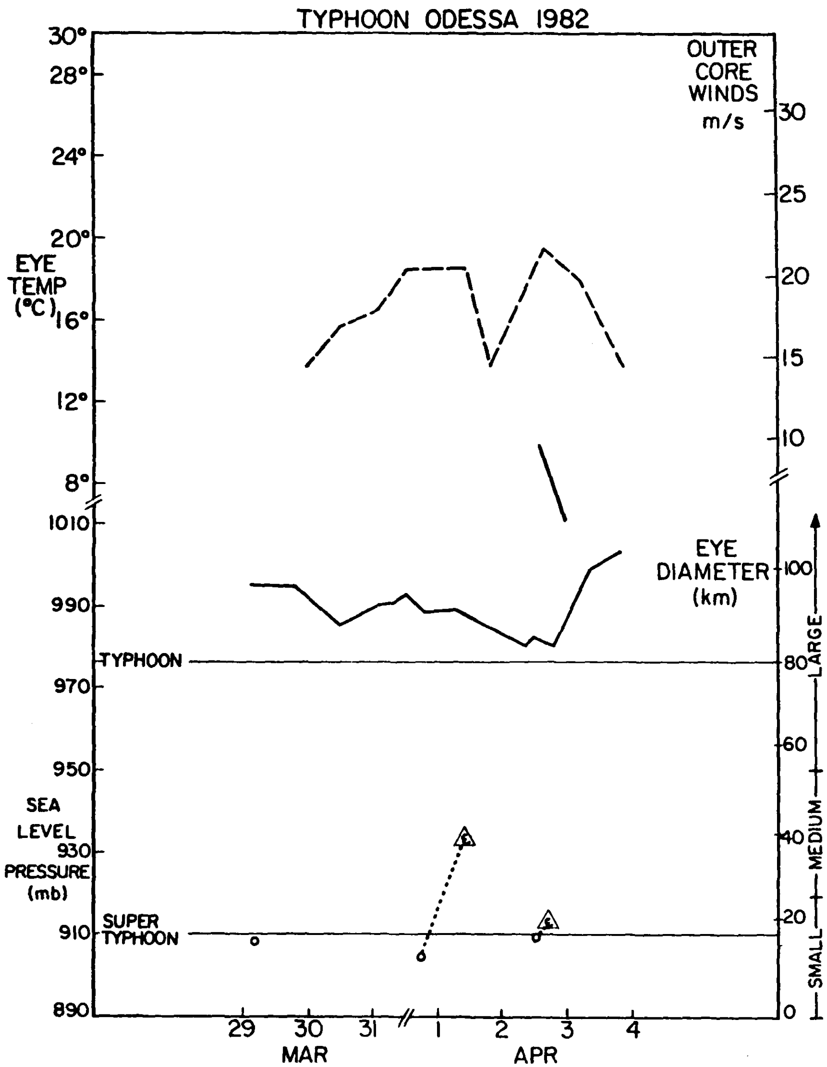
TYPHOON ODESSA 1982
EYE TEMP (°C)
OUTER CORE WINDS m/s
EYE DIAMETER (km)
SEA LEVEL PRESSURE (mb)
TYPHOON
SUPER TYPHOON
SMALL
MEDIUM
LARGE
MAR
APR

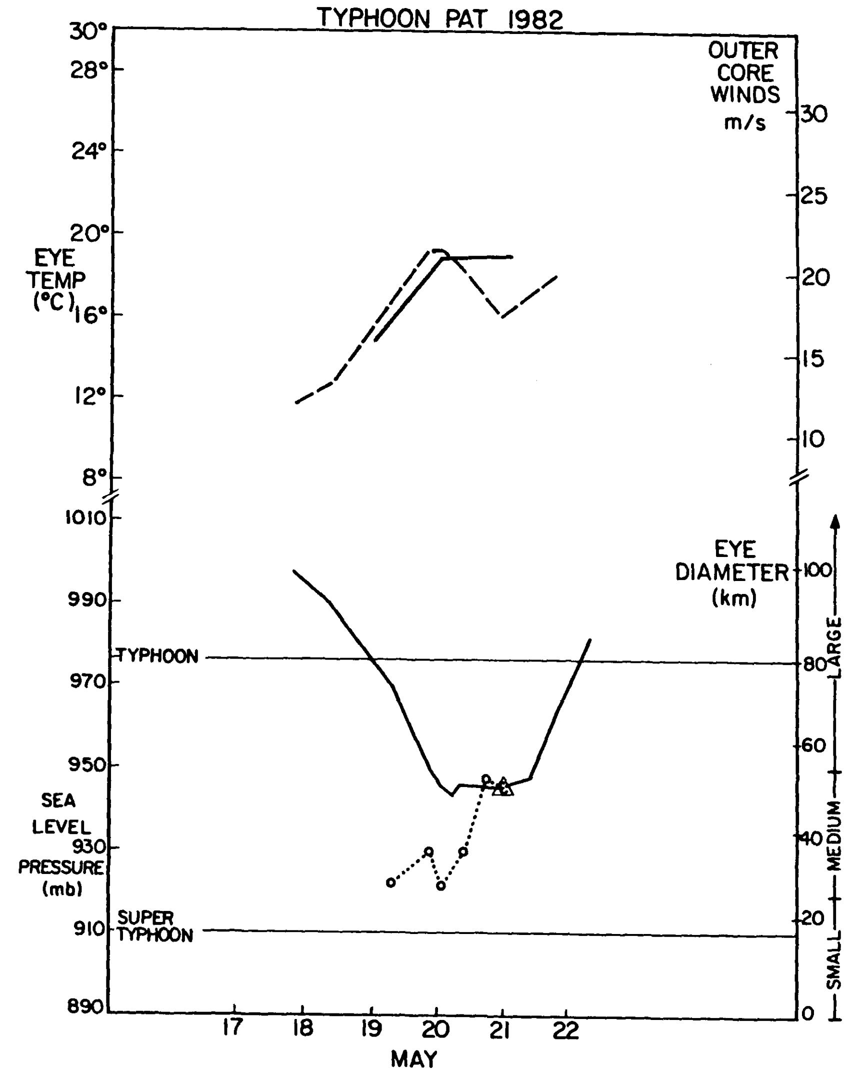
TYPHOON PAT 1982
EYE TEMP (°C)
OUTER CORE WINDS m/s
EYE DIAMETER (km)
SEA LEVEL PRESSURE (mb)
TYPHOON
SUPER TYPHOON
SMALL
MEDIUM
LARGE
MAY

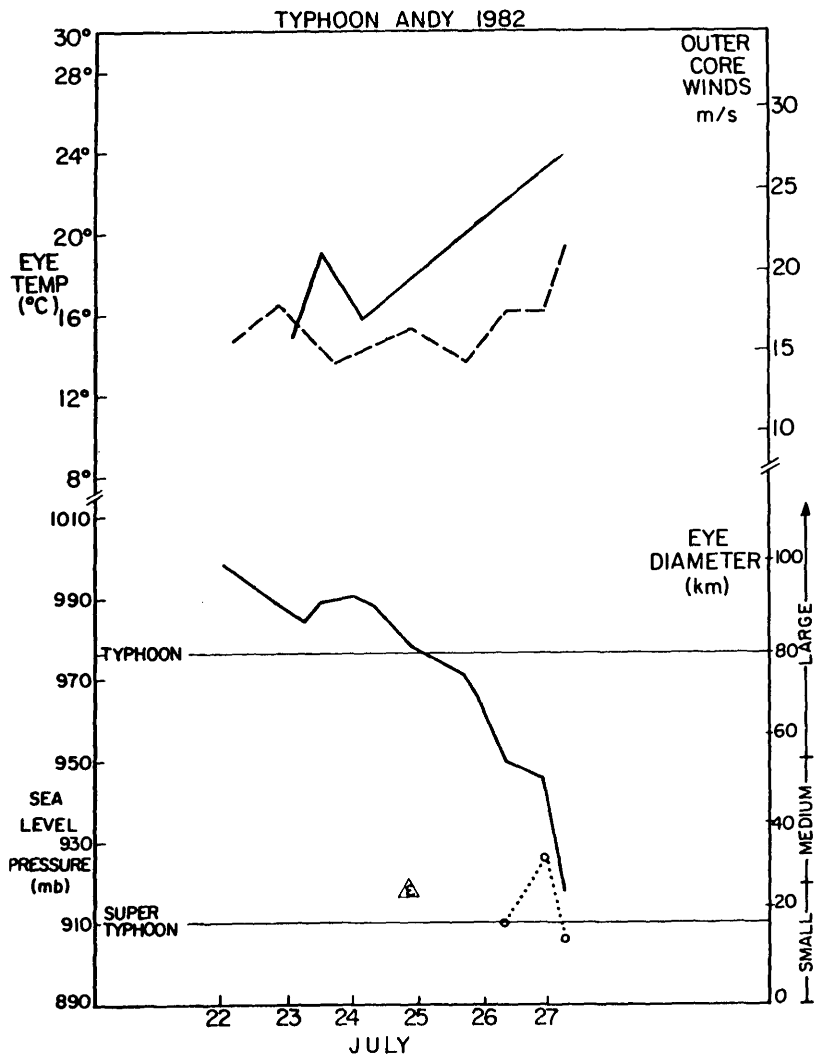
TYPHOON ANDY 1982
30°
28°
24°
20°
16°
12°
8°
EYE
TEMP
(°C)
OUTER
CORE
WINDS
m/s
30
25
20
15
10
1010
990
970
950
930
910
890
TYPHOON
SUPER
TYPHOON
SEA
LEVEL
PRESSURE
(mb)
EYE
DIAMETER
(km)
100
80
60
40
20
0
LARGE
MEDIUM
SMALL
22
23
24
25
26
27
JULY

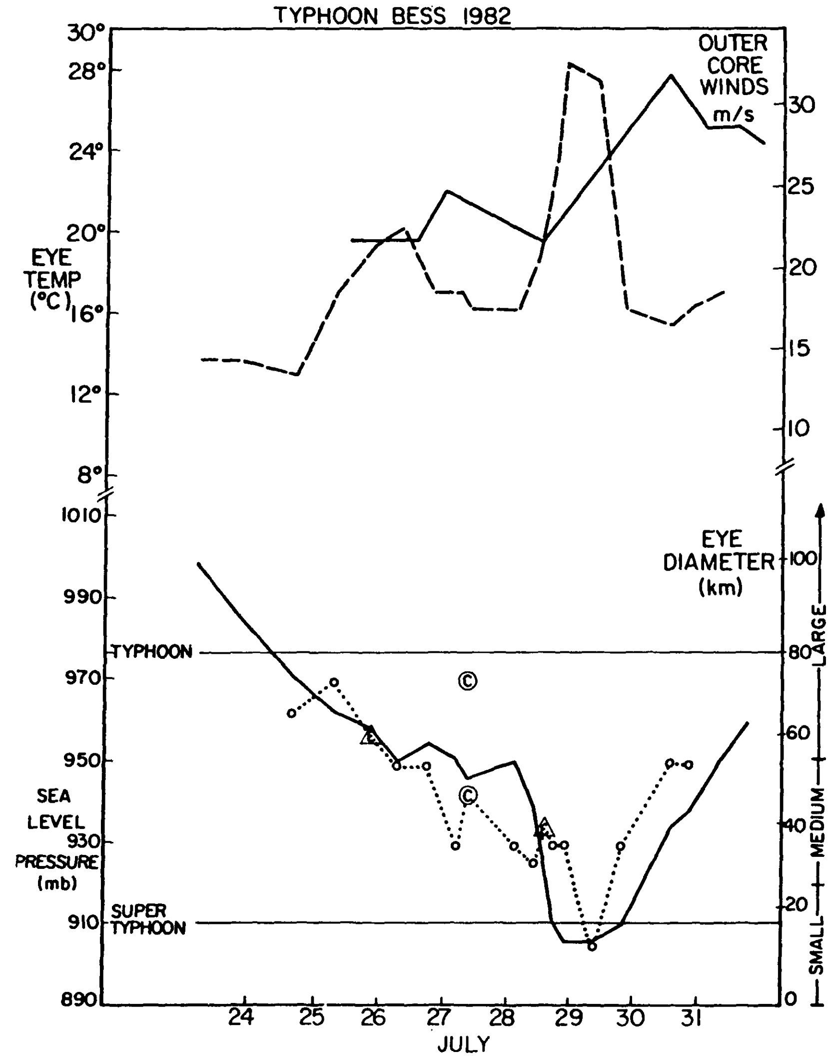
TYPHOON BESS 1982
30°
28°
24°
20°
16°
12°
8°
EYE
TEMP
(°C)
OUTER
CORE
WINDS
m/s
30
25
20
15
10
1010
990
970
950
930
910
890
TYPHOON
SUPER
TYPHOON
SEA
LEVEL
PRESSURE
(mb)
EYE
DIAMETER
(km)
100
80
60
40
20
0
LARGE
MEDIUM
SMALL
24
25
26
27
28
29
30
31
JULY

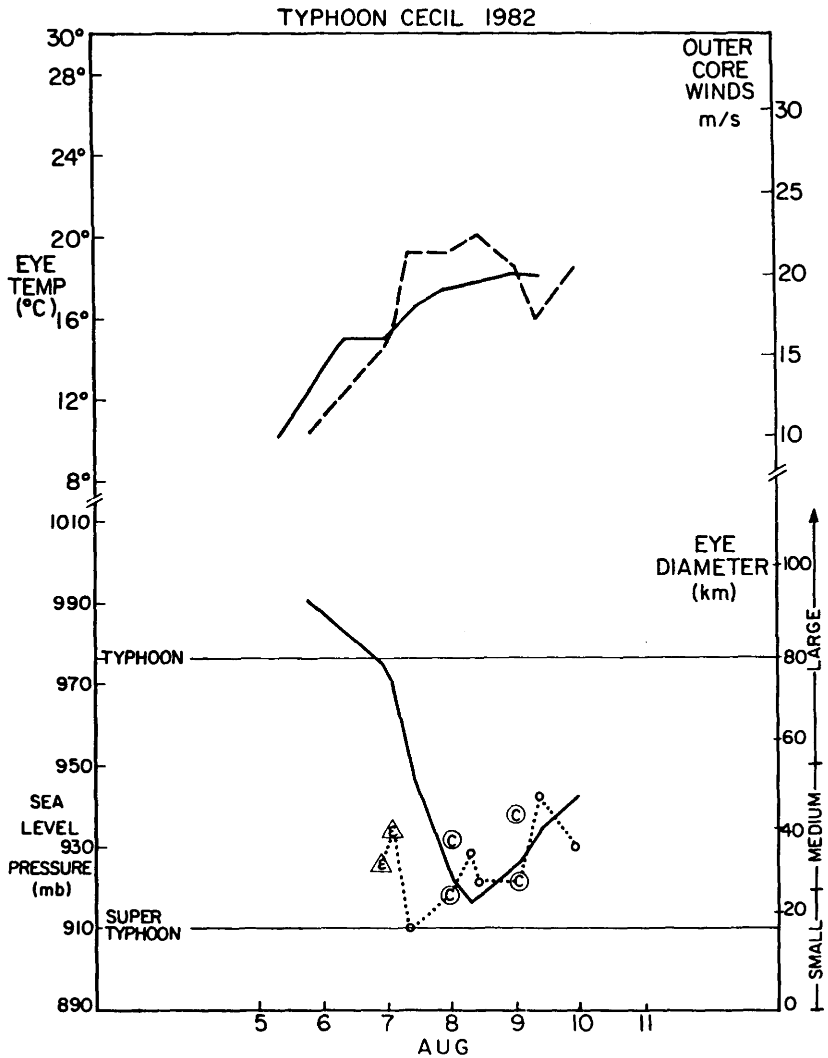
TYPHOON CECIL 1982
EYE TEMP (°C)
30°
28°
24°
20°
16°
12°
8°
OUTER CORE WINDS m/s
30
25
20
15
10
1010
990
970
950
930
910
890
SEA LEVEL PRESSURE (mb)
TYPHOON
SUPER TYPHOON
EYE DIAMETER (km)
100
80
60
40
20
0
LARGE
MEDIUM
SMALL
5
6
7
8
9
10
11
AUG

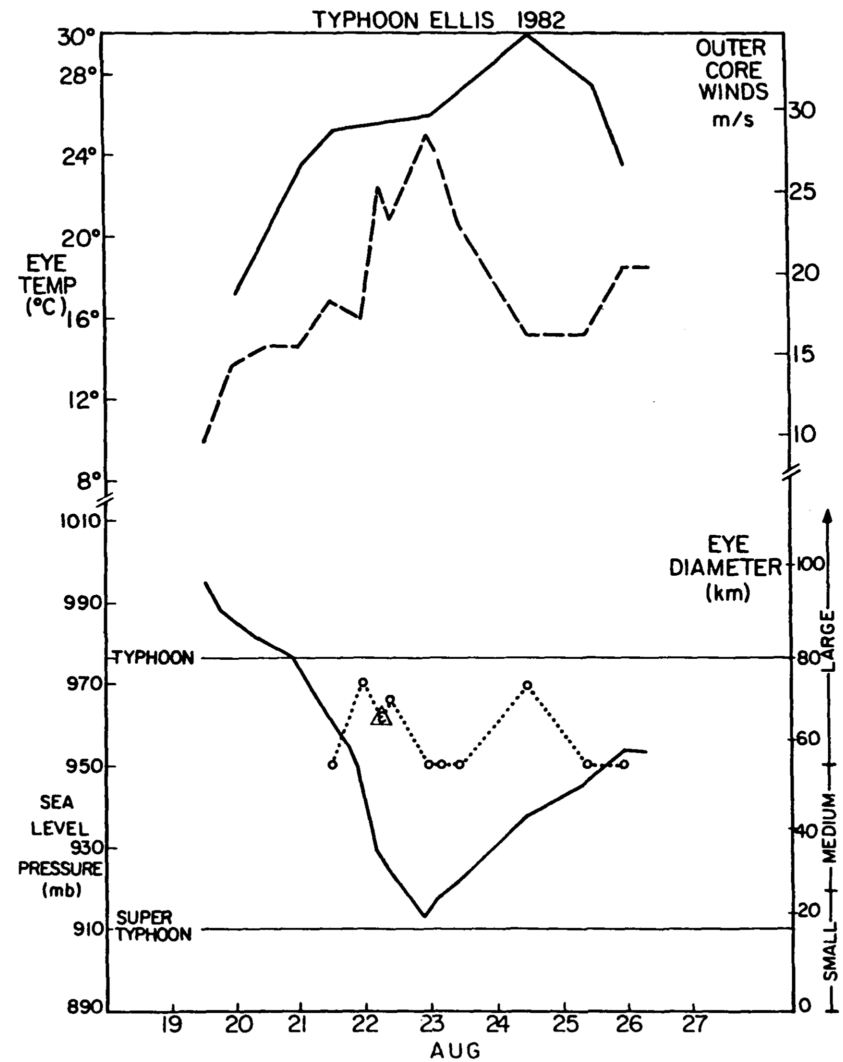
TYPHOON ELLIS 1982
EYE TEMP (°C)
30°
28°
24°
20°
16°
12°
8°
OUTER CORE WINDS m/s
30
25
20
15
10
1010
990
970
950
930
910
890
SEA LEVEL PRESSURE (mb)
TYPHOON
SUPER TYPHOON
EYE DIAMETER (km)
100
80
60
40
20
0
LARGE
MEDIUM
SMALL
19
20
21
22
23
24
25
26
27
AUG

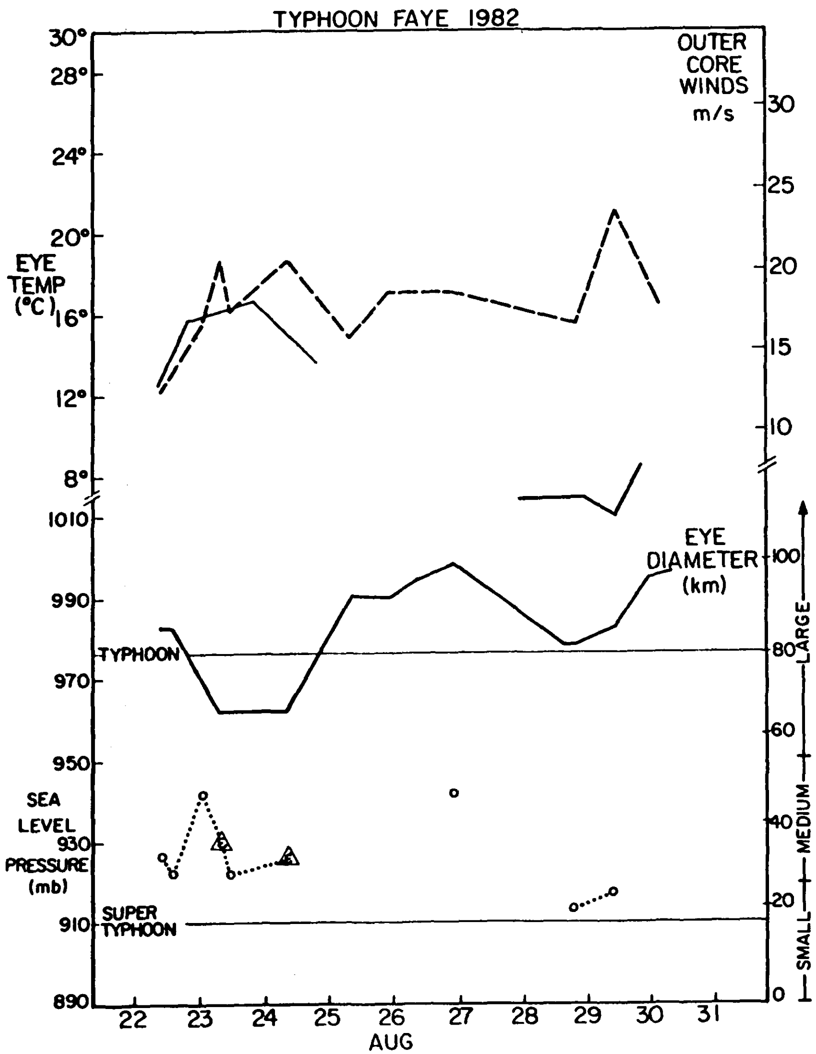
TYPHOON FAYE 1982
EYE TEMP (°C)
30°
28°
24°
20°
16°
12°
8°
OUTER CORE WINDS m/s
30
25
20
15
10
SEA LEVEL PRESSURE (mb)
1010
990
970
950
930
910
890
TYPHOON
SUPER TYPHOON
EYE DIAMETER (km)
100
80
60
40
20
0
LARGE
MEDIUM
SMALL
22
23
24
25
26
27
28
29
30
31
AUG

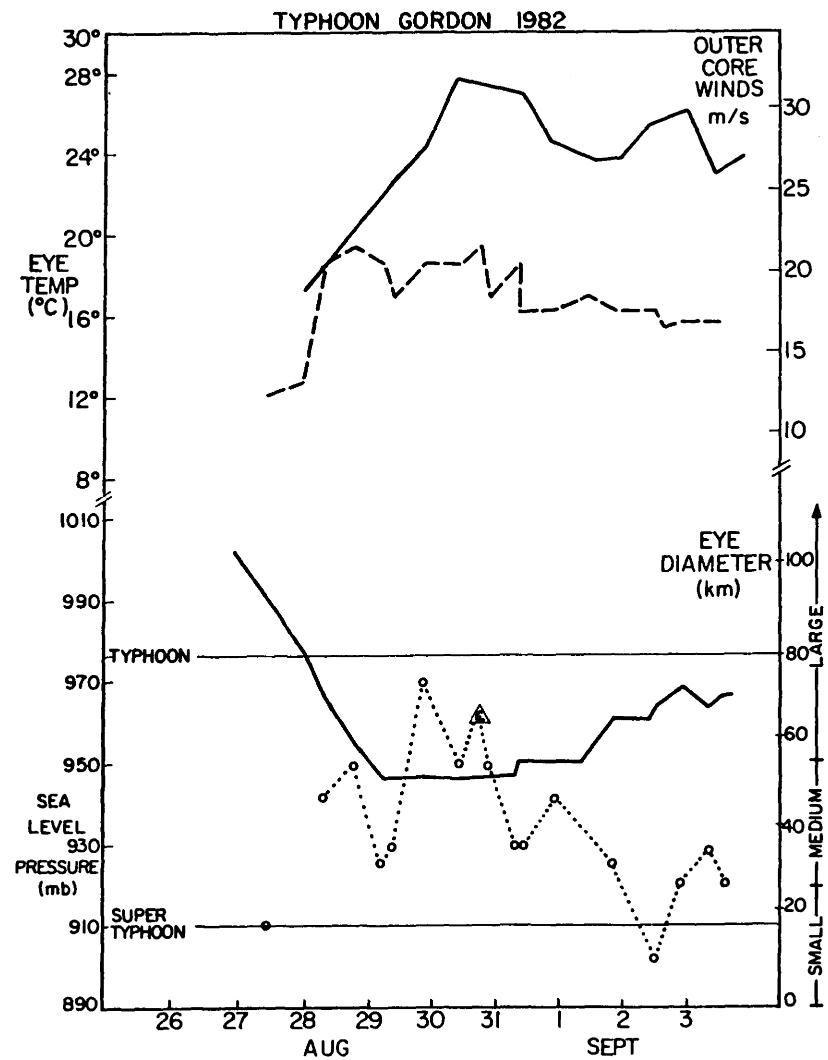
TYPHOON GORDON 1982
EYE TEMP (°C)
30°
28°
24°
20°
16°
12°
8°
OUTER CORE WINDS m/s
30
25
20
15
10
SEA LEVEL PRESSURE (mb)
1010
990
970
950
930
910
890
TYPHOON
SUPER TYPHOON
EYE DIAMETER (km)
100
80
60
40
20
0
LARGE
MEDIUM
SMALL
26
27
28
29
30
31
1
2
3
AUG
SEPT

TYPHOON KEN 1982

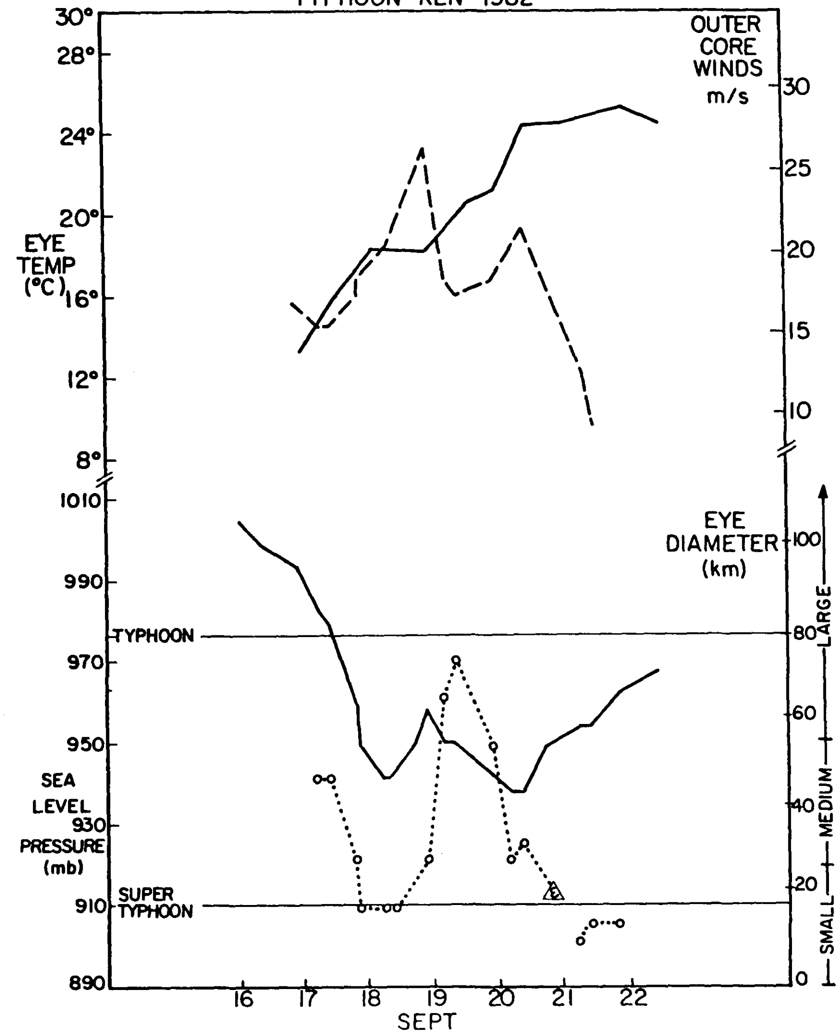

SUPERTYPHOON MAC 1982

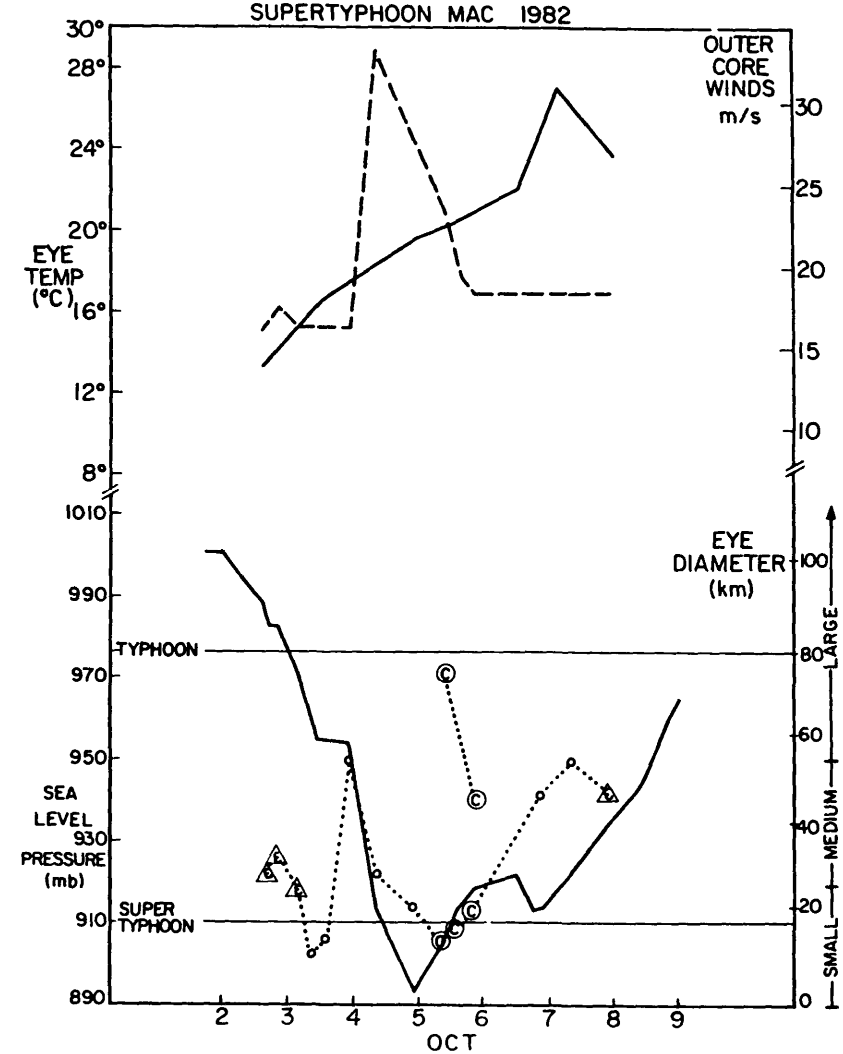

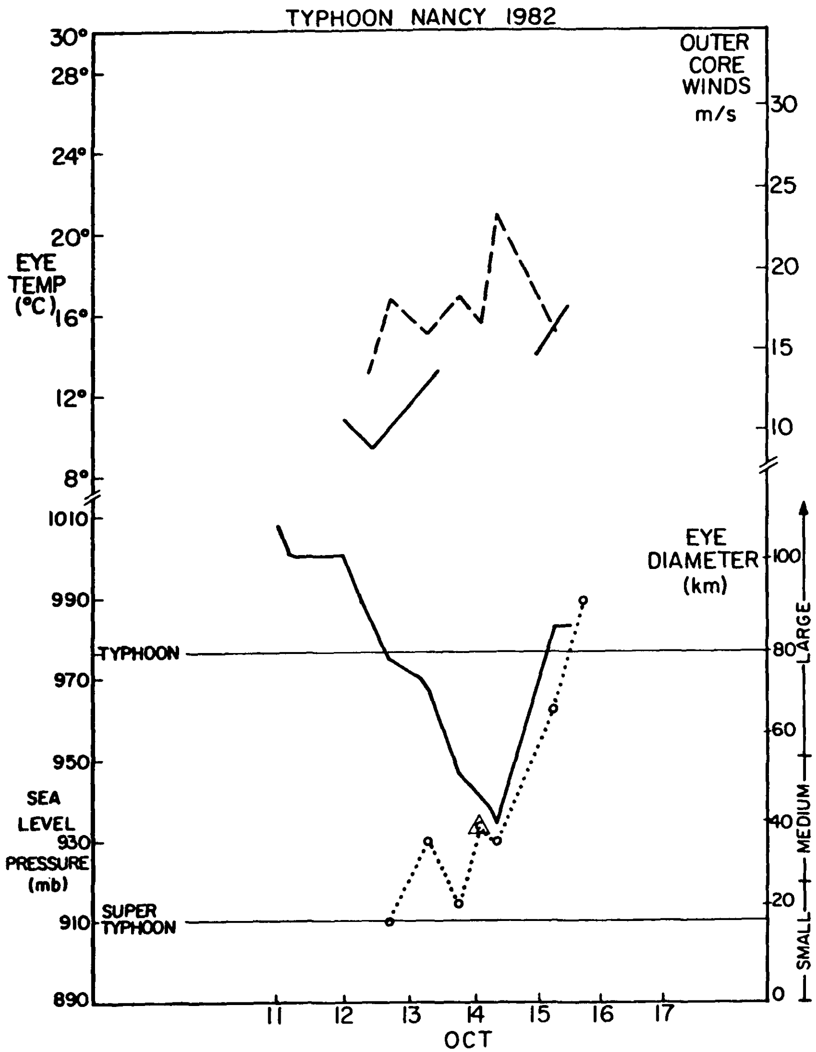
TYPHOON NANCY 1982
OUTER CORE WINDS m/s
EYE TEMP (°C)
30°
28°
24°
20°
16°
12°
8°
30
25
20
15
10
1010
990
970
950
930
910
890
EYE DIAMETER (km)
100
80
60
40
20
0
LARGE
MEDIUM
SMALL
TYPHOON
SUPER TYPHOON
SEA LEVEL PRESSURE (mb)
11
12
13
14
15
16
17
OCT

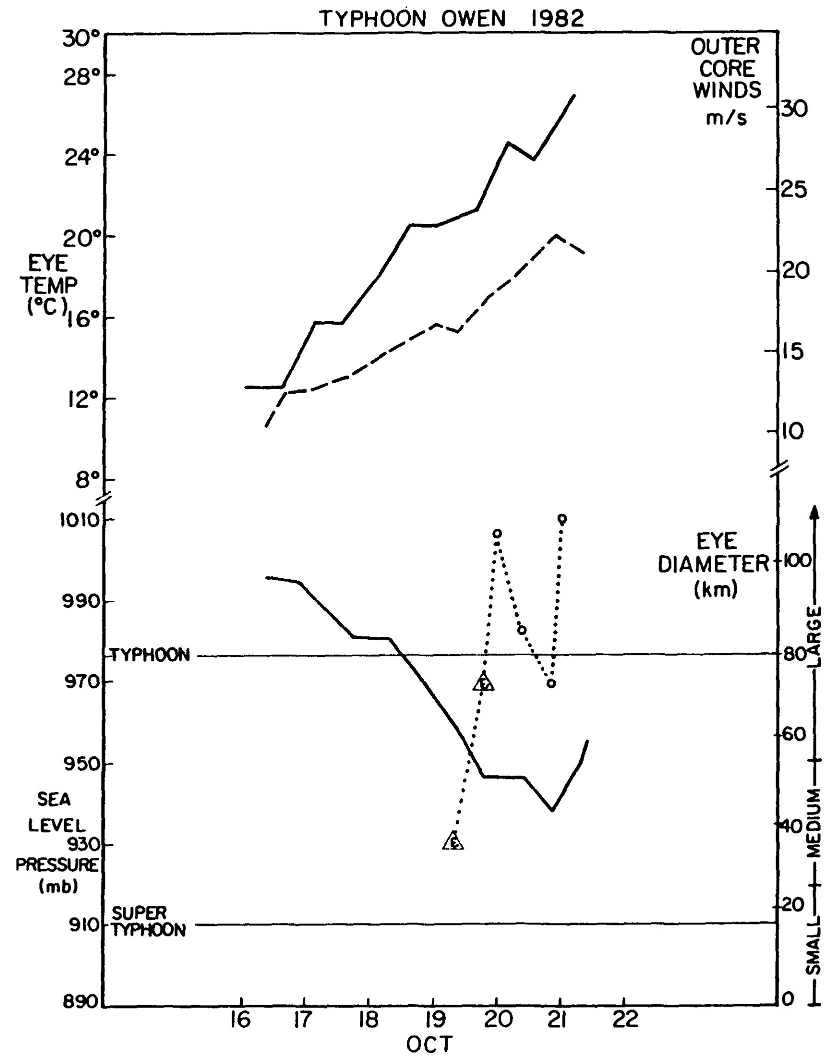
TYPHOON OWEN 1982
OUTER CORE WINDS m/s
EYE TEMP (°C)
30°
28°
24°
20°
16°
12°
8°
30
25
20
15
10
1010
990
970
950
930
910
890
EYE DIAMETER (km)
100
80
60
40
20
0
LARGE
MEDIUM
SMALL
TYPHOON
SUPER TYPHOON
SEA LEVEL PRESSURE (mb)
16
17
18
19
20
21
22
OCT

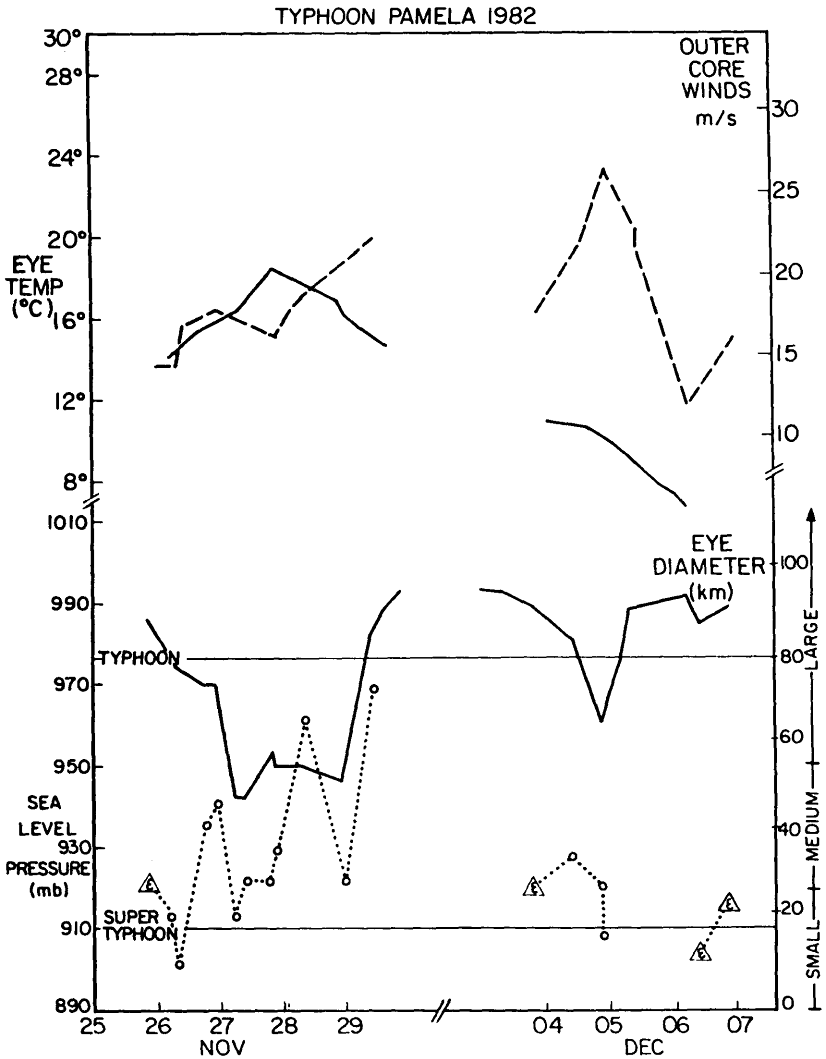
TYPHOON PAMELA 1982
EYE TEMP (°C)
30°
28°
24°
20°
16°
12°
8°
OUTER CORE WINDS m/s
30
25
20
15
10
EYE DIAMETER (km)
100
80
60
40
20
0
LARGE
MEDIUM
SMALL
SEA LEVEL PRESSURE (mb)
1010
990
970
950
930
910
890
TYPHOON
SUPER TYPHOON
25
26
27
28
29
04
05
06
07
NOV
DEC

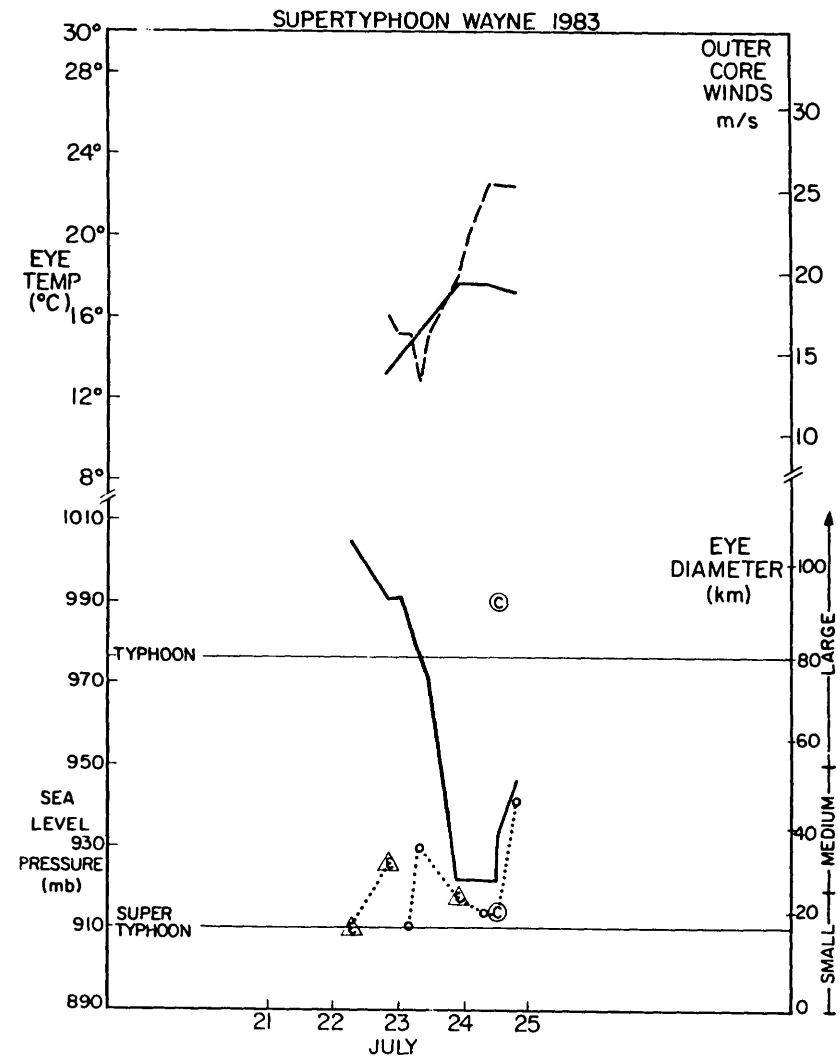
SUPERTYPHOON WAYNE 1983
EYE TEMP (°C)
30°
28°
24°
20°
16°
12°
8°
OUTER CORE WINDS m/s
30
25
20
15
10
EYE DIAMETER (km)
100
80
60
40
20
0
LARGE
MEDIUM
SMALL
SEA LEVEL PRESSURE (mb)
1010
990
970
950
930
910
890
TYPHOON
SUPER TYPHOON
21
22
23
24
25
JULY

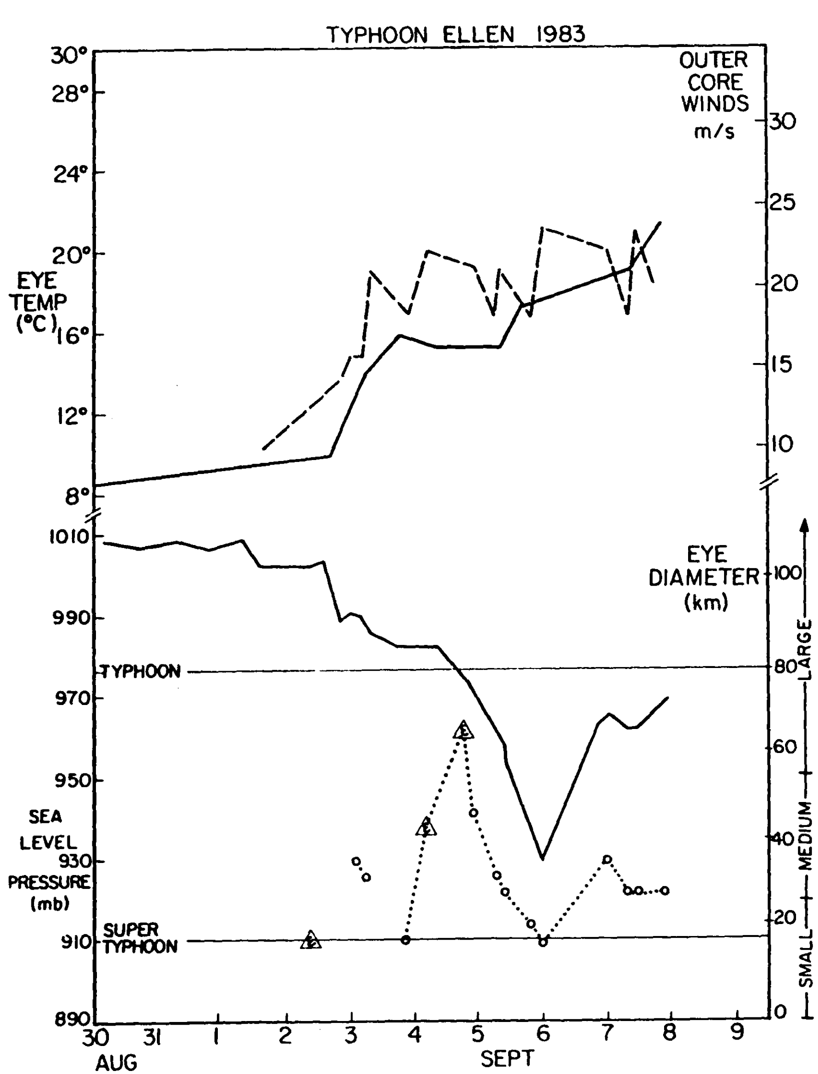
TYPHOON ELLEN 1983
EYE TEMP (°C)
OUTER CORE WINDS m/s
EYE DIAMETER (km)
SEA LEVEL PRESSURE (mb)
TYPHOON
SUPER TYPHOON
LARGE
MEDIUM
SMALL
30 AUG
SEPT

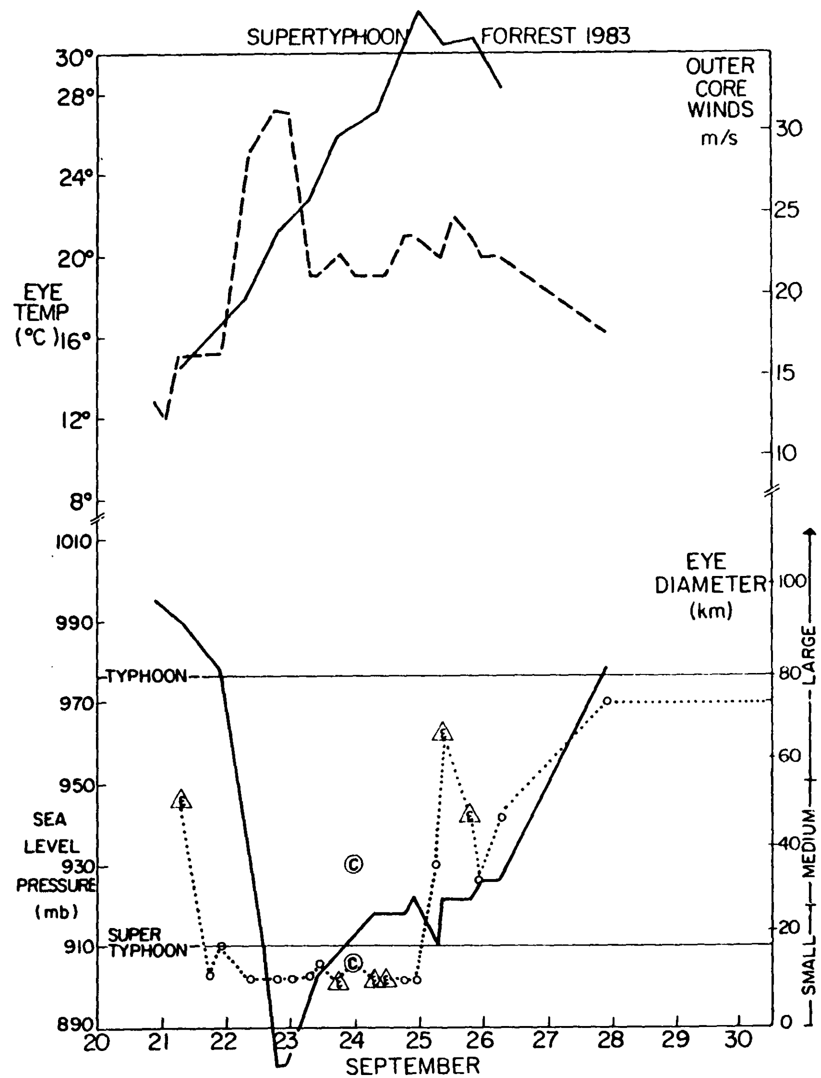
SUPERTYPHOON FORREST 1983
EYE TEMP (°C)
OUTER CORE WINDS m/s
EYE DIAMETER (km)
SEA LEVEL PRESSURE (mb)
TYPHOON
SUPER TYPHOON
LARGE
MEDIUM
SMALL
SEPTEMBER

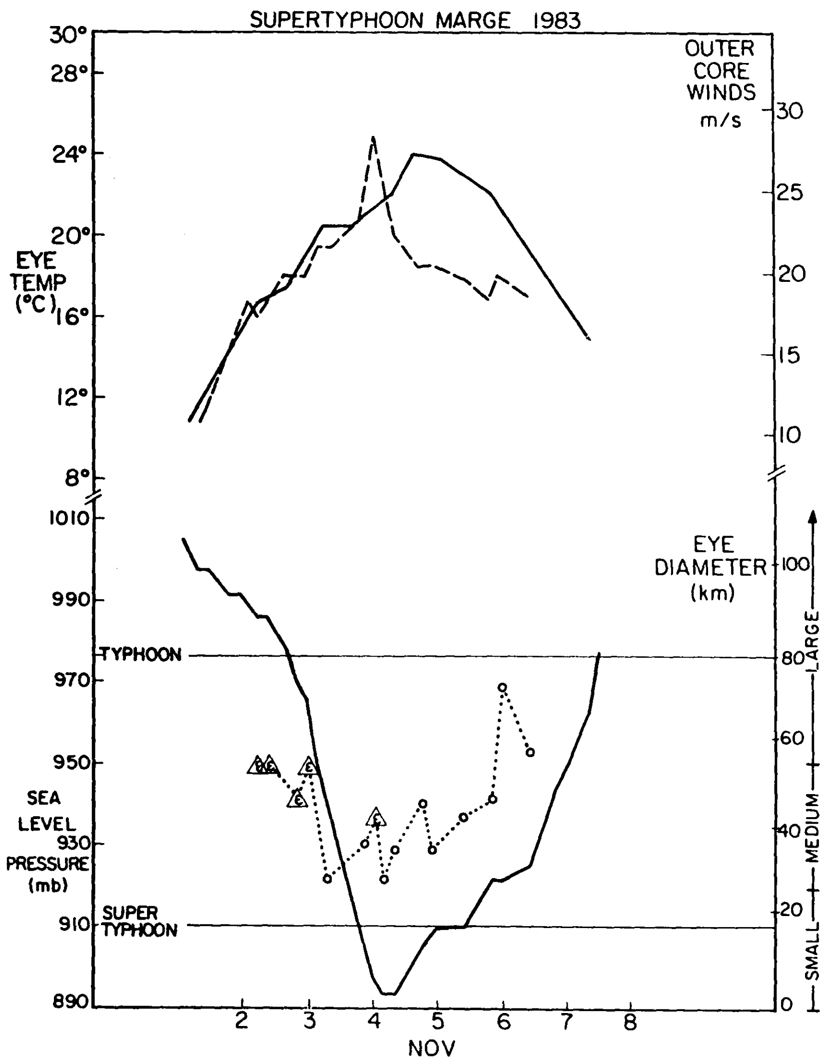
SUPERTYPHOON MARGE 1983
OUTER CORE WINDS m/s
EYE TEMP (°C)
EYE DIAMETER (km)
SEA LEVEL PRESSURE (mb)
TYPHOON
SUPER TYPHOON
SMALL
MEDIUM
LARGE
NOV

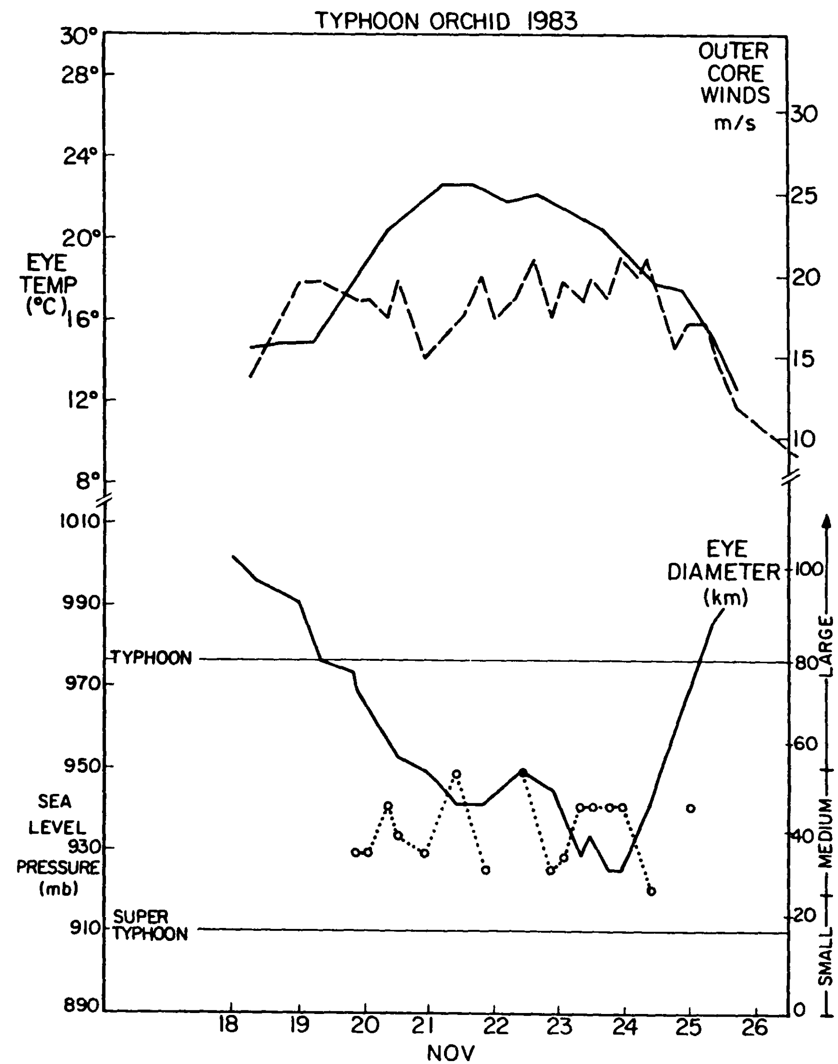
TYPHOON ORCHID 1983
OUTER CORE WINDS m/s
EYE TEMP (°C)
EYE DIAMETER (km)
SEA LEVEL PRESSURE (mb)
TYPHOON
SUPER TYPHOON
SMALL
MEDIUM
LARGE
NOV

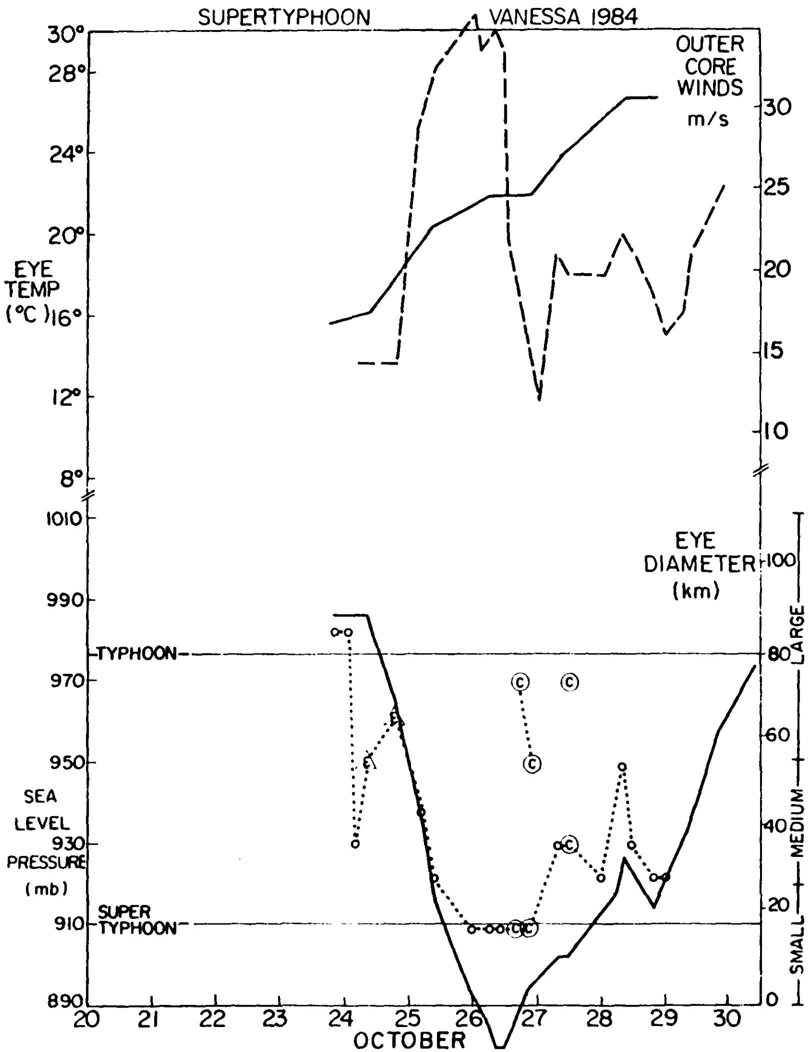
SUPERTYPHOON VANESSA 1984
OUTER CORE WINDS m/s
EYE TEMP (°C)
30° 28° 24° 20° 16° 12° 8°
30 25 20 15 10
EYE DIAMETER (km)
SEA LEVEL PRESSURE (mb)
1010 990 970 950 930 910 890
TYPHOON
SUPER TYPHOON
100 80 60 40 20 0
LARGE MEDIUM SMALL
20 21 22 23 24 25 26 27 28 29 30
OCTOBER

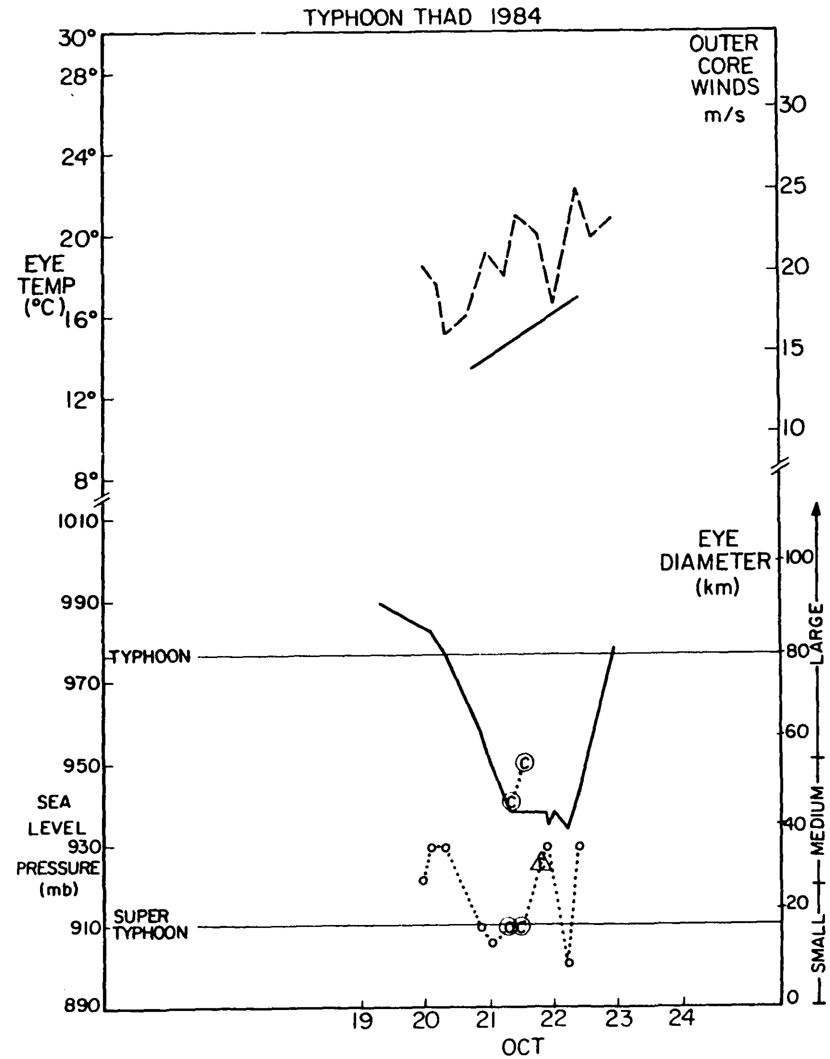
TYPHOON THAD 1984
OUTER CORE WINDS m/s
EYE TEMP (°C)
30° 28° 24° 20° 16° 12° 8°
30 25 20 15 10
EYE DIAMETER (km)
SEA LEVEL PRESSURE (mb)
1010 990 970 950 930 910 890
TYPHOON
SUPER TYPHOON
100 80 60 40 20 0
LARGE MEDIUM SMALL
19 20 21 22 23 24
OCT

TYPHOON CARY 1984

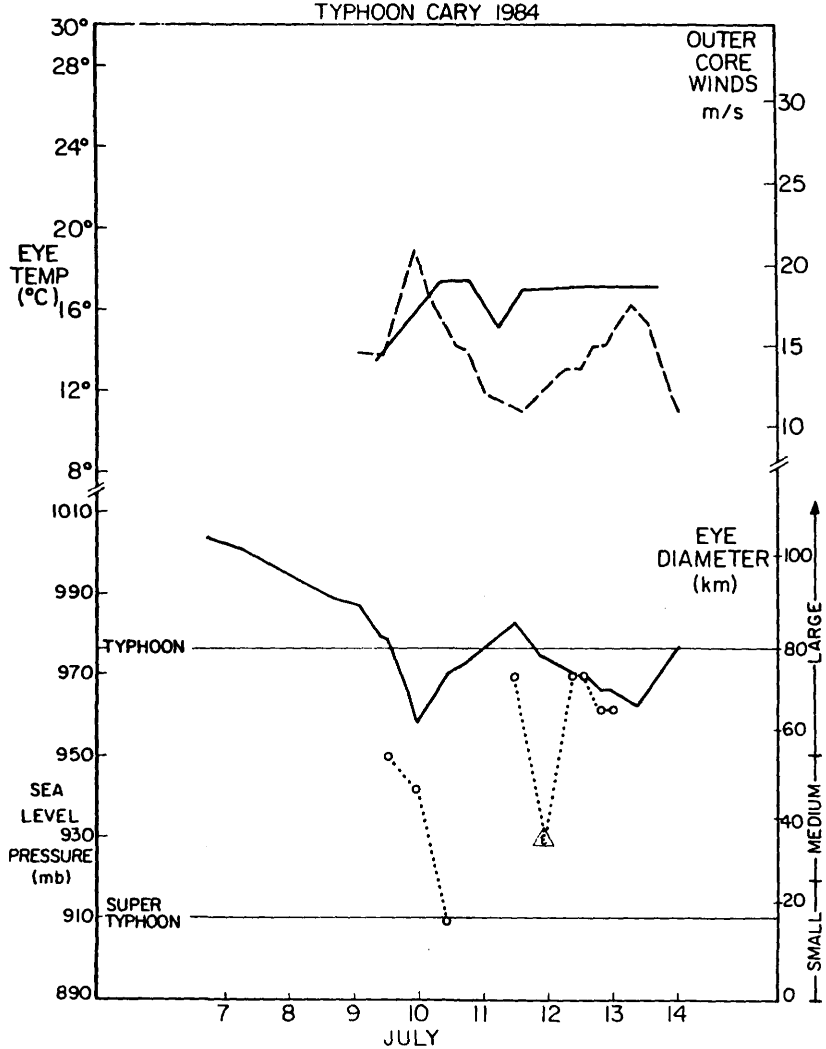

TYPHOON DINAH 1984

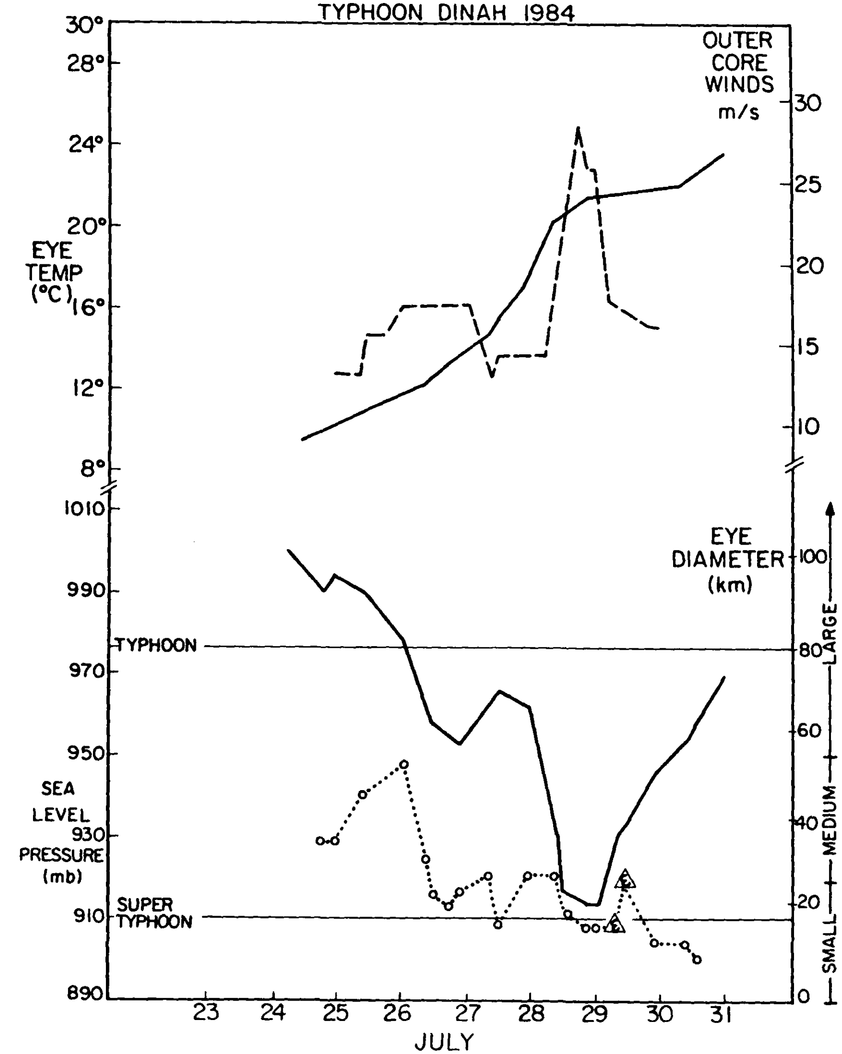

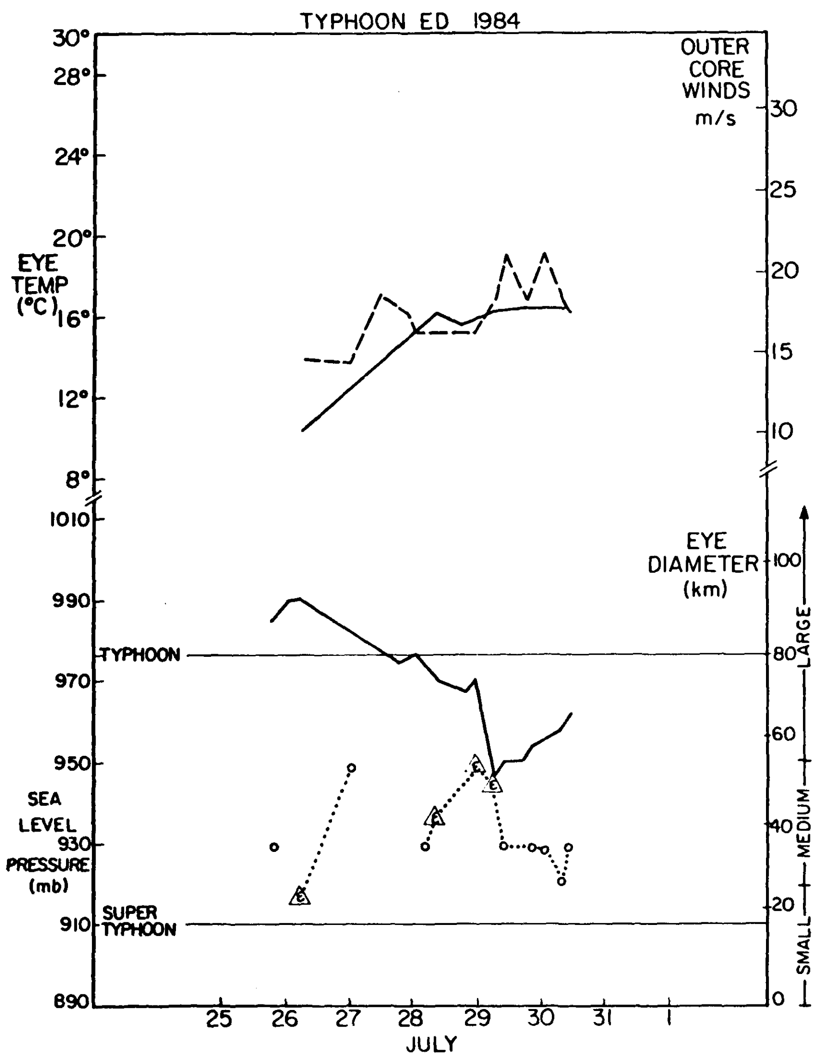
TYPHOON ED 1984
OUTER CORE WINDS m/s
EYE TEMP (°C)
30°
28°
24°
20°
16°
12°
8°
30
25
20
15
10
EYE DIAMETER (km)
SEA LEVEL PRESSURE (mb)
1010
990
970
950
930
910
890
TYPHOON
SUPER TYPHOON
100
80
60
40
20
0
LARGE
MEDIUM
SMALL
25
26
27
28
29
30
31
1
JULY

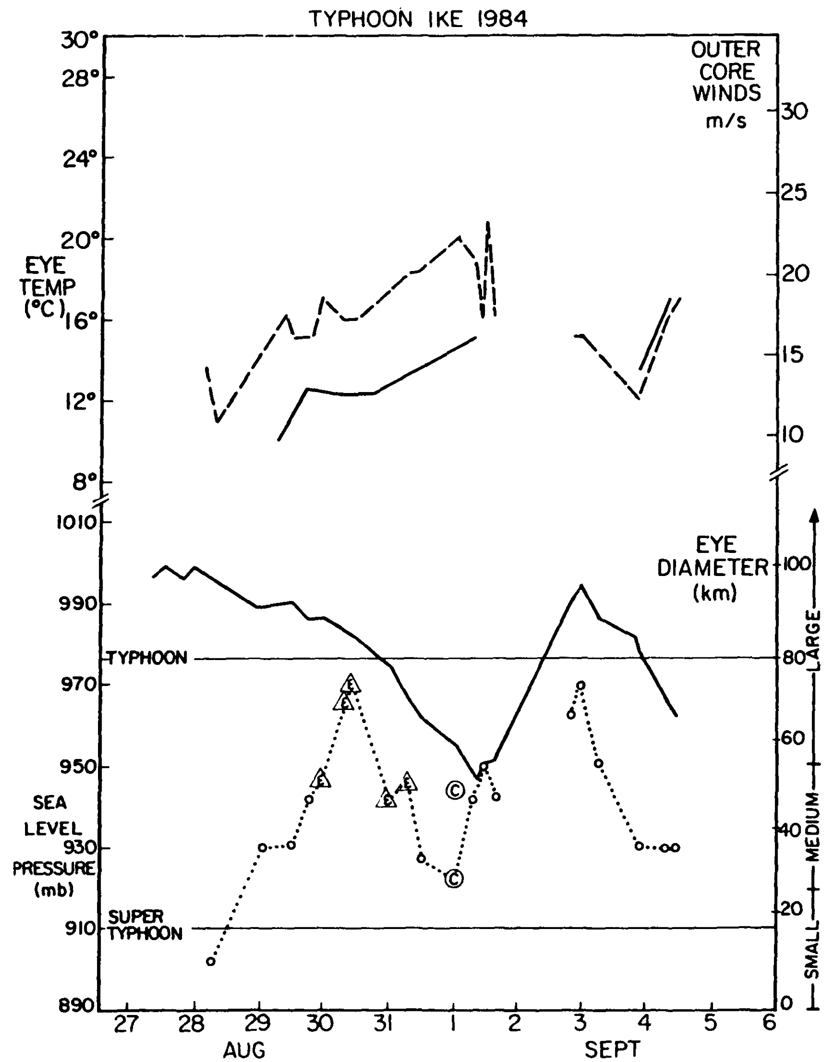
TYPHOON IKE 1984
OUTER CORE WINDS m/s
EYE TEMP (°C)
30°
28°
24°
20°
16°
12°
8°
30
25
20
15
10
EYE DIAMETER (km)
SEA LEVEL PRESSURE (mb)
1010
990
970
950
930
910
890
TYPHOON
SUPER TYPHOON
100
80
60
40
20
0
LARGE
MEDIUM
SMALL
27
28
29
30
31
1
2
3
4
5
6
AUG
SEPT

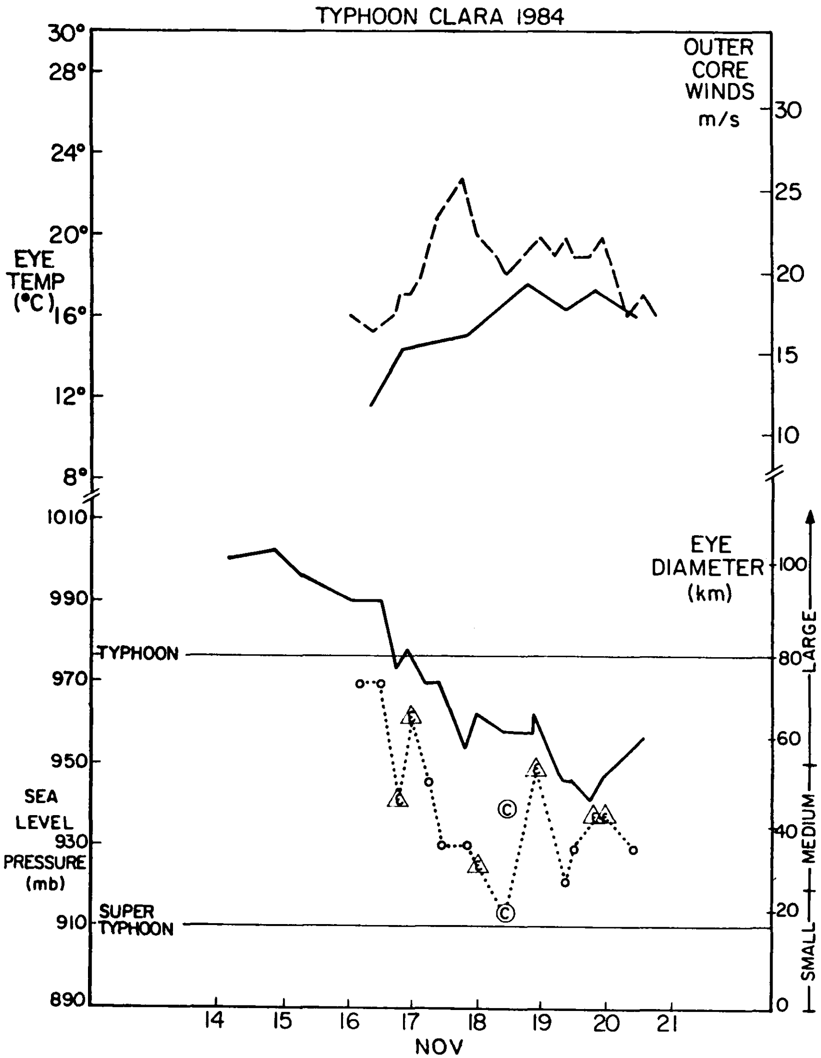
TYPHOON CLARA 1984
OUTER CORE WINDS m/s
EYE TEMP (°C)
EYE DIAMETER (km)
SEA LEVEL PRESSURE (mb)
TYPHOON
SUPER TYPHOON
LARGE
MEDIUM
SMALL
NOV

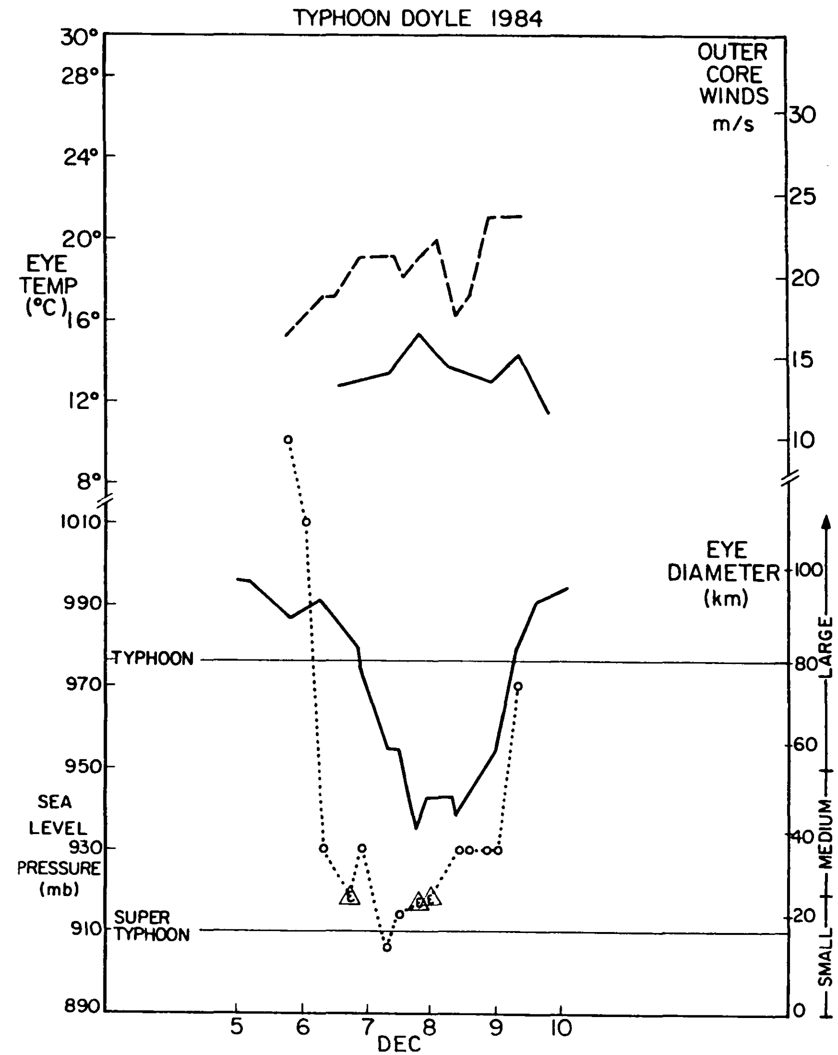
TYPHOON DOYLE 1984
OUTER CORE WINDS m/s
EYE TEMP (°C)
EYE DIAMETER (km)
SEA LEVEL PRESSURE (mb)
TYPHOON
SUPER TYPHOON
LARGE
MEDIUM
SMALL
DEC

TYPHOON AGNES 1984

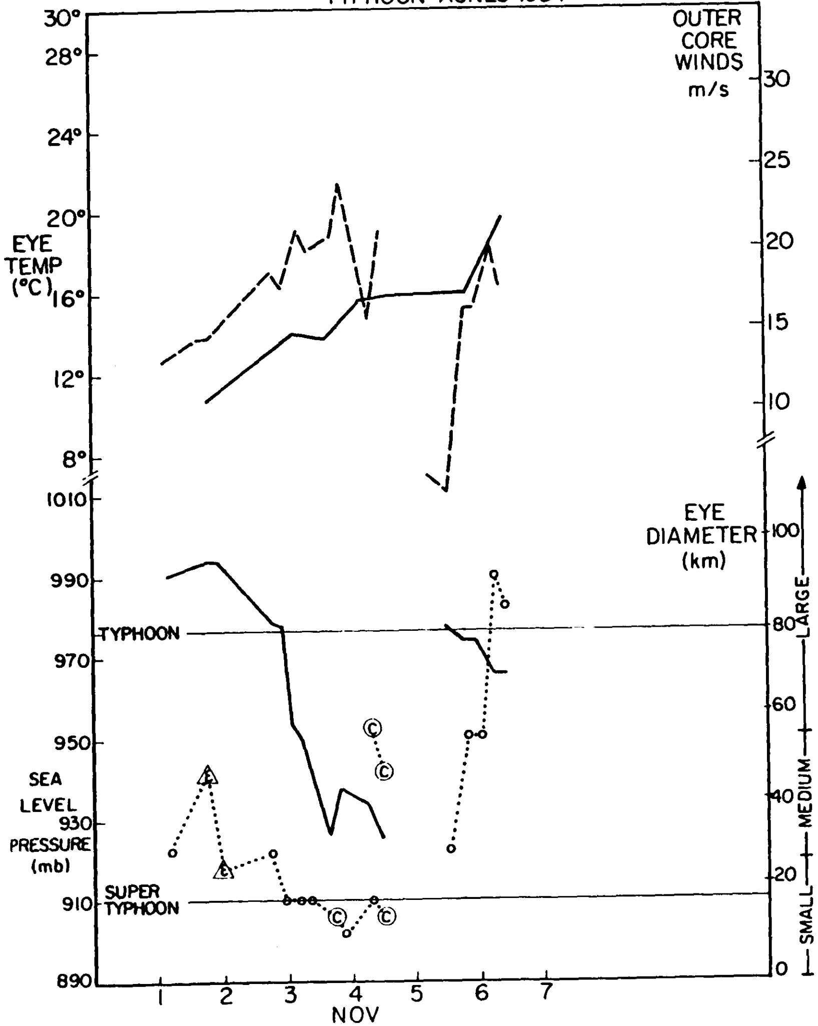

SUPERTYPHOON BILL 1984

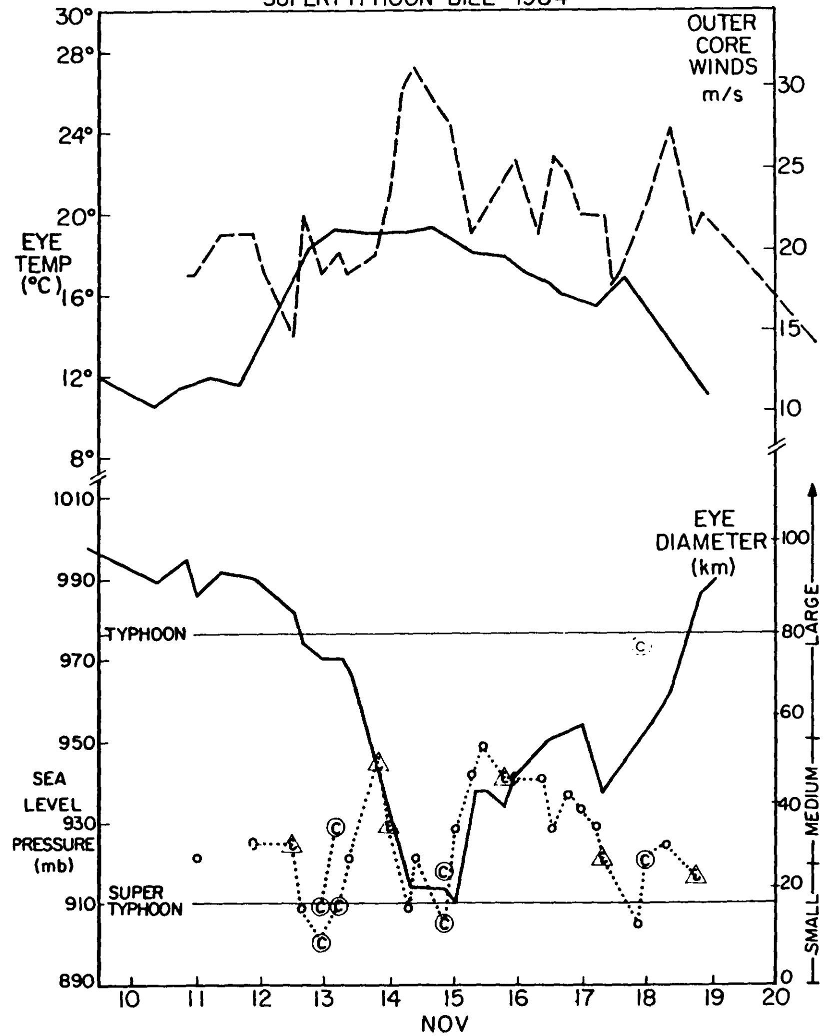

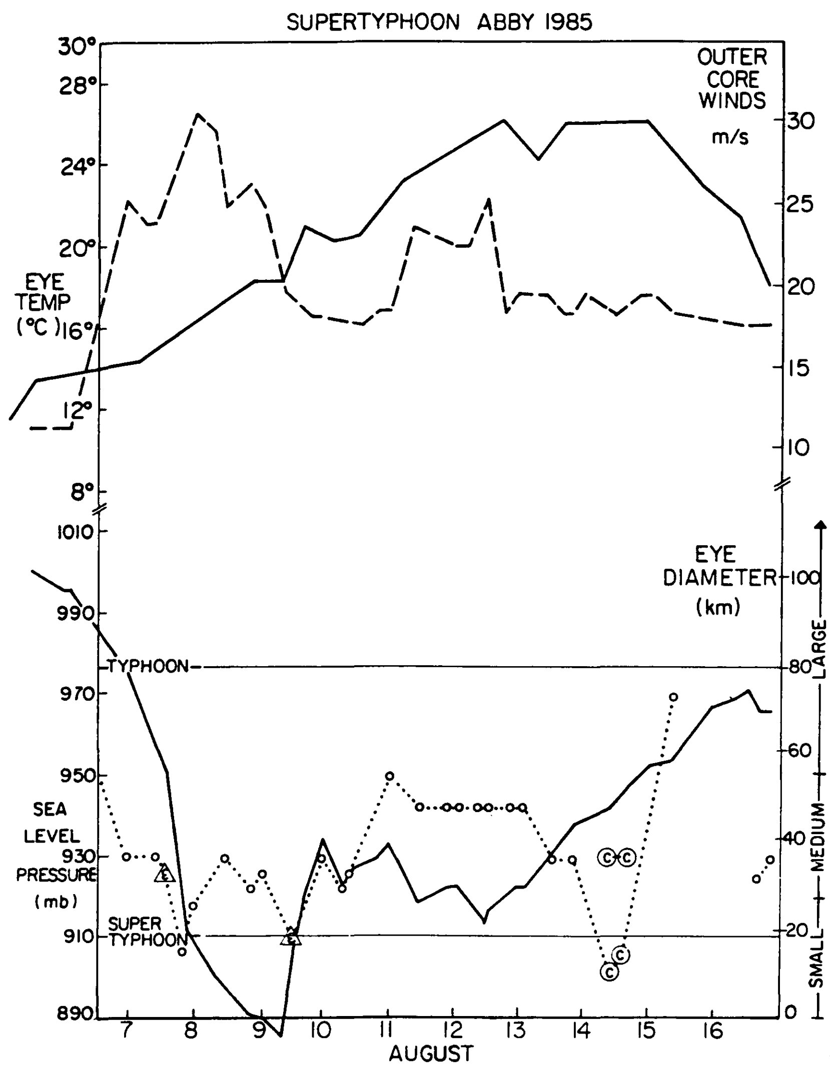
SUPERTYPHOON ABBY 1985
30°
28°
24°
20°
EYE TEMP (°C)
16°
12°
8°
OUTER CORE WINDS m/s
30
25
20
15
10
1010
990
TYPHOON
970
950
SEA LEVEL PRESSURE (mb)
930
910
SUPER TYPHOON
890
EYE DIAMETER (km)
100
80
60
40
20
0
LARGE
MEDIUM
SMALL
7
8
9
10
11
12
13
14
15
16
AUGUST

Appendix B

DATA PROCESSING

This study is based on five years of flight data of the northwestern Pacific Ocean basin. Many years went into the processing of this data set which involved several steps to complete.

The first step consisted of gathering the data. This involved a trip to the NOAA's National Climate Data Center at Asheville, NC, where the original forms are stored. Locating, sorting and copying the forms took two weeks. In this and all steps it was vital that someone who had worked with these forms before, take a direct role in overseeing the entire process. This precluded non-cyclone data from being incorporated into a strictly tropical cyclone study.

Preparing the forms for key punching involved highlighting only that information which was needed for the research. Dates were checked to ensure against observer error. This step was critical since observations with the wrong date would be matched with the wrong center from which to navigate. All remarks which accompanied the form were checked in case equipment problems invalidated the reported observations. This step took three months.

Key-punching the information into the computer entailed a massive effort. Realize that all information was handwritten onto seven different forms by dozens of different observers. Combine in-flight turbulence with an overloaded trainee and the difference between a "2" and a "7" often took a committee to decipher, one of which had to be someone knowledgeable with the code. It was at this step that all data which included a code denoting equipment problems were excluded. We were primarily concerned with navigational and wind measuring equipment. If either of these were faulty, the entire mission was scrapped. Missions with other equipment problems, such as an inoperative dew-point hygrometer, were retained with the bad data entered as missing. Seven-man months of effort went into this step.

Once all the data were placed into the computer, it was the job of the programmer to translate all seven codes and their modifications over the years into a common and usable format. Error checks were incorporated all along the way. Low-level missions which were labelled 'cyclone' and later developed into a named storm were traced back and named at the earliest possible stage. The coupling of an experienced programmer with someone intimately familiar with the codes allowed the completion of this step in two man-years.

Aircraft usually spent 4 hours taking observations in the storm area but positioned the center only twice. Therefore, the next step entailed navigating all data to an appropriate moving center position. To accomplish this, a supplemental data set was used. Cyclone center motion was most completely traced by JTWC forecasters and compiled in their 'Best Track' position archive. These position data were used to provide aircraft-measured centers with an appropriate heading and speed so that all observations could be appropriately navigated. This step took four months of programming.

It was at this point that an analysis of the data could commence. Particular attention was given this data set in these early stages of analysis with the realization that results which stand on a clean and carefully processed data sample will provide the best results. Considering the fact that typhoons are inherently quite variable to begin with, only a clean data set would allow meaningful results to stand out. Massive data sets have the potential of providing many answers but require such meticulous handling.

Overall, the task of processing 5 years of flight data involved an enormous effort. Three and a half years went into just the compiling of this data set. Evidently, it is easy to see why no one before has attempted such a task. It was vital to the completion of this job that someone familiar with the code and the method of observing be responsible for this job. This has always been a military person. Those military personnel returning from assignments in Guam (to go to school) are typically given 21 months to complete a Master's degree and 3 years for a Ph.D. This time allowance often falls far short of what is required simply to place the data into a semblance of order and well before any analysis can be done. The only way the author (who did fly in Guam for nearly three years in the Air Force) accomplished this task was with the full support of Professor Gray who continually provided me with the resources necessary to get the job done in as rapid a manner as possible.

Appendix C

VORTEX-AVERAGED MAXIMUM WIND AND NORMALIZED WIND PROFILES

It is vital to both forecaster and researcher to have an objective method for estimating the maximum wind speed of a tropical cyclone. The procedure developed here provides a consistently objective method of estimating an azimuthally averaged 700 mb maximum wind speed. Without this procedure adjustments would have been required for estimates of surface winds, cyclone motion, and wind asymmetry in the natural coordinate system. The method used here relied instead on the shape of the height profile unique to each flight mission not to a particular surface gust factors.

C.1 Vortex-Averaged Estimate of Maximum Wind

As noted in Weatherford and Gray (1987a), the doppler wind equipment used on board the WC-130 aircraft occasionally attenuated in the heavy rain that accompanied convection within the eyewall. Therefore some doubt was cast on the reliability of the measured values for maximum wind and the radius of maximum wind in cases with well developed eyewalls. Nevertheless, it is the value of the maximum wind speed that is most crucial to any tropical cyclone damage forecast. This need necessitated the systematic estimation of maximum winds using an analytical approach given flight observations of the pressure profile or outer wind speeds, both of which were reliably measured.

Prior attempts to find an accurate estimate of the cyclone's maximum wind include solving the modified Rankine vortex equation (Depperman 1947):

$$VR^{\propto} = V_{max}R^{\propto}_{max} \tag{C.1}$$

where V is the tangential wind at radius R, V_{max} is the maximum tangential wind at radius R_{max}, and $\propto$ is the shape of the curve to assure from constant angular momentum. This equation can be solved simultaneously through a sum of squares method to obtain alpha ($\propto$) and V_{max}, given the abundant and reliable wind data that lay outside the eyewall region. However, although this method can be solved analytically, tests showed that it was very sensitive to the placement of the RMW. A sensitivity study involving an intense typhoon revealed that the maximum wind varied six meters per second for every kilometer change in radius of maximum wind (RMW). Hence, an error in the RMW of five kilometers could result in a maximum wind estimate 30 ms^{-1} in error. One could thus incur large spurious maximum wind errors from this technique. Since the azimuthal mean RMW was often difficult to measure precisely, this method proved too unreliable for the purpose here.

A method presently in use at JTWC (Atkinson and Holliday, 1977) to estimate the maximum surface wind speed avoids use of 700 mb flight-level winds. This method is based on empirically derived estimates the maximum surface wind speed from observations of maximum winds on island stations. In practice, maximum winds are estimated from the difference between the cyclone's central and environmental pressure values. This high reliance on the MSLP alone raises some doubt as to this wind estimate. As Fig. C.1 shows, similar central pressure values may result in very different pressure gradients.

Holland (1980) recognized these difficulties and attempted to account for the maximum wind speed and RMW as a function of varying shapes of the surface pressure profile rather than MSLP alone. Holland's method of maximum wind estimation was found to be reliable and was utilized in this analysis. This method involves the fitting of height data to a logarithmic hyperbola from which the maximum slope would provide a height

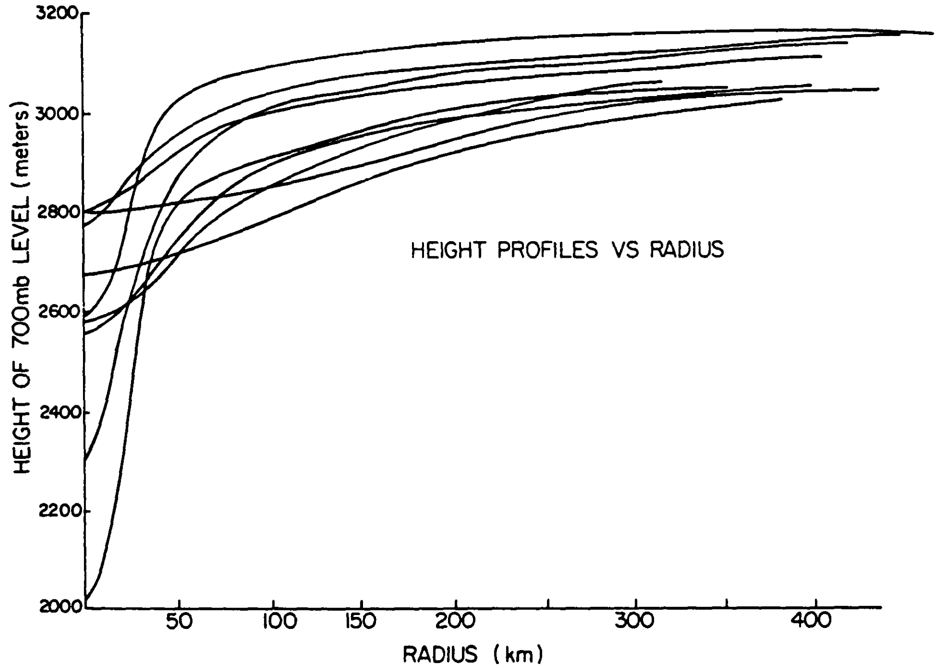

Figure C.1: An assortment of differing 700 mb height profiles of tropical cyclones of the 1980-84 data set.

gradient that can be applied to the gradient or cyclostrophic wind equations for deriving estimates of the maximum wind speed. Holland's scheme is believed to be more accurate than either the Atkinson-Holliday method or the (sometimes attenuating) Doppler wind measurement itself. The superiority of the Holland method over that of Atkinson-Holliday lies in the reliance on case by case variations in the shape of the height curve rather than just the minimum height or pressure value by itself.

Prior to applying Holland's scheme, a pilot study was made on a data set for which height data and maximum winds were already available. Shea and Gray (1973) compiled data for inside 1° radius of the center of Atlantic hurricanes from 1957 to 1969 (Gray and Shea, 1975). Although these missions also used Doppler wind equipment, there was a basic difference between these missions and the missions that comprised the 1980-1984 set. In the Pacific, data were taken every 55km (0.5°) along each radial pass with one additional wind measure at the radius of maximum wind. If the Doppler system attenuated, this wind measurement was missed. In the Atlantic, however, wind reports were automatically recorded every 100 meters and later averaged for every 2.5 n mi (4.6 km) for Shea and Gray's purposes. Doppler attenuation was thus easily identified and missions in error were excluded. Only those missions flown at 700mb were used in order to closely match the 700 mb 1980-84 northwestern Pacific data set used here. In addition, data from hurricanes Anita (1977) and Allen (1980) were also tested. In lieu of the Doppler wind system, data for these storms were obtained using the Inertial Navigation System (INS). All height data for each hurricane were fit to a logarithmic hyperbola in a least-squares manner from which a cyclostrophic wind was derived. This value was compared with the observed four-radial leg averaged maximum wind speed and found to correlate at 0.92. Based on these results, it was decided that this scheme would provide a reasonable estimate of the vortex-averaged maximum wind.

Holland's equation:

$$ln(h_n - h_c/h - h_c) = A/r^b \tag{C.2}$$

was used to solve for the scaling parameters A and b through a sum of squares best fit approach. Other values in C.2 include h_n, the (700 mb) height of the environment; h_c, the height at the center, and h, the height at radius r. The International Mathematics and Statistical Library (IMSL) routine used to make this calculation relied on a Levenberg-Marquardt algorithm in order to solve for the unknowns A and b as described in Brown and Dennis (1972), Levenberg (1944), and Marquardt (1963). Table C.1 lists the hurricanes used in the test and compares the observed and calculated maximum speed values along with the RMW obtained using Holland's method. Note that the hurricane with the greatest error was Allen of 1980 as its MSLP reached an unusually low 899 mb central pressure. Figure C.1 shows a plot of the observed versus calculated height profiles for Allen. In this extreme case even a slight error in the calculated profile can produce large errors in the maximum wind estimate. Radial accelerations may also be non-negligible. Gradient wind estimates were compared with cyclostrophic winds with little significant observed difference. As a result, the simpler cyclostrophic estimate was applied to the 1980-1984 northwestern Pacific data set. Figures C.2 and C.3 show how Holland's scheme approximated the height profiles of the 1980-1984 Pacific data sets for Supertyphoon Wynne and Typhoon Owen.

Table C.1: Comparison of observed quadrant averaged maximum wind speeds and their radii with the Holland estimate for 19 test cases of Atlantic hurricanes.

Hurricane	Date	Radius of Max (km)		Maximum Wind (m s^{-1})	
Name	(Yr-Mo-Da)	Observed	Holland Estimate	Observed	Holland Estimate
HANNAH	591001	46	37	40	37
HANNAH	591002	35	39	33	44
ANNA	610721	41	19	33	34
CARLA	610908	74	61	38	40
CARLA	610909	70	46	42	45
FLORA	631003	19	19	57	54
FLORA	631010	113	80	31	36
DORA	640905	54	56	43	39
DORA	640907	67	80	35	34
DORA	640908	89	80	31	36
DORA	640909	72	93	32	34
GLADYS	640917	35	28	46	41
GLADYS	640917	46	28	48	52
HILDA	641002	54	65	43	43
ISBELL	641014	24	19	30	38
DONNA	600907	33	37	55	55
ANITA	770901	24	24	68	64
ALLEN	800807	17	15	67	79
ALLEN	800808	19	17	56	56

A climatological average value was chosen for the environmental height. The value used for the height of the environment in the northwestern Pacific was 3130 meters. This value was derived from an average of 700 mb height observations 6° to 8° radius from cyclone centers. The tropical cyclone MSLP for this study varied from 1007 mb to 878 mb and estimated maximum 700 mb wind speeds varied from 5 to 76 ms^{-1}. Table C.2 lists the average, median, standard deviation and range of values found for the scaling parameters A and b, the calculated maximum wind speed and RMW obtained with Holland's scheme for the 5-year data set used here. Figure C.5 shows a good correlation (0.93) between

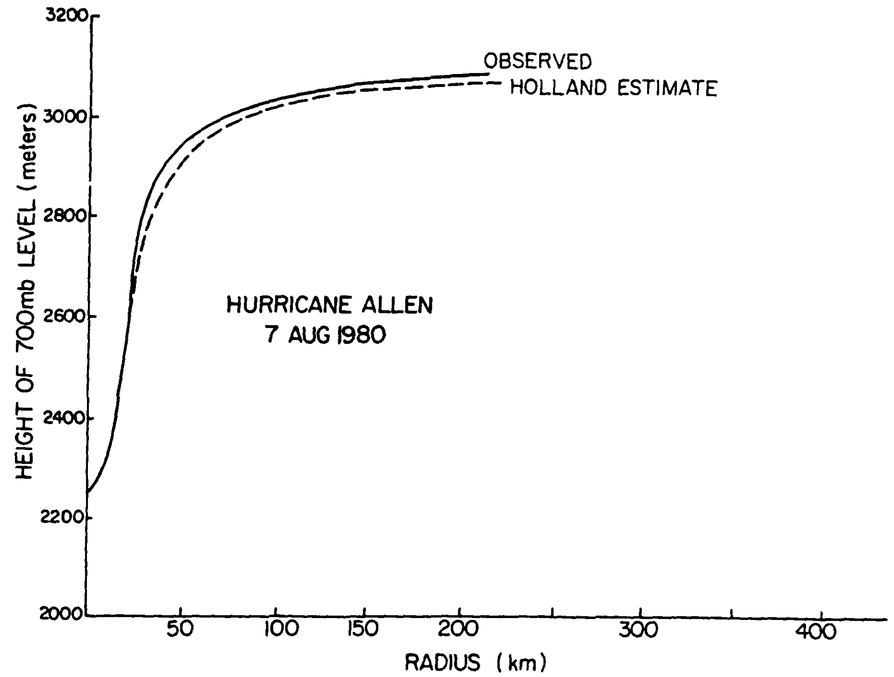

Figure C.2: 700 mb height vs radius profiles for the observed and Holland-estimated shapes.

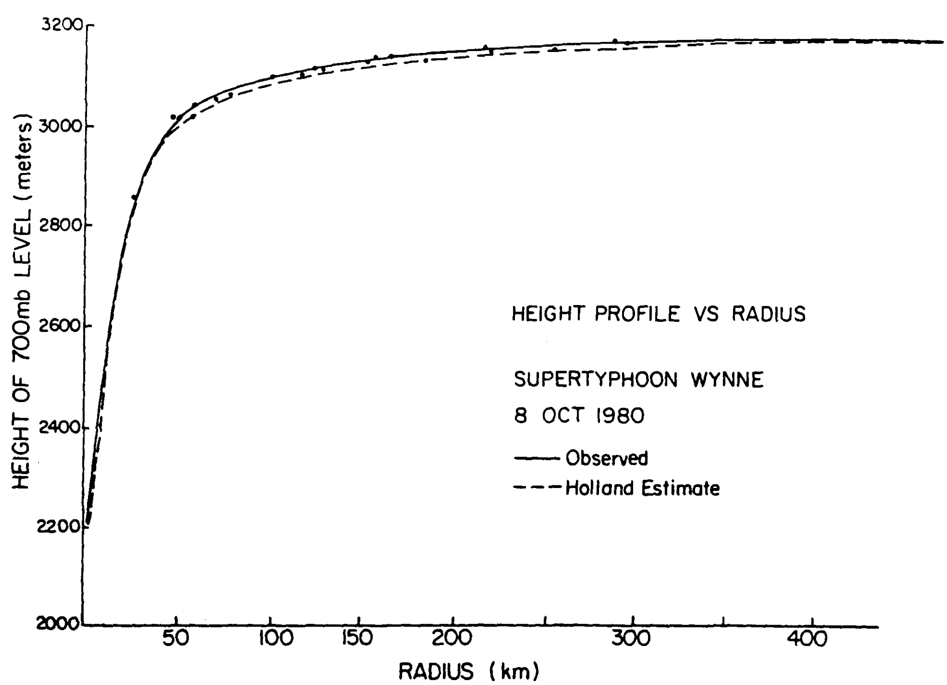

Figure C.3: 700 mb height vs. radius profiles for the observed curve (actual data points shown) and the Holland-estimate for Supertyphoon Wynne.

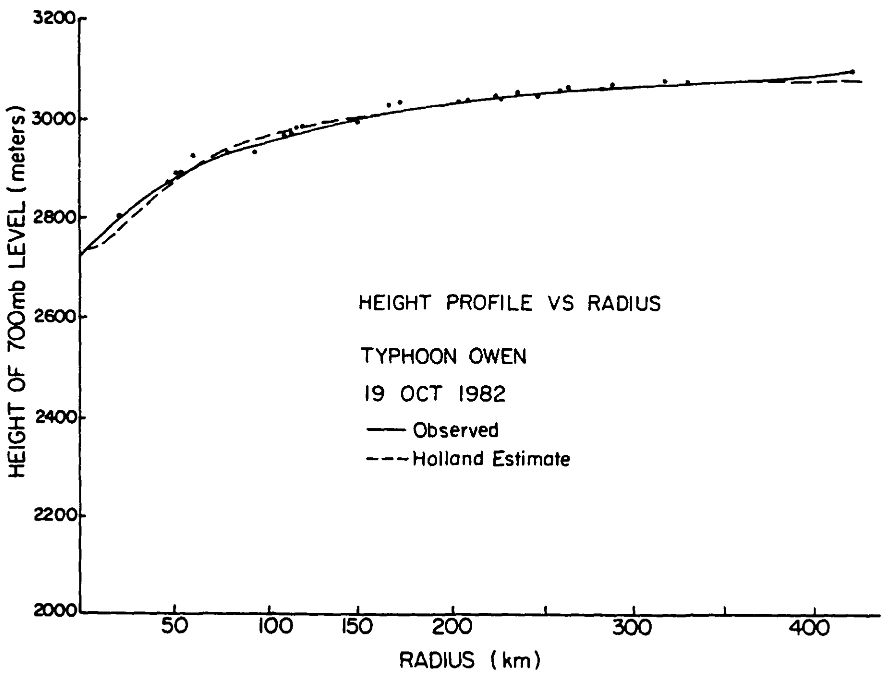

Figure C.4: 700 mb height vs. radius profiles for the observed curve (actual data points shown) and the Holland-estimate for Typhoon Owen.

the estimated and observed MSLP, implying that even though the pressure gradient can play a major role in determining the maximum wind speed, the minimum pressure value dominates. When the observed maximum winds were compared with the MSLP, the correlation coefficient was 0.88 (Weatherford and Gray 1987a).

C.2 The Normalized Wind Profile

When modelling the wind profile of tropical cyclones, it is convenient to characterize the tangential wind field in terms of a normalized structure. Conceptually, as the maximum wind changes, the entire wind field should respond and change accordingly. A straightforward way to approach the problem of scaling these changes would be to normalize the wind profile for the value of the maximum wind and by the radius of maximum wind speed (RMW). This approach could systematically account for variations in both the maximum wind speed and its position relative to the center. In this way, the normalized

Table C.2: Statistics on the Holland derived scaling paramenters A and b that best fit height data to a logarithmic hyperbola and the resultant estimates of Radius of Maximum Wind speed (RMW) and maximum wind speed as applied to the 780 missions of the northwestern Pacific data set.

PARAMETER	AVERAGE	STANDARD DEVIATION	MEDIAN	RANGE
A (km)	118	± 243	44	1 - 2081
	.99	± .29	.97	.1 - 2.1
RMW (km)	61	± 50	48	7 - 330
MAX WIND (ms-1)	32	± 13	30	5 - 76

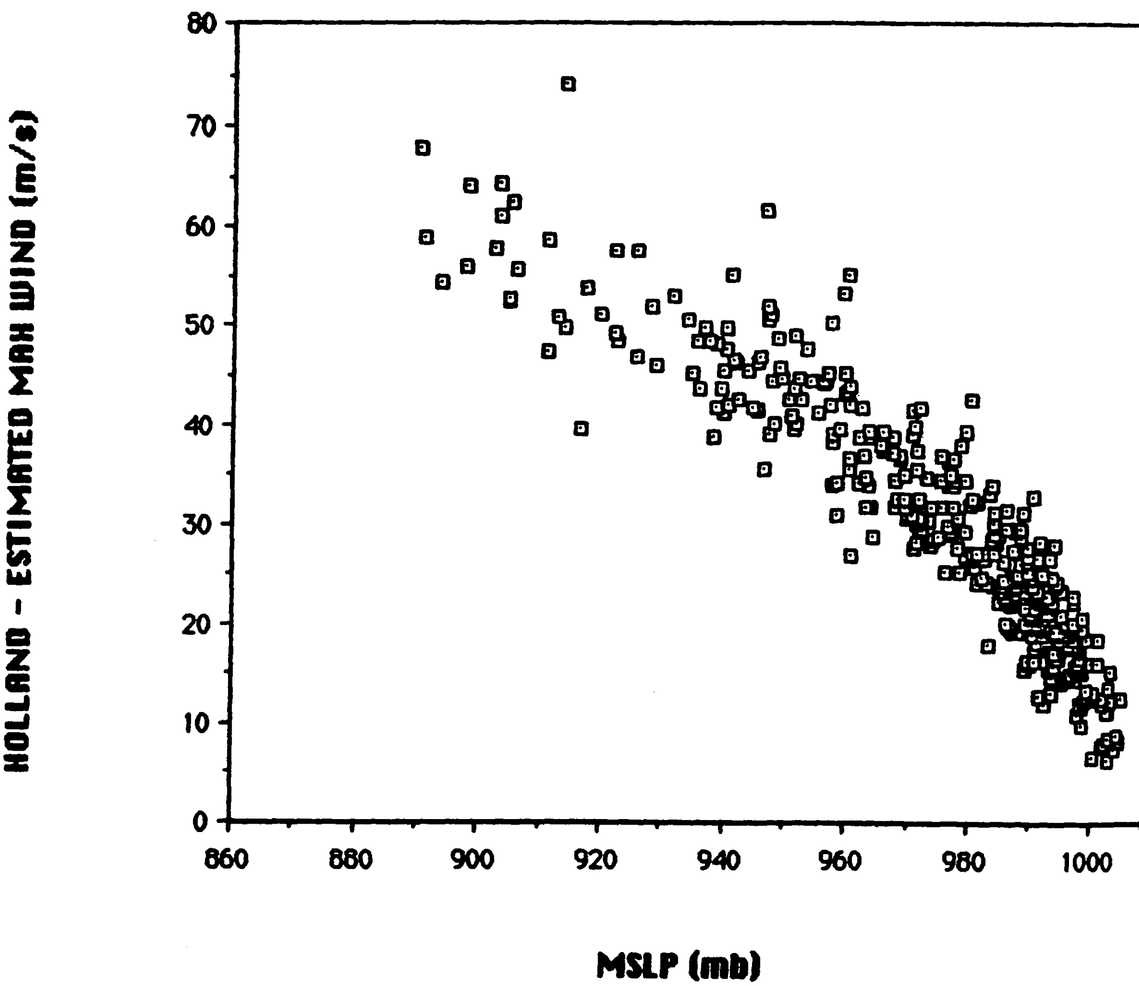

Figure C.5: Scatter plot of the Holland method estimated maximum wind speeds versus the accompanying MSLP for all cyclones used in the present study.

wind profile should remain the same as the RMW contracts while the cyclone intensifies and then expands as the MSLP fills. The potential applications for such a representation are great in that observations of the maximum winds could be obtained, either directly by aircraft measurement or indirectly from satellite analysis (Dvorak, 1975) and then applied to regions beyond the RMW. Since the results in this paper show considerable changes in the outer core as well as the inner core, a question to be addressed was whether or not the changes in the Outer Core Strength (the region between 1° to 2.5° radius) precisely reflect changes in the value and radius of the maximum wind or more simply, can the wind profile be simplified when normalized to the RMW?

We tested this concept by examining wind profiles observed for the 101 cyclones in this data set. The procedure used observed values of the RMW and the Holland-estimates of the maximum wind speed to scale the wind profile. In those cases when RMW was not accurately measured because the Doppler wind equipment attenuated, observations of the eyewall diameter were employed instead. From data for hurricane flights of the late 1950's through 1970's in which the Doppler wind equipment did not attenuate, a regression equation was derived for the best fit RMW given the MSLP and eyewall diameter. The result, which explained 73% of the variance is given by Eq. C.3.

$$RMW = -133 + .1468(MSLP) + .967(\text{ eye radius}) \tag{C.3}$$

where the RMW and eye radius are in nautical miles and MSLP is in millibars.

Figure C.6 shows the radial wind profiles of seven different cyclones. Figure C.7 shows these same profiles but where the normalized radius is expressed as multiples of the RMW and the wind speed is normalized by the maximum wind speed as

$$\text{normalized wind speed} = V_t/V_{t-max}. \tag{C.4}$$

Profile variability was little reduced when compared with the unnormalized profiles (compare Figs. C.3 and C.4).

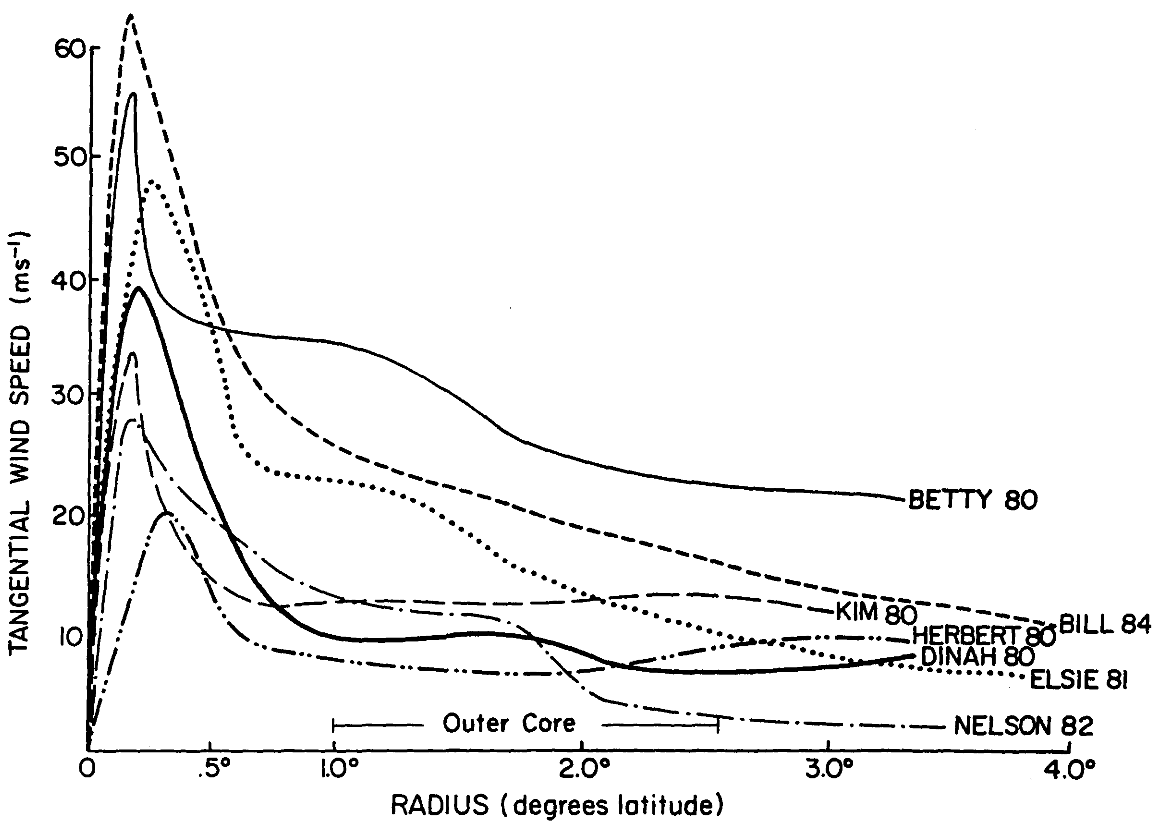

Figure C.6: Actual tangential wind profiles for seven tropical cyclones. The outer core extends from $1°to2.5°$ radius.

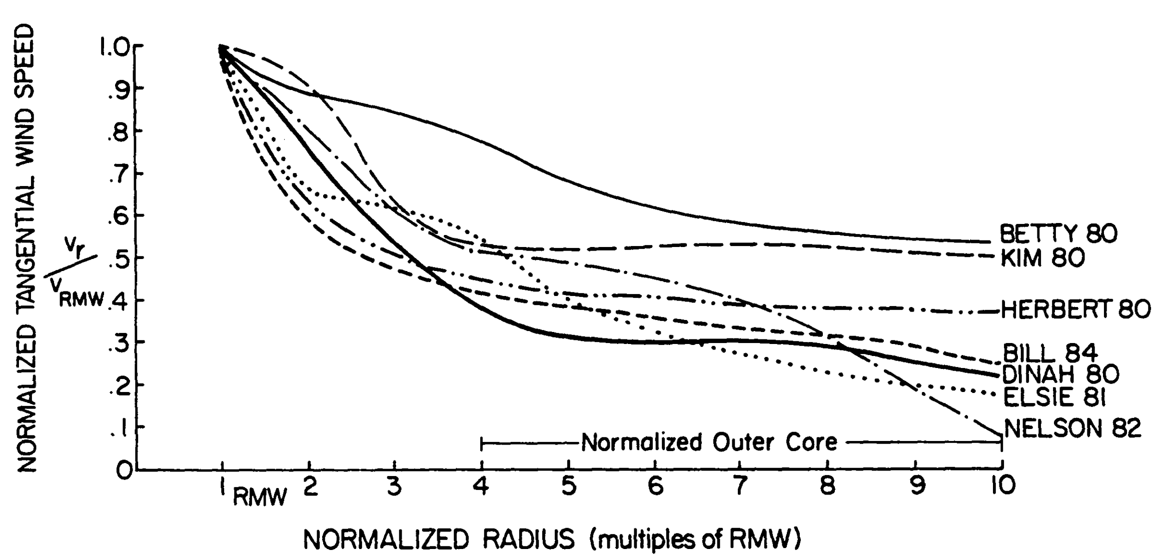

Figure C.7: Normalized tangential wind profiles in which radius varies as multiples of RMW and wind speed values are a fraction of the maximum wind value. A comparable outer core extends from 4 to 10 times the RMW.

An attempt was also made to construct a normalized Outer Core wind Strength, or NORM-OCS. The standard OCS, as shown in Fig. C.6, is the area weighted average tangential wind speed between 1° to 2.5° radius. However, RMW values varied in time with each storm system. It was found that, on average, the outer core extended across a radius which varied from 4 to 10 times the RMW. Normalized OCS values were then computed for area-weighted values corresponding to values 4 to 10 times the RMW. Comparisons were made using the maximum wind/normalized OCS ratio versus the max wind/OCS ratio to see if the normalized method would reduce the observed variability between inner and outer core winds. Notice in Fig. C.8 that for all cases, the actual OCS (Fig. C.9) correlated much better with the maximum wind (-.42) than did the normalized OCS values (-.02 in Fig C.9). When only intensifying cases were compared, as shown in Fig. C.10, the non-normalized plot again correlated better (-.67) than the normalized plot (-.09) as seen in Fig. C.11. The results in Figs. C.8-C.10 implies that in the intensifying phase, the higher the maximum wind speed, the smaller the ratio of inner core to outer core speeds for the un-normalized cases. The normalized cases show no relationship whatsoever.

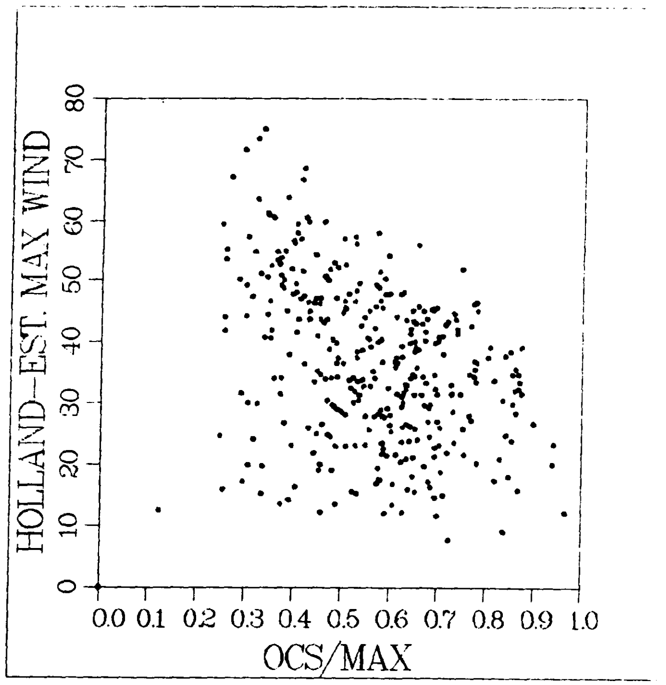

Figure C.8: Scatter diagram of the maximum wind speed vs. the ratio of OCS/maximum wind speed for a random number of cyclones.

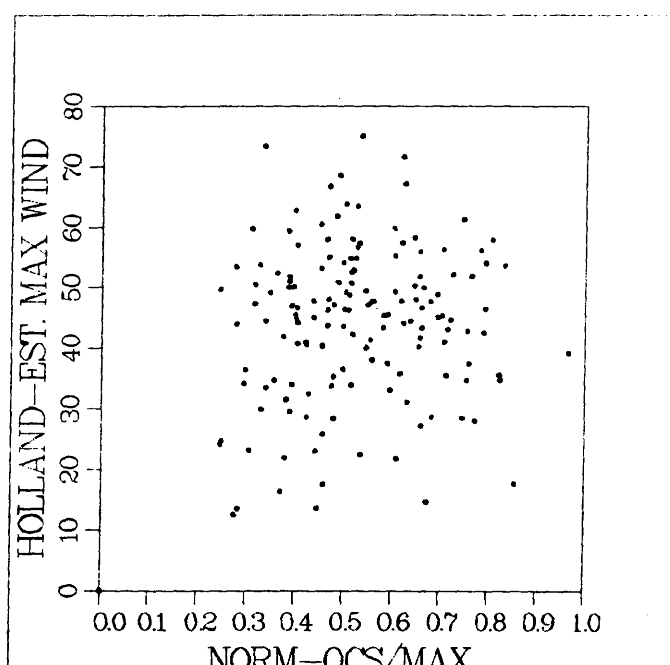

Figure C.9: Scatter diagram of the maximum wind speed vs. the ratio of the normalized OCS/maximum wind speed for the same cyclones as in Fig. 2.17.

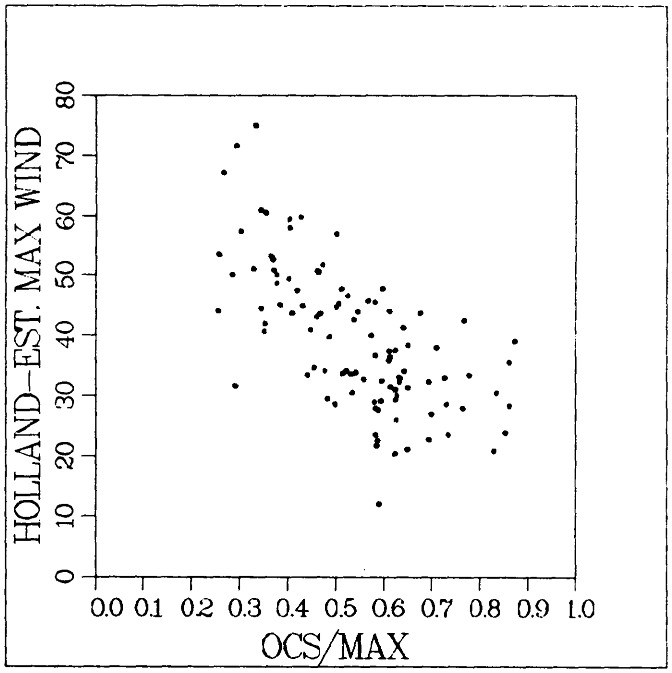

Figure C.10: Scatter diagram of the maximum wind speed vs. the ratio of OCS/maximum wind speed for intensifying cyclones.

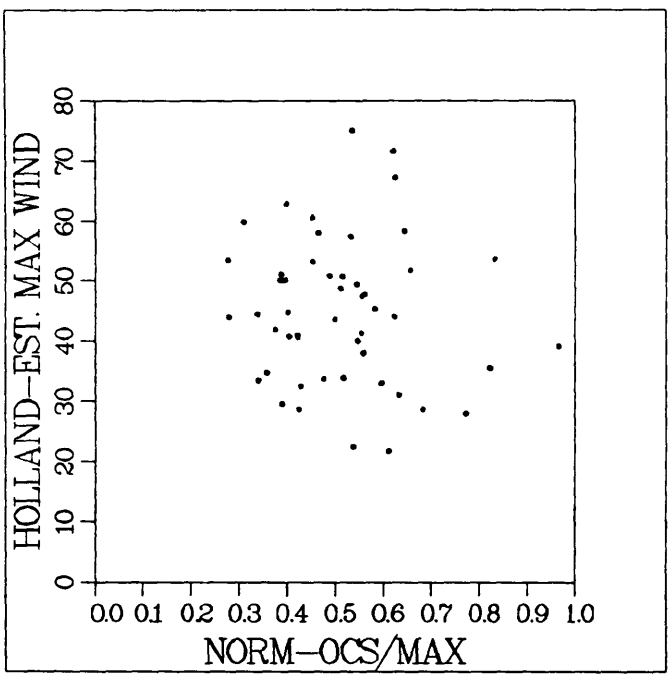

Figure C.11: Scatter diagram of the maximum wind speed vs. the ratio of the normalized OCS/maximum wind speed for the same cyclones as in Fig. 2.19.

The method employed here was compromised by the range of observations provided by the aircraft. When the RMW was smaller than the average value of 28 km, it was a simple matter to obtain wind observations at radii 10 times the RMW because missions routinely extended that far. However, for an RMW much beyond 28 km, winds at 10 RMW were often not available and thus this scheme became weighted towards smaller cyclones.

W. M. GRAY'S FEDERALLY SUPPORTED RESEARCH PROJECT REPORTS SINCE 1967

CSU Dept. of Atmos. Sci. Report No.	Report Title, Author, Date, Agency Support
104	The Mutual Variation of Wind, Shear and Baroclinicity in the Cumulus Convective Atmosphere of the Hurricane (69 pp.). W. M. Gray. February 1967. NSF Support.
114	Global View of the Origin of Tropical Disturbances and Storms (105 pp.). W. M. Gray. October 1967. NSF Support.
116	A Statistical Study of the Frictional Wind Veering in the Planetary Boundary Layer (57 pp.). B. Mendenhall. December 1967. NSF and ESSA Support.
124	Investigation of the Importance of Cumulus Convection and ventilation in Early Tropical Storm Development (88 pp.). R. Lopez. June 1968. ESSA Satellite Lab. Support.
Unnumbered	Role of Angular Momentum Transports in Tropical Storm Dissipation over Tropical Oceans (46 pp.). R. F. Wachtmann. December 1968. NSF and ESSA Support.
Unnumbered	Monthly Climatological Wind Fields Associated with Tropical Storm Genesis in the West Indies (34 pp.). J. W. Sartor. December 1968. NSF Support.
140	Characteristics of the Tornado Environment as Deduced from Proximity Soundings (55 pp.). T. G. Wills. June 1969. NOAA and NSF Support.
161	Statistical Analysis of Trade Wind Cloud Clusters in the Western North Pacific (80 pp.). K. Williams. June 1970. ESSA Satellite Lab. Support.
—	A Climatology of Tropical Cyclones and Disturbances of the Western Pacific with a Suggested Theory for Their Genesis/Maintenance (225 pp.). W. M. Gray. NAVWEARSCHFAC Tech. Paper No. 19-70. November 1970. (Available from US Navy, Monterey, CA). US Navy Support.
179	A diagnostic Study of the Planetary Boundary Layer over the Oceans (95 pp.). W. M. Gray. February 1972. Navy and NSF Support.
182	The Structure and Dynamics of the Hurricane's Inner Core Area (105 pp.). D. J. Shea. April 1972. NOAA and NSF Support.
188	Cumulus Convection and Larger-scale Circulations, Part I: A Parametric Model of Cumulus Convection (100 pp.). R. E. Lopez. June 1972. NSF Support.
189	Cumulus Convection and Larger-scale Circulations, Part II: Cumulus and Meso-scale Interactions (63 pp.). R. E. Lopez. June 1972. NSF Support.

CSU Dept. of Atmos. Sci. Report No.	Report Title, Author, Date, Agency Support
190	Cumulus Convection and Larger-scale Circulations, Part III: Broadscale and Meso-scale Considerations (80 pp.). W. M. Gray. July 1972. NOAA-NESS Support.
195	Characteristics of Carbon Black Dust as a Tropospheric Heat Source for Weather Modification (55 pp.). W. M. Frank. January 1973. NSF Support.
196	Feasibility of Beneficial Hurricane Modification by Carbon Black Seeding (130 pp.). W. M. Gray. April 1973. NOAA Support.
199	Variability of Planetary Boundary Layer Winds (157 pp.). L. R. Hoxit. May 1973. NSF Support.
200	Hurricane Spawned Tornadoes (57 pp.). D. J. Novlan. May 1973. NOAA and NSF Support.
212	A Study of Tornado Proximity Data and an Observationally Derived Model of Tornado Genesis (101 pp.). R. Maddox. November 1973. NOAA Support.
219	Analysis of Satellite Observed Tropical Cloud Clusters (91 pp.). E. Ruprecht and W. M. Gray. May 1974. NOAA/NESS Support.
224	Precipitation Characteristics in the Northeast Brazil Dry Region (56 pp.). R. P. L. Ramos. May 1974. NSF Support.
225	Weather Modification through Carbon Dust Absorption of Solar Energy (190 pp.). W. M. Gray, W. M. Frank, M. L. Corrin, and C. A. Stokes. July 1974.
234	Tropical Cyclone Genesis (121 pp.). W. M. Gray. March 1975. NSF Support.
—	Tropical Cyclone Genesis in the Western North Pacific (66 pp.). W. M. Gray. March 1975. US Navy Environmental Prediction Research Facility Report. Tech. Paper No. 16-75. (Available from the US Navy, Monterey, CA). Navy Support.
241	Tropical Cyclone Motion and Surrounding Parameter Relationships (105 pp.). J. E. George. December 1975. NOAA Support.
243	Diurnal Variation of Oceanic Deep Cumulus Convection. Paper I: Observational Evidence, Paper II: Physical Hypothesis (106 pp.). R. W. Jacobson, Jr. and W. M. Gray. February 1976. NOAA-NESS Support.
257	Data Summary of NOAA's Hurricanes Inner-Core Radial Leg Flight Penetrations 1957-1967, and 1969 (245 pp.). W. M. Gray and D. J. Shea. October 1976. NSF and NOAA Support.
258	The Structure and Energetics of the Tropical Cyclone (180 pp.). W. M. Frank. October 1976. NOAA-NHEML, NOAA-NESS and NSF Support.

CSU Dept. of Atmos. Sci. Report No.	Report Title, Author, Date, Agency Support
259	Typhoon Genesis and Pre-typhoon Cloud Clusters (79 pp.). R. M. Zehr. November 1976. NSF Support.
Unnumbered	Severe Thunderstorm Wind Gusts (81 pp.). G. W. Walters. December 1976. NSF Support.
262	Diurnal Variation of the Tropospheric Energy Budget (141 pp.). G. S. Foltz. November 1976. NSF Support.
274	Comparison of Developing and Non-developing Tropical Disturbances (81 pp.). S. L. Erickson. July 1977. US Army Support.
—	Tropical Cyclone Research by Data Compositing (79 pp.). W. M. Gray and W. M. Frank. July 1977. US Navy Environmental Prediction Research Facility Report. Tech. Paper No. 77-01. (Available from the US Navy, Monterey, CA). Navy Support.
277	Tropical Cyclone Cloud and Intensity Relationships (154 pp.). C. P. Arnold. November 1977. US Army and NHEML Support.
297	Diagnostic Analyses of the GATE A/B-scale Area at Individual Time Periods (102 pp.). W. M. Frank. November 1978. NSF Support.
298	Diurnal Variability in the GATE Region (80 pp.). J. M. Dewart. November 1978. NSF Support.
299	Mass Divergence in Tropical Weather Systems, Paper I: Diurnal Variation; Paper II: Large-scale Controls on Convection (109 pp.). J. L. McBride and W. M. Gray. November 1978. NOAA-NHEML Support.
—	New Results of Tropical Cyclone Research from Observational Analysis (108 pp.). W. M. Gray and W. M. Frank. June 1978. US Navy Environmental Prediction Research Facility Report. Tech. Paper No. 78-01. (Available from the US Navy, Monterey, CA). Navy Support.
305	Convection Induced Temperature Change in GATE (128 pp.). P. G. Grube. February 1979. NSF Support.
308	Observational Analysis of Tropical Cyclone Formation (230 pp.). J. L. McBride. April 1979. NOAA-NHEML, NSF and NEPRF Support.
—	Tropical Cyclone Origin, Movement and Intensity characteristics Based on Data Compositing Techniques (124 pp.). W. M. Gray. August 1979. US Navy Environmental Prediction Research Facility Report. Tech. Paper No. CR-79-06. (Available from the US Navy, Monterey, CA). Navy Support.

CSU Dept. of Atmos. Sci. Report No.	Report Title, Author, Date, Agency Support
—	Further Analysis of Tropical Cyclone Characteristics from Rawinsonde Compositing Techniques (129 pp.). W. M. Gray. March 1981. US Navy Environmental Prediction Research Facility Report. Tech. Paper No. CR-81-02. (Available from the US Navy, Monterey, CA). Navy Support.
333	Tropical Cyclone Intensity Change—A Quantitative Forecasting Scheme. K. M. Dropco. May 1981. NOAA Support.
—	Recent Advances in Tropical Cyclone Research from Rawinsonde Composite Analysis (407 pp.). WMO Publication. W. M. Gray. 1981.
340	The Role of the General Circulation in Tropical Cyclone Genesis (230 pp.). G. Love. April 1982. NSF Support.
341	Cumulus Momentum Transports in Tropical Cyclones (78 pp.). C. S. Lee. May 1982. ONR Support.
343	Tropical Cyclone Movement and Surrounding Flow Relationships (68 pp.). J. C. L. Chan and W. M. Gray. May 1982. ONR Support.
346	Environmental Circulations Associated with Tropical Cyclones Experiencing Fast, Slow and Looping Motions (273 pp.). J. Xu and W. M. Gray. May 1982. NOAA and NSF Support.
348	Tropical Cyclone Motion: Environmental Interaction Plus a Beta Effect (47 pp.). G. J. Holland. May 1982. ONR Support.
—	Tropical Cyclone and Related Meteorological Data Sets Available at CSU and Their Utilization (186 pp.). W. M. Gray, E. Buzzell, G. Burton and Other Project Personnel. February 1982. NSF, ONR, NOAA, and NEPRF Support.
352	A Comparison of Large and Small Tropical Cyclones (75 pp.). R. T. Merrill. July 1982. NOAA and NSF Support.
358	On the Physical Processes Responsible for Tropical Cyclone Motion (200 pp.). Johnny C. L. Chan. November 1982. NSF, NOAA/NHRL and NEPRF Support.
363	Tropical Cyclones in the Australian/Southwest Pacific Region (264 pp.). Greg J. Holland. March 1983. NSF, NOAA/NHRL and Australian Government Support.
370	Atlantic Seasonal Hurricane Frequency, Part I: El Nino and 30 mb QBO Influences; Part II: Forecasting Its Variability (105 pp.). W. M. Gray. July 1983. NSF Support.
379	A Statistical Method for One- to Three-Day Tropical Cyclone Track Prediction (201 pp). Clifford R. Matsumoto. December, 1984. NSF/NOAA and NEPRF support.
—	Varying Structure and Intensity Change Characteristics of Four Western North Pacific Tropical Cyclones. (100 pp.). Cecilia A. Askue and W. M. Gray. October 1984. US Navy Environmental Prediction Research Facility Report No. CR 84-08. (Available from the US Navy, Monterey, CA). Navy Support.

CSU Dept. of Atmos. Sci. Report No.	Report Title, Author, Date, Agency Support
—	Characteristics of North Indian Ocean Tropical Cyclone Activity. (108 pp.). Cheng-Shang Lee and W. M. Gray. December 1984. US Navy Environmental Prediction Research Facility Report No. CR 84-11. (Available from the US Navy, Monterey, CA). Navy Support.
391	Typhoon Structural Variability. (77 pp.). Candis L. Weatherford. October, 1985. NSF/NOAA Support.
392	Global View of the Upper Level Outflow Patterns Associated with Tropical Cyclone Intensity Change During FGGE. (126 pp.). L. Chen and W. Gray. October, 1985. NASA support.
394	Environmental Influences on Hurricane Intensification. (156 pp.). Robert T. Merrill. December, 1985. NSF/NOAA Support.
403	An Observational Study of Tropical Cloud Cluster Evolution and Cyclogenesis in the Western North Pacific. (250 pp.). Cheng-Shang Lee. September, 1986. NSF/NOAA support.
—	Factors Influencing Tropical Cyclone Genesis as Determined from Aircraft Investigative Flights into Developing and Non-Developing Tropical Disturbances in the Western North Pacific. Michael Middlebrooke. October, 1986 (70 pp.). NSF/NOAA support.
—	Recent Colorado State University Tropical Cyclone Research of Interest to Forecasters. (115 pp.). William M. Gray. June, 1987. US Navy Environmental Prediction Research Facility Contractor Report CR 87-10. Available from US Navy, Monterey, CA. Navy support.
428	Tropical Cyclone Observation and Forecasting With and With and Without Aircraft Reconnaissance. (105 pp.) Joel D. Martin. May, 1988. USAF, NWS, ONR support.
429	Investigation of Tropical Cyclone Genesis and Development Using Low-level Aircraft Flight Data. (94 pp.) Michael G. Middlebrooke. May, 1988. USAF, NSF support.
436	Environmental and convective influence on tropical cyclone development vs. non–development. (105 pp.) Patrick A. Lunney. December, 1988.